Energy Monitoring and Verification of Ground-Coupled Heat Pumps:

Utilizing Live Building Control Data in the Wisconsin Institutes for Discovery

by

Russell Knudson

A thesis submitted in partial fulfillment of the requirements for the degree of

Master of Science

(Mechanical Engineering)

at the

UNIVERSITY OF WISCONSIN-MADISON

2013

Blank

Approved by

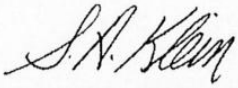

Professor Sanford A. Klein

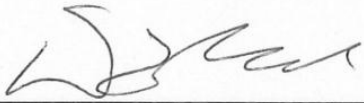

Professor Douglas T. Reindl

Blank

ACKNOWLEDGMENTS

There is a long list of people to thank, but I will try to keep it brief. The present research would not have been possible without John S. Nelson. Among many other duties, John is adjunct faculty of UW Civil Engineering and consultant to the Wisconsin Alumni Research Foundation – specifically for coordinating research on the environmental impact of the Wisconsin Institutes for Discovery facility. John was the principal contact at the Wisconsin Institutes for Discovery and assisted with much of the document gathering and overall project mentoring. In addition, the research was funded through the John S. Nelson Distinguished Graduate Fellowship program. In this way, John served as benefactor, enabler, and mentor to the project, for all of which I am humbly grateful.

Much is indebted to the principal advisors to the project – Douglas T. Reindl and Sandford A. Klein. Doug and Sandy were eternally critical, made efforts to be available often, and (somehow) were enjoyable to be around and work with. Doug's insights regarding building systems, HVAC, and engineering professionalism were of critical importance to the research. Sandy's inventiveness and creativity were great motive powers during the project. Additionally, the course work and final exams administered in Sandy's classes made the research a piece of cake. Most of all, I appreciate the lessons learned from Doug and Sandy regarding the importance of the fundamentals and the value of practicality.

A note of gratitude to Professor Gregory F. Nellis, who served as the third member of the project review committee. Greg's input on the project was of direct influence to the research, and his heat transfer courses and his Heat Transfer textbook had a broader influence. A big thank you to the members of the UW Solar Energy Lab of 2011 to 2013. The SEL (13th floor of the Engineering Research Building) was at times a constructive place to work, a great place to chalkboard ideas, and sometimes a little too much fun. There are many to thank, but in particular, thank you to Mandy Pertzborn for her guidance, and to Rogelio Rosas and Diego Fonseca for their extra efforts regarding many research challenges.

The initial understanding of the building equipment and general operation of building systems was due to the patience and efforts of John G. Davis from UW Engineering Professional Development. Shadowing and first-hand experience was also gained from many of the technical staff that paid visit to the building, such as the commissioning team and representatives from various equipment manufacturers. There were also many who were of great assistance from the UW Facilities, Planning, and Management Department, namely: Tim Collins, Adam Griffin, Ken Wolff, Wayne Vander Ark, Dave Sherman, and Jeff Polei. The complexity of construction projects, issues inherent in building operations, and the impact of buildings on the environment are too important to be allowed to be bridled by politics. The author hopes that the transparency and cooperation observed in the present research will be a continued and ever-improving trend in building research.

Finally, a thank you to members of the UW Nelson Institute's Culture, History, and Environment group (CHE), many of whom provided insights to the research that kept the project in a broader context and inspired a greater appreciation for the values to be found within the discipline of engineering. In particular, the author is grateful to: Professor Cathy Middlecamp – for the many discussions and shared mysteries within the WID; Garrett Dash Nelson – for the friendship and adventures in the built environment; and Professor Bill Cronon – for mentorship in and out of the classroom.

Table of Contents

Acronyms and Definitions

IBA	Intelligent Building Architecture system, used for data trending
BAS	Building Automation System, responsible for building HVAC controls
WFM	Water Flow Meter
BCS-T	Temperature Sensor, Basement Chilled water Supply
CEW-T	Temperature Sensor, Condenser Entering Water
CHWS-T	Temperature Sensor, Campus Chilled Water Supply
CHWR-T	Temperature Sensor, Campus Chilled Water Return
CLW-T	Temperature Sensor, Condenser Leaving Water
CWR-T	Temperature Sensor, Campus Chilled Water Return #2
CWS-T	Temperature Sensor, Campus Chilled Water Supply #2
EEW-T	Temperature Sensor, Evaporator Entering Water
ELW-T	Temperature Sensor, Evaporator Leaving Water
GEW-T	Temperature Sensor, Campus Chilled Water Return
GLW-T	Temperature Sensor, Condenser Leaving Water
GUR-1-T	Temperature Sensor, Geo-Loop "University" Return (#1)
GER-2-T	Temperature Sensor, Geo-Loop "East Orchard" Return (#2)
GWR-3-T	Temperature Sensor, Geo-Loop "West Orchard" Return (#3)
GCR-4-T	Temperature Sensor, Geo-Loop "Campus" Return (#4)
SMT-1	Temperature Sensor, Surface-Mounted #1
SMT-2	Temperature Sensor, Surface Mounted #2
WHS-T	Temperature Sensor, Recovered-Reheat Supply
WHR-T	Temperature Sensor, Recovered-Reheat Return
Cx	The process of commissioning building mechanical equipment by a commissioning team.
As-Built	A document or schematic that provides information about the building status post-construction, which can differ from what was intended or designed.
BAS	Building Automation System, a computerized building information system that manages and automates the control of the building mechanical equipment.
IBA	Intelligent Building Architecture, a computerized building information system used for monitoring the status of building equipment and building resource consumption. Similar to the BAS, however the IBA is less commonly used for control purposes.
MEP	All building systems and functions that are operated by Mechanical, Electrical, or Plumbing equipment.
Point (data)	A Point signifies any measurement or calculation that is stored in the various building information systems and used for either control or monitoring of building operations.
Contractor(s)	During building construction, the contractor is an entity responsible for implementing a specific job.
BOD	Basis of Design, a document created during the planning of the construction of WID
WCCF	West Campus Cogeneration Facility

Chapter 1. Motivations and Objectives

1.1 Energy Use in U.S. Buildings

Improving methods in the design and operation of buildings represent a significant potential for immediate and continual energy conservation. Increasing rates of energy production and consumption, particularly pertaining to the burning of fossil fuels, has been linked to rapid environmental change; most notably the increasing concentration of greenhouse gases in the Earth's atmosphere and historical environmental events such as substantial decrease in the area of polar ice caps. (IPCC 2007) Energy consumption and availability are also major factors in the U.S. national economy and have been recognized as key components in issues of economic stability and national security.

In 2011, the combined end-use energy consumption of the U.S. residential and commercial buildings was 39.5 quadrillion Btu; 40% of the nation's total energy consumed (Figure 1-1). Occupant expectations in the U.S. with regard to indoor comfort and a growing awareness of indoor health play a major part of building energy use. In commercial buildings, heating, ventilation, and cooling accounted for the single largest energy end-use, representing 27% of the electrical, 52% of natural gas, and 31% of fuel oil consumption. (EIA 2013)

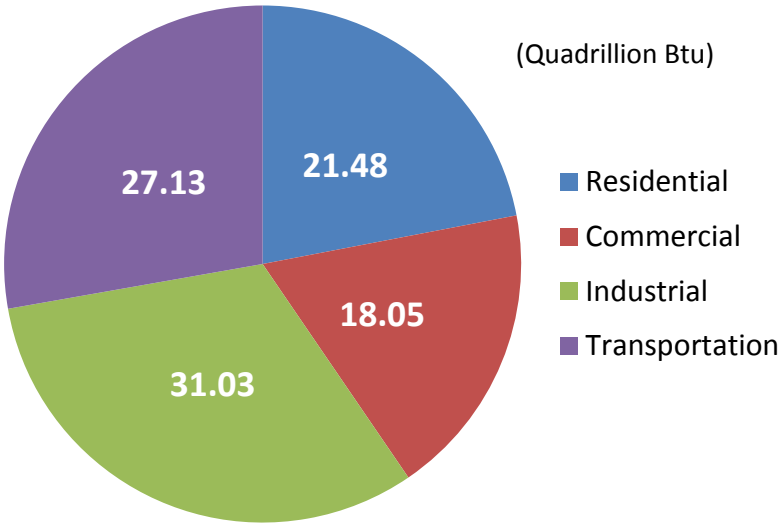

Figure 1-1 – End-use energy consumption by sector (EIA Data, 2011)

1.2 Federal Initiatives and Legislation Regarding Energy Conservation in Buildings

Under the 2007 Energy Independence and Security Act, Congress authorized the creation the Office of Federal and Commercial High-Performance Green Buildings. Administered through the General Services Administration, the Office promotes and coordinates "green building" for new Federal or commercial buildings.[1] (EISA 2007) One stated focus of the Office is to engage in public outreach activities that identifies and organizes educational resources regarding green building, and to maintain a green building clearinghouse (i.e.

[1] The definition for a "high-performance green building" under the Act is 176 words long. To summarize, a high-performance green building means a building that takes into consideration substantial reductions in energy and water use, and decreased environmental impact.

database).[2] (Building Database 2013) Of significant interest to the present research, the Office targets "cost-effective technologies and practices"; the definition of which is generally any technology that meets the requirements of the Act. Only one technology is mentioned specifically, and that is the geothermal (i.e. ground-coupled) heat pump. (EISA, T. IV, Sec. 401 (6), 2007)

One of the major provisions made under the Office of High Performance Green Buildings was to create a consortium (i.e. public-private business partnerships) responsible for developing and establishing programs "for the development and establishment of zero net energy commercial buildings".[3] The Commercial Building Consortium (CBC) was established in 2008 and is administered under the Department of Energy (DOE). The goal of the initiative is for any newly constructed commercial building in the U.S. to qualify as net-zero by 2030, 50% of the existing building stock by 2040, and all existing commercial buildings by 2050.

Another major piece of legislation, the Energy Conservation and Policy Act requires that State commercial building codes meet or exceed the requirements within Standard 90.1, created and maintained by the American Society of Heating Refrigeration and Energy (ASHRAE). The DOE conducted an analysis in 2011 and determined that the 2010 version of 90.1 were to be adopted by States by July 2013. Using 240 computer energy simulations,

[2] As of June 2013, the Wisconsin Institutes for Discovery was not registered on the clearinghouse.

[3] Net zero, or zero-net-energy building, is defined as one in which the balance of energy needs during typical operation are provided by sources that do not produce greenhouse gases.

the DOE analysis concluded that 18.5 percent building site energy would be saved if 90.1-2010 was adopted over 90.1-2007. (DOE 2011)

1.3 State of Wisconsin Incentive Program – Focus on Energy

Financial incentives are available from the State for energy efficient designs and retro-fitting in buildings. The Focus on Energy program was created in 2001 to administer incentives to Wisconsin residents and building project developers for investing in methods to reduce energy use. The program is funded by the state's investor-owned energy utilities and participating municipal and electric cooperative utilities. Participation by the utilities was mandated by the state under Wisconsin Statute §196, ordering that each utility contribute 1.2% of its annual operating revenue to the program. (WI Statute 196, section 374) In 2012, the Focus on Energy program administered $31,233,437 to nonresidential program participants at the cost of $19,074,976 to operate the program.

Energy savings by the Focus on Energy program are projected based on the claims that are submitted by participating businesses and residences. The program performs some verification of the energy savings, using methodologies listed in the International Performance Measurement and Verification Protocol (IPMVP) to perform validations. As an example of the evaluation capabilities of the program, Focus on Energy performed measurement evaluations for 164 non-residential buildings out of 6,429 that participated in 2012.

1.4 Energy Efficiency Rating and Certification Programs

There are many non-regulatory programs and standards that rate building design for energy. In 1992 the U.S. Environmental Protection Agency created Energy Star, a program aimed at

guiding individuals and businesses to achieve energy efficiency. The program strives to boost the adoption of efficient technologies and practices by certifying commercial products and publishing educational material. Energy Star hosts a database and ranking system for commercial buildings, within which a building owner regularly submits utility bill information in order to determine the relative performance of the building compared to national averages. Several characteristics of the building (e.g. operating hours, size, type of equipment within, etc.) are used to establish the benchmark for comparison.[4] (Energy Star 2013) Though Energy Star is attractive for being a no cost program that based on measurements and actual performance, its focus is limited to energy and utilities and is not considered a "whole building" analysis tool.

The most widely recognized building certification program is the Leadership in Energy and Environmental Design (LEED) certification program administered by the non-profit organization the U.S. Green Building Council (USGBC). The LEED program rates design and retro-fit plans for new and existing buildings. LEED rating systems are based on a point system analysis that is composed of categories including the design, construction, and operation of the building. In the most current version for new commercial buildings, LEED 2009, buildings are awarded (i.e. certified) with levels ranging in order of increasing

[4] As of June 2013, 41 facilities were listed in Madison as qualifying and participating in the Energy Star program.

superiority from certified, silver, gold, or platinum. Since 2010, the GSA has been requiring that all new federal buildings be LEED Gold certified as part of the EISA Sec. 436(h).[5]

Building certifications such as LEED are attractive because they have the potential to guide a building design toward greater efficiency and therefore greater return on the investment. For LEED, the registration and certification process comes with a fee that depends, generally, on the size of the building. Using a pertinent example, a 330,000 ft^2 building would cost about $16,000 in fees.[6] However, there are added costs associated with certification programs like LEED. The obvious costs in most situations would stem from the investments necessary to achieve the LEED rating (e.g. more energy efficient mechanical equipment, commonly known as incremental costs). In addition, there is a tendency for greater fees to be charged by architects and engineers for "green" designs. LEED certified buildings are generally perceived as providing healthier indoor/outdoor environments and cheaper operating costs, the building property and market values have been shown to be higher, however the long-term effects are still unknown. (Burr 2008) (Dermisi 2009)

Because the LEED program awards are distributed following a review of the building's design documentation, it is important to note that LEED certifications are based more on

[5] At the time of this writing, the U.S. GSA Office of High-Performance Green Buildings was in a public comment period regarding the review of building certification programs to be used to guide the design and construction for all future GSA buildings. The decision was narrowed to three finalists, and the chosen program was expected to be announced in the summer of 2013.

[6] Calculation based on $0.045 per sq. ft. and a $900 registration fee. http://www.usgbc.org/leed/certification/fees/overview

intention rather than actual performance. Mangasarian et al studied comparisons in water and energy saving between LEED-certified and non-LEED buildings owned by the U.S. Navy. The study showed that not all LEED-certified buildings achieved the stated goal in energy or water savings, and in some cases, the LEED-certified facilities performed worse in energy or water reduction than their non-LEED counterpart. (Mangasarian 2010) Four out of eleven buildings studied showed greater energy consumption for the LEED-certified building compared to its commercial counterpart. Two of eleven buildings showed greater water consumption for the LEED-certified building.

Through a partnership with the USGBC and the Illuminating Engineering Society of North America, ASHRAE created standard 189.1 "Standard for High-Performance Green Buildings" as a supplement to the minimum building code standard 90.1. Standard 189.1 has mandatory provisions for renewable energy requirements and includes provisions for consideration of building site characteristics such as heat island effect, for example. The National Renewable Energy Laboratory conducted a comparative analysis of 16 building models using either Standard 90.1-2007 or Standard 189.1-2009. The models showed that results varied somewhat by climate, and more strongly by building type. The study showed that Standard 189.1 would provide 30 percent site energy savings on average as compared to Standard 90.1-2007, with 15% site energy savings for an out-patient healthcare facility, to as high as 42% energy savings for a warehouse type facility. (NREL 2010) At the time of this writing, ASHRAE 189.1 was yet to be built into U.S. law.

1.5 Laboratory Facilities

Lab facilities present a unique challenge for designers attempting to reduce energy use. Lab facilities are, in general, energy intensive compared to commercial buildings of comparable size. Labs typically have significantly higher ventilation rate requirements, in many cases using 100% outside air with no recirculation. Therefore, space heating and/or cooling loads are significantly higher. In addition, internal heat gains are often higher in labs depending on the nature of the lab equipment and activity. Finally, many lab facilities have requirements for space conditioning and ventilation at all hours of the day, especially those with vivariums (i.e. space for living organisms) or patients (e.g. hospitals).

Though labs are a growing segment of the building sector, they constitute a small part of the U.S. building energy use and have not been incorporated into national programs such as Energy Star. Sponsored by the U.S. DOE and EPA, the Labs21 program was created to identify best practices related to energy efficiency. In order to do so, Labs21 compiled information for lab facilities based on normalized parameters including: gross floor area, lab area, climate, lab type, lab use, occupancy schedule, ventilation requirements, and equipment loads. (Matthew 2003) Labs21 created an online tool that generates an estimated energy baseline (i.e. "benchmark") based on the input information.[7]

1.6 Research Objectives

The current research effort aims to assess the energy performance of the heating and cooling system at the Wisconsin Institutes for Discovery - a high-performance LEED Gold laboratory

[7] The Labs21 benchmarking tool has been relocated from the DOE and is now hosted by the International Institute for Sustainable Laboratories.
http://www.i2sl.org/resources/toolkit/benchmark.html

facility on the campus of UW-Madison. Specifically, this project will measure the field-performance of aground-couple heat pump system and compare the in-situ performance with the original system design expectations. Performance will be expressed in terms of both the capacity (cooling and heat recovery) and efficiency. The system's efficiency will be compared to the efficiency of alternative means of heating and cooling the facility. In addition, the measured performance of the heat pump equipment will be compared to the manufacturer's rated performance information as part of the analysis. Finally, investigations were conducted to determine optimal (i.e. most efficient) methods of operating the system.

Chapter 2. Overview of the WID

2.1 Background of the Wisconsin Institutes for Discovery

The Wisconsin Institutes for Discovery is both the name of a group of research institutes at the University of Wisconsin-Madison and the facility that houses the institutes. The 330,000 ft^2 facility is officially referred to as the "Discovery building" or the "W.I.D.", but colloquially the acronym is pronounced as one word (rhymes with "bid"; IPA: wɪd). The WID was originally envisioned as both a laboratory and mixed-use facility, primarily to house research in the fields of the biomedical sciences. The building also has a ~70,000 ft^2 publicly accessible ground floor with three restaurants and space that hosted events ranging from lectures to weddings.

The WID was conceived for and houses twin research institutes, the privately-owned Morgridge Institute for Research, and the state-owned Wisconsin Institute for Discovery. The cost of the design, construction, and capital within the WID totaled $210 million ($640/ft^2). The Wisconsin Alumni Research Foundation (WARF) owns half of the building, building site, and the operations within the building from a contribution of $110 million. WARF leases their half of the building to the non-profit Morgridge Institute, named after John Morgridge, alumnus of UW-Madison and former chairman of Cisco Systems. He, along with his wife Tashia, contributed $50 million to the WID construction. The other half of the building and the building site is owned by the University Of Wisconsin Board Of Regents, based on a $50 million contribution from the State of Wisconsin.

The intended scope of the building and its impact within the UW-Madison community were made publicly aware in "town hall meetings" held in 2007, where discussions were held to inform the public of the building's design, organizations' objectives and purpose, and to solicit public feedback. (UW News 2009) In particular, the WID was envisioned to be designed, constructed, and operated with a significant reduction in environmental impact, compared to buildings of similar size and function. Design goals regarding the building's environmental impact revolved around the concept of a "100 year building" and the Basis of Design (BOD) outlines general protocols for the long-term operation, maintenance, and even destruction of the building. At the forefront of the BOD were goals for the facility to, during typical operation, consume 50% less energy than a benchmark facility of similar size and purpose. (BOD 2011)

From its inception, the WID building has been a high profile building project, partly due to the activities and people associated with the WID, but undoubtedly due to the scale and ambitions of the building itself. Photographed in Figure 2-1, the WID displays awards that have been granted to the WID organization for the building. The awards range from recognition of the architectural design to the building's intended sustainability goals, among them the R&D magazine 2012 "Lab of the Year" award, the Association for the Advancement of Sustainability in Higher Education 2012 "Innovation in Green Building" award, and the Focus on Energy 2011 "Award for Excellence in Sustainability and Energy Efficiency".

Figure 2-1 - Awards displayed in ground floor of WID[8]

2.2 WID's Commitment to Reduced Energy Use and LEED Certification

The WID was designed to use 50% less energy (on a per square foot basis) than a benchmark building of similar size and type. The UW Biochemistry Addition, a 220,000 ft^2 lab facility constructed in 1998, served as the baseline of comparison for the WID design engineers. (FP&M 2007) The Department of Energy's Labs21 benchmarking toolkit was used to

[8] Other awards pictured: (1) American Society of Interior Designers "Platinum Design Award", (2) Wisconsin Commercial Real Estate Women "2011 Impact Award", (3) American Council of Engineering Companies "2012 Engineering Excellence, Best of State Award", (4) American Institute of Architects "2011 Distinguished Accomplishments in Architecture".

estimate the energy use of the Biochem building. The toolkit is an online tool that estimates the energy usage of a lab facility based on normalized specifications such as the square footage, type of work and activity within the lab, approximate geographical location and climate. The WID design engineers reported that the Biochem building was estimated to use around 570 MBtu/GSF/yr.[9] During the design phase, an energy model of the WID facility was created using eQuest modeling software. The planned performance of WID based on the energy model exceeded the early expectations for energy savings of 50%. The final model of WID indicated that the estimated energy consumption was 180 MBtu/GSF/year, which represents a 68% energy savings as compared to the estimate for the Biochem building. (Energy Model 2011)

According to the WID basis of design (BOD), the energy reduction goals of the proposed building design were based on the U.S. Green Building Council's "Leadership in Energy and Environmental Design" (LEED) building certification program. Specifically, the most current rating system available at the time, LEED version 2.2 required a design energy (cost) savings of 42% compared to a baseline. In 2006, the USGBC announced the future rating system for new commercial buildings would require a reduction of building-based carbon emissions by 50% compared to a baseline. The designers of the WID reported that, though the building was registered as part of the LEED program and was expected to "achieve a strong level of performance", the most important goal of the building design was to "focus on meaningful and substantive initiatives… and accept the LEED rating that comes with [the established sustainability objectives]." (BOD 2011) In this way, the WID designers were

[9] Measured data was not reported, and possibly not available to the designers.

vocal about being inspired by the goals established by the LEED program, but only considered LEED recognition as secondary to the internally-established design goals.

During the present research, criticisms of LEED and similar building design accreditation programs were increasingly public discussion and in the popular press. (USA Today 2012) Suspicions of LEED awardees, particularly larger institutions of the kind that were commonly under public scrutiny for lacking environmental considerations, were suspect of "green washing" or "point mongering" (i.e. methods of feigning responsible actions in lieu of meaningful investment in conservation efforts). A year after its official opening in late 2010, the WID was the first laboratory in Wisconsin to receive the LEED Gold certification, the second highest LEED rating for new constructions. (Kelly 2011) Though it has been publicized by news outlets and the WID website, the WID had not publicly displayed recognition of its LEED certification a year and a half after receiving the certification.[10]

From the building's initial opening in December 2010, the WID offered itself as a "Living Laboratory" to certain researchers at the UW. Examples of previous works that directly involved the WID facility can be found in (N. C. Taylor 2012) and (Azar 2012). As will be discussed in subsequent chapters of this report, the WID Green Team staff granted physical access to the building, to building services and personnel such as the facility technicians and I.T. department, remote access to building automation and data systems, and was responsive regarding suggested system changes throughout the project. The support for research, such as

[10] Displaying a LEED plaque at a prominent location within the building was a custom for many LEED certified facilities.

the current project, is one example of the WID's committed effort to establish actual performance verification regarding the facility's design, operation, and impact. However, the high publicity value of "sustainability" remained an item that was difficult to quantify and was considered an inescapable consideration regarding the inclusion of many of the building's supplemental energy features.

2.3 Overview and Design of the Ground-Coupled Heat Pump System

The BOD lists 38 "baseline energy efficiency measures" that were fundamental to the WID's design; examples include: (1) glycol energy recovery loops from exhaust air stream; (2) four enthalpy recovery heat exchangers; (3) overnight fresh-air purge and cool down in the atrium; (4) solar thermal system for domestic hot water heating; (5) chilled beams used for cooling in laboratory spaces; (6) LED for task lighting; and (7) and expanded thermal comfort range in the public accessible areas as compared to many building designs.[11]

As stated, the major focus of the present research was the energy savings created by the WID ground-coupled heat pump system (GCHP). The GCHP system consisted of six heat pump modules, each with two compressors at 35 tons of cooling capacity (nominal). The heat pumps were hydronically connected to a closed-loop, vertical bore ground heat exchanger (GHX) as its primary means of heat rejection (heat pumps in cooling mode) and heat sourcing (heat pumps in heating mode). The GHX consisted of 77 vertical bores at depths of 300 feet that were located around the perimeter of the building and in one section across the

[11] Using large indoor plants and high amounts of natural lighting, the design of the publicly accessible floor was to give the occupant the perception of being outdoors. In doing so, the designers had confidence the temperature condition range could be widened to 80°F in the summer (traditionally 76°F) and 65°F in the winter (traditionally 68°F).

street. A representation of the GHX in relation to the WID building is shown in Figure 2-2. More detail and specifications of the ground-coupled heat pump systems can be found in Appendix B.

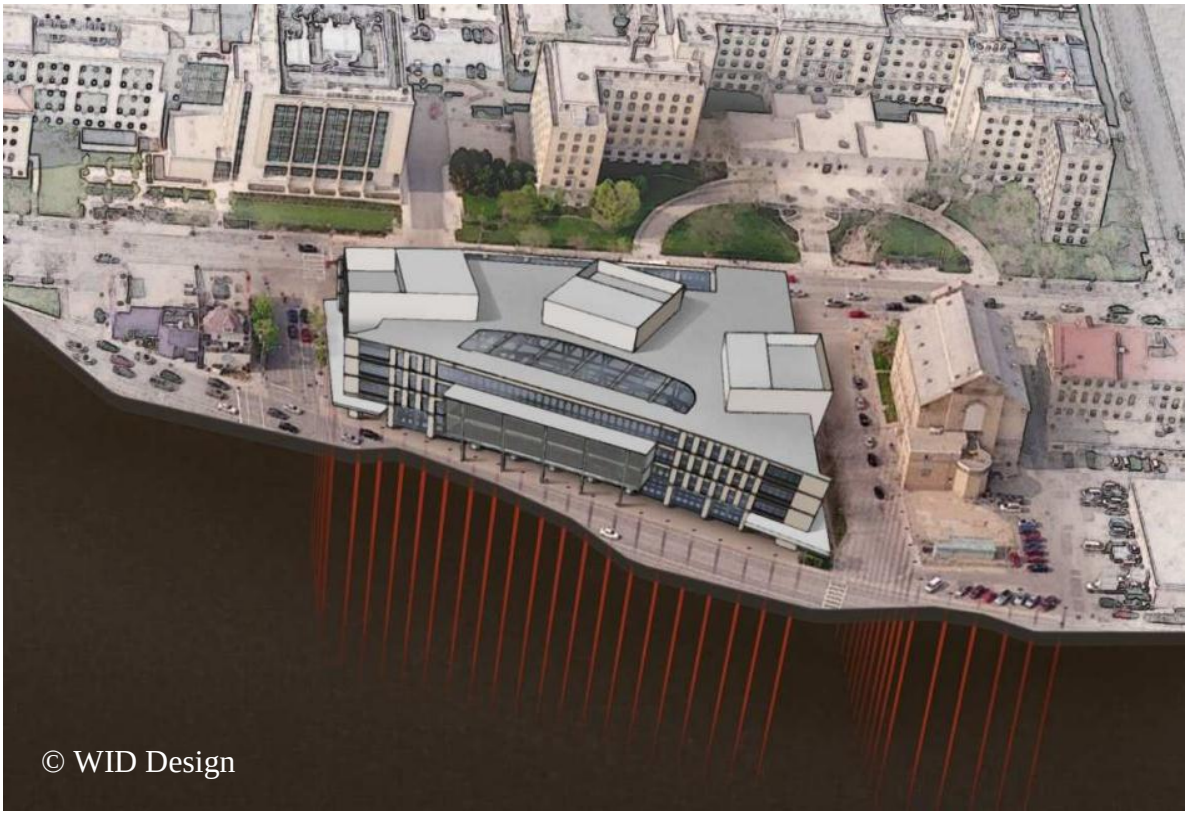

Figure 2-2 - Representation of the WID and the ground heat exchanger around the perimeter and under the building

The GCHP system was one of many of the energy efficiency (i.e. "sustainability") measures that were documented as "supplemental initiatives" in the basis of design. These initiatives were not part of the building's early design framework, but were included in the building plan after re-investing funds in the project contingency. Other examples of supplemental initiatives include the solar hot water system, the intelligent building architecture data

collection system, and the building's LED lighting. (G. K. Austin 2011) The total cost of the GCHP system was not reported in the construction documents, but initial cost estimates were reported as $1,250,000. (Architects 2008) Of the 50% projected energy savings of the WID design, the GCHP was estimated to contribute 10% of the savings.[12] (BOD 2011)

Because the WID is a cooling-dominated building (i.e. a cooling load was present at all times of the year), the heat pumps were sized to meet the year-round cooling requirements, also known as the "base cooling load", which consisted of cooling requirements associated with the in-house data center, process chilled water, and closet electrical and communication equipment. (BOD 2011) [13] [14] Figure 2-3 is a photograph of the WID server farm, the largest year-round cooling load. The estimated peak cooling load of the building was 2395 tons, and the design cooling capacity of the heat pumps was 385 tons, indicating that the heat pumps were to provide 16% of the peak cooling capacity to the building.[15] Twenty-four inch campus chilled water mains were piped into the WID mechanical room to supply the majority of the

[12] A final note on energy savings: the WID BOD does not specify whether the 10% projected energy savings of the GCHP was site (i.e. energy saved at the building) or source (energy saved for the district system which WID is a part of). Neither the energy model nor BOD indicate the estimated or measured efficiencies of the campus chilled water and steam supplies, which would be needed to make the determination.

[13] The design cooling capacity of the heat pumps was reported as 385 tons (Heat Pump Equipment Submittal document). The year-round server farm cooling load was estimated at 123 tons (BOD 2011) pg. 8-52, but the year-round cooling demand of the process loads was not reported. The peak process cooling load was estimated at 365 tons (BOD 2011) pg. 8-20).

[14] Process cooling loads are typically defined as loads that do not pertain to human comfort. However, in the WID the process loads include the load created by "chilled beams" which are used to cool laboratory spaces.

[15] The base, ventilation, and vivarium cooling load design estimates were summed to find the total design cooling load. (BOD 2011)

peak cooling, shown in Figure 2-4. Utility chilled water was not available year-round on the UW campus, so the GCHP was designed to provide the total base cooling in the off-cooling season and during times when campus chilled water is unavailable.

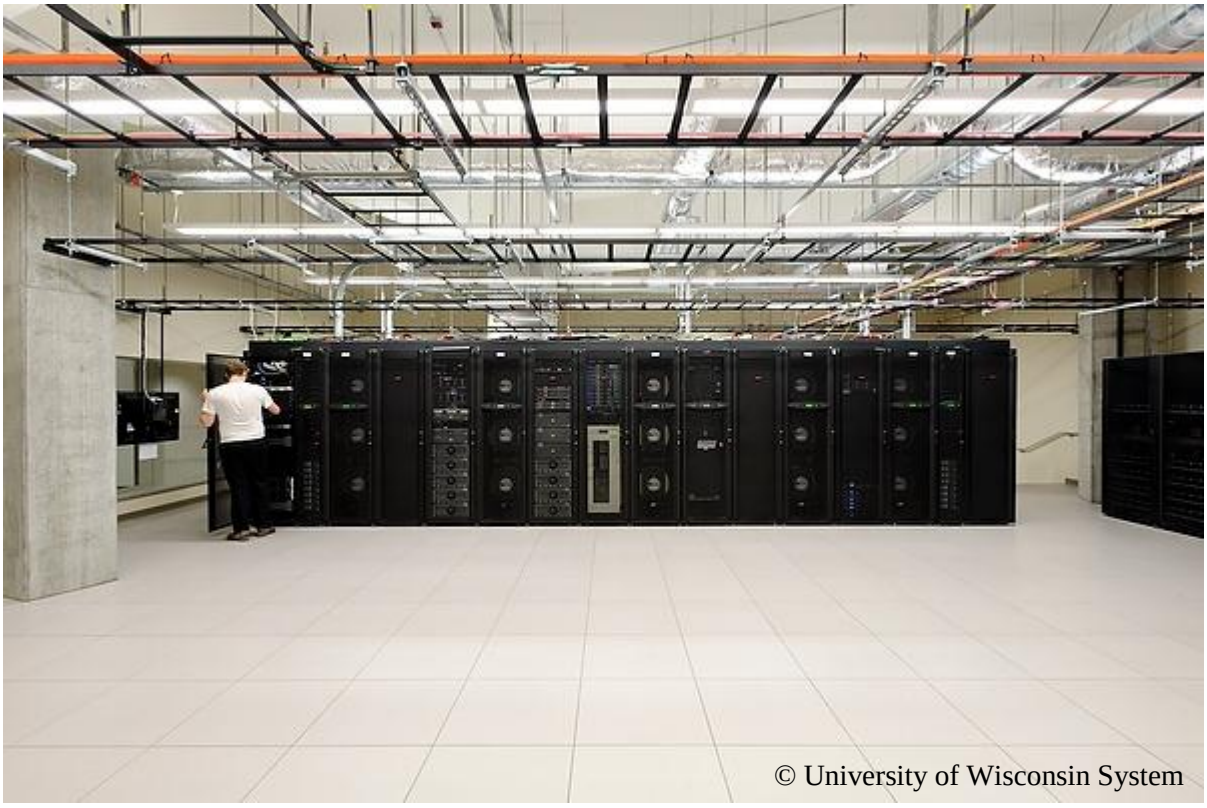

Figure 2-3 – Inside the partially occupied WID server farm, the largest planned, year-round cooling load in the building[16]

[16] Photo from the University of Wisconsin Systems, Campus Photo Library, by Jeff Miller, File ID: 14359

Figure 2-4 – Twenty-Four Inch Campus Chilled Water Supply and Return Mains at WID

According to the design, one advantage to cooling with on-site heat pumps was the possibility of operating them as "heat recovery chillers" to displace the need for campus steam for reheat. Recovering heat from the heat pumps is accomplished by re-directing the flow of hot condenser water to the building reheat loops, which is otherwise heated with campus utility steam. The remainder of the heat rejection is to be accomplished by circulating the hot condenser water through the GHX. The heat recovery aspect of the system is crucial to achieving the planned energy efficiency targets for the building.

Not only was the heat recovery operation closely linked to the heat rejection capabilities of the system (and subsequently the condensing temperatures and heat pump efficiency), but the sizing and design of the heat pumps to produce water hot enough for use as reheat could produce the tendency for the system to operate at higher condenser water temperatures. Finally, it should be noted that at the time of this writing, the campus utility operation

produced an abundance of low pressure steam (as a byproduct of steam turbine power generation) that was suitable for use in building reheat. It was not known what utility costs, if any, were billed to the WID for low pressure steam, or what the dependability of the steam supply was. However, the abundance of campus steam called into question the value of the heat recovery aspect of the system.

Finally, the possibility of operating the heat pumps for either cooling or heating (sometimes referred to as a hybrid heat pump system) was a significant part of the WID energy efficiency operations. Coupling the heat pumps to a ground heat exchanger, rather than conventional source/sink methods (e.g. cooling tower), would theoretically allow for more consistent ambient temperature conditions and is favorable for either condenser heat rejection in warm seasons or evaporator heat sourcing in cold seasons. However, as will be discussed in the following section, there are implementation challenges in such a system; namely the additional valving and piping required to accommodate changing the system between heating and cooling modes.

2.4 Early Issues Identified during Commissioning and Detection of System Leaks

The results of the WID commissioning process and early findings by the on-site facility technicians formed the starting point of the present research. For a complex lab facility such as the WID, commissioning is a practical necessity. Commissioning (shortened as “Cx”) is also a fundamental requirement for building certification programs such as LEED. As part of the WID sustainability goals defined in the BOD, a Cx team was hired to do what was described as “fundamental systems and enhanced commissioning”. The final Cx report, in the

form of the “As-Commissioned Controls Sequences”, indicated that the GHX appeared to have a lower heat rejection capacity than originally planned and that the hot water production mode (i.e. heat pumps in heating mode) was more adversely affected. (Controls 2012)

During initial operation of the heat pump system, the return condenser water temperatures were often in excess of 100°F (design temperature was 85°F). The commissioning team recommended that the heat pumps operate in cooling mode as the normal sequence until further notice. The implications of this recommendation were that the WID had a year-round cooling load and therefore the system operating only in cooling would not impact overall operation. However, it was not understood what the impact would be to the long-term performance of the GHX (i.e. would only heat rejection lead to continually increasing ground temperatures).

The Cx report also indicated that the heat pumps appeared unstable and cycled as frequently as every 3 to 4 minutes. The details of the control sequence for the heat pumps was not documented or not reported to the Cx team. In addition, heat pumps had been shutting off occasionally due to refrigerant high-pressure cutout warnings (high condenser water temperatures). The heat pump internal software was subsequently updated which lowered the HP cycling time to 20 minute cycle times, on average. By the end of the Cx process, the team had not received more detailed sequences for the heat pump system. (Correspondence 2011)

By design, WID’s the chilled water system was directly connected to the campus chilled water distribution. Inherent in the design of WID’s hydronic system is a connection between

the chilled water side of the building's loop and the heating side of the building as well as the condenser water side of the heat pumps. Because the campus chilled water system operates at significantly higher system pressures (120 psi on the campus chilled water distribution, vs. 50 psi in the condenser/reheat water loop) there is a risk of leakage of chilled water to the heat rejection side of the hydronic system. During routine reheat coil maintenance in the fall of 2012, WID facility technicians discovered that the reheat system pressure had increased significantly, and the cause was pinpointed as leakage of higher pressure campus chilled water flowing through the valves intended to isolate chilled water from the condenser water system. Because the GCHP is only operating in cooling mode, valves that enable the GCHP system to operate in either cooling or heating mode were permanently blocked off. Following this change, the system pressures returned to normal and the leak problem was resolved. The long-term impact of the permanent isolation of these two loops is that the GCHP system will not be able to operate in heating mode unless other modifications are pursued (e.g. installation of valves that can hold against a higher operating pressure differential). The following chapter discusses the initial work that was done to understand the layout of the systems and to determine whether additional instrumentation would be required to meet the research objectives and to investigate the issues discussed in this section.

Chapter 3. Proposal and Installation of Additional Instrumentation

3.1 Introduction

There are on the order of 23,000 live data points in WID for building automation, equipment diagnostic, and energy monitoring purposes.[17] Given such a large array of data, coupled with the intent of the building designers to make the WID facility itself available for research (i.e. a "Living Lab"), one would naturally assume that all (or most) of the specific data required for the present research would come from sensors already in place. However, it was clear from post-construction documentation that several of the key variables being measured were not available from existing sensors. Preliminary inspection of the building equipment and the building data systems (i.e. recorded data) further revealed a gap in the required data sensors.

An overview of the research plan along with a preliminary report of the lack of data sensors was presented at an introductory meeting with members of the University of Wisconsin-Madison Facilities, Planning, & Management department (FP&M) and the WID building project team ("Green Team"). All agreed to participate in a feasibility study for installing additional sensors in order to collect the data required to support this research. Due to the complexity and size of the ground-coupled heat pump (GCHP) system, the feasibility study would first require a thorough physical inspection of the existing mechanical equipment and sensor instrumentation, along with a detailed overview of the research objectives. FP&M

[17] Running a "discovery" on all of the field controllers that were connected to the Intelligent Building Architecture system (IBA) turned up 22,554 points. A "point" is defined as any trended metric or collection of data. Some examples of data points are: A sensor reading (e.g. a zone temperature), a calculated value (e.g. energy rate measured by a BTU meter), or a setpoint value to be used in control logic. A collection of historical data for a particular metric is also considered one data point (i.e. collection of values for a particular metric over long periods of time; one history collection equals one data point).

Engineering developed a cost estimate for purchasing and installing the additional instrumentation. Full security access to WID mechanical equipment rooms was granted, along with read-only access to both of the primary building data systems. Discussed in this chapter, the proposal included: (1) A list of any additional sensors required to fulfill the research objectives, (2) the necessary accuracy required for the sensors, and (3) recommendations for the logical and physical locations of the sensors.

3.2 Sensor Guidelines

To ensure an appropriate level of data accuracy, the instrumentation used in the present research would necessarily be installed and calibrated according to the manufacturer's specifications. Because the WID heat pump system utilizes water as the working fluid on the evaporator and condensers, all sensors must be correspondingly compatible. An infrastructure for electronic data storage was available through the Building Automation System (BAS) and/or the Intelligent Building Architecture (IBA) system. Therefore, it was desirable that the requested instrumentation provide time-trended readings at configurable time steps to be stored electronically for historical trending purposes to be used for monthly and annual energy analysis. Measurement devices that provided only physical readouts (i.e. pressure gauges and thermometers without a computer connection) were limited for use only as a secondary source of data intended for diagnostics and sensor verification. Figure 3-1 shows examples of primary and secondary measurement instrumentation: a differential pressure meter with a signal transmitter (primary), and two glass thermometers that did not provide digital output (secondary).

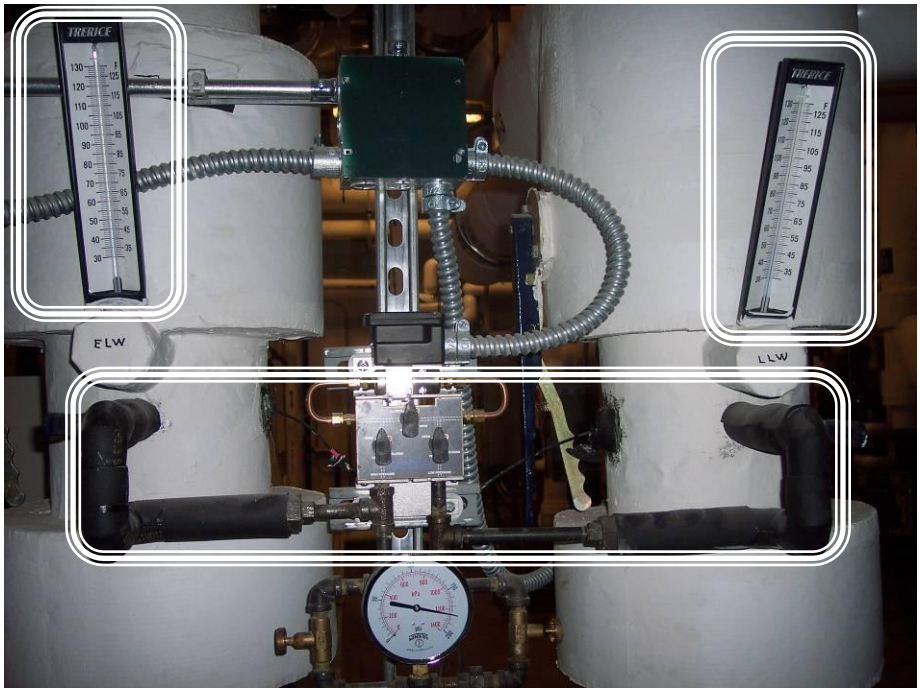

Figure 3-1 - Contrasted measurement devices: a differential pressure sensor (middle) that was eligible to be a primary data source and thermometers (sides) which were not.

The sensors chosen to be a primary source of data are independent of the equipment being studied. For example, data sensors on-board or directly integrated with larger subsystems (e.g. temperature sensors located internal to the HP units) will not be used for determining the equipment's operating capacity or efficiency, but used solely for independent data comparison. The desire to utilize independent sensors was several-fold. In order to ensure data accuracy, sensors must be available to be maintained or recalibrated without affecting internal operation of equipment. Any changes made to on-board sensors would most likely result in unnecessary downtime for the mechanical equipment. In the same vein, any equipment maintenance could similarly affect the on-board sensor readings, which would impact data collection. Finally, a separation from the instrumentation and equipment was

desirable to ensure that equipment internal logic or computer activity did not confound the sensor measurements. In the present research, sensors for temperature, differential pressure, and flow rate that were internal to the HP units were only considered as secondary data sources.

With the above guidelines in mind, sensors that were previously installed by the UW Direct Digital Controls group (DDC), for building automation and diagnostic purposes, were generally suitable for the data collection required by this research. Two examples of instrumentation that were installed prior to the research are shown in Figure 3-2. The instrumentation that was previously installed and utilized in the research is provided in Table 3-2. To determine the existence and location of instrumentation, contractor documentation was reviewed as discussed in the following section.

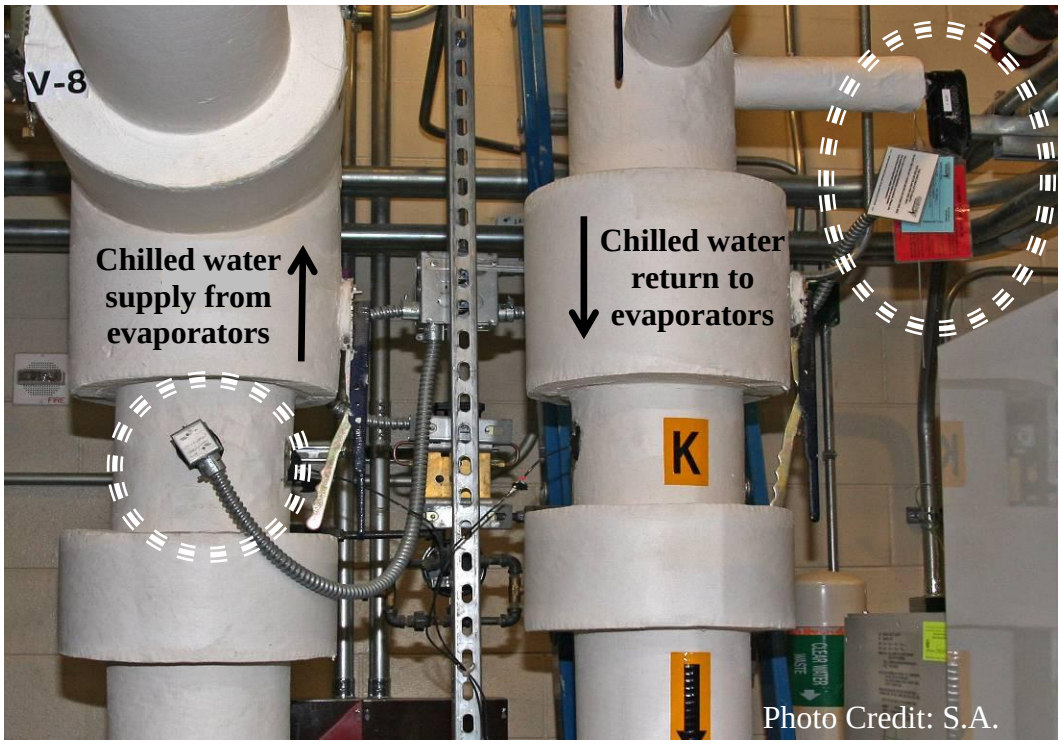

Figure 3-2 - Two examples of previously installed sensors that were suitable for use in this research are circled, a resistance temperature detector (left) and a volumetric flow meter (right).

3.3 Reviewing As-Built Documentation

From reviewing post-construction (i.e. "As-Commissioned") contractor documents, created by a team consisting of the controls contractor, the building commissioning team, and UW DDC, it became evident that additional instrumentation was needed to accomplish several key performance calculations. However, some conflicting information was observed between different versions of the documents and it was unclear whether the documentation was up-to-date and verified. The documents were used to guide the initial explorations of the system configuration and to predict a lack of sensor instrumentation.

For example, Figure 3-3 contains a clip of an As-Commissioned controls schematic. The heat pumps are represented by the Evaporator/Condenser box near the center and hydronic piping

extends outward to the hydronic pumps (labeled P7, P8, P12, and P11), modulating three-way valves (labeled V-1 and V-2), and a representative symbol of the geo-exchange field (labeled “Geothermal Well Field”). All other symbols are control sensors: temperature sensors (labeled LWT or EWT depending on orientation), flow meters (WFM-1 and WFM-2), and differential pressure sensors directly on either side of the HPs.

From the figure, it can be seen that there is no temperature sensor on the evaporator entering water (near label #1). Therefore, it would not be possible to measure the water temperature drop across the evaporators or, more importantly, the cooling capacity of the heat pumps. Similarly, it can be seen that no temperature sensor is present at the inlet of the HP condensers (near #2). A temperature sensor is at the outlet of the geo-exchange field (sensor GTES-LWT). However, mixing may occur by valve V-2 depending on the flow of condenser water. Therefore, the temperature difference across the condensers could not be measured, and subsequently the heat rejected from the condensers could not be quantified. Finally, it was not clear from the documentation if the electrical power consumed by the HPs was measured, which would make it impossible to measure the efficiency or attempt to close an energy balance.

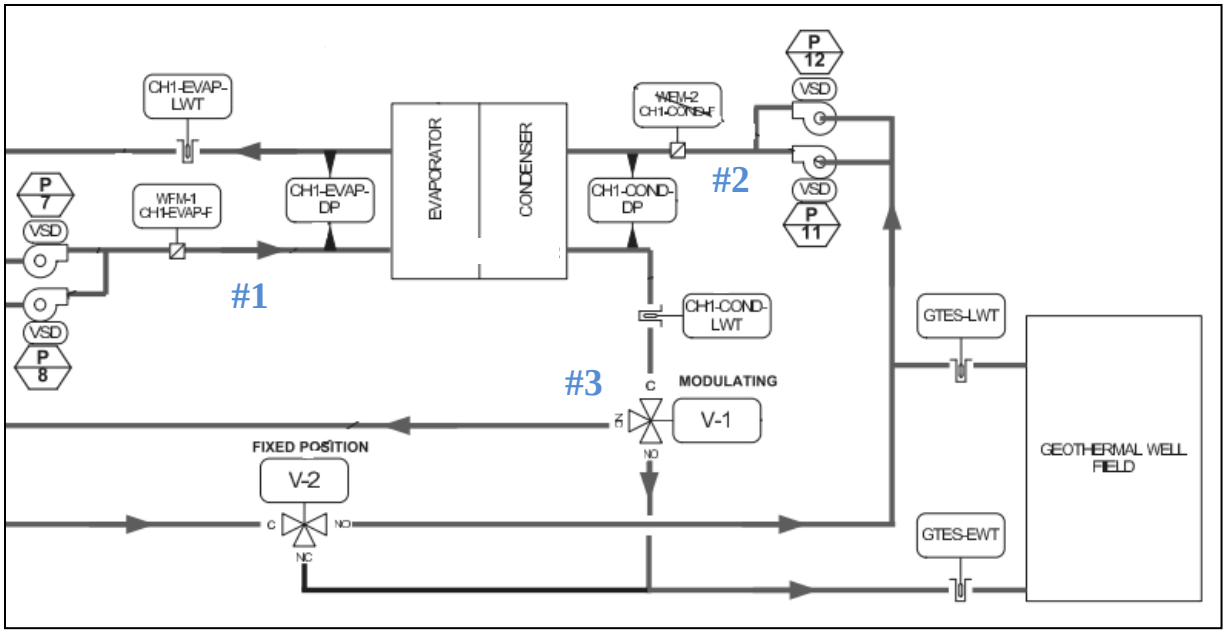

Figure 3-3 – Clip of a Control Schematic (numbering added by author as a guide to the discussion below)

Extending the inspection of Figure 3-3 further, the hydronic flow entering valve V-2 is returning from the reheat recovery loop (not shown in the figure). Only the summation of hydronic flow is measured at the condenser by flow meter WFM-2, and therefore individual flow rates within the reheat recovery loop and the geo field are unknown. The individual energy transfers to/from the reheat and geo-field sub-loops therefore could not be measured. As mentioned, these documents had yet to be verified and it was possible that changes to the equipment or instrumentation had been made during construction.

The above discussion does not detail all of the instrumentation gaps suggested by the contractor documentation, but serves as an example for the considerations taken into account in the following sections. Other sources for preliminary investigation regarding data instrumentation were the available data points within the building information systems themselves. However, the data systems did not reveal additional points beyond the control

documentation. The possibility of their being undocumented or disconnected instrumentation motivated a closer inspection of the equipment associated with the WID GCHP system.

3.4 Inventory of Devices

An inventory of all mechanical equipment, hydronic pipe layout, and data sensors related to the WID GCHP was collected. A majority of the equipment of interest to the present research was located in the WID basement mechanical equipment room and the penthouse mechanical floor of the building. A majority of the hydronic piping was thermally insulated, but otherwise in plain sight within the mechanical equipment rooms.

Figure 3-4 – Hydronic piping with the heat pump units displayed at the center

Spaces above ceilings were accessed as needed in order to confirm equipment or piping details. In some instances, it was not possible to physically access equipment or

instrumentation such as in the “chases” that ran piping between building floors. In the circumstances where equipment could not be physically accessed, it was assumed those locations did not contain instrumentation or relevant equipment other than the piping. Various documents created by the mechanical contractors were relied upon to understand the pipe path and connections in the inaccessible areas.

Equipment connected to the system via electrical connections were also investigated and included in the inventory. The electrical power monitors that were used for power consumption measurements of the heat pumps and hydronic pumps, and the variable speed drives of the hydronic pumps, were located. Finally, BTU meters (i.e. computer devices that measure hydronic energy transfer and related metrics) were located and their connections to individual instrumentation were confirmed.

The actual locations of devices were compared to the contractor drawings, and in some cases clarifications or corrections of the contractor documentation were necessary. For example, Figure 3-5 and Figure 3-6 demonstrate the difference between the contractor documentation to the physical location for the geo-field return temperature sensor (“GTES-LWT”). In Figure 3-5, it would appear possible to measure the temperature difference across the entire geo-exchange field. In actuality, the supply and return for the “Campus Drive” geo-field sub-loop was separate from the common manifold for the other three sub-loops. From Figure 3-6, we can see that the Campus Drive loop flow stream (and therefore the temperature) could not be sensed by GTES-LWT. A more detailed schematic was necessary to accurately display the configuration, as shown in Figure 3-7.

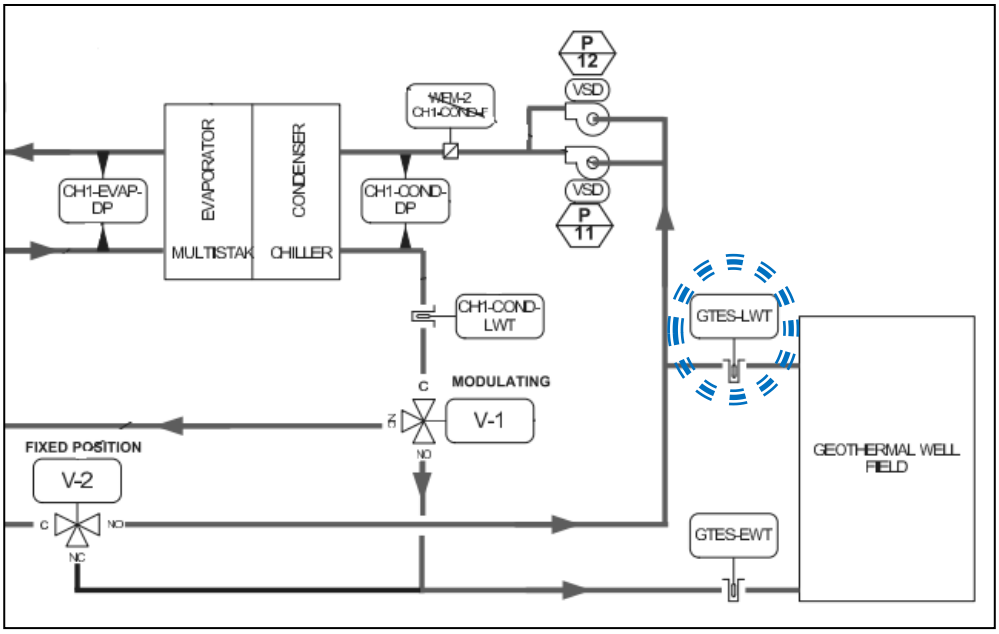

Figure 3-5 - Contractor Schematic with geo-field return temperature sensor "GTES-LWT"

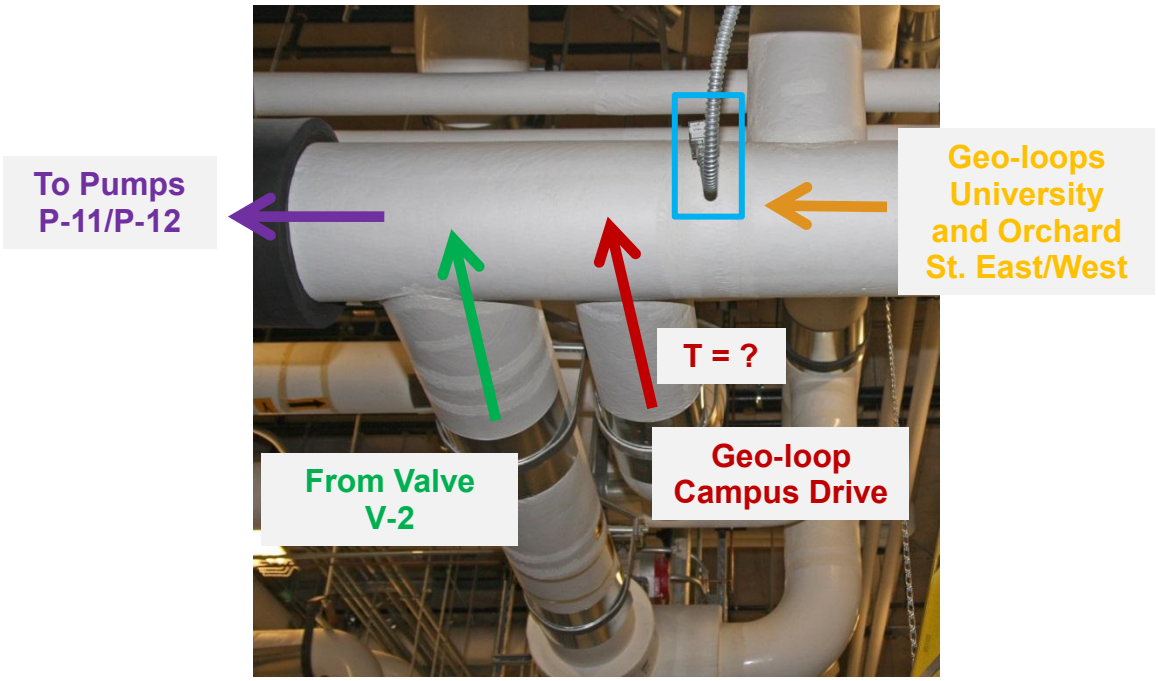

Figure 3-6 – Actual configuration near GTES-LWT (indicated with a box)

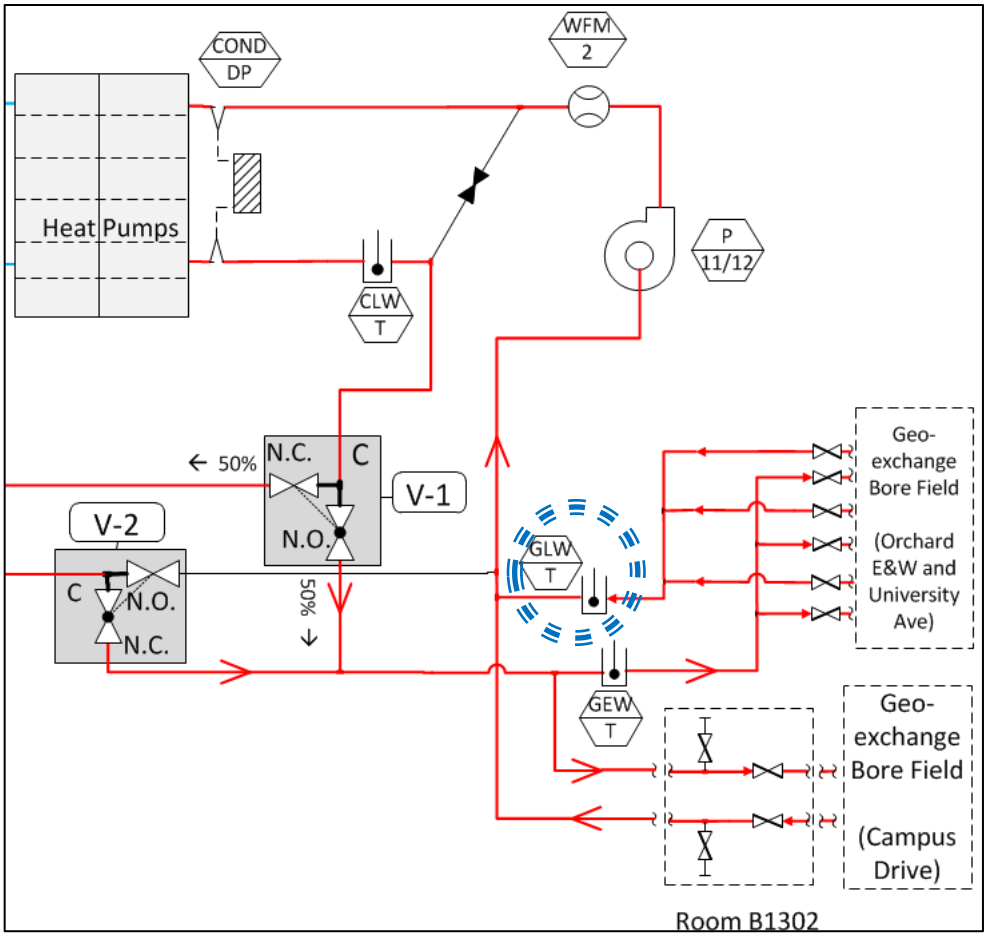

Figure 3-7 – Snippet of updated schematic with GTES-LWT (now labeled GLW-T) circled

As illustrated, temperature sensor GLW-T was located such that it could not measure the temperature of one of the four geo-field sub-loops. Due to space limitations and the installed piping layout, there was not a more favorable location for the GLW-T sensor and additional instrumentation would be needed to verify and accurately measure the geo-field bulk leaving water temperature.

All additional instrumentation requested for the present research is listed in Section 3.6. Comparing contractor documentation to the actual system indicated that more detailed and updated schematics of the system were not only desirable, but necessary to understand the

system operations and available instrumentation/equipment. All equipment and instrumentation related to the WID GCHP that was discovered during the inventory discussed in this section is provided in Figure 3-8 and Figure 3-9.[18]

[18] Due to the number of details in the system, all WID contractor drawings were created to be printed on D-size sheets. Condensed versions of the system drawings created by the author are provided herein for legibility. D-size drawings were created and provided to the WID staff for future use.

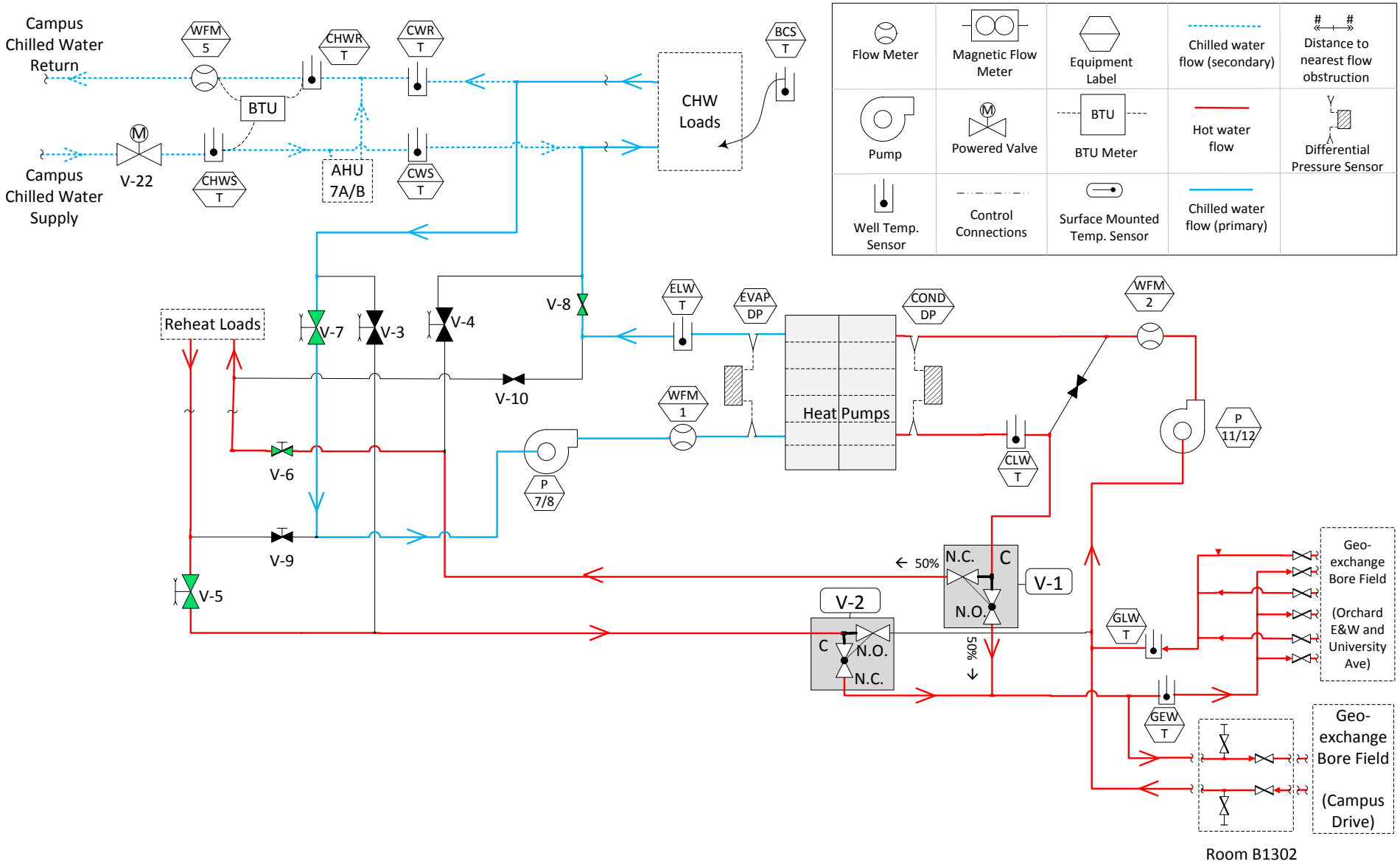

Figure 3-8 –Schematic of the WID GCHP System As-Built at the initiation of the present research

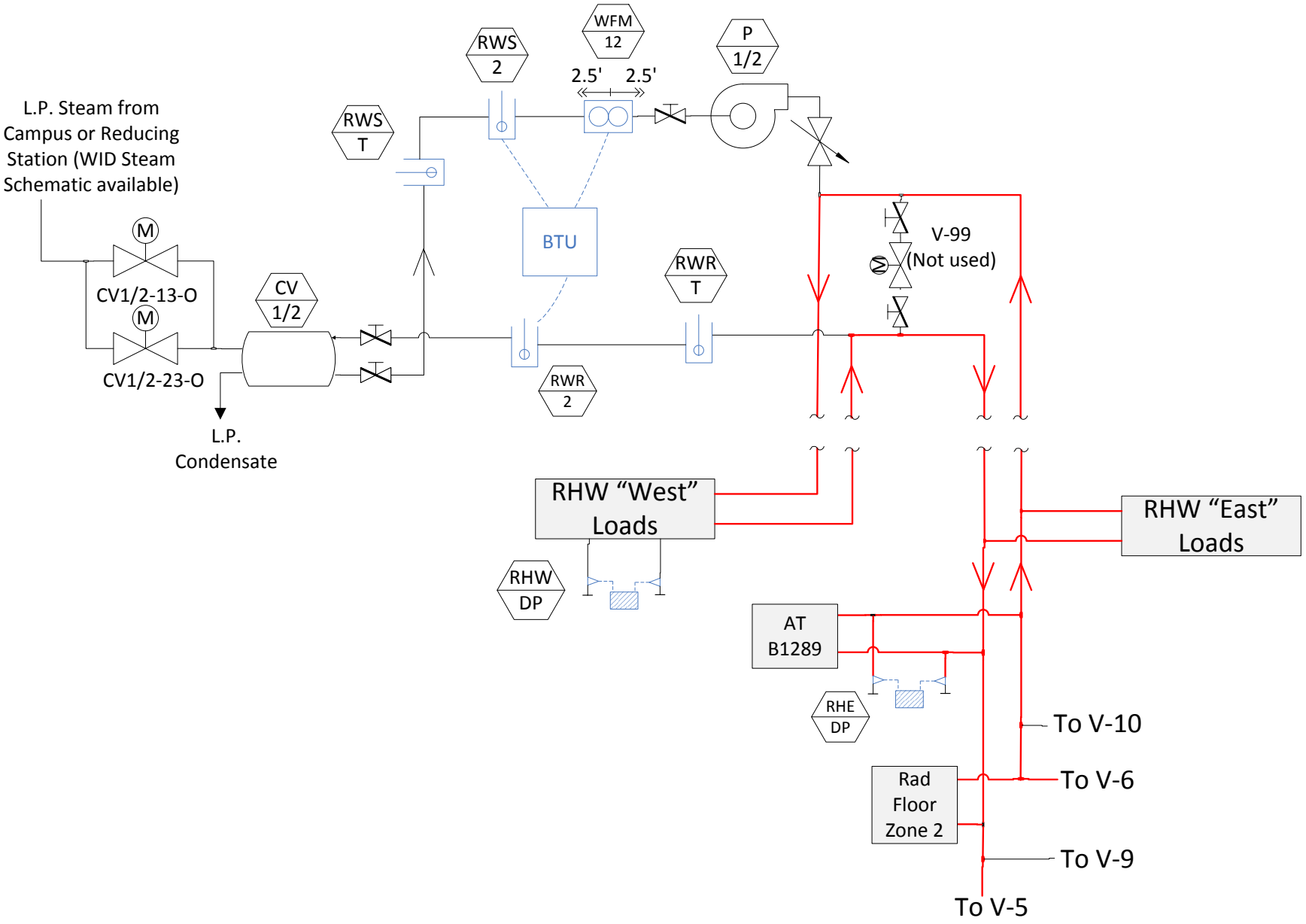

Figure 3-9 - As-Built Schematic of the Penthouse Reheat Loop

3.5 Accuracy Requirements for the Requested Instrumentation

The accuracy requirements for additional instrumentation were back-calculated based on specified accuracies for key measurements. The primary measurements of interest were the hydronic energy flows to/from the heat pumps and the condenser heat rejection loops. Target accuracy requirements for key measurements were based on AHRI Standard 330, which requires that the cooling capacity and efficiency of the heat pumps be calculated to within ±5% uncertainty. (AHRI 1998)

As introduced in Section 3.3, Figure 3-3, it was observed that the water temperature returning to the HP evaporators was not measured. To measure the cooling capacity of the heat pumps the volumetric flow rate of chilled water through the HP evaporators would be measured by a flow meter (WFM-1), installed prior to the present research, with a manufacturer-listed accuracy of ±2% (reading).[19] The uncertainty of the measured cooling capacity, with the heat pumps operating at design conditions, was propagated in EES for various evaporator water temperature measurement uncertainties. Figure 3-10 shows the propagated uncertainty of the cooling capacity measurement with increasing uncertainty of the evaporator water temperature rise and the increasing uncertainty of the supply/return evaporator water temperature sensors on the lower and upper abscissae, respectively. The cooling capacity would be measured at ±5% uncertainty if the accuracy of the water temperature drop across

[19] It was known early in the present research that the location of flow meter WFM-1 was not within manufacturer installation specifications. The additional error encountered due to the proximity of an upstream pipe elbow was not determined until the sensor verification work discussed in Chapter 4.

the evaporators was measured at or within ±0.61°F.[20] Therefore, the accuracy of the supply and return evaporator water temperature sensors were then required to be at or within ±0.43°F.

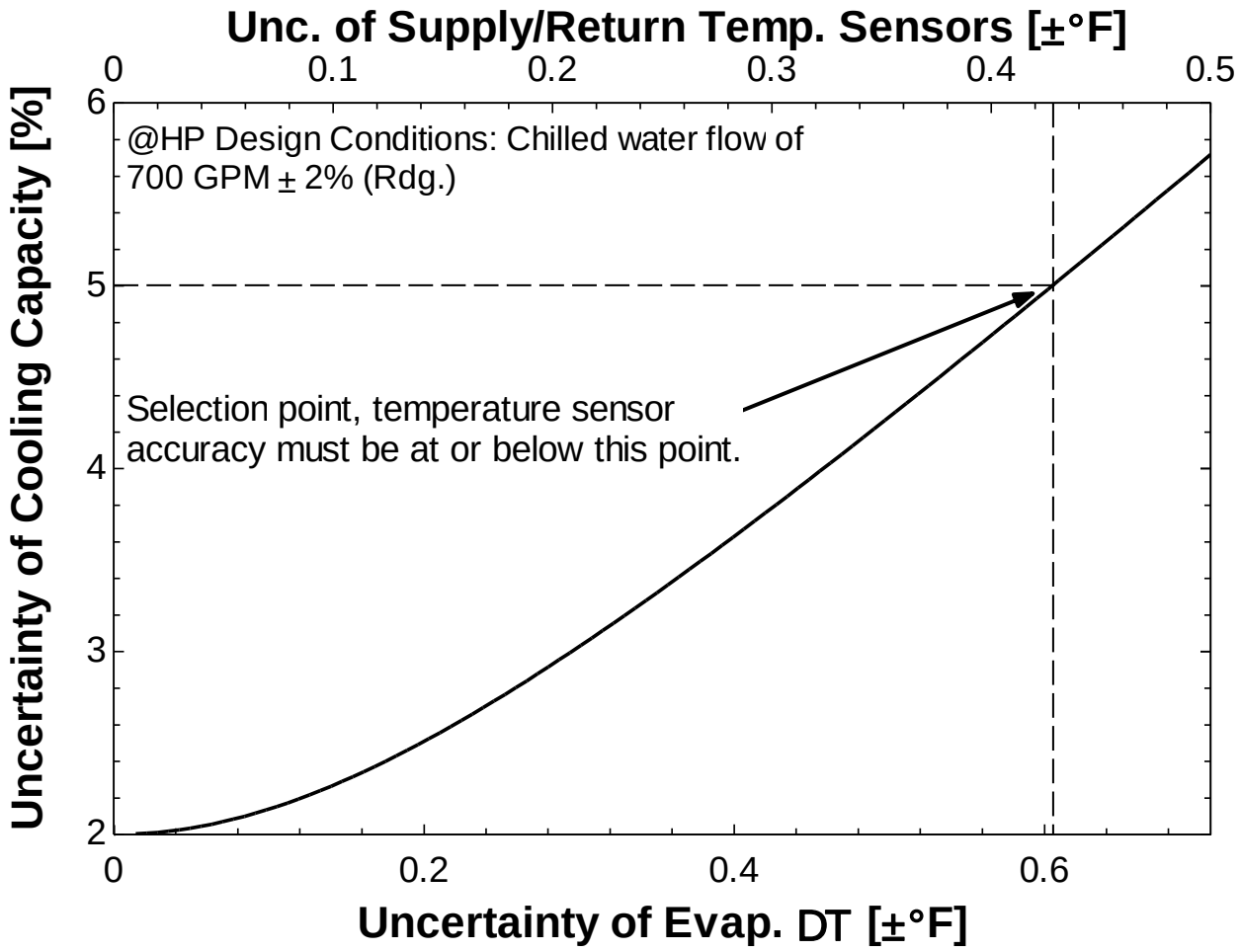

Figure 3-10 – Propagated uncertainty plot showing the required accuracy of the HP evap water temp sensors

[20] The equations used to calculate the HP cooling capacity and uncertainty can be found in Appendix A. Design conditions of the chilled water side of the heat pumps, from the heat pump equipment submittal document, were: leaving chilled water temperature of 44°F, return chilled water temperature of 57.2°F, chilled water flow rate of 700 GPM, and electrical power input of 342.3 kW.

Temperature sensor ELW-T, installed at the evaporator water outlet prior to the present research, met the accuracy requirement with a manufacturer-listed accuracy of ±0.35°F at 70°F. Therefore, a sensor of equal accuracy would be appropriate to measure the water temperature returning to the evaporator. A similar calculation methodology as above showed that evaporator water temperature measurements at ±0.35°F allowed the COP of the heat pumps to be measured at or within the ±5% target accuracy.

While selecting additional instrumentation, the accuracies of previously installed instrumentation were assumed to be at the manufacturer-listed accuracies. A more thorough verification of instrumentation was conducted following the installation of all required sensors for the present research, and is discussed in Chapter 4.

3.6 Proposal for Additional Instrumentation

A proposal for the instrumentation necessary for the present research was presented to FP&M and the WID staff. Two lists were compiled: one of the sensors that were requested to be purchased and installed (provided in Table 3-1), and a second of the sensors that were already available and would be used in the research (Table 3-2). Each list included a description of the instrumentation and recommended accuracy. The recommended physical location of each of the sensors listed in Table 3-1 were marked within the WID mechanical equipment room. The recommended logical locations of the requested (new) sensors were added to the As-Built schematic, shown in Figure 3-11.

Short Name	Description	Recommended Accuracy
CEW-T	HP Condenser-side Entering Temp	±0.35°F at 70°F
EEW-T	HP Evaporator-side Entering Temp	±0.35°F at 70°F
WHS-T	Reheat Supply Temperature	±0.35°F at 70°F
WHR-T	Reheat Return Temperature	±0.35°F at 70°F
GUR-1	Return Temp, Geo Loop 1	±0.35°F at 70°F
GER-2	Return Temp, Geo Loop 2	±0.35°F at 70°F
GWR-3	Return Temp, Geo Loop 3	±0.35°F at 70°F
GCR-4	Return Temp, Geo Loop 4	±0.35°F at 70°F
DPT-1	Diff. Pressure Transmitter, Geo Loop 1	±1% (Reading)
DPT-2	Diff. Pressure Transmitter, Geo Loop 2	±1% (Reading)
DPT-3	Diff. Pressure Transmitter, Geo Loop 3	±1% (Reading)
DPT-4	Diff. Pressure Transmitter, Geo Loop 4	±1% (Reading)
WFM-13	Return Reheat Volumetric Flow Rate	±1% (Reading)
WFM-14	Total Geofield Volumetric Flow Rate	±1% (Reading)
SMT-1	Surface Temp Sensor, Condenser In	±0.1% at 32°F (0°C)
SMT-2	Surface Temp Sensor, Condenser Out	±0.1% at 32°F (0°C)

Table 3-1 - Instrumentation/Monitoring Points Requested to be Installed

Short Name	Description	Listed Accuracy
WFM-1	HP Evaporator Flow Meter	±2% (reading)
WFM-2	HP Condenser Flow Meter	±2% (reading)
WFM-5	Campus CHW Flow Meter	±2% (reading)
WFM-12	Campus Reheat Flow Meter (*not functional*)	±0.20% (reading)
CLW-T	HP Condenser-side Leaving Temp	±0.35°F at 70°F
ELW-T	HP Evaporator-side Leaving Temp	±0.35°F at 70°F
CWS-T	Campus CHW Supply Temp	±0.35°F at 70°F
CWR-T	Campus CHW Return Temp	±0.35°F at 70°F
RWS-T	Campus RHW Supply Temp	±0.35°F at 70°F
RWR-T	Campus RHW Return Temp	±0.35°F at 70°F
V-1	Supply/Geo Modulating Valve Position	-
V-2	Return/Geo Modulating Valve Position	-
V-21	Pump-21 Valve Position	-
V-22	Campus CHW Supply Valve Position	-
P-21	Campus CHW Pump VFD Signal	-
P-1	Reheat Pump VFD Signal	-
P-2	Reheat Pump VFD Signal	-
P-7	HP Evaporator-side Pump VFD Signal	-
P-8	HP Evaporator-side Pump VFD Signal	-
P-11	HP Condenser-side Pump VFD Signal	-
P-12	HP Condenser-side Pump VFD Signal	-
T-3	In-Line CHW Return Temp	±0.35°F at 70°F
T-2	In-Line CHW Supply Temp	±0.35°F at 70°F
GEW-T	Partial Geo-field Entering Temperature	±0.35°F at 70°F
GLW-T	Partial Geo-field Leaving Temperature	±0.35°F at 70°F
CHW-DP	Penthouse CHW Differential Pressure	±0.25%
RHW-DP	Reheat Differential Pressure	±0.25%
EVAP-DP	HP Evaporator-side Differential Pressure	±0.25%
COND-DP	HP Condenser-side Differential Pressure	±0.25%
WFM-6	Additional CHW Flow Meter	±2% (reading)
WFM-7	Additional CHW Flow Meter	±2% (reading)
WFM-8	Additional CHW Flow Meter	±2% (reading)
WFM-9	Additional CHW Flow Meter	±2% (reading)
WFM-10	Additional CHW Flow Meter	±2% (reading)
WFM-11	Additional CHW Flow Meter	±2% (reading)
HP Capacity	Multistack Capacity Output Signal	-
CV1-13-O	Campus Reheat Steam Valve Position	-
CV2-13-O	Campus Reheat Steam Valve Position	-
CV1-23-O	Campus Reheat Steam Valve Position	-
CV2-23-O	Campus Reheat Steam Valve Position	-

Table 3-2 - Instrumentation/Monitoring Points Available and Required

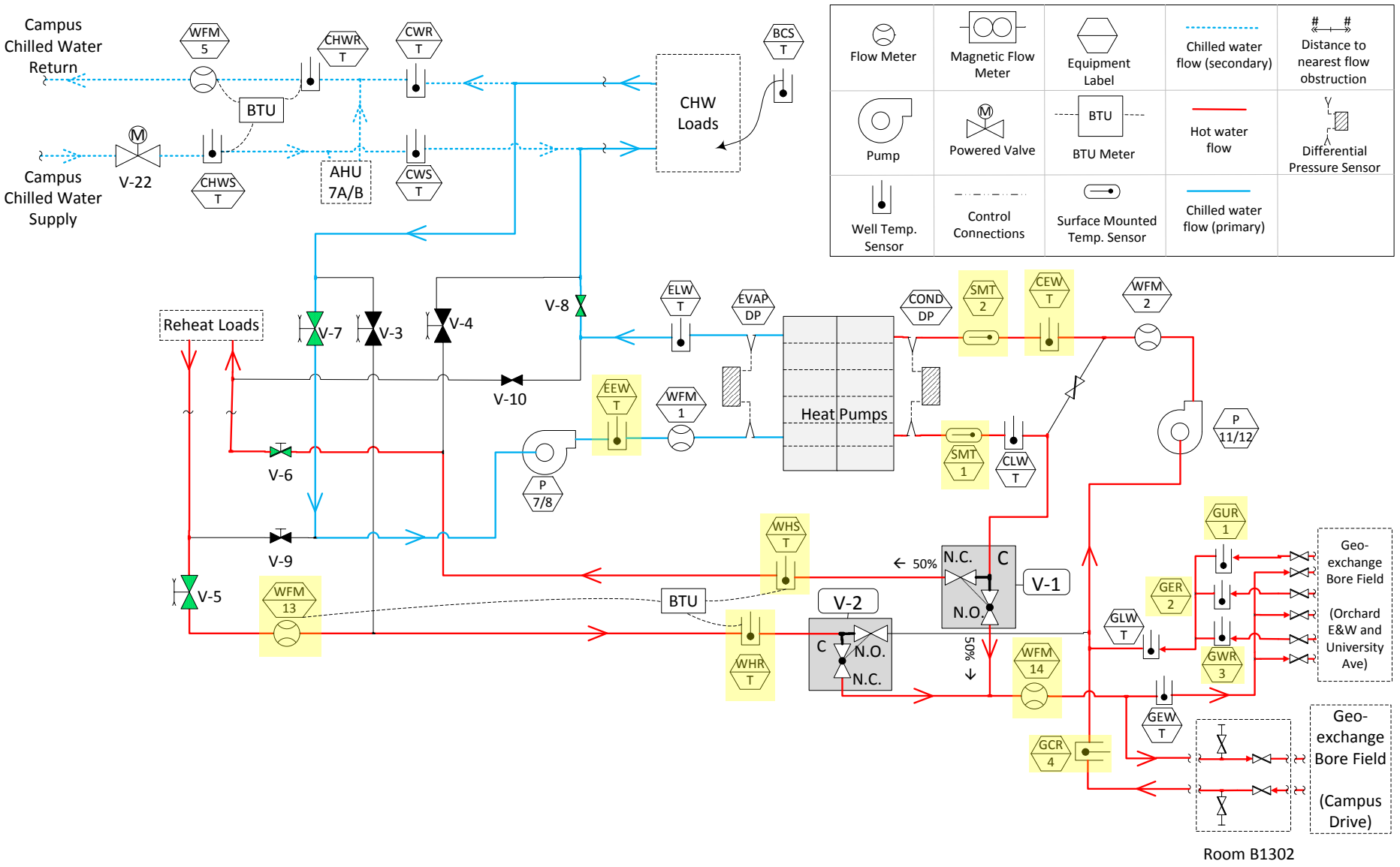

Figure 3-11 – As-Built System schematic, requested (new) sensors are highlighted.

3.7 Cost Estimate and Implementation of Additional (Requested) Sensors

A team of engineers from FP&M reviewed the proposal for additional instrumentation and verified that the proposal was accurate during a walk-through of the WID mechanical rooms. FP&M agreed to purchase and install the requested instrumentation and estimated the cost of the project to be $18,600. Figure 3-12 shows the estimated cost breakdown for the project. The WID project lead met with WARF and secured the funding for the project.

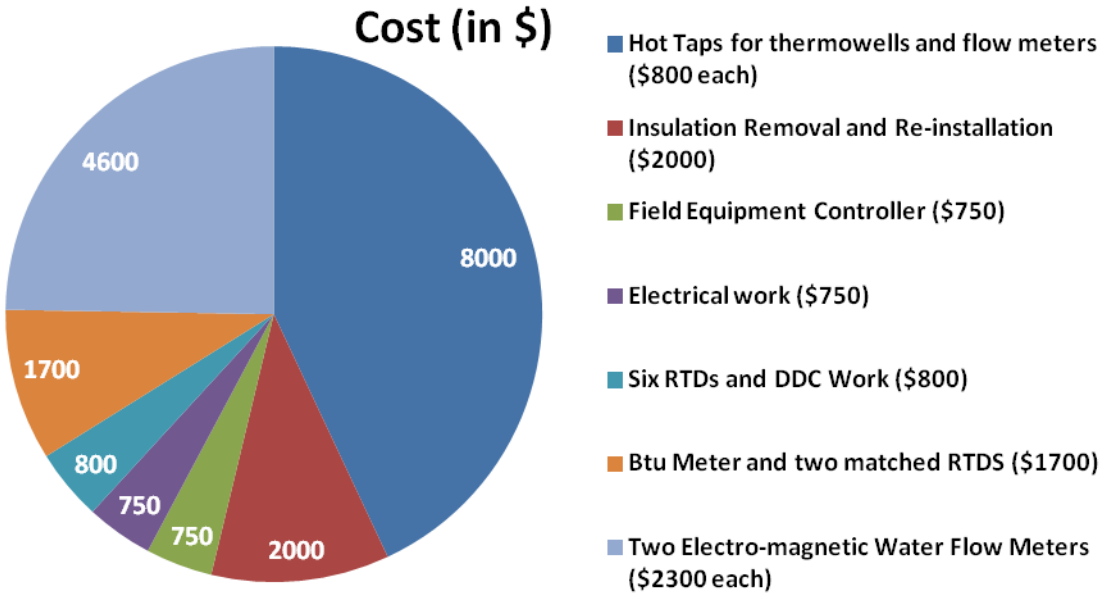

Figure 3-12 - Cost estimate breakdown of project to install additional instrumentation for WID GCHP analysis

Following the cost estimate, FP&M made several recommendations to the original proposal. From their experience, FP&M did not recommend purchasing and installing differential pressure transmitters on the geo-field sub loops. The differential pressure sensors were expensive and typically of low quality and dependability. The sensors were part of the original proposal in an effort to infer the hydronic flow rate through each of the geo-field

sub-loops. Based on FP&M's recommendations, the differential pressure sensors were removed from the proposal.

Sensor calibration was not part of FP&M's installation processes for typical building instrumentation. Furthermore, FP&M did not provide a quote for the cost of calibrating the new instrumentation, but stated that the cost would be outside of the agreed upon quote and funding. Therefore, the necessity for calibration was determined during post-installation verification. Purchasing and installation of the requested instrumentation began in March 2012 and concluded mid-June. The following chapter discusses the work performed to verify and calibrate (if necessary) the original and added instrumentation.

Chapter 4. Instrumentation Verification

4.1 Introduction

Following the installation of additional temperature and flow sensors, all measurement devices related to the research were verified with both independent test techniques and data comparisons where applicable. Depending on the operating conditions of the system, situations existed where redundant temperature and flow rate measurements were available for direct comparison to assess sensor agreement. Field-verification steps were performed to ensure that the instrumentation was installed appropriately and that each physical sensor corresponded to the data point trended in the IBA and BAS data systems. Independent sensor verification tests consisted of using an ultrasonic flow meter to verify the measurements of the field-installed water flow meters; and room temperature water bath tests were conducted as a means of verifying the field-installed temperature sensors. Finally, the corrected/calibrated sensor measurements were further verified using “mass balance” and “energy balance” checks.

The sensor corrections defined in this chapter were applied to the measured data used for the analyses in the remainder of the present research. Therefore, it was crucial to document the verification steps performed and the resulting sensor corrections. Of the temperature and flow sensors that were deemed critical to the present research, only the penthouse reheat water flow meter (WFM-12) could not be verified due to a faulty electronics board on the

BTU meter that the WFM-12 was attached to.[21] Diagrams are provided in the following sections as needed. However, a schematic of all critical instrumentation and equipment for the present research can be found in Figure 4-1 and Figure 4-2.

[21] FP&M worked with the manufacturer to repair the faulty BTU meter, but it was not repaired before the research was concluded. The water flow rate through the reheat loop while in Mode 1A (reheat with campus steam) could not be measured.

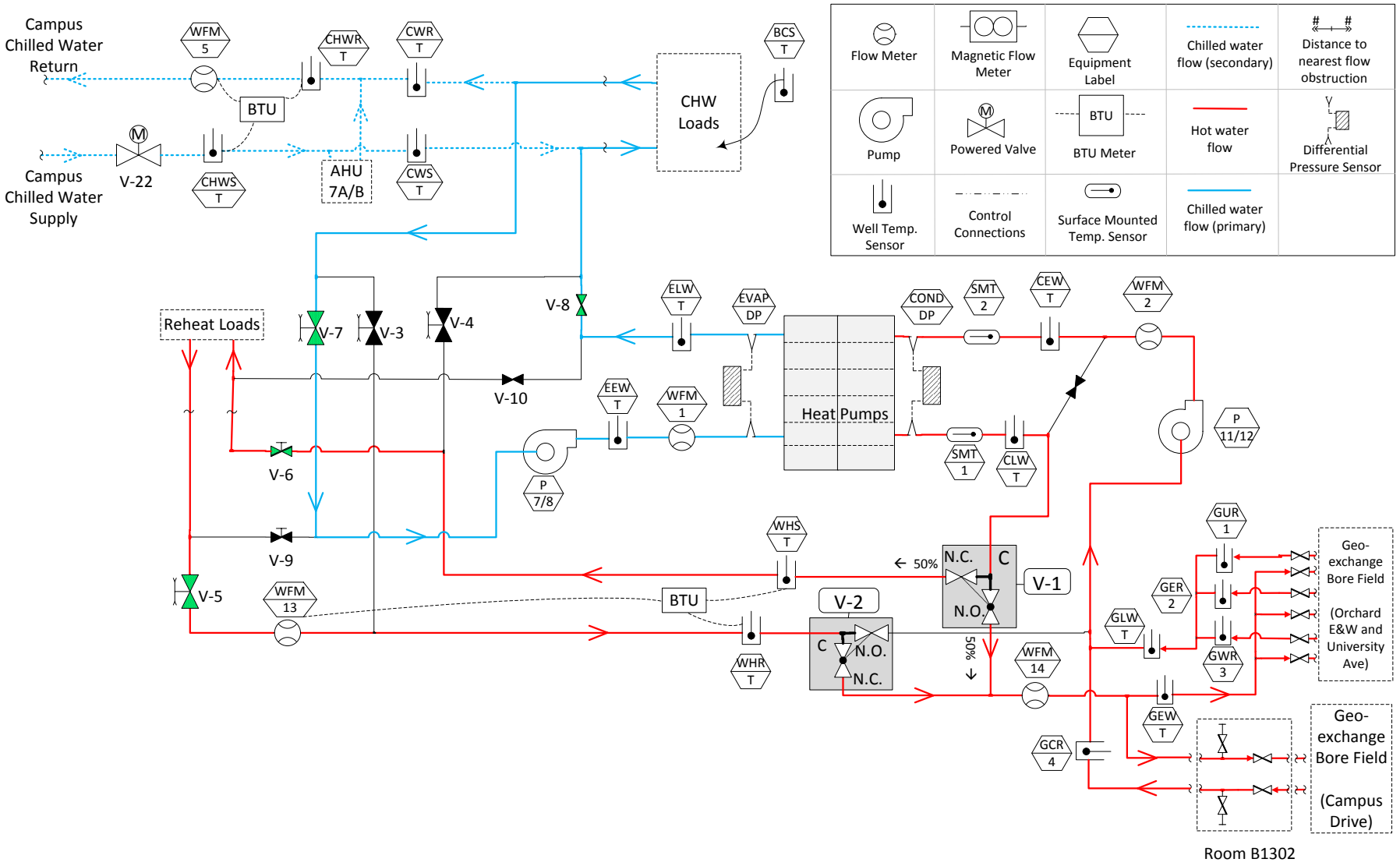

Figure 4-1 – GCHP system schematic, operating in "cooling with heat recovery" mode with critical sensors

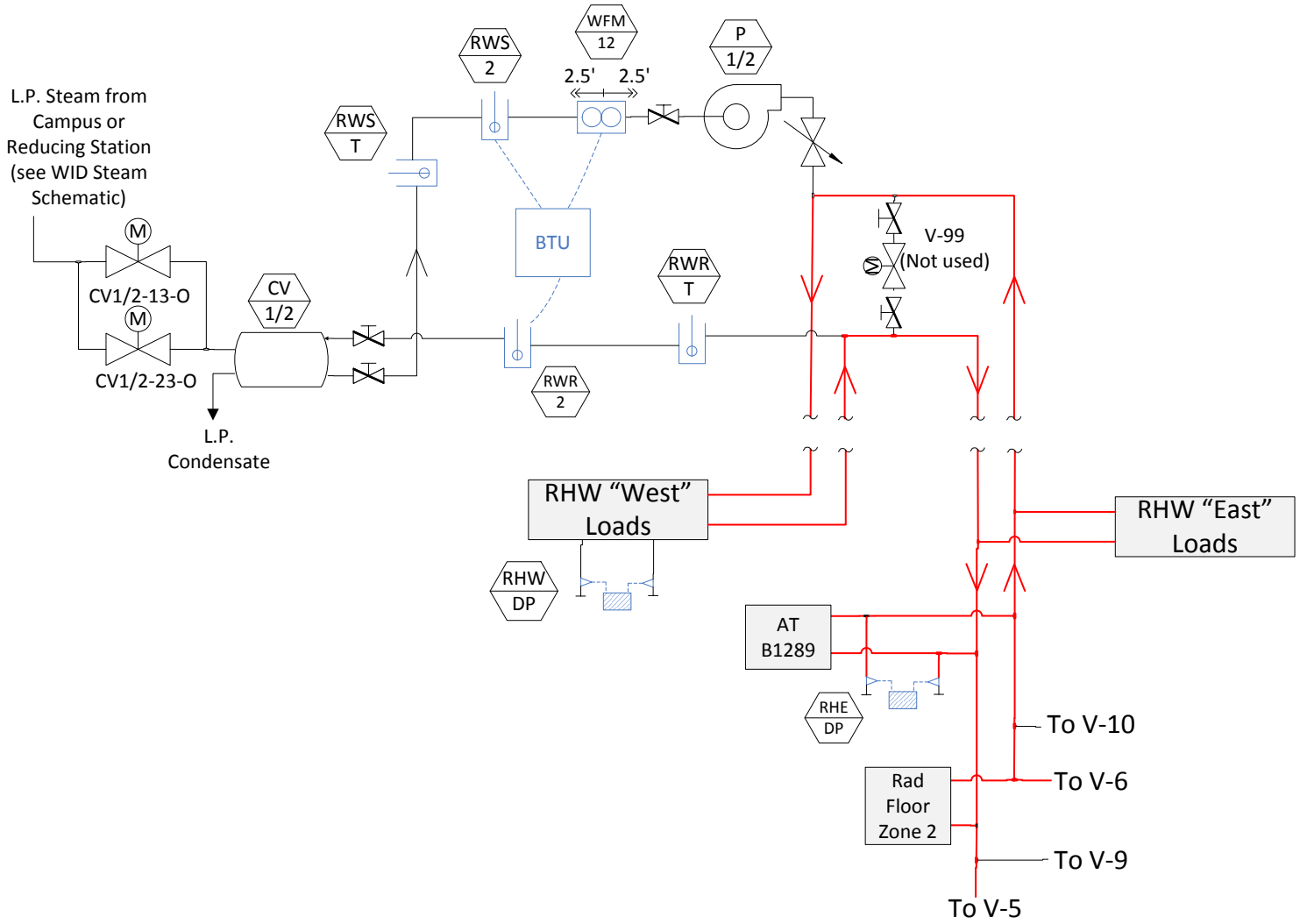

Figure 4-2 - Penthouse Reheat System layout, shown as operating with reheat supplied by GCHP system

4.2 Comparing and Calibrating Temperature Sensors

4.2.1 Single-Point Calibration Method

Due to budget and time limitations, FP&M did not field calibrate the temperature sensors following the installation process. The sensor manufacturers provided calibration information. However, there were several reasons a sensor could drift after installation, such as the use of a longer lead wire to connect the sensor to the communication bus or damage to the sensor during shipment/installation. The critical sensors for this research were investigated to determine if any corrections were needed.

It was assumed that any temperature sensor corrections required would be accommodated by a single-point calibration technique. Single-point calibrations were proposed as acceptable for this research for two reasons. First, more exacting calibration profiles (e.g. two-point or polynomial functions) are most useful for temperature conditions that vary widely for a given sensor span. In typical operation of the heat pump system, the ranges of likely temperature conditions at each sensor location were small compared to the span of the sensors. For example, from July 2012 to October 2012 the water temperature conditions at the heat pump condenser inlet remained within a 27°F range (91°F to 118°F) while the sensor manufacturer's nominal temperature range was 190°F (32°F to 158°F).

One possible caveat to single-point calibrations was that, due to the multiple modes of operation of the system, the sensors that monitored chilled water temperatures while the system was in cooling mode would necessarily monitor hot water temperatures while in heating mode, and vice versa. For example, while in cooling mode, the condenser entering

water temperature sensor (CEW-T) monitored relatively hot water returning from the geo-field or reheat loop back to the HP condenser. While in heating mode, CEW-T would monitor relatively cold water returning from the geo-field to the HP evaporator (i.e. the evaporator and condenser effectively trade places between the two modes). In scenarios where a single temperature sensor monitored two ranges of temperatures, it is conceivable that the single-point sensor correction at the higher, condenser water temperatures may not be suitable for the sensor at lower, evaporator water temperatures.[22] The range of temperatures available for confirming the sensor calibrations were dictated by the conditions produced by the system while in cooling mode, discussed further in the section that follows.

Additionally, the Building Automation System (BAS) only allowed for single-point (i.e. constant) sensor corrections through the building control infrastructure. Though it was possible to correct temperature data post-data collection with more sophisticated calibration profiles, it would be desirable to enable temperature corrections at the source of the data, within the BAS system, in order to make available more accurate temperature readings for system controls and for future research groups at the WID.

4.2.2 Directly Comparing Temperature Data

Temperature sensors were verified and calibrated by comparing multiple, independent sensors where appropriate comparisons could be made. System operating conditions existed where multiple temperature sensors were in-line for a particular hydronic flow. Therefore the sensor measurements were effectively redundant and could be directly compared.

[22] It was not possible to test the accuracy of sensor calibrations in the heat pump heating operating mode.

Necessarily, a reference temperature sensor was chosen to compare or adjust the other coincident sensors. Ideally, agreement amongst several temperature sensors would provide the reference temperature used for calibrating.

Where available, temperature sensors connected to a BTU meter were used as reference temperature sensors. The temperature sensors connected to a BTU meter were factory calibrated using a two-point calibration and each BTU temperature sensor came with a slope and temperature offset to be programmed into the BTU meter computer after installation. Additionally, the BTU temperature sensors had higher manufacturer-listed measurement accuracy compared to the other temperature sensors in the system (±0.2°F and ±0.35°F, respectively). BTU meters are indicated in Figure 4-1 and their respective temperature sensors were: WHS-T, WHR-T, CHWS-T, and CHWR-T.

To illustrate the methods used to compare and calibrate temperature sensor data, Figure 4-3 shows that sensor GEW-T was located in the same hydronic flow as temperature sensors WHS-T, CLW-T, and SMT-1 whenever valve V-1 was in its normally-open position (splits the flow) and valve V-2 was in normally open (sends all flow from recovered-to-reheat loop directly back to the heat pump condensers). Data at ten minute intervals were collected for the "GEW-T Group" of sensors (GEW-T, WHS-T, CLW-T, and SMT-1) while valve V-1 and V-2 were in their normally open positions. Assuming that the piping insulation adequately prevented ambient heat transfer in the piping segments between the sensors, indicated sensor readings should agree within their measurement uncertainties and could be adjusted until agreement was made. No time synchronization was necessary to directly

compare sensor measurements as the hydronic flow rate was sufficiently large and pipe distances between coincident sensors were sufficiently small.[23] The unadjusted (i.e. raw) data are provided in graphical form in Figure 4-4.

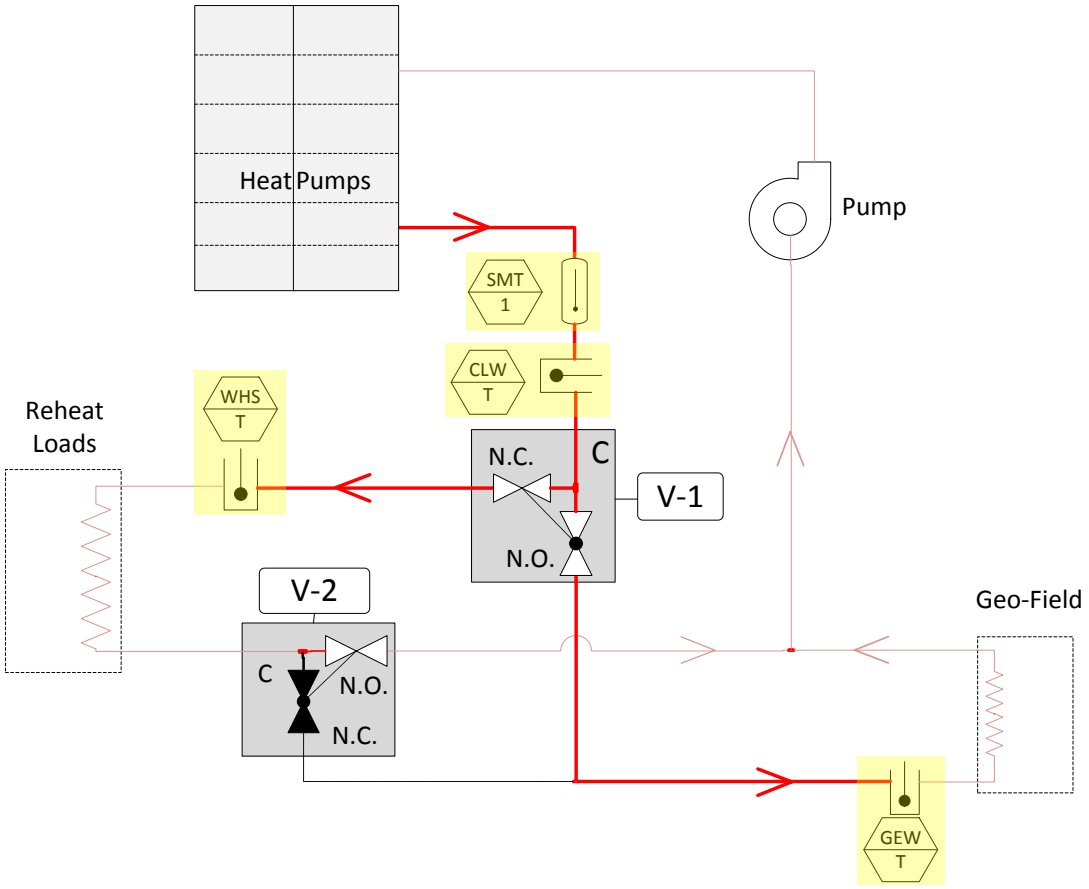

Figure 4-3 - Coincident Temp. Sensors to GEW-T, sensors used for comparison are highlighted.

[23] Except for sensor BCS-T and the penthouse sensors shown in , all research temperature sensors were located in the WID mechanical equipment room. No direct comparisons were made between sensors more than 20 feet of pipe length apart. At an average flow rate of 500 GPM and a pipe diameter of 8 inches, the travel time between sensors would be around 6 seconds.

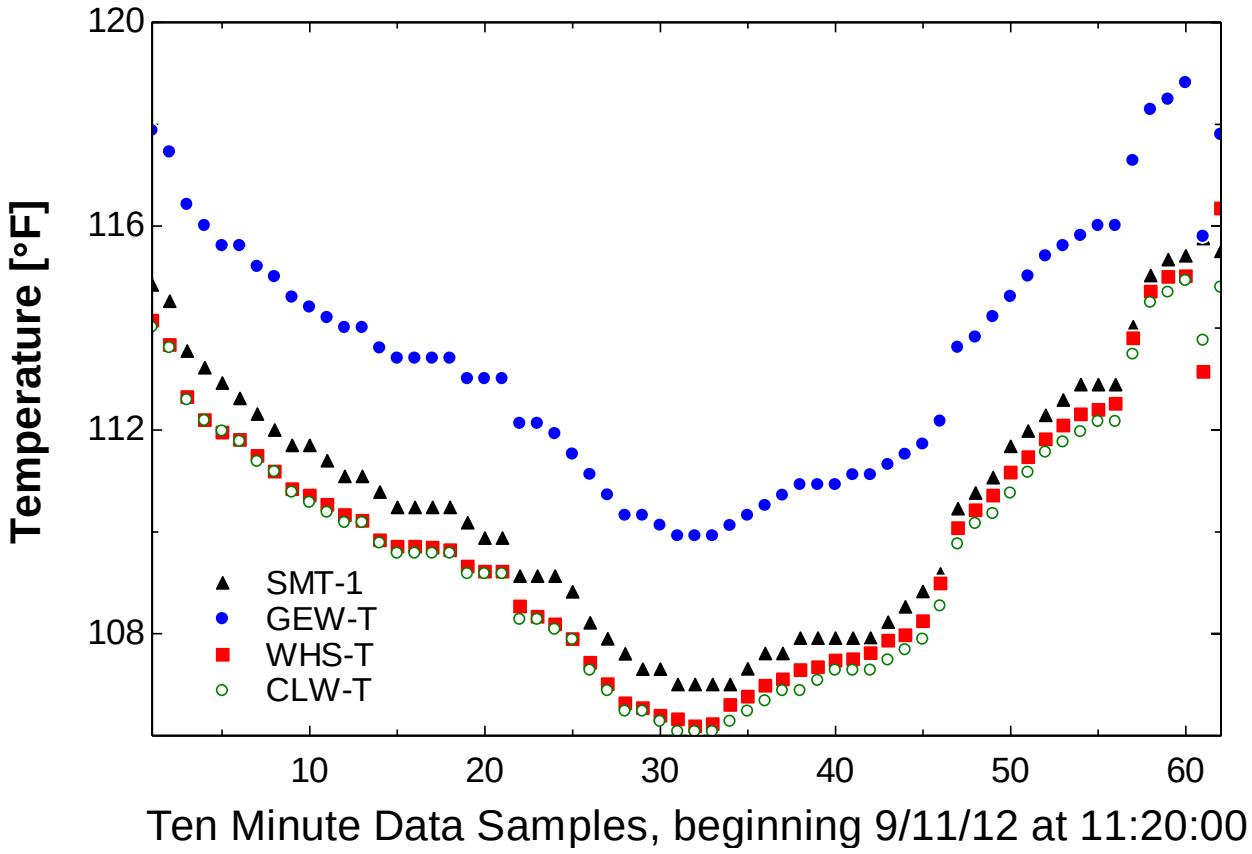

Figure 4-4 – Raw temperature data from the GEW-T Group sensors.

The single-point offset correction for a sensor was calculated by averaging the difference between the sensor's temperature readings and the readings from a designated reference sensor, using:

$$Offset = \frac{\sum_i \left(T_{ref,i} - T_{x,i}\right)}{N} \quad \textbf{(4-1)}$$

where i represents a data point used in the calculation,

N is the number of data points,

T_{ref} is the reference temperature sensor reading in °F,

and T_x is the temperature reading in °F from the temperature sensor to be verified.

For the GEW-T Group of sensors, WHS-T was chosen as the most appropriate reference sensor because it was connected to a BTU meter (i.e. was factory-calibrated and had a higher rated accuracy). Using sensor WHS-T as the reference sensor in Eq. (4-1), raw temperature data (i.e. without any temperature corrections) for sensors GEW-T, CLW-T, and SMT-1 were used to calculate the necessary offset corrections for those sensors, as shown in Table 4-1. The average absolute temperature differences between the corrected sensors and WHS-T were calculated to test the accuracy of the calculated offset corrections (shown in column four of Table 4-1). For each case, the temperature difference was less than the magnitude of the sensor's measurement uncertainty, 0.22°F and ±0.35°F respectively; therefore the temperature corrections were considered acceptable. The closeness of fit (denoted with R^2) to the reference measurements was calculated for each sensor. The procedure to calculate R^2 is provided in Appendix B.

Sensor Name	**Offset [°F]**	**Ref. Sensor**	**Avg. Abs. ΔT (Ref. - Sensor)[°F]**	**R^2 of Corrected Value [%] (62 data points compared)**
GEW-T	-3.6	WHS-T	0.14	99.19
SMT-1	-0.7	WHS-T	0.22	97.9
CLW-T	+0.1*	WHS-T	0.17	98.43
WHS-T	N/A	N/A	N/A	N/A

Table 4-1 – Calculated Temperature Offsets and Standard Errors for GEW-T Group of Sensors

* The offset calculated for CLW-T was smaller than the sensor's measurement uncertainty, and therefore was not used.

The largest correction value was for sensor GEW-T, with a calculated offset of 3.6°F (negative).[24] The relatively high calculated offset for GEW-T motivated further inquiries. It was considered possible that steam-heated reheat water was leaking through the normally closed leg of valve V-2 and mixing with the water flow that entered the geo-field, causing higher measured temperatures at GEW-T. However, temperature information at sensor WHR-T revealed that the average return-from-reheat temperatures were 105°F (as compared to the 114°F average temperature sensed by GEW-T as shown in Figure 4-4). Therefore, it was not possible that a leak was causing GEW-T to read 3.6°F higher than the other comparable sensors.

All temperature sensors intended for use in the research were investigated similarly as discussed for the GEW-T Group of sensors above. A network of the sensors used for data comparisons is shown in Figure 4-5, where the factory-calibrated (reference) sensors are in bold and the arrows indicate the direction that data were passed to inform the calibrations (e.g. the calibration for sensor CWR-T was informed by comparing it's temperature data with that of sensor CHWR-T).

[24] The correction calculated for GEW-T by comparing temperature data was in close agreement with room temperature thermometer tests, discussed in Section 4.2.4.

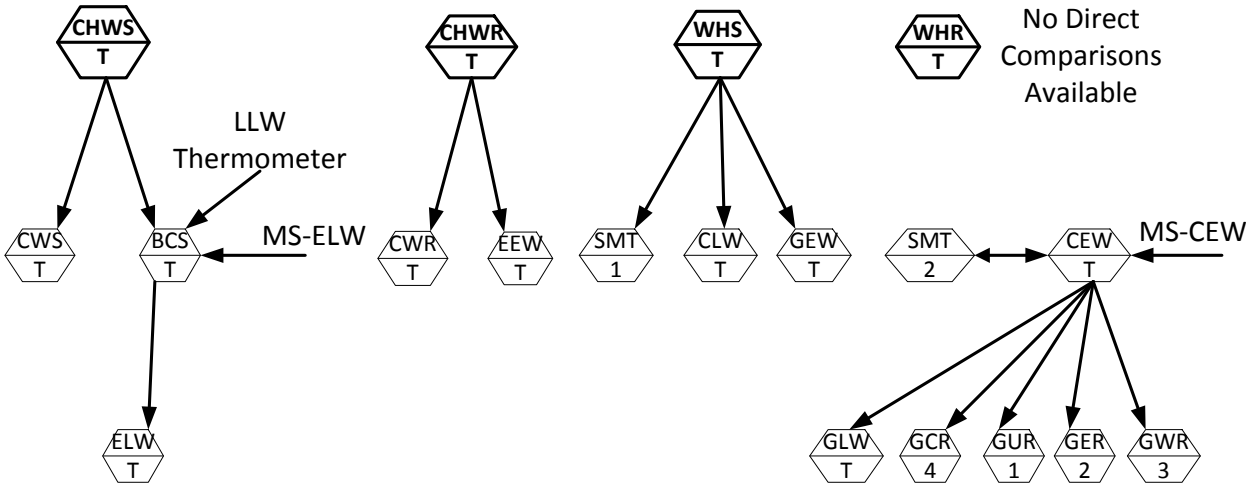

Figure 4-5 - Comparison network for temperature sensors

Of the available temperature sensors, the condenser water inlet sensor (CEW-T) was the only sensor that could not be directly compared to another RTD of higher or equal accuracy or quality. Surface mounted temperature sensors monitoring the water temperature on the heat pump condenser inlet and built-in glass thermometers were available for comparing the temperature measured by CEW-T (refer to Appendix C). Because the reheat return and geo-field return water were mixed before crossing CEW-T, the temperatures measured by WHR-T and GLW-T could be used to verify that CEW-T remained bounded by the two sensors (shown in Figure 4-6).

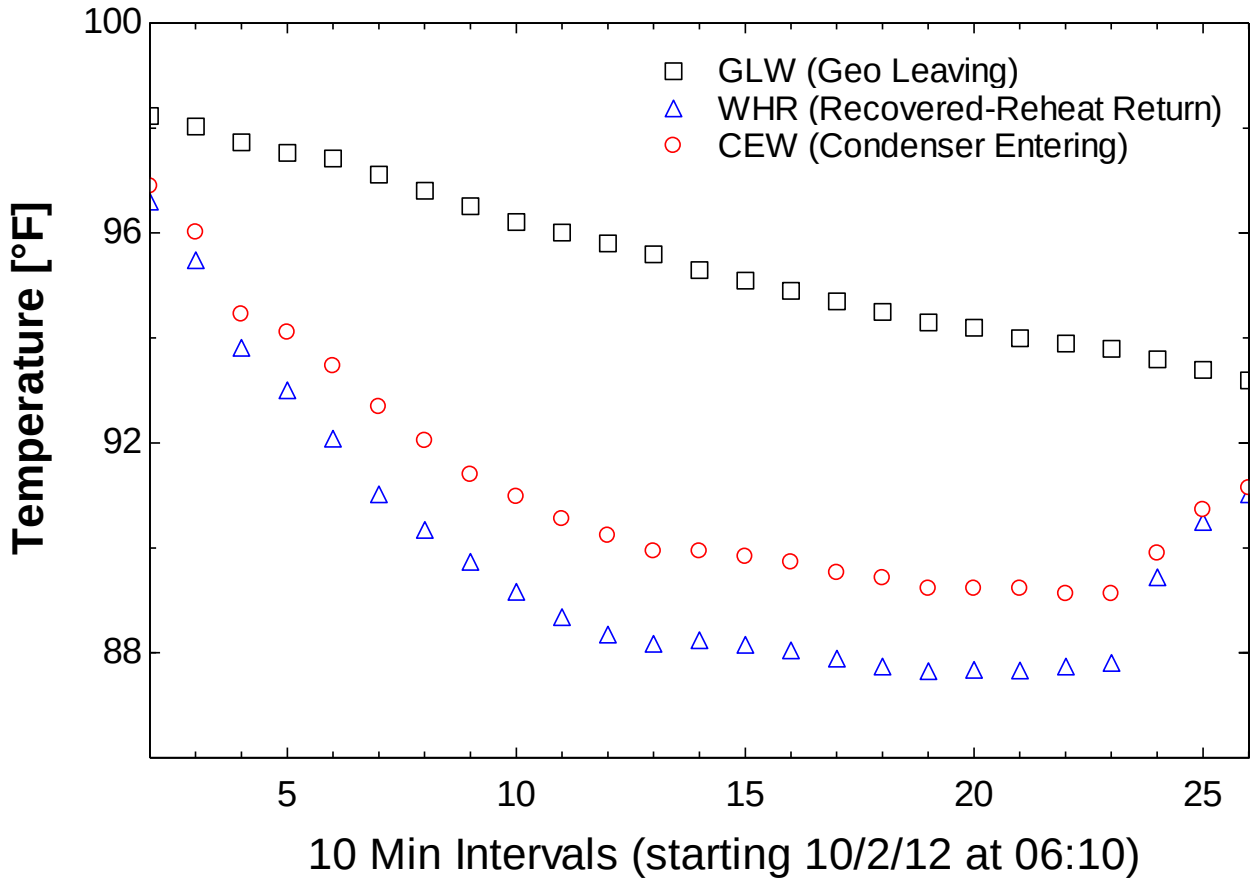

Figure 4-6 - The reheat return (WHR) and geo-field return temps (GLW) were used to verify CEW-T fell between.

Comparative data used for all temperature sensor calibrations are provided graphically in Appendix C. The results of the sensor comparisons, including the calculated offsets to be used for single-point calibrations, as well as the closeness of fit (R^2) between the calibrated sensor measurement and its reference sensor, are included in Table 4-2. In addition, the results of the field-verification tests for each sensor (discussed in Section 4.2.4) are included in the table. All temperature sensors listed in Table 4-2.

Sensor	Calculated Offset [°F]	Reference Sensor	Temp Range of Comparison [°F]	Time of Data Comparison	# of Data points	R^2 [%]	*Field Offset [°F]
BCS-T	+0.1	CHWS-T	39 – 42	9/5/12 03:20	16	68	+0.6
CEW-T	0	SMT-2	89 – 97	10/2/2012 06:10	29	99.2	-1
CHWS-T	F.C.	N/A	N/A	N/A	N/A	N/A	†
CHWR-T	F.C.	N/A	N/A	N/A	N/A	N/A	†
CLW-T	+0.1	WHS-T	106 – 115	9/11/12 03:00	62	98.4	+0.5
CWR-T	-1.3	CHWR-T	49 – 55	8/15/12 00:00	121	99.6	†
CWS-T	-1.7	CHWS-T	41 – 42	9/5/12 03:20	16	92.3	+0.25
EEW-T	-1.7	CHWR-T	49 – 55	8/15/12 00:00	121	98.9	-0.25
ELW-T	+0.6	BCS-T	44 – 47	9/24/12 01:00	16	66	+0.5
GEW-T	-3.6	WHS-T	106 – 115	9/11/12 03:00	62	99	-3
GLW-T	-2.5	CEW-T	~82	1/16/13 13:40	-	-	0
GUR-1-T	-2.5	CEW-T	~82	1/16/13 14:03	-	-	-1
GER-2-T	-3	CEW-T	80 – 85	1/16/13 13:55	-	-	-0.5
GWR-3-T	-0.5	CEW-T	80 – 82	1/16/13 13:47	-	-	-0.5
GCR-4-T	-1	CEW-T	82 – 84	1/16/13 13:10	-	-	-0.75
SMT-1	-0.7	WHS-T	106 – 115	9/11/12 03:00	62	97.9	-2.5
SMT-2	0	CEW-T	89 – 97	10/2/2012 06:10	29	99.2	-0.5
WHS-T	F.C.	N/A	N/A	N/A	N/A	N/A	-0.5
WHR-T	F.C.	N/A	N/A	N/A	N/A	N/A	+0.25

Table 4-2 – Offsets applied to critical temperature sensors.

* Field offset column values are from the tests discussed in Section 4.2.4.
† Was not possible to field-verify the sensor due to physical access limitations.
F.C. indicates the sensor was factory calibrated.

For the remainder of the research, temperature corrections were made post-data collection, meaning that the offsets were not incorporated into the BAS. Rather, all temperature corrections were applied to the logged data as part of a routine Q/A process. The necessary sensor adjustments were reported to the DDC group for their consideration to incorporate into building controls at the conclusion of the research. The temperature corrections defined in this section were verified by comparing measured energy rates through system components (i.e. “energy balances” discussed in Section 4.4).

4.2.3 EEW-T Installation Issue Identified from Sensor Data Comparisons

Using a similar procedure as outlined in Sections 4.2.2, comparisons of temperature data for sensor EEW-T and other related sensors revealed issues with the sensor's physical installation. It was determined that sensor EEW-T was not fully inserted in its thermowell and, coupled by the fact that the pipe area surrounding the sensor had not yet been insulated, large disparities were observed when compared with independent temperature sensors. Only one RTD was available by which to compare sensor EEW-T.[25] In order to have a third reference for comparison, temperature readings from a glass thermometer installed prior to this project directly in the evaporator inlet pipe were manually recorded every two minutes. Temperature data for sensor EEW-T consistently indicated higher than other comparable temperature sensors by nearly 10°F and did not follow the same trend as the other sensor readings (Figure 4-7).

[25] MS-EEW-T: the only comparable digital temperature sensor to EEW-T. It was located internal to the heat pumps at the evaporator inlet.

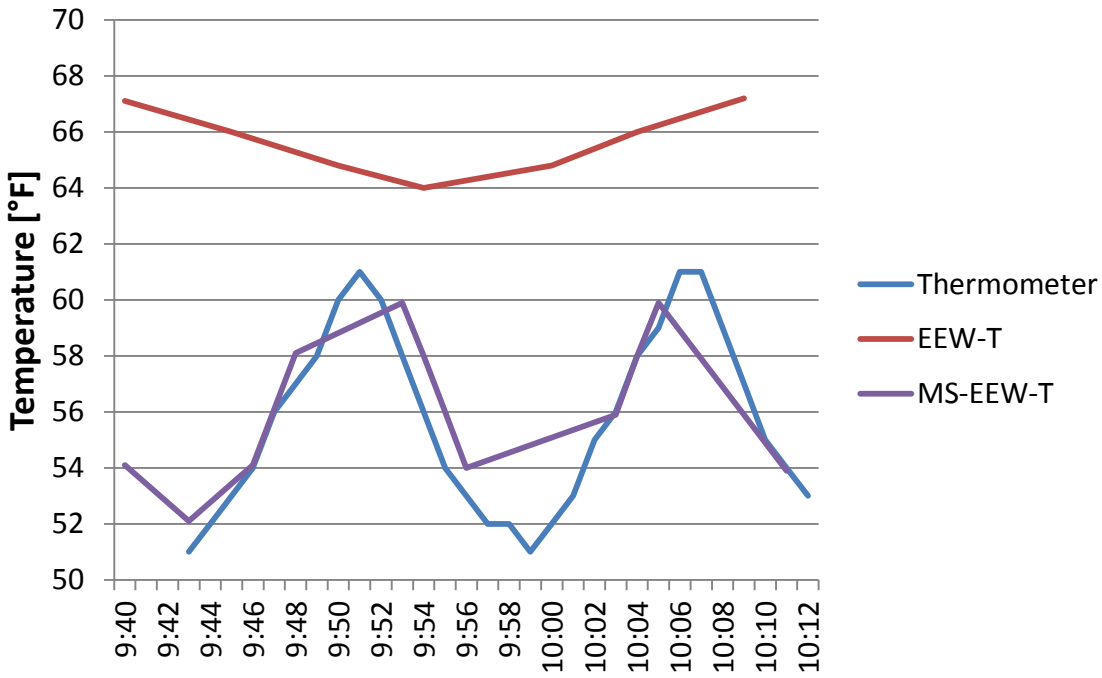

Figure 4-7 – Temperature comparisons for EEW-T

Due to such large disagreement between EEW-T and other comparable temperature sensors, an additional test was conducted to substantiate the error of the EEW-T sensor. The EEW-T sensor was removed from the pipe and submerged in a bath maintained at room temperature. Surprisingly, EEW-T temperature data read accurately, indicating a temperature difference of only 0.2°F (as compared to a thermometer in the water bath). The EEW-T sensor was then installed back in its original location in the pipe. The surrounding pipe area and sensor mounting were insulated by FP&M near the end of July 2012, and little change was seen regarding the temperature difference (error) between EEW-T and the other sensors.

The mounting structure of the sensor was investigated, which consisted of: the weldolet added to the pipe during the "hot tap" installation procedure and a threaded fitting, an adapter

bushing, a second bushing with a set-screw to secure the sensor, and finally the sensor casing which holds the sensor sheath and wiring (Figure 4-8). Because the thermowell was inside of the pipe and could not be examined externally, it was difficult to determine the extent that the sensor was inserted fully into the thermowell. The second bushing was removed from the sensor mount to allow more clearance for inserting the sensor. The sensor sheath was re-inserted into the adapter until it was clear that the tip of the sensor probe reached the end of the thermowell.

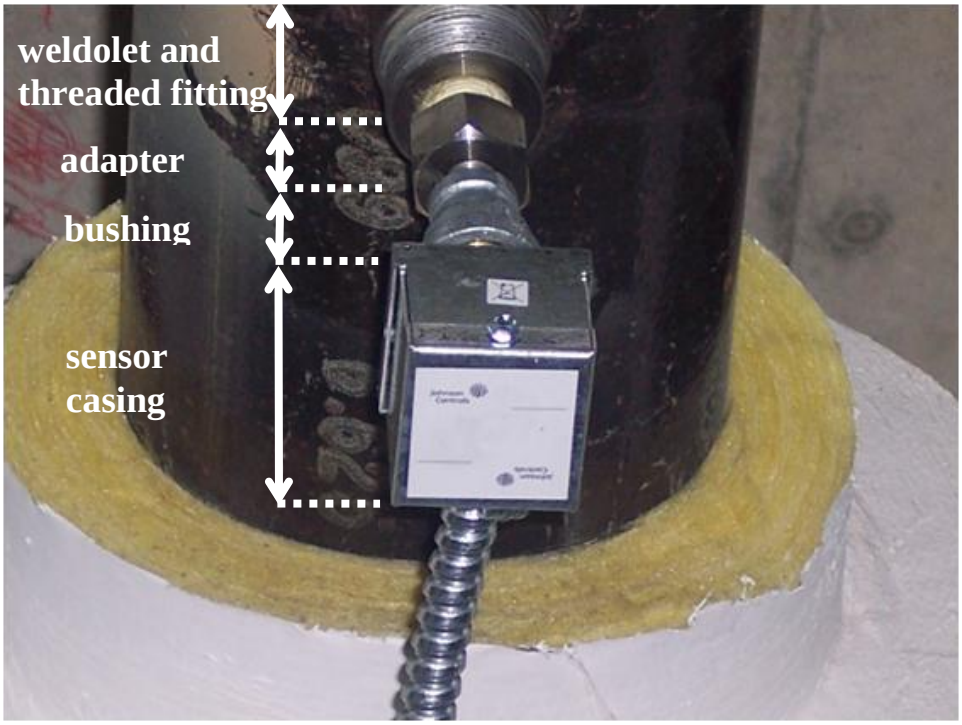

Figure 4-8 – Sensor EEW-T and surrounding pipe area.

As shown in Figure 4-9, data recorded before and after this time period clearly indicated that the full insertion of the sensor probe reduced the disparities between EEW-T and MS-EEW-T. The average difference between the sensors decreased from an average of 8°F to an average of 2°F. Sensor EEW-T was left installed without the second bushing to maintain data recording accuracy. FP&M was notified of the issue with the original sensor installation and

was to modify the mounting structure to ensure the sensor remains fully submerged in the thermowell and secured appropriately. The result of this test instigated similar field-verification "sanity checks" to be conducted for all temperature sensors involved in the research and is the subject of the following section.

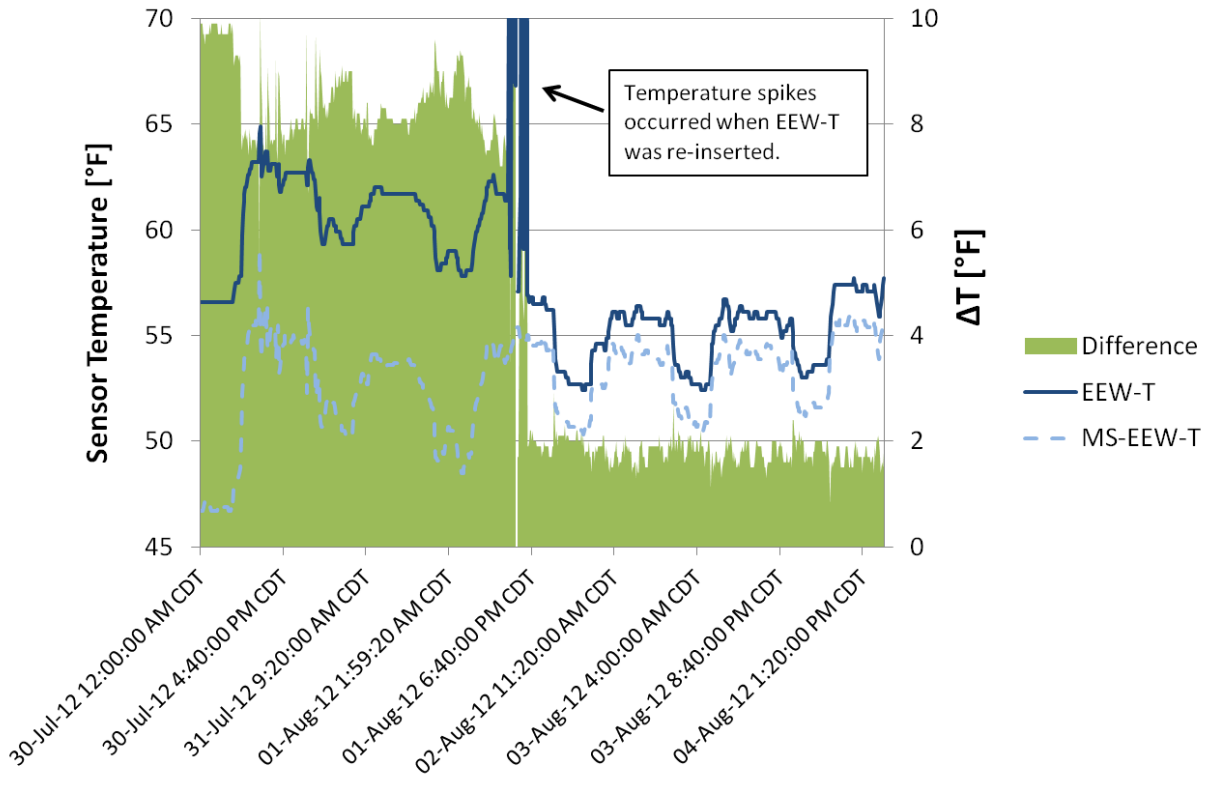

Figure 4-9 - EEW-T, MS-EEW-T temperatures, and the difference between them before and after EEW-T was fully inserted in the thermowell.

4.2.4 Field-Verifying Temperature Sensors

All temperature sensors critical to the research were removed and their temperature readings were compared to a thermometer reading in a water bath maintained at room temperature (Figure 4-11). One purpose of this test was to validate the temperature sensor offsets found from comparative data (discussed in Section 4.2.2). The tests revealed that two of twenty-

two sensors indicated temperatures more than ±1°F different than the thermometer reading and the results can be found in Table 4-2.

Figure 4-10 – Temperature sensor ELW-T removed from pipe. Thermally-conductive paste can be seen on the sensor sheath and casing, and on the inside of the mounting bushing.

Two temperature sensors showed readings much different than the thermometer: the geo-field entering water (GEW-T) and the surface-mounted sensor on the condenser leaving water leg (SMT-1). The GEW-T sensor consistently indicated 3°F higher temperature readings than the thermometer, which was in close agreement with the calibration offset determined for GEW-T in Section 4.2.2 (an offset of -3.5°F).

Sensor SMT-1 was installed to study the efficacy of non-intrusive temperature measurement, which was planned as part of a future phase of the research. The SMT-1 sensor indicated a temperature reading of 2.5°F higher than the thermometer at room temperature. While it was installed on the surface of the condenser leaving water pipe, recorded data from SMT-1

indicated it read consistently too high by 0.75°F compared to similar sensors (Table 4-2). Because the compared data were closer to the temperature conditions typical of SMT-1, the calibration offset was kept at -0.75°F for the sensor.

Figure 4-11 – GUR-T sensor sheath and thermometer submersed in room temperature water.

4.2.5 Issues Found from Field-Verifying Sensors

Three types of issues were noted while field-verifying the sensors: (1) sensors could not be accessed physically, (2) some sensors were missing thermally-conductive paste in their thermowells, or (3) sensor data could not be accessed. Three temperature sensors, all of which were installed prior to the beginning of this research, could not be physically accessed

with a ladder or lift due to height and equipment obstructions. [26]As such, these sensors could not be field-verified.

Figure 4-12 – Looking up, temperature sensors CWR-T at 20 feet and cannot be physically accessed with a ladder or lift.

In the process of removing and testing the temperature sensors, it was noted that three sensor sheaths did not have thermally-conductive paste. [27] Thermally-conductive paste is typically included in order to improve the thermal communication between the sensor and the thermowell inserted into the fluid stream. Because the GCHP system can be run in both heating a cooling modes, it was imperative that all sensors were checked for paste, as the sensors could monitor either hot or cold fluid streams depending on the mode of operation. A request to add thermal paste to the three sensors was submitted to FP&M, whom responded within one day to add paste to the more critical sensors (CEW-T and GUR-T). Because

[26] Three temperature sensor that were inaccessible to test: chilled water return #1 (CHWR-T), Campus chilled water return #2 (CWR-T), and campus chilled water supply #1 (CHWS-T).
[27] Three temperature sensors that did not have thermally-conductive paste: Condenser entering water (CEW-T), campus chilled water supply #2 (CWS-T), and the University St. geofield loop return temperature (GUR-T). Note that, in Figure 4-11, no paste can be seen on sensor GUR-T.

sensor CWS-T was difficult to access without the use of lift equipment and because it was a redundant (secondary) sensor FP&M proposed to add paste to CWS-T at a later time when all four of the campus chilled water temperature sensors could be accessed and tested. [28]

To study the impact of conductive paste being added to sensor CEW-T, temperature data from before and after the addition of paste were compared with a like sensor.[29] No appreciable difference was observed, which was a reasonable result given that the typical ambient temperature of the WID mechanical room was 85°F (i.e. within 1°F of the average condenser entering water temperature during the data period). The before and after temperature comparisons are shown in Figure 4-13. Regardless of the impact witnessed here, it is the view of this research that thermal paste is critical for temperature sensors related to the WID heat pump system, as the paste provides thermal communication between the sensor and the thermowell. It was expected that a greater error due to ambient heat gain would have been shown if the system was running in heating mode (i.e. the CEW-T sensor would be measuring chilled water temperature), however it was not possible to perform a test due to the system's inability to operate in heating mode.

[28] Sensor CHWS-T is used for primary data for the district chilled water supply temperature, and therefore CWS-T provided redundant measurements.
[29] SMT-2, which is installed in the same location and should agree with CEW-T. A full assessment of comparable sensors such as CEW-T and SMT-2 is discussed in Section 4.2.2.

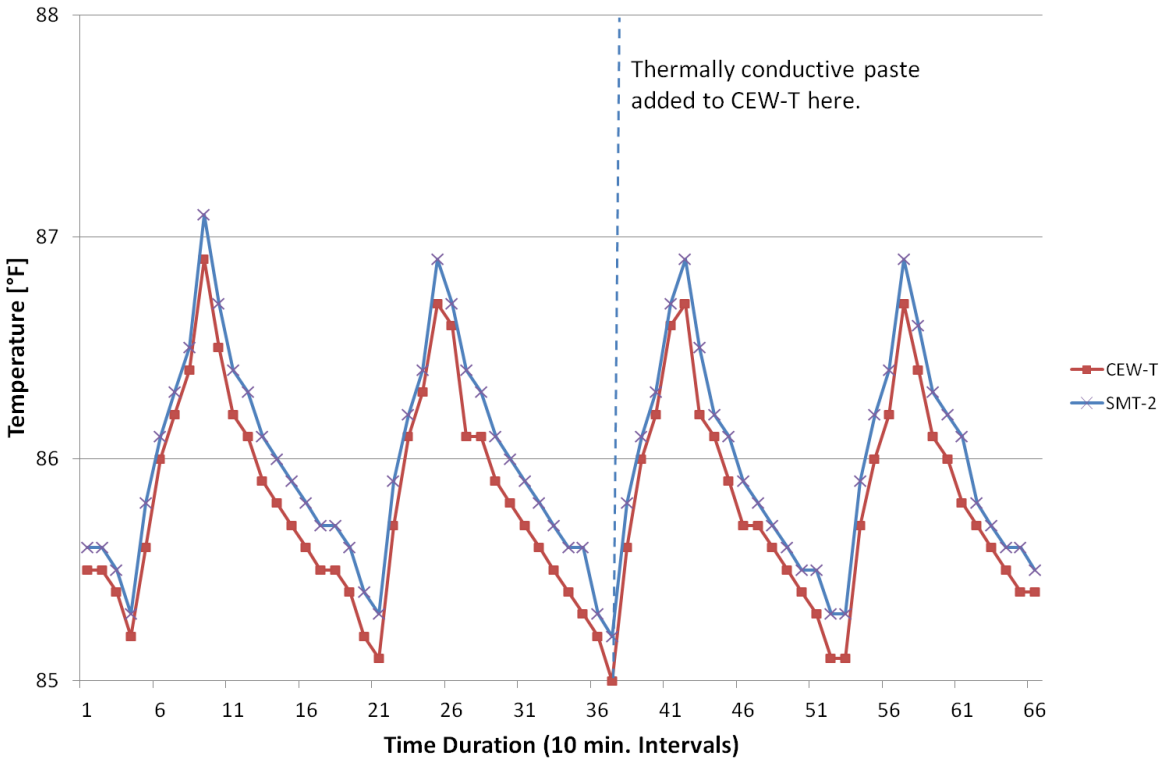

Figure 4-13 – Before and after thermally-conductive paste added to CEW-T, no evident impact was observed.

When field-verifying the sensors, the third type of issue found was related to communication issues between the sensor and the BAS. For example, wiring/communication issues were discovered when removing the temperature sensors installed on the steam reheat supply. It was found that the return and supply temperature sensors (RWR-2 and RWS-2) associated with the steam reheat BTU meter were not registering correctly on the BTU meter computer screen. The meter screen was displaying incorrect (constant) temperature values and did not change when the sensors were removed from the pipe and submerged in two different temperature baths. More importantly, it was then discovered that the recorded data in the

BAS for RWR-2 and RWS-2 were incorrectly named and the data being trended was actually from the redundant sensors RWR-T and RWS-T.

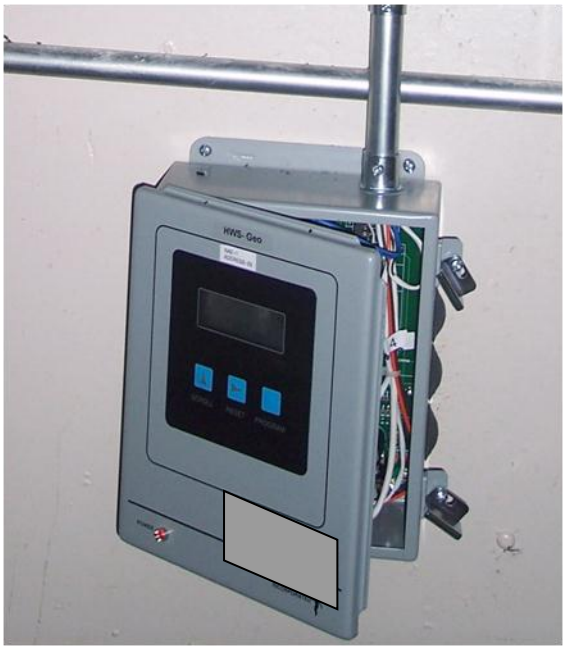

Figure 4-14 – Open BTU Meter Computer with Display. The wiring inside connects to two RTDs and one

Sensors RWR-2 and RWS-2 (the sensors belonging to the BTU meter) were higher accuracy, calibrated temperature sensors, while RWR-T and RWS-T were lower accuracy RTDs and were to be more useful as secondary sensors. Once notified, FP&M determined that the sensor wiring had come loose in the BTU meter and while attempting to fix the problem they determined that the motherboard of the meter computer needed to be replaced. The BTU meter manufacturer was unable to fully resolve the hardware issue in order to initiate data trending for the reheat hydronic flow rate and supply/return fluid temperatures during the research, therefore the steam energy consumed to meet the building reheat load was not measured. Without physically testing the sensors the connection issue would have been difficult to detect.

The steps taken to calibrate, field-verify, and test the research temperature sensors proved useful. Single-point calibrations were developed for all sensors showing appreciable disagreement with independent sensors located within the same system location (Table 4-2). An installation issue was identified for the heat pump chilled water return temperature (EEW-T) that revealed an error of 11.5°F in the original measurement. Further field tests revealed missing thermal conductivity paste, wiring issues, and a hardware fault in the reheat BTU meter. The temperature calibration values defined in this section were further verified using energy balance methods (Section 4.4), but first the water flow meter verification is discussed in the following section.

4.3 Verifying the Water Flow Meters

The methods used to verify the water flow meters are discussed in this section. Beyond assuring that the flow data were accurate, flow meter verification was motivated by several known issues for the installed water flow meters. The FP&M engineering team was skeptical of the quality of the turbine-type flow meters (WFM-1 and WFM-2) that had been installed prior to the research, but budget limitations prevented upgrading the flow meters. In addition, meter WFM-1 was installed in close proximity to an upstream elbow, and flow meter WFM-2 has been calibrated for a pipe size different than the pipe which it was installed on.

The verification techniques discussed in this Section revealed that the BAS and IBA data points linked to flow meters WFM-1 and WFM-2 had been mislabeled and, because of the mislabel, had also been calibrated incorrectly. Several tests were conducted before discovering that the flow meter data were interchanged, and as a result, the results of tests

were often unclear and contrary to expectations. To indicate to the reader the tests in which the flow data between WFM-1 and WFM-2 were unknowingly interchanged, an asterisk is appended to the flow meter name (e.g. WFM-1* and WFM-2*). Upon the discovery of the mislabeled flow meters in Section 4.3.5, the asterisk is removed from the meter names.

4.3.1 Initial Ultrasonic Comparisons

An ultrasonic flow meter (UFM), made available by UW FP&M Engineering, was used to field-verify the readings from the installed flow meters (Figure 4-16a).[30] Tests were conducted to record independent flow rate measurements for the following installed flow meters: WFM-14 (geo-field supply flow rate), WFM-13 (recovered-to-reheat supply flow rate), WFM-1* (heat pump evaporator water flow rate) and WFM-2* (heat pump condenser water flow rate). The field tests were conducted in four different locations, where the UFM was installed in as favorable a location as possible (i.e. away from flow obstructions or elbows) on the same straight run of pipe as the flow meter of interest. In many cases, the UFM was installed just upstream of the flow meter. During testing, sufficient time was permitted for the UFM to settle to a relatively constant value. Readings were recorded from the UFM display computer (Figure 4-16b) and instantaneous flow rate values for the flow meter in question were recorded from the IBA and time synchronized.[31]

---

[30] Information on the ultra-sonic flow meter: General Electric, model "TransPortPT878"

[31] "Instantaneous" is used here to denote that the real-time value of the installed flow meter did not come from trended data, as was most data used in the research, but rather from watching and recording updating "live" data reported at regular intervals on a program from the IBA computer. The use of instantaneous data allowed for immediate comparison between the installed flow meter and the ultra-sonic flow meter. Time synchronization errors may have been on the order of one second due to the requirement that the instantaneous flow meter readings be recorded by hand.

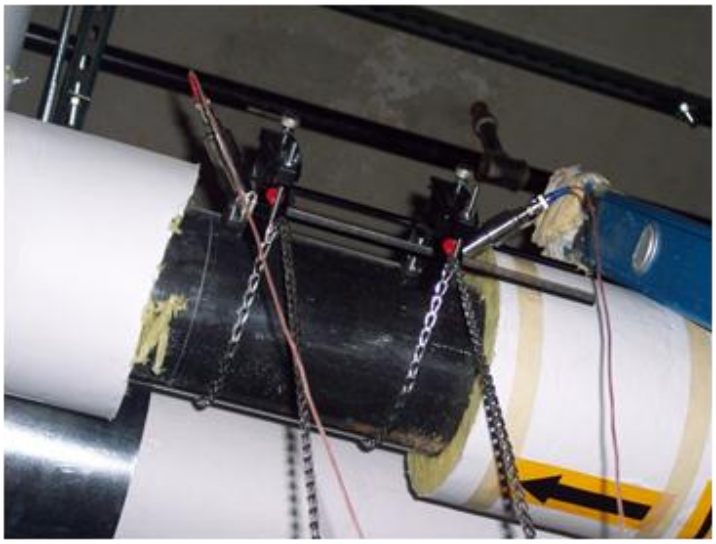

Figure 4-16a - Ultrasonic Flow Meter: Pictured are the transducers, mounting harness, and connection wires. The meter is installed on a section of 8" pipe after the insulation was removed.

Figure 4-16b – Ultrasonic Flow Meter Data Display Computer

The results of these tests showed that the newly installed electro-magnetic flow meters (WFM-13 and WFM-14) both agreed within three percent of the UFM. The two turbine-type flow meters that monitored the heat pump evaporator water flow (WFM-1*) and the heat pump condenser water flow (WFM-2*) showed less agreement. The results of the UFM tests are shown in Table 4-3.

Meter Tested	*Flow meter [GPM]*	*UFM [GPM]*	*Difference [GPM]*	*% Diff.*
WFM-13 (reheat)	302	312	9.6	3%
WFM-14 (geo)	635	655	20	3%
WFM-1* (evap)	353	512	159	45%
WFM-2* (cond)	729	623	-106	15%

Table 4-3: Comparisons between UFM and Primary Flow Meters

The agreement between the electro-magnetic flow meters (WFM-13 and WFM-14) and the UFM was within the manufacturer-listed uncertainty of the UFM, 3% and ±5% (reading)

respectively. The agreement observed for the electro-magnetic flow meters was considered sufficient, and no further UFM comparison tests were conducted for the electro-magnetic meters. Additional verification for WFM-13 and WFM-14 came from comparing measured flow data between the condenser, geo-field, and reheat water loops and is discussed further in Section 4.4.1. Due to the large disagreement for the heat pump evaporator and condenser water flow meters, further tests were conducted and are discussed in the following section.

4.3.2 Additional Tests for WFM-1* (Installed Close to Pipe Elbows)

Flow meters WFM-1* and WFM-2* were turbine-type, insertion flow meters and were installed prior to the research to monitor the aggregate flow rate of chilled water through the heat pump evaporators and heat pump condensers (in chilled water production mode). It was known from the initial review of the system equipment that the HP evaporator water flow meter (WFM-1*) was not installed in accordance with manufacture site selection guidelines, which recommended that the meter be installed ten pipe diameters downstream and five pipe diameters upstream of any flow obstruction. The flow meter was installed on a 6 inch diameter chilled water pipe, and due to a lack of straight runs of pipe near the heat pumps, the meter was only four pipe diameters downstream of a 90° elbow and only two pipe diameters upstream from another 90° elbow (Figure 4-17).

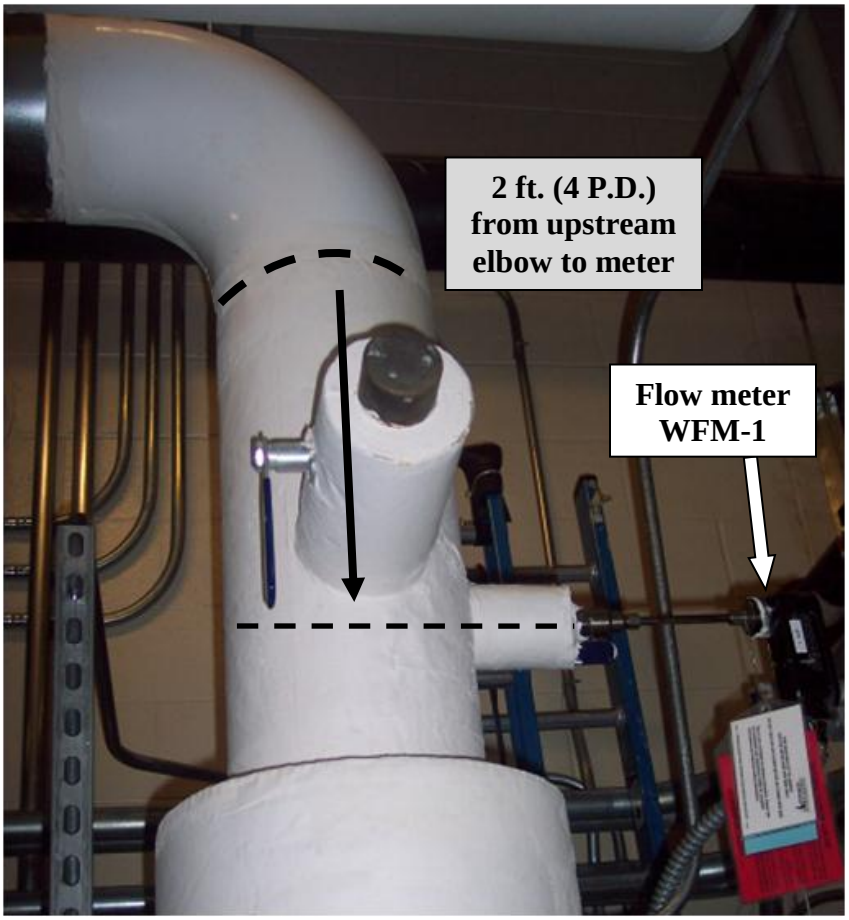

Figure 4-17 – HP chilled water flow meter was installed only four pipe diameters downstream of elbow. Ten pipe diameters were recommended by manufacturer guidelines.

The turbine flow meter location was fixed and could not be relocated without considerable re-installation and hot-tapping procedures. To perform additional comparison tests, a new location was determined for the UFM that was still within the same hydronic flow path, with no intervening branch piping, as the chilled water meter, but allowed for sufficient lengths of straight pipe before and after the UFM.[32] The purpose of new UFM location was to attempt

[32] If relocation of flow meter WFM-1 were possible, it would not be recommended to re-locate the meter to the new UFM testing location. The UFM testing location was appropriate for verifying WFM-1; however, it would be not be possible for the WFM-1 flow meter to measure the water flow rate while the system was configured in heating mode.

to remove any measurement errors in the UFM that were previously caused by elbows near the chilled water flow meter.[33] (Figure 4-18)

In addition to the new location for the UFM, a range of flow rates were used to compare the UFM and WFM-1* flow measurements. With assistance from WID mechanical staff, the speed of one chilled water hydronic pump (P-7) was increased from 30 to 50 Hz to cause a change in the chilled water flow while flow rate measurements were recorded.

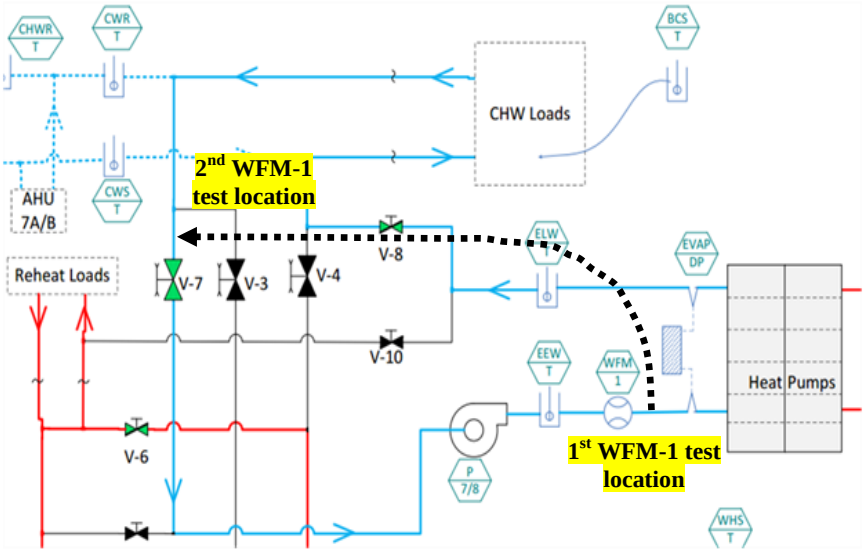

Figure 4-18 – Change of UFM test location with respect to WFM-1*. 2nd location allowed more distance for the UFM from flow obstructions.

The results of the test showed varying disagreement between the UFM and flow meter WFM-1*, with an average percent difference of 9% (Figure 4-19). The results indicated much closer agreement than the 45% error found in the first test (outlined in Section 4.3.1). However, the fluctuations in WFM-1* data did not match the trend expected by gradually increasing the pump speed; the flow behavior measured by the UFM was closer to the flow

[33] The UFM was re-located to allow for ten pipe diameters upstream to the nearest pipe elbow or flow obstruction, sufficient for the clearance recommended by the UFM manufacturer to ensure a fully developed flow profile.

expected.[34] It was therefore not clear from the test whether or not significant error was being caused by the close proximity of WFM-1* to up and downstream elbows.

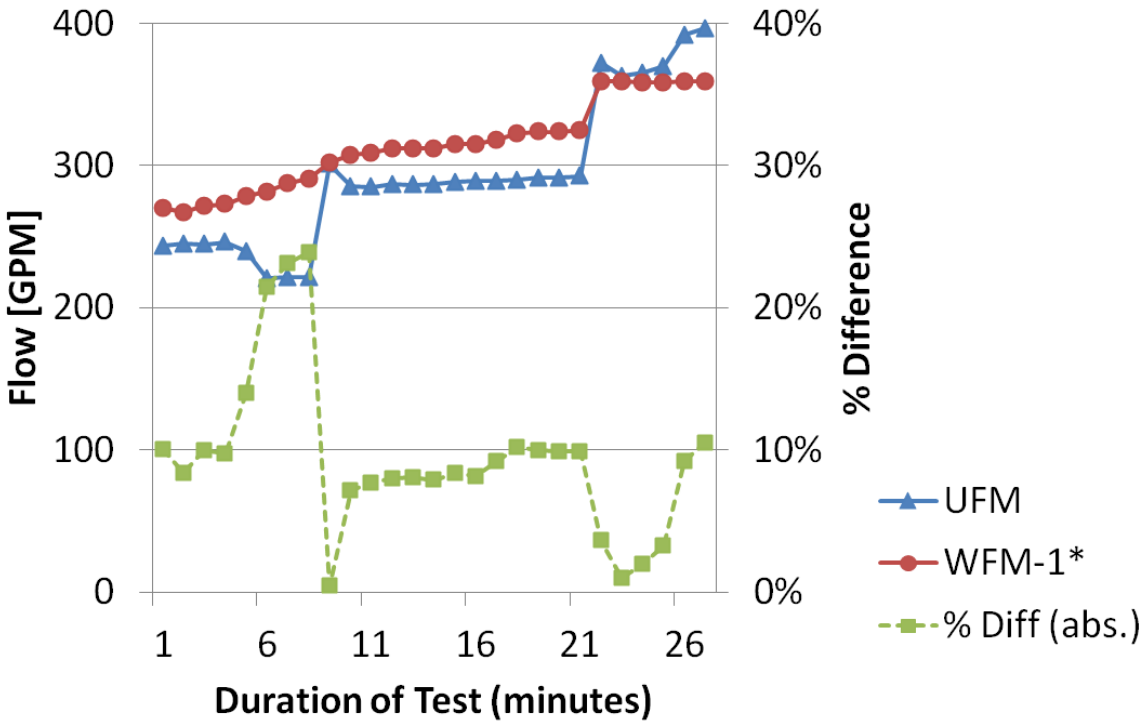

Figure 4-19 – UFM vs. WFM-1* during second comparison with UFM

Additional tests were conducted to determine the relationship between the responses of the water flow meters under varying pumping conditions, as described in the following section.

[34] The fact that the trend of WFM-1* did not closely match what was expected, and observed by the UFM, was perhaps the first clue that the meter data was coming from a different flow meter (i.e. WFM-1 and WFM-2 were switched). It was a reasonable that both the UFM (measuring chilled water flow) and WFM-1 (measuring condenser water flow) both increased simultaneously, considering that any increase in heat pump load would necessitate increased water flow to maintain the system setpoints on both the chilled and condenser water loops. Additionally, because WFM-1 had been calibrated for the wrong pipe size, the actual reading of WFM-1, if spanned appropriately, would have indicated flow rates a factor of 1.74 larger, and therefore a much wider discrepancy would have been seen for the data displayed in Figure 4-19.

Additional ultrasonic test comparisons were performed to verify the chilled water flow meter measurements, discussed in Section 4.3.7.

4.3.3 Variable Pumping Flow Tests

At a time when the heat pumps could be shut off and the building cooling load be met solely by campus chilled water, an additional flow test was conducted whereby the speed of the condenser water pumps was manually changed to manipulate the condenser water flow. During the test, data were collected for flow meters WFM-2* and WFM-14. Because valve V-1 was in its closed position, the total condenser water flow was passing through the geofield. Therefore, WFM-14 would agree with WFM-2* assuming there was no leak in V-1.

The variable drives to the condenser water hydronic pumps (P-11 and P-12) were manually decreased to their minimum frequency of 15 Hz. Over the course of one hour, the speed of pump P-11 was gradually increased to observe and compare the flow as measured by the condenser water flow meter WFM-2* and the geo-field water flow meter WFM-14. To indicate the operation of the pump during the test, the electrical power consumed by P-11 was trended on the IBA synchronously in time with the measured flow rates. The results are presented in Figure 4-20 and Figure 4-21.

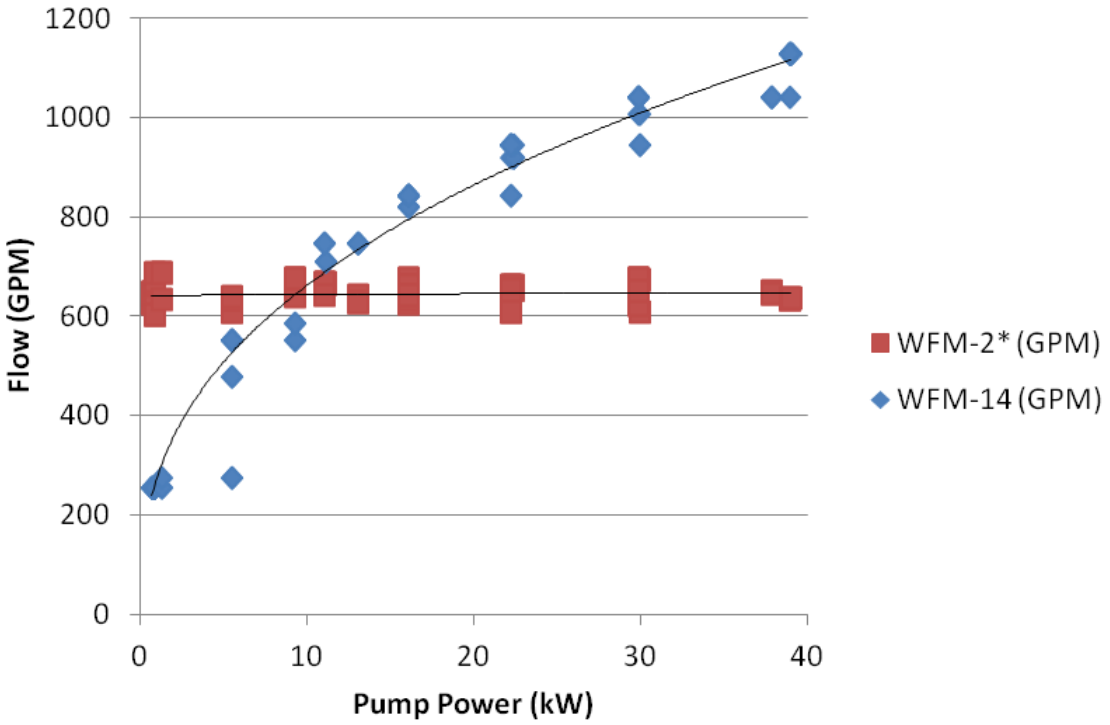

Figure 4-20 – One hour of flow rate data for WFM-2* and WFM-14 vs. Condenser Pumping Power

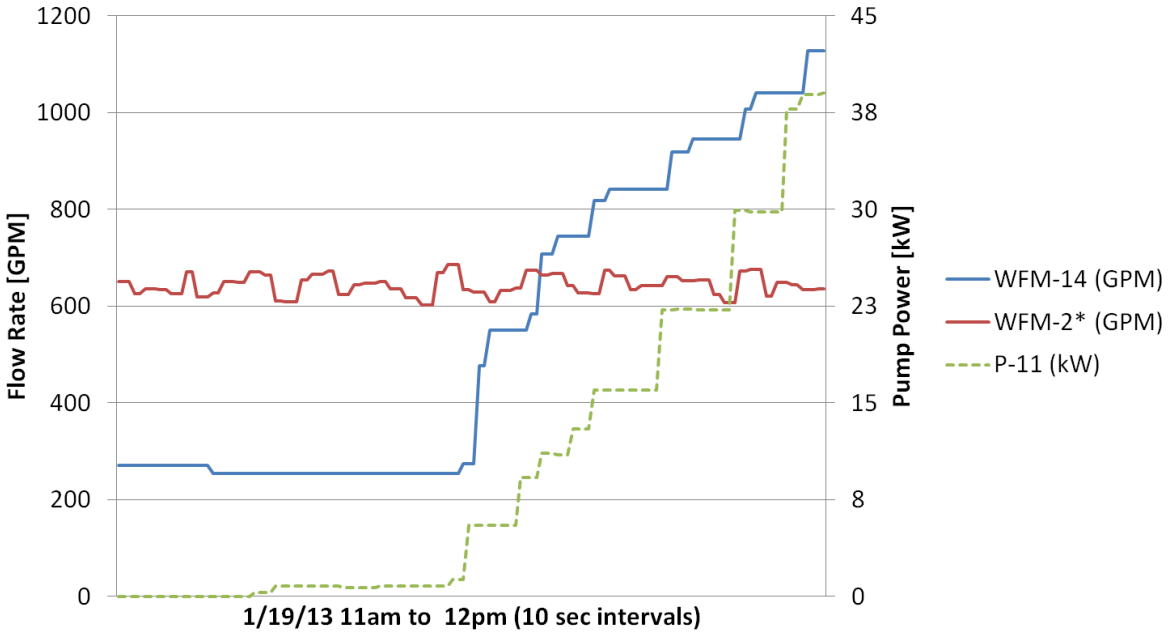

Figure 4-21 - Measured Flow rates and overlaid pumping power

The results of the test strongly indicated an issue with the condenser water flow rate as measured by WFM-2*. The flow rate measured by WFM-14 behaved as expected with an asymptotic increase in flow rate as the pump speed (i.e. pumping power) increased. The nearly constant response of WFM-2* made the flow meter data suspect.

4.3.4 Flow Meter Field-Verification

Similar to the temperature sensor field verification tests discussed in Section 4.2.4, the condenser water flow meter was physically removed from the pipe to validate its connection with data point WFM-2. During the test period, flow rate measurements from the WID water flow meters were recorded at fifteen second intervals and the data is presented in Figure 4-22. Upon removing the condenser water flow meter, the measured flow rate for data point WFM-2* showed no significant change; rather, the measured flow rate WFM-1* plummeted from 150 GPM to a constant 4.3 GPM. The flow measured by WFM-1* returned around 150 GPM at the same time the flow meter was re-installed. For further verification, the evaporator water flow meter (originally thought to be connected to data point WFM-1*) was removed from the pipe and flow data from WFM-2* decreased sharply from 513 GPM to a nearly constant 7 GPM while the meter was removed.

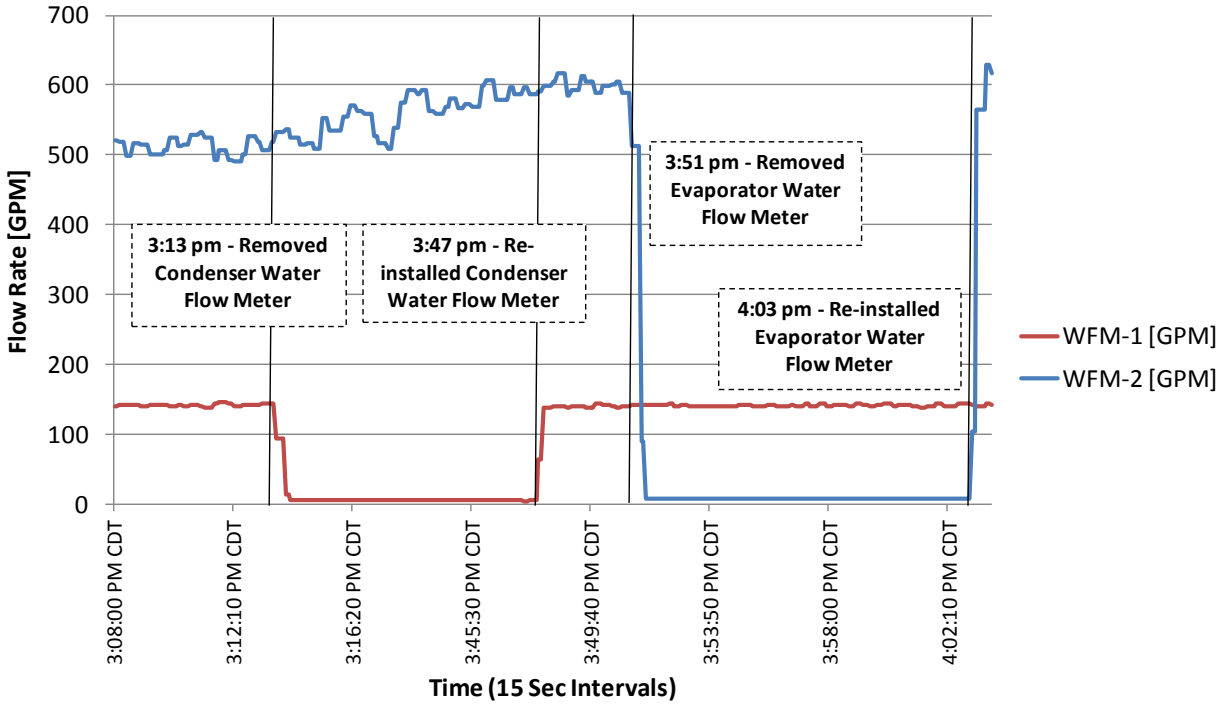

Figure 4-22 - Flow measurements for WFM-1 and WFM-2 during flow meter field verification tests

The field verification tests gave sufficient proof that the data points for the evaporator and condenser water flow meters had been mislabeled, not only in the IBA but also in the BAS, as compared to the meters' nametag labeling and the WID construction/controls documentation. The geo-field water flow meter was also field-verified and showed that the meter corresponded to data point WFM-14 and labeled correctly. The recovered-to-reheat water flow meter could not be field-verified, because at the time of testing it was out of operation due to a faulty electrical connection. However, the relationship between modulating valve V-1 operation and WFM-13 flow rate data were used to validate that the meter corresponded to the appropriate data point.

Correcting the evaporator and condenser water flow meter data were not as straight-forward as simply interchanging the data for WFM-1 and WFM-2 post data collection. The condenser water flow meter had been sized incorrectly and, to re-calibrate the meter, FP&M had applied a correction factor to the flow rate measurements. Unknowingly, FP&M had applied the correction factor to the wrong data point (i.e. the correction factor was applied to the evaporator flow rate data). The following section discusses the flow meter calibration, correction factor, and the methods used to re-calibrate and re-correct the flow data for meters WFM-1 and WFM-2.

4.3.5 Re-Calibrating WFM-2 for a Different Pipe Size

With the help of FP&M engineers, closer inspection of the condenser water flow meter revealed that the flow meter was incorrectly sized for the pipe it had been installed on. The meter's tag indicated it was sized for a six inch diameter pipe, but the heat pump condenser water pipe was an eight inch pipe. In order to re-calibrate the condenser water flow meter to the eight inch pipe, the insertion depth of the flow meter and the signal range of the meter needed to be adjusted.

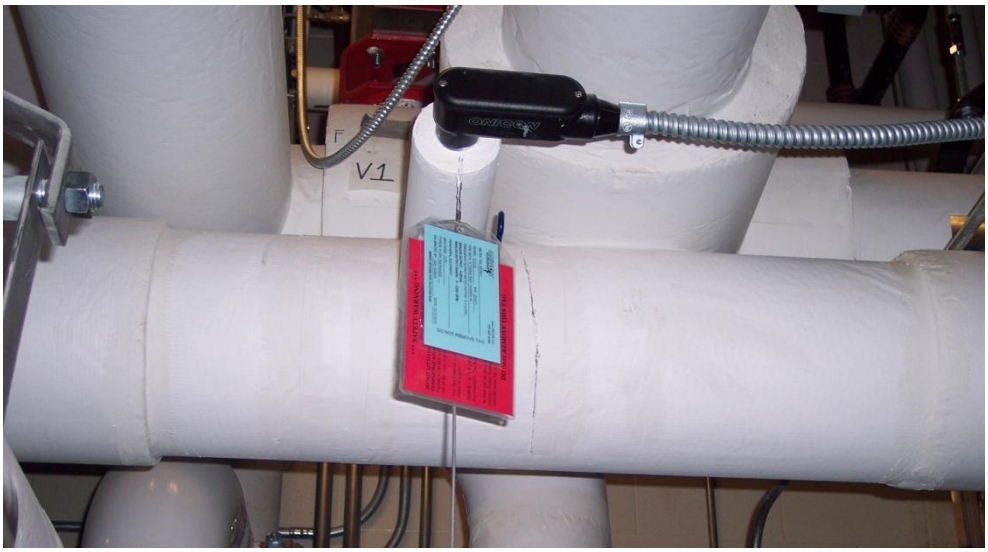

Figure 4-23 – WFM-2: sized and calibrated for a 6 inch pipe, but installed on 8 inch pipe.

An "insertion depth gage" was provided by the flow meter manufacturer for each flow meter that was installed in the WID. As the name suggests, the gage was used during installation to position the depth of each meter (i.e. the radial distance into the pipe that the meter's turbines were located, see Figure 4-24). The purpose of the depth gage was to locate the meter turbines at 1/3 the pipe inner diameter inside of the pipe wall; the location the meter was factory-calibrated and the approximate location that the average flow velocity would be expected in a fully developed flow profile (Figure 4-25). Because the original gage that was used to install the condenser water flow meter was for a six inch pipe application, engineers from FP&M, with assistance from the flow meter manufacturer, re-positioned the condenser water flow meter using a new insertion depth gage with a length of 13 $^{7}/_{8}$ inches, as compared to the original gage with a length of 14 ½ inches.[35]

[35] The dimensions of the flow meter were not measured as it was not possible to fully remove the meter from the pipe. The decreased gage length made sense, as the increased diameter of the actual pipe would require the flow meter turbines be moved deeper into the pipe. The

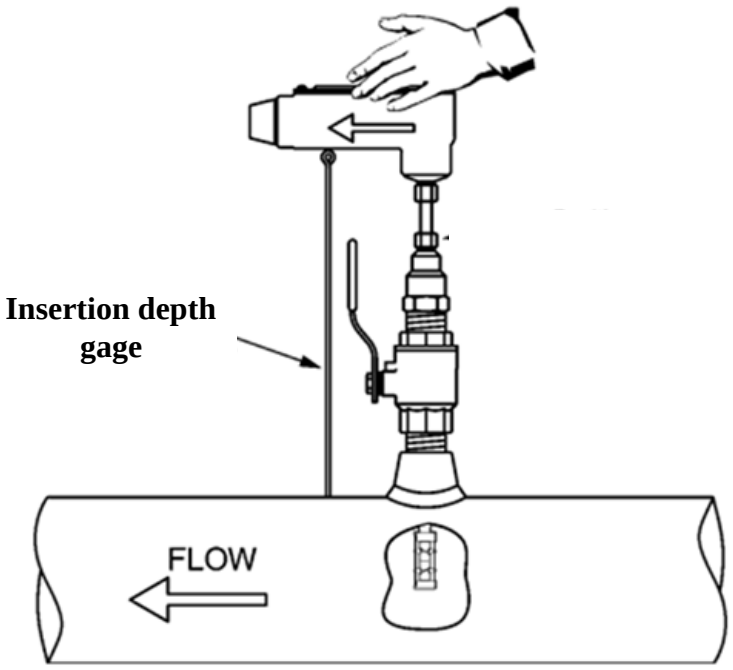

Figure 4-24 - Turbine-type flow meter installed in pipe with Depth Gage, cut-away showing turbines (Image from Flow Meter Manufacturer)

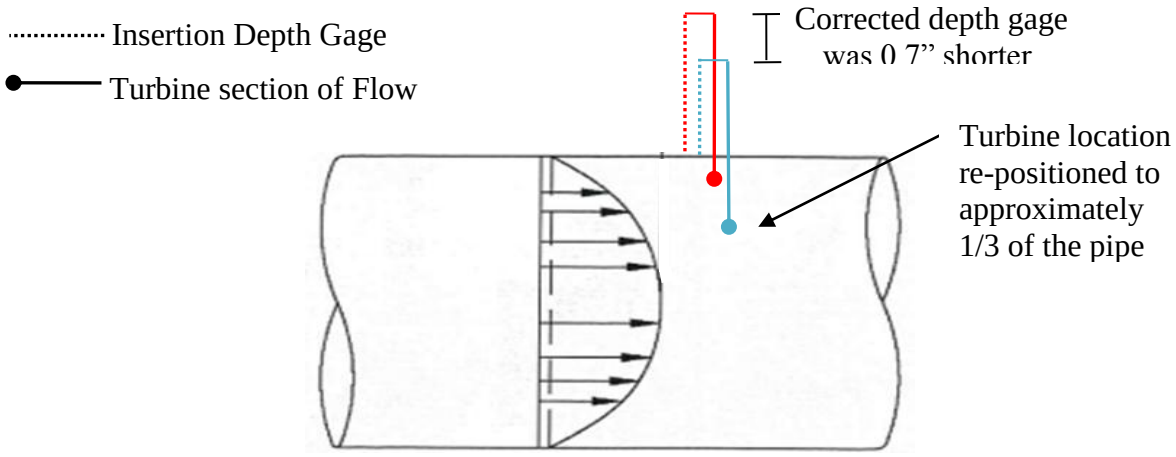

Figure 4-25 – Flow meter depth re-location and velocity profile in a pipe with fully developed flow (Not

previous (incorrect) gage length of 14 ½ inches was equal to that of the evaporator water flow meter which was also sized for a 6 inch pipe.

In addition to re-positioning, a correction factor was applied to the recorded flow measurements to account for the meter being calibrated for a six inch pipe, rather than an eight inch pipe. In effect, the condenser water flow rate was corrected by multiplying the measured flow rate by 1.74, a value approximately equal to the ratio of the actual pipe cross sectional area to the cross sectional area of the pipe that the meter was intended for.[36] To aide in understanding the theory and application of the flow correction, a generalized discussion of the turbine flow meter operation is included here.

In general, the turbine-type flow meter measures the fluid velocity by sensing the rotational speed of a freely rotating turbine that is situated with its axis parallel to the passing fluid. As the turbine is spun by the fluid, the turbine blades pass a fixed electrode and an electromagnetic pulse is recorded. The sensed fluid velocity within the pipe is therefore recorded by counting the electromagnetic pulses. The meter's volumetric flow rate is then determined by multiplying the sensed velocity by the cross sectional area of the pipe, and hence any change in pipe size will necessitate a correction.

[36] The correction factor that was applied to the condenser water flow rate measurements took into account the cross-sectional area that the actual flow meter turbines and turbine arm covered within the pipe.

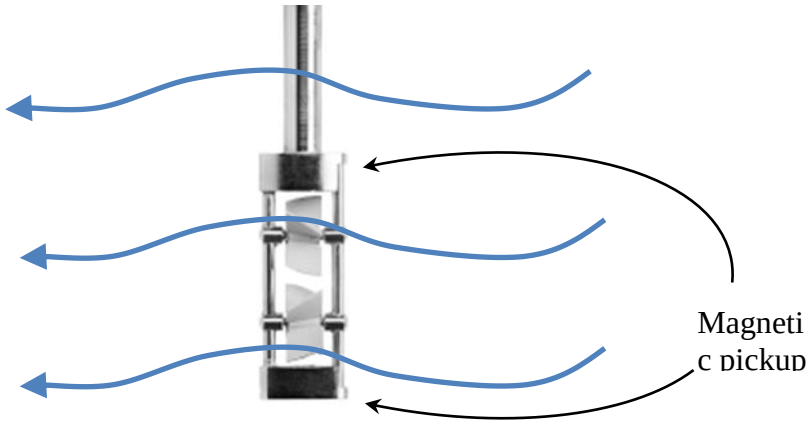

Figure 4-26 - View Perpendicular to Flow Meter turbines, arrows indicate direction of water flow

In the case of the turbine-type meters found in the WID, each flow meter contained two individual turbines at the fluid end of the meter, the electromagnetic pulses of both were averaged, and that average was converted by electronics on-board of the flow meter to an output signal in a range from 4 to 20 milliamps. The milliamp signal was then transmitted to a BAS field controller and "spanned" to a volumetric flow rate value based on the meter's flow output range. The flow range for the condenser water flow meter, as calibrated by the manufacturer, was 0 to 1200 GPM.[37] For illustration purposes, Figure 4-27 shows a simplified movement of information in its various forms from fluid flow measurement with a turbine-type flow meter.

[37] All of the flow meters installed in WID had basic information included on an information card that hung from the flow meter. The card included information such as model number and calibration information.

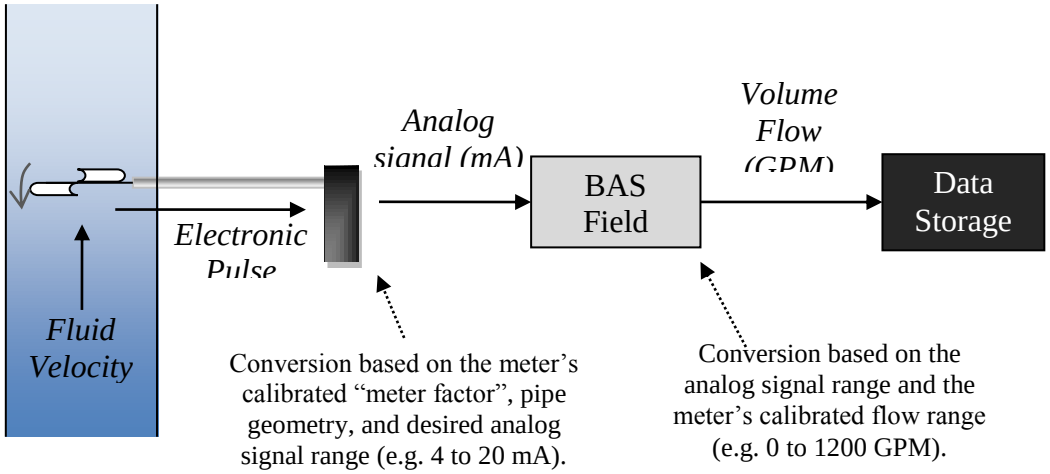

Figure 4-27 – Simplified schematic of data movement when measuring volumetric fluid flow

In order to re-calibrate the condenser flow meter to a larger pipe size, a correction factor was needed to account for the larger pipe cross sectional area. The simplest method to apply the correction factor was to "re-span" the volume flow rate conversion on the BAS field controller to a new flow rate range. Originally, the span of the meter programmed into the BAS was from 0 to 1200 GPM. A rough estimate for the necessary flow correction would come from considering that the maximum flow of 1200 GPM was based on the manufacturer calibration for the largest allowable water velocity, equal to 16.18 ft/s. In the larger, 8 inch pipe, a water velocity of 16.18 ft/s would be associated with a volumetric flow rate of 2522 GPM; hence the need to re-span the meter flow range for the new pipe size by roughly 2522/1200, or 2.1.

A more exact re-span factor was supplied by the meter manufacturer which accounted for the cross-sectional area of the submerged turbines and turbine arm within the pipe. The manufacturer supplied re-span factor was equal to 1.74, corresponding to a maximum water

flow rate of 2086 GPM. The manufacturer re-span factor was programmed into the BAS field controller by FP&M. To confirm that the analog signal output of the flow meters were re-spanned as expected, analog signal tests were conducted and are discussed in the following section.

4.3.6 Confirming the Flow Meter Span with a Multimeter

To verify the volumetric flow rate span of meters WFM-1 and WFM-2, the analog output signal was measured with an electronic multimeter and compared to the flow measurement recorded in the BAS. The flow meter output signal was directly measured from the internal circuitry within the flow meter. The flow meter manufacturer provided commissioning documentation that instructed the analog output signal was communicated through the leads indicated in Figure 4-28.

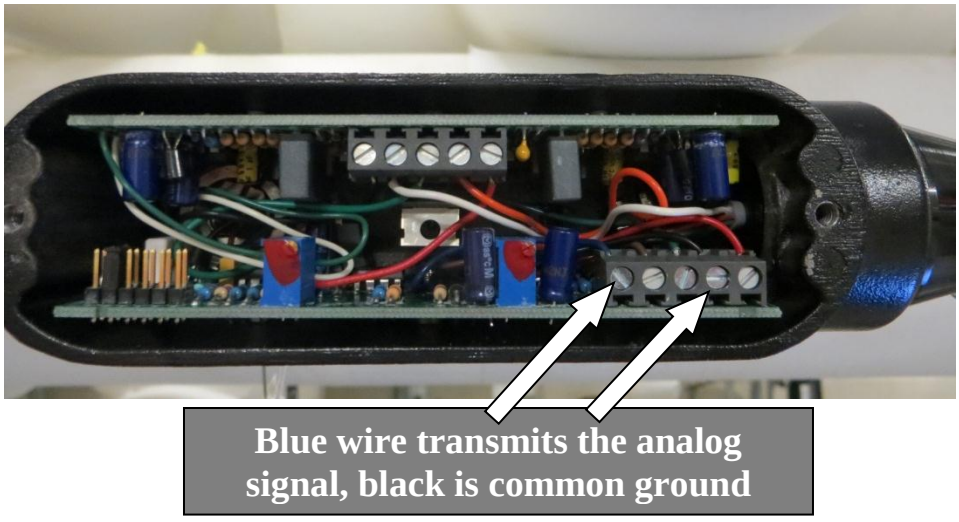

Figure 4-28 - Internal circuit board of flow meter with the cover removed.

The multimeter measurement of the output signal in milliamps (DC) was recorded synchronously in time with the flow meter measurement as recorded in the IBA. The output

signal was then spanned for flow rate ranges 0 to 1200 GPM and a range of 0 to 2086 GPM and compared to the IBA measured data. The data from the tests are provided in Figure 4-29 and Figure 4-30.

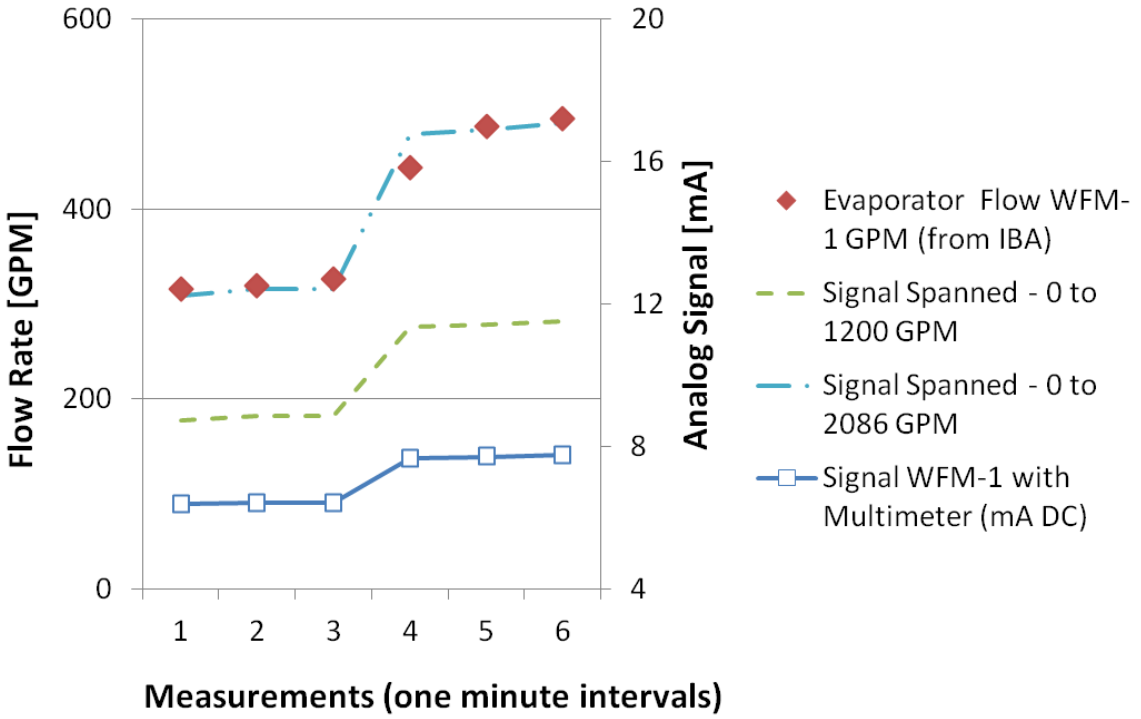

Figure 4-29 - Multimeter Test of Evaporator Water Flow Meter WFM-1

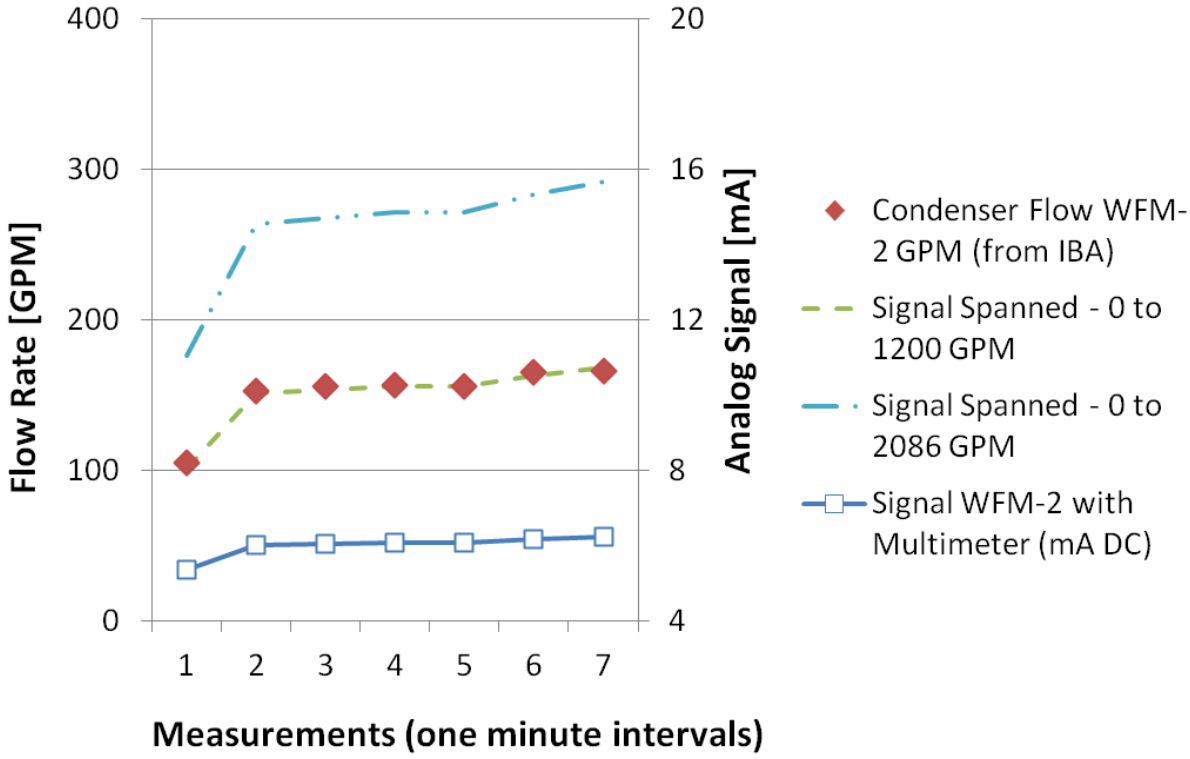

Figure 4-30 - Multimeter Test of Condenser Water Flow Meter WFM-2

The results of the multimeter tests confirmed that the mislabeled data points had caused FP&M to re-calibrate the wrong flow meter. The flow span for the condenser water flow meter (WFM-2) had not been re-spanned for the larger pipe diameter, but instead had incorrectly remained spanned from 0 to 1200 GPM. Conversely, the analog signal from the evaporator water flow meter (WFM-1) was being spanned for a flow range of 0 to 2086 GPM, which was incorrect for the meter's calibration and pipe size.

For the remainder of the research, flow meter data for WFM-1 and WFM-2 were corrected post-process, meaning that no changes were made on the IBA, BAS, or BAS field controller. Following data collection, the data labels were interchanged so as to match the WID documentation, such that the data recorded for the evaporator flow meter was labeled WFM-1 and the data recorded for the condenser water flow meter was labeled WFM-2. Secondly, the flow rate data for the evaporator flow meter were spanned back to a flow rate range of 0 to 1200 GPM, and the condenser water flow rate was spanned to a flow range of 0 to 2086 GPM. The re-labeling and re-spanning of the flow meters were accomplished using the following:

$$WFM_1 = WFM_{2,IBA}\frac{1200}{2086} \quad \textbf{(4-2)}$$

$$WFM_2 = WFM_{1,IBA}\frac{2086}{1200} \quad \textbf{(4-3)}$$

4.3.7 Final UFM Tests of Chilled Water Flow

Coincident flow rate data from meters WFM-1 and WFM-2 had not been recorded in the ultrasonic flow meter comparisons discussed in Sections 4.3.1 through 4.3.3. After determining the flow meter data from WFM-1 and WFM-2 needed to be switched, additional ultrasonic flow meter tests were performed. Due to the availability of the UFM test equipment and the operating conditions of the GCHP system, a final test was performed for chilled water flow meter WFM-1 only. Flow rate data for the geo-field and reheat loops were used to further verify the flow measured by WFM-2, discussed in Section 4.4.1.

The UFM was installed using the methods outlined and location identified in Section 4.3.2. The cooling demand on the heat pumps was low at the time of the test. Therefore, a valve that allowed water flow to bypass two air handling units in the WID penthouse was opened to allow the system to push the design chilled water flow rate to 700 GPM.[38] Additionally, internal valves at the HP evaporators were opened, consequently decreasing the water pressure drop across the HP evaporators which in-turn caused the chilled water pump drives to automatically increase the pump speed. Once the target flow rate was reached as measured by flow meter WFM-1 data collection began for the UFM using the methods outlined in Section 4.3.1.

Results of the test showed that the UFM and WFM-1 agreed within 6% on average. However, a wider agreement of 10% on average was observed for flow rates smaller than 600 GPM. The data are presented in Figure 4-31, where the significant changes in flow rate

[38] System design conditions were from the heat pump equipment submittal construction document.

indicate the time during the test where valves were opened and pump speed increased. The broad fluctuations observed in the flow rates measured by WFM-1 were suspect as the pump speed and HP internal flow valves were held constant, especially considering the relatively constant measurement by the UFM.

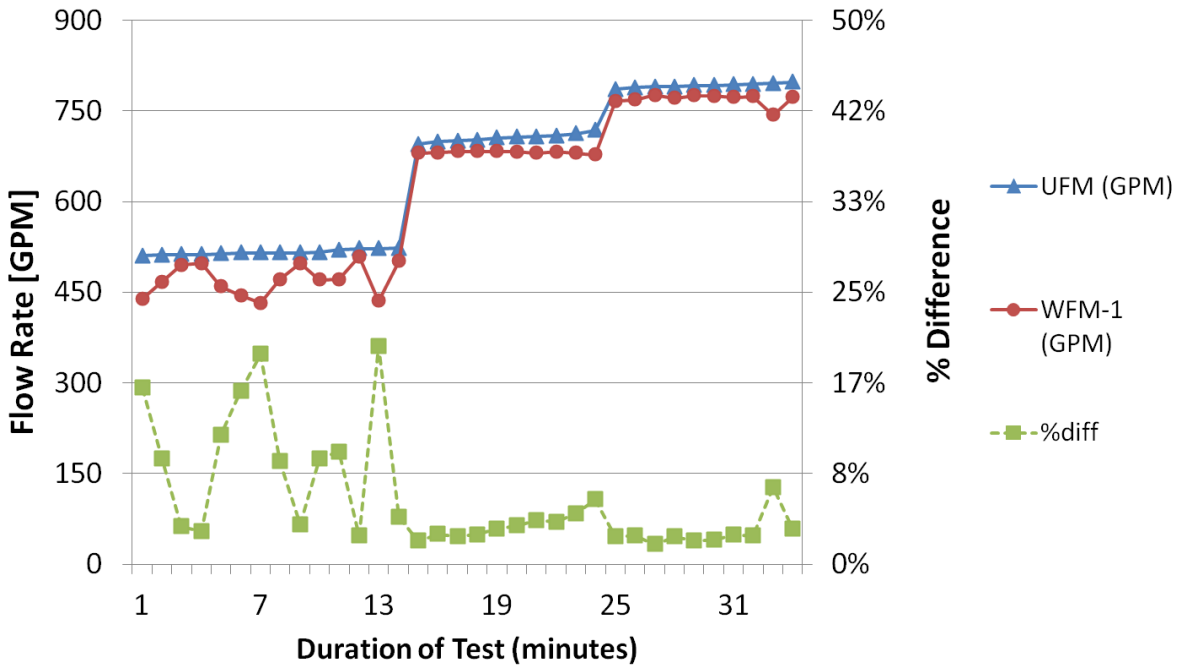

Figure 4-31 - Final UFM Comparison Tests for WFM-1

Due to the results of testing with the UFM and the proximity of the upstream pipe elbow, it was determined necessary to apply an elevated measurement uncertainty to the measurements of the evaporator water flow meter WFM-1. The UFM tests suggested that, especially for lower water flow rates, the measurement uncertainty be increased to as high as ±10% (reading). Though not directly comparable to the turbine-type meters used in this research, Woo and O'Neal determined that insertion flow meters installed at a similar

proximity of an elbow, as observed for WFM-1, showed flow measurement errors on the order of ±10%. (Woo 2006)[39] Because the measurement confidence and certainty of the ultrasonic flow meter was not high enough to justify a proper calibration of meter WFM-1, the measurement uncertainty of WFM-1 was increased from the manufacturer-rated ±2% (of reading) to ±10% (of reading).

The effect of the elevated measurement uncertainty of WFM-1 on energy measurements was noticeable but not detrimental. At larger temperature drops across the HP evaporators (e.g. 14°F), the heat pump cooling measurement uncertainty increased from ±7% to ±12% with the added WFM-1 uncertainty. The effect of the increased WFM-1 uncertainty is much less significant for cooling measurements for smaller evaporator temperature drops.

Flow meter verification tests in this section indicated that all flow meters but one agreed reasonably well with the ultrasonic flow meter. Additional flow verification procedures using the hydronic pump manufacturer's pump curves were considered, but were not useful for the research; refer to Appendix C. In the following section, the flow rate measurements, along with the temperature corrections discussed in Section 4.2, are further verified using mass balance and energy balance techniques.

---

[39] Woo and O'Neal studied a paddle-wheel type flow meter at various distances from a pipe elbow. Their study indicates as large as a 10% measurement error for paddle-wheel flow meters in similar pipe geometry and installed at a location similar to that of WFM-1 and its upstream pipe elbow (i.e. four pipe diameters downstream in a 6 inch pipe with elbow curvatures of 2.5 inches at an angle of 0° away from the elbow). One caveat: Woo also showed that fluid velocity (i.e. flow rate) does not have a significant impact on measurement error, and that the error is only a function of pipe/elbow geometry and flow meter proximity. It was observed for WFM-1 that the flow velocity had an impact in the difference between the ultrasonic flow meter and WFM-1.

4.4 Measurement Verification through Mass and Energy Balances

The configuration of the system hydronic loops and the location of the installed water flow meters allowed for secondary checks to verify the mass flow of water and energy flows were conserved. Equations to calculate the quantities, and the measurement uncertainty those quantities, discussed in this section can be found in Appendix A.

4.4.1 Condenser Water Flow (Mass) Balances

The condenser water flow, as measured by flow meter WFM-2, was compared against the measured geo-field and recovered-to-reheat water flows, as measured by WFM-14 and WFM-13, respectively. Flow rate data were collected for a time period when the geo-field and reheat recovery loop flows were in parallel. In other words, condenser water was recovered to the reheat loop through valve V-1 and valve V-2 was in the “geo-field bypass” N.O. position. Figure 4-32 provides the relative location of the equipment used to measure the mass flows and the bold red circle indicates the location the mass balance was applied.

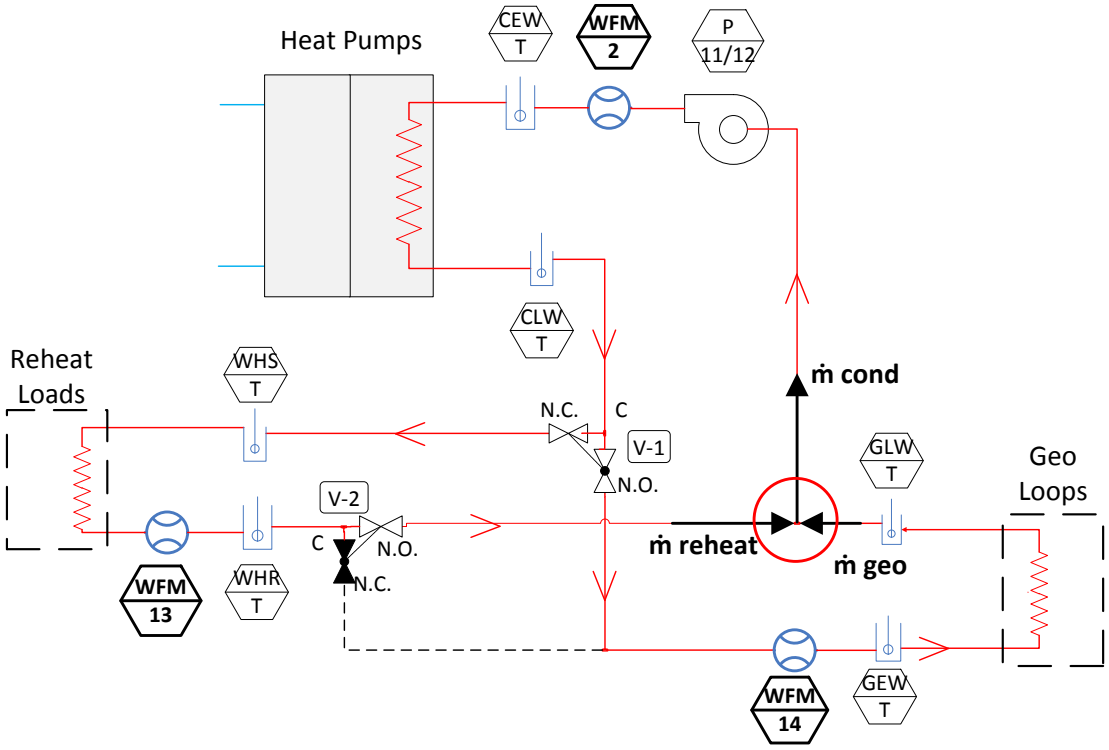

Figure 4-32 - Mass Balance Diagram on the Heat Rejection Loops, the location of the mass balance is circled in red

Because there were no other inputs, outputs, or storage of water flow during the steady operation of the system, the mass flow would balance according to:

$$\dot{m}_{Cond} = \dot{m}_{Reheat} + \dot{m}_{Geo} \quad \textbf{(4-4)}$$

The water mass flow through each loop was calculated using the measured volumetric flow rates and the water density at each flow meter, making the balance equation:

$$\dot{V}_{WFM2}\rho_{WFM2} = \dot{V}_{WFM13}\rho_{WFM13} + \dot{V}_{WFM14}\rho_{WFM14} \quad \textbf{(4-5)}$$

The change in density of water between the flow meter locations was calculated for wide operating temperature and pressure conditions using thermophysical property data for water

programmed into EES.[40] It was determined that the water density changed as much as 0.3%, therefore it was reasonable to approximate the water density as constant, simplifying Eq. (4-4) into:

$$\dot{V}_{WFM2} = \dot{V}_{WFM13} + \dot{V}_{WFM14} \quad \textbf{(4-6)}$$

Thirty-minute averages of the flow measurements were used to eliminate discrepancies in the travel time between the flow meters. Shown in Figure 4-33, the flow measured by WFM-2 was 2% different on average than the sum of flows from WFM-13 and WFM-14. The agreement between the flow measurements was within the measurement uncertainties of the flow meters.

[40] To simulate wide operating conditions, a maximum water pressure drop (30 ft H_2O) and maximum water temperature rise (20°F) across the HP condenser was used to calculate the difference between the water density at the condenser inlet (near WFM-2) and the geo-field inlet (near WFM-14).

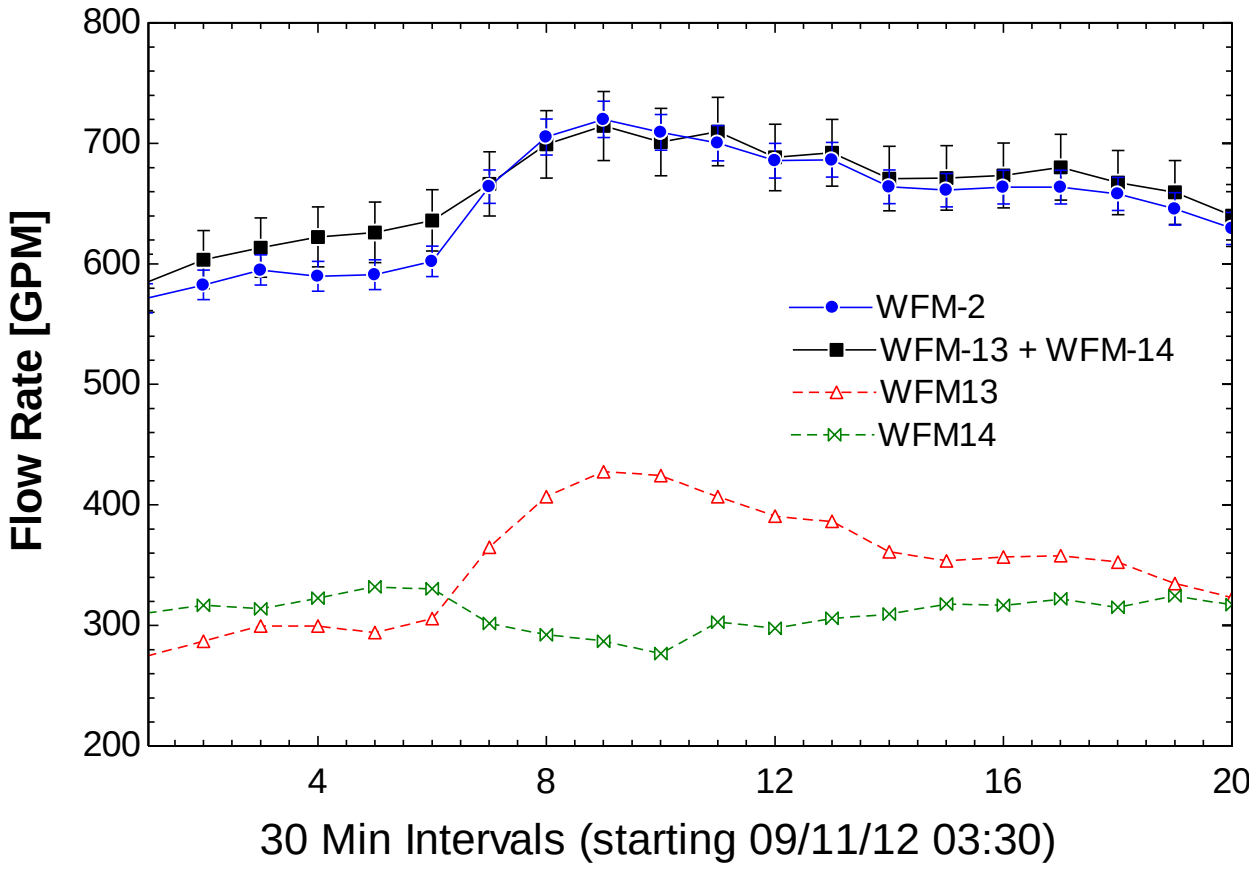

Figure 4-33 - Condenser, reheat, and geo-loop flow rates when V-2 was closed to bypass geo-field

The redundancy of the flow meters on the heat rejection loops allowed for mass balance comparisons during all modes of operation. Due to a lack of redundant flow meters, independent water flow verifications were not possible for the flow meters on the chilled water side of the heat pump. The heat pump and chilled water energy balance comparisons discussed in the following sections provide additional verification for both the chilled water and heat rejection water sides of the HP.

4.4.2 Energy Balance on the Heat Pumps

As a means of additional measurement verification, the measured cooling rate, heat rejection rate, and electrical power consumption of the heat pumps were used to determine if energy balances were observed in accordance with conservation of energy principles. The energy transfers and relevant measurement instrumentation for the heat pump energy balance are shown in Figure 4-34.

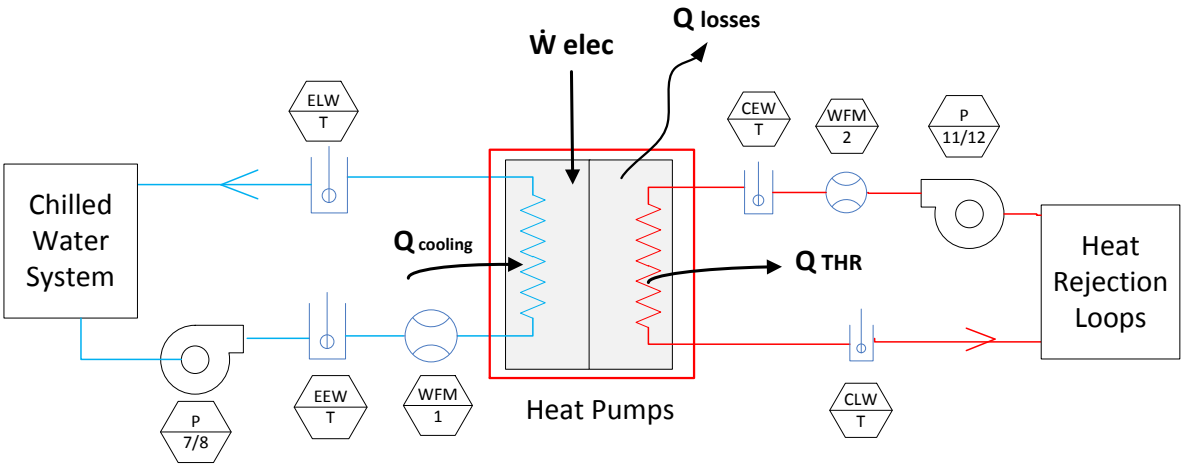

Figure 4-34 – Measured Energy Balance around the Heat Pumps

For heat pumps operating steadily, the measured energy rates would obey the first law if conformed to:

$$\dot{Q}_{cooling} + \dot{W}_{elec} = \dot{Q}_{THR} + \dot{Q}_{losses} \quad \textbf{(4-7)}$$

where $\dot{Q}_{cooling}$ is the measured HP cooling–Eq. (A-1),

$\dot{Q}_{THR}$ is the measured HP total heat rejection,

$\dot{W}_{elec}$ is the measured HP power consumption in kW,

and $\dot{Q}_{losses}$ is the thermal energy transferred from the equipment to the ambient.

The $\dot{Q}_{losses}$ term was not measured and was estimated to be small. To make direct comparisons, the thermal energy rate terms in Eq. (4-7) were converted to consistent units of kW using the following:

$$\dot{Q}_{cooling}[kW] = \dot{Q}_{cooling}[tons]\ 3.516852\frac{kW}{tons} \quad \textbf{(4-8)}$$

$$\dot{Q}_{THR}[kW] = \dot{Q}_{THR}\left[\frac{MBtu}{hr}\right]\ 0.2931\frac{kW\ hr}{MBtu} \quad \textbf{(4-9)}$$

As with the mass balances discussed in Section 4.4.1, measured data were averaged over 30-minute intervals to attempt to remove errors caused by system transients. Data from time periods when relatively large water temperature differences across the HP condensers and evaporators were desirable due to the higher measured certainty.

In Figure 4-35, the left and right side results of Eq. (4-7) are plotted for twenty consecutive 30-minute intervals. The uncertainties displayed in the figure were calculated using sensor measurement uncertainties as discussed in Appendix A. As shown, the sum of the measured HP energy rate inputs $(\dot{Q}_{cooling} + \dot{W}_{elec})$ was on average 15% larger than the measured energy rate out of the HP $(\dot{Q}_{THR})$. The data used in the calculation are provided in Appendix C.

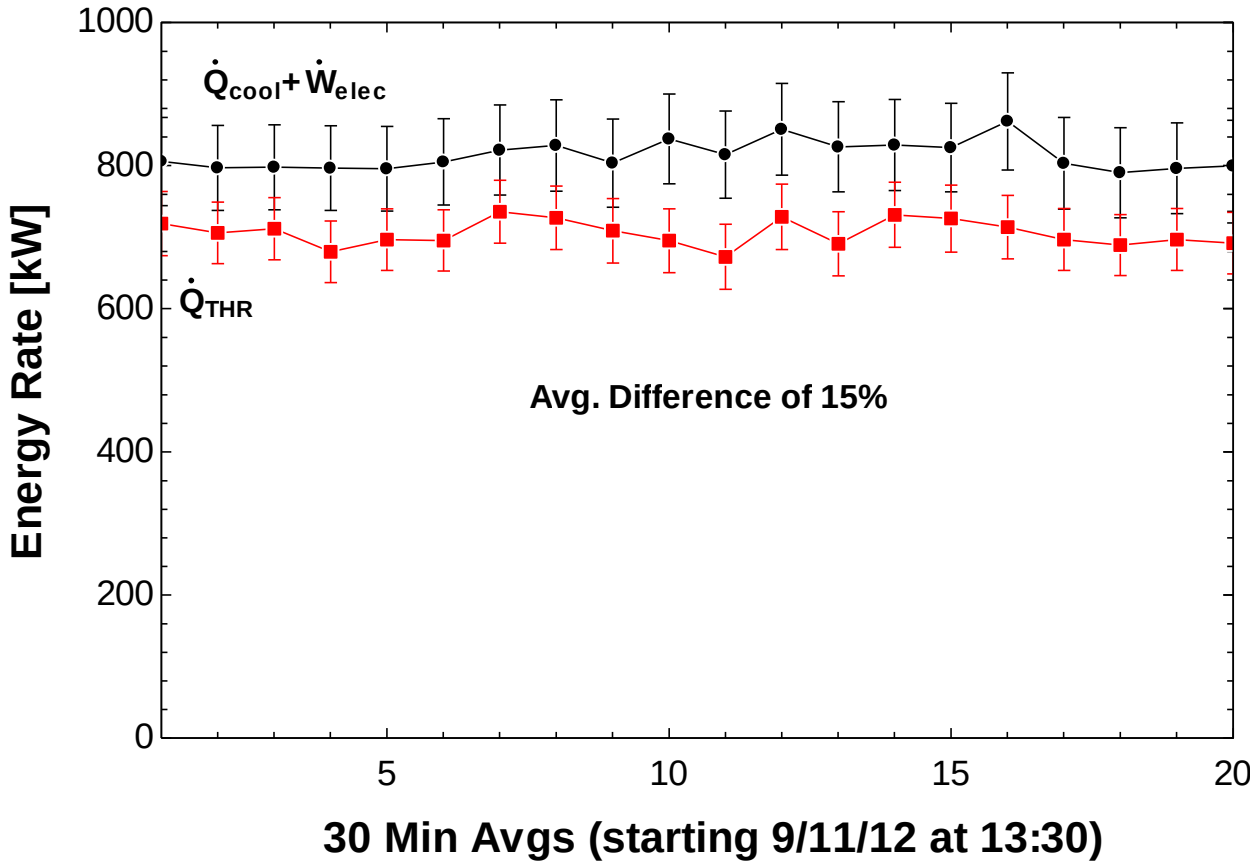

Figure 4-35 - Heat Pump Energy Balance at High Cooling Load

The results of the HP energy balance were encouraging. A larger measured energy rate input to the HPs was reasonable, as ambient heat losses from the equipment (i.e. the heat rejected by the cooling fans on the heat pump electronics) were unaccounted for in the above measurement data.

A second HP energy balance comparison is plotted in Figure 4-36 for a time period where the HPs were operating at low cooling load conditions. The water temperature differences across the evaporators and condensers were small at low load conditions; therefore the measurement uncertainties were high. The left and right sides of Eq. (4-7) were observed to be within 20%

and within measurement uncertainty. As with the high cooling load energy balance, the measured energy inputs showed slightly larger than the measured outputs, staying within reasonable expectations for measured error due to unaccounted for energy losses. The data used in calculating the low cooling load energy balance are provided in Appendix C.

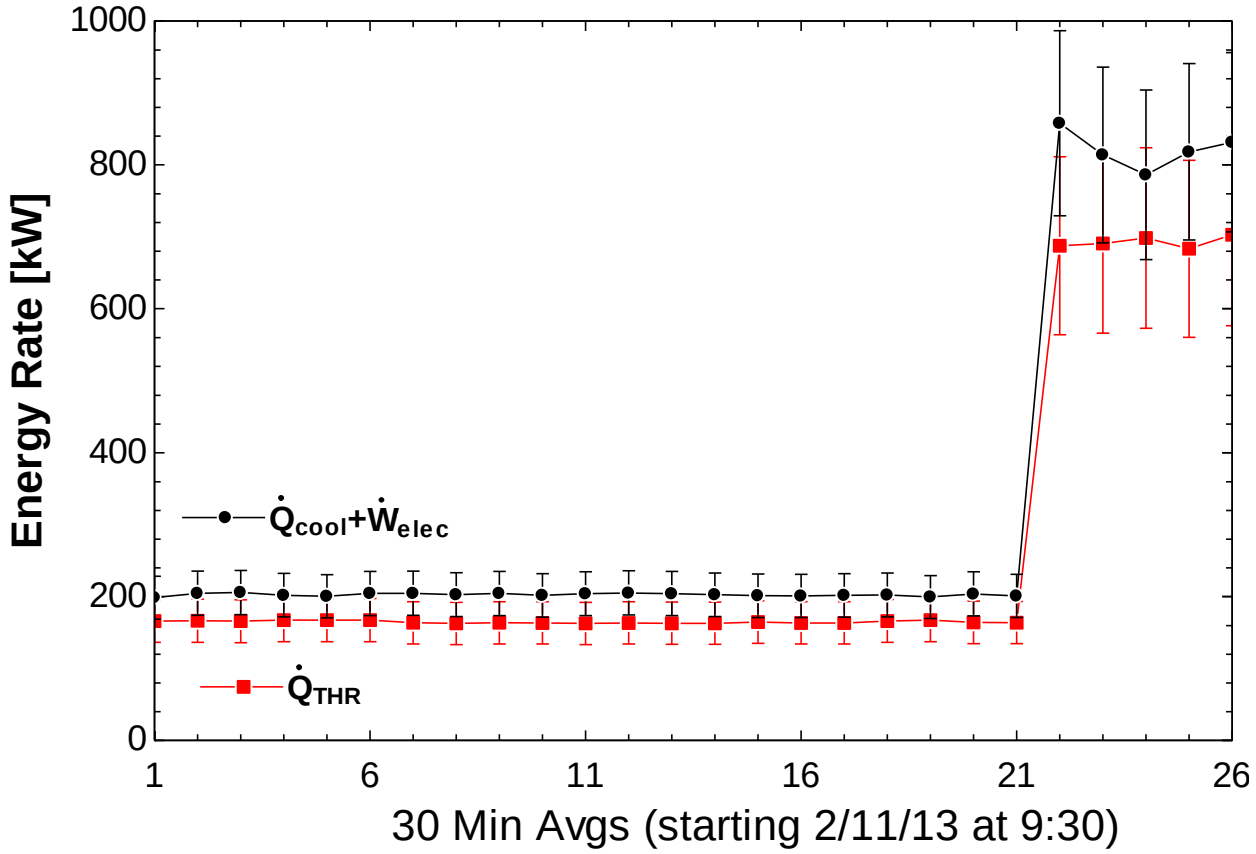

Figure 4-36 - Energy Balance at Low Cooling Loads

The measured cooling, electrical power consumption, and total heat rejected by the heat pumps were integrated for time periods of one month and compared as in Eq. (4-7). All terms were converted to consistent units of watts using Eqs. (4-8) and (4-9). The results indicated that the energy balanced within 10% on average, with the inputs consistently larger than the

measured outputs (i.e. obeyed Second Law) and the integrated energy inputs and outputs were within measurement uncertainty for most months. The data is shown in Figure 4-37.

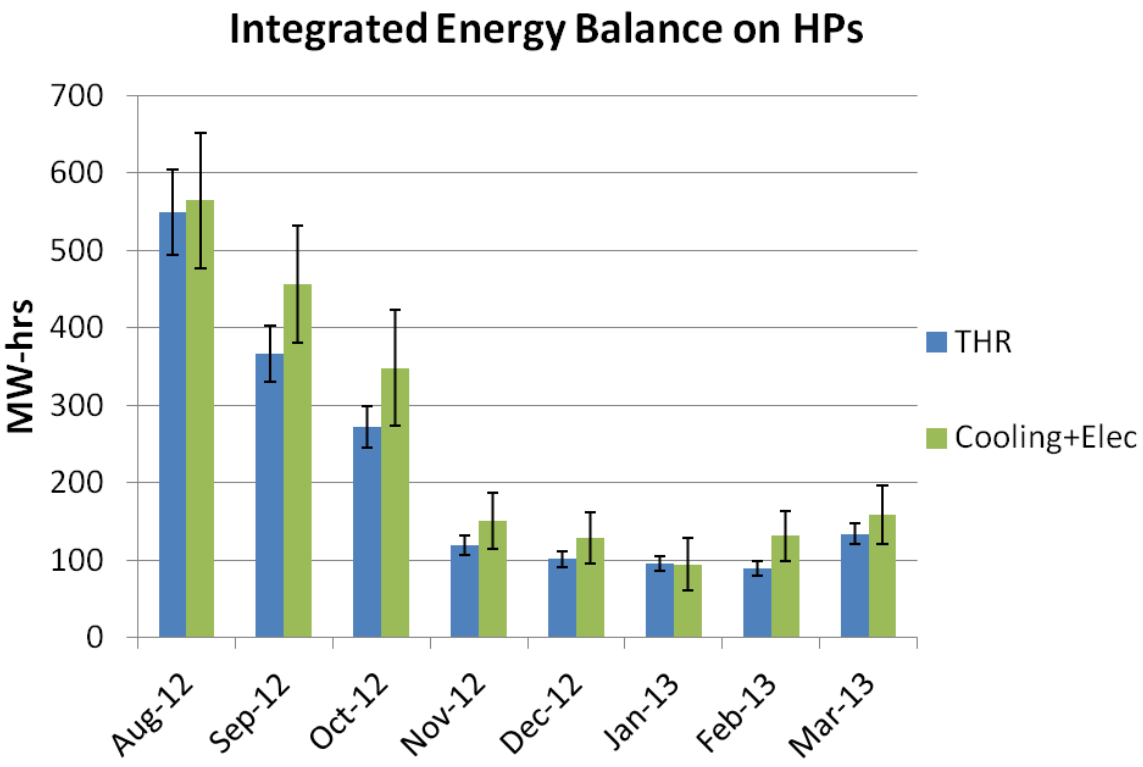

Figure 4-37 - Integrated Energy Balance on HPs

4.4.3 Heat Rejection and Chilled Water Loop Energy Balances

Additional opportunities existed to verify the measurements used to measure the energy rates within the system. In this section, four scenarios are presented that allowed for measured energy balance checks. The measured heat transfer within the heat rejection loops (recovered reheat and geo-field) could be compared at three different system configurations: (1) reheat and geo-field heat rejection occurred in series; (2) the reheat and geo-field heat rejection

occurred in parallel; and (3) the geo-field was the only available heat rejection. Lastly, the cooling energy supplied to the building loads could be compared (i.e. balanced) against the measured cooling supplied by the heat pump and the campus chilled water loop.

The energy balances presented in this Section are similar in their methodology to each other and to the HP energy balances of 4.4.2. For brevity, only the first energy balance scenario will be discussed in detail. The following energy balances will be presented in an abbreviated format where: a brief description and system schematic are given indicating the locations of sensors used in the relevant measurements; an equation is provided to show how the energy balance was performed; and the resulting data are provided in a figure along with measurement uncertainties.

As shown in Figure 4-38, the rejection loops could be configured such that the reheat and geo-field energy transfer occurred in parallel (i.e. the return water from the recovered-to-reheat loop was directed to the geo-field for additional cooling). Assuming no pipe heat loss or system water leaks within the heat rejection loops, the total heat rejected from the HP condensers would necessarily equal the heat recovered to the reheat loop plus the heat rejected to the geo-field:

$$\dot{Q}_{THR} = \dot{Q}_{Reheat} + \dot{Q}_{Geo} \quad \textbf{(4-10)}$$

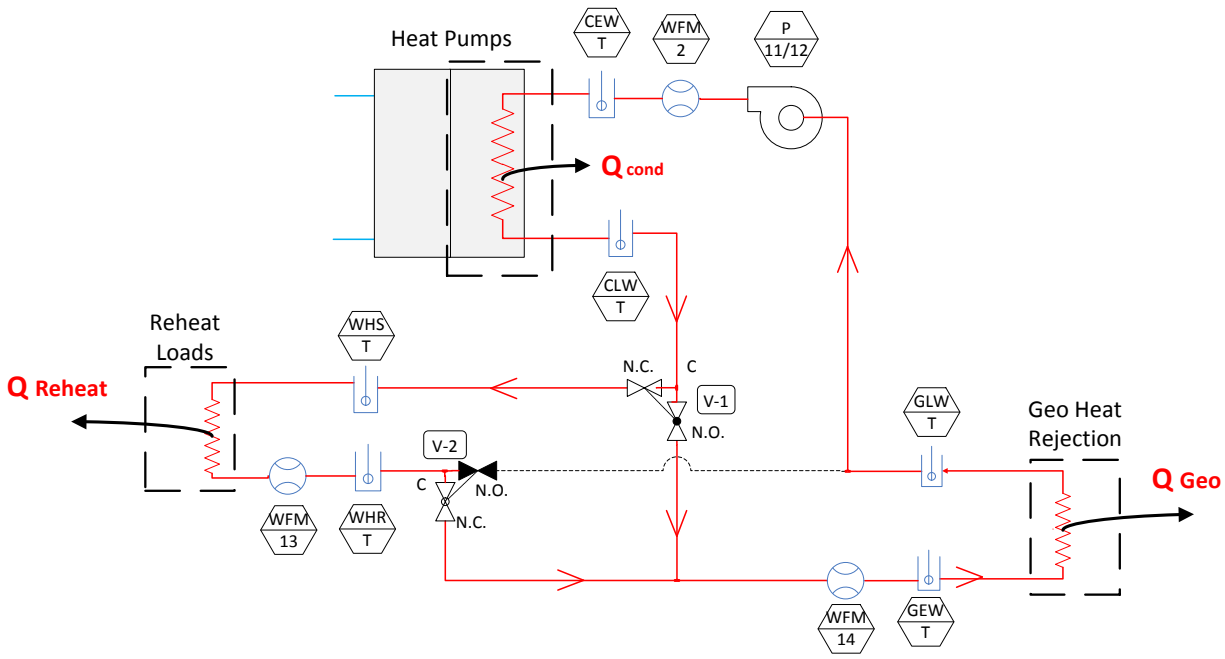

Figure 4-38 - Energy Balance on System Heat Rejection Loops, Reheat and Geo in Series

The terms in Eq. (4-10) were calculated with measured data and it was observed that the left and right sides agreed within 1% on average. The results are plotted in Figure 4-39 and the measured $\dot{Q}_{Reheat}$ and $\dot{Q}_{Geo}$ are included in the Figure to show the proportion of heat rejection during the time period. The data used in the calculation are provided in Table .

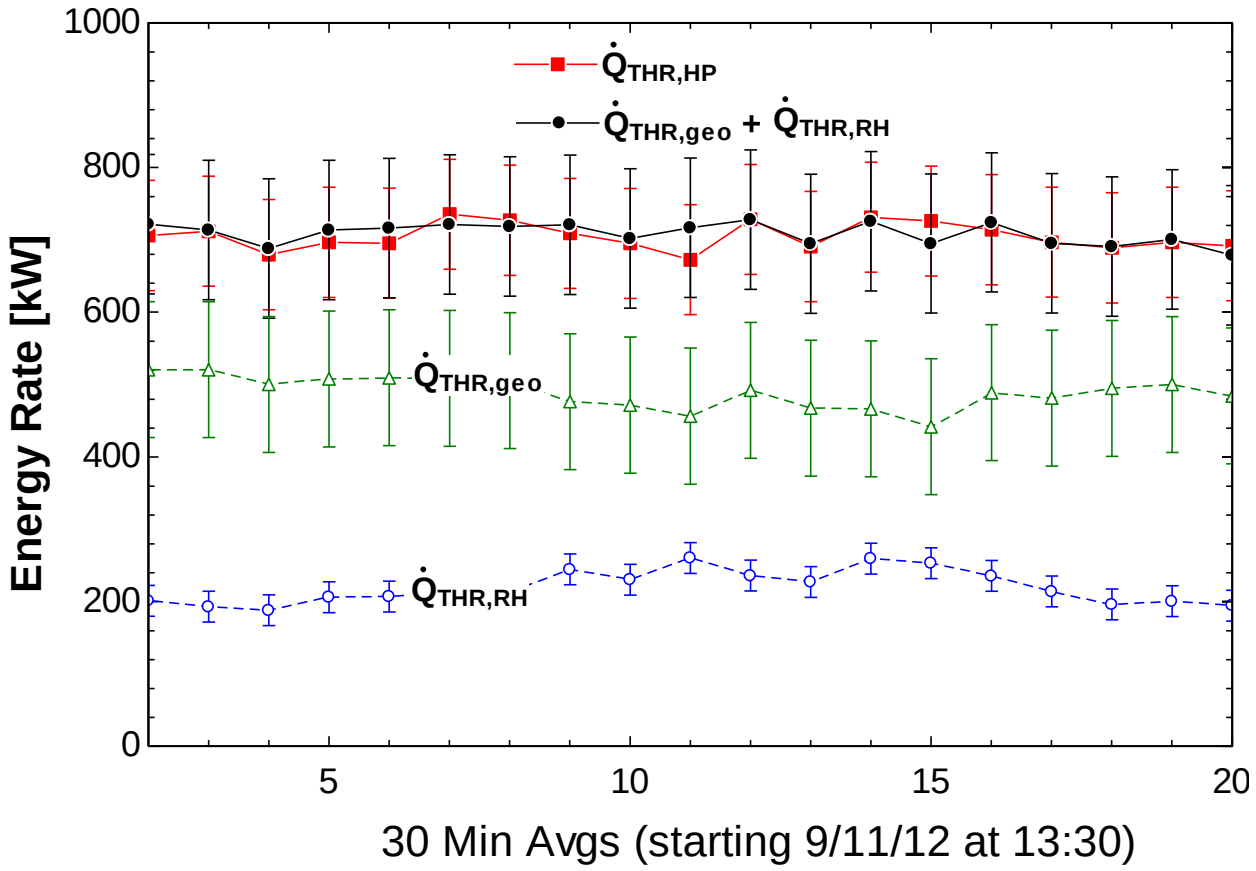

Figure 4-39 - Measured heat rates for the HP condenser heat rejection and the sum of the heat rejection loops.

As shown in Figure 4-40, the heat rejection loops would also operate such that the recovered-to-reheat system was in parallel with the geo-field (i.e. return water from the recovered-to-reheat loop bypass the geo-field). Because the geo-field and reheat loops were the only systems allowing heat rejection, the measured total heat rejected from the HP condensers should equal the sum of the measured heat rejected to the reheat and geo-loops, and Eq. (4-10) was used for confirming energy balanced appropriately.

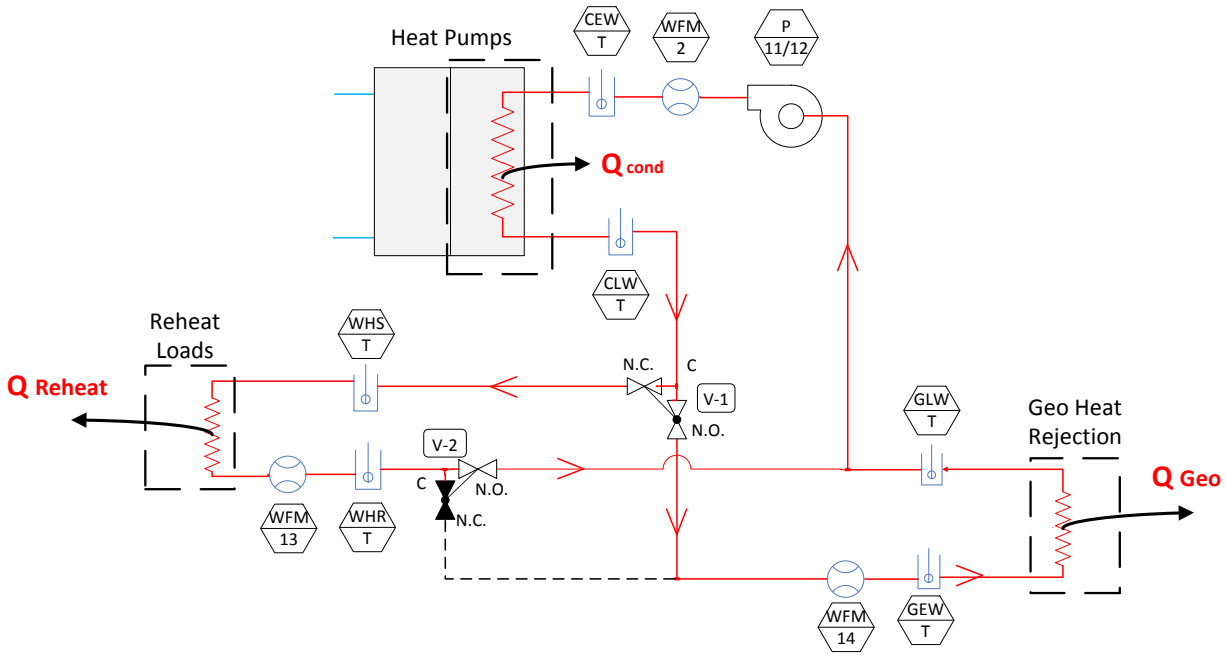

Figure 4-40 - Energy Balance on Heat Rejection Loops, Geo and Reheat in Parallel

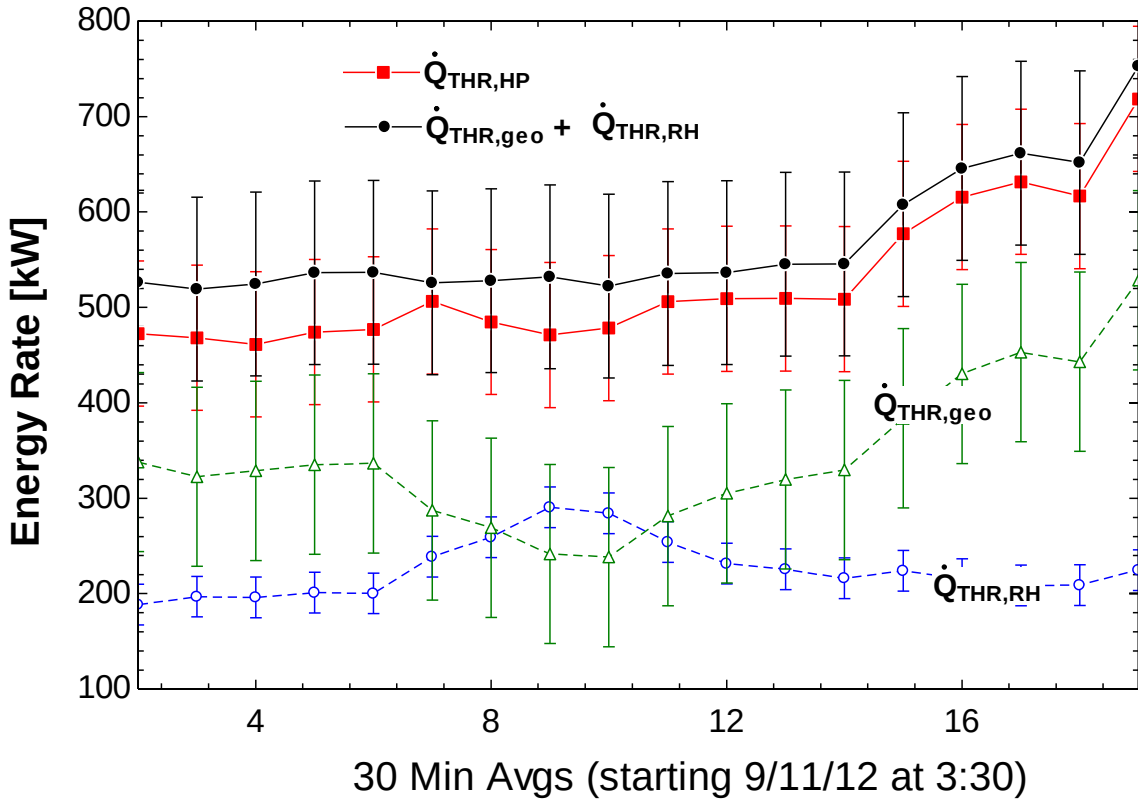

Figure 4-41 – Heat Rejection Energy Balance, Geo and RH Loops in Series

As shown in Figure 4-42, the final configuration of the heat rejection loops was such that the condenser water was too cool for use as reheat and the geo-field was the only system used for heat rejection, suggesting that the heat rejected from the HPs must equal the measured heat rejected by the GHX. An example of the "geo-field only" energy balance scenario is presented in Figure 4-43.

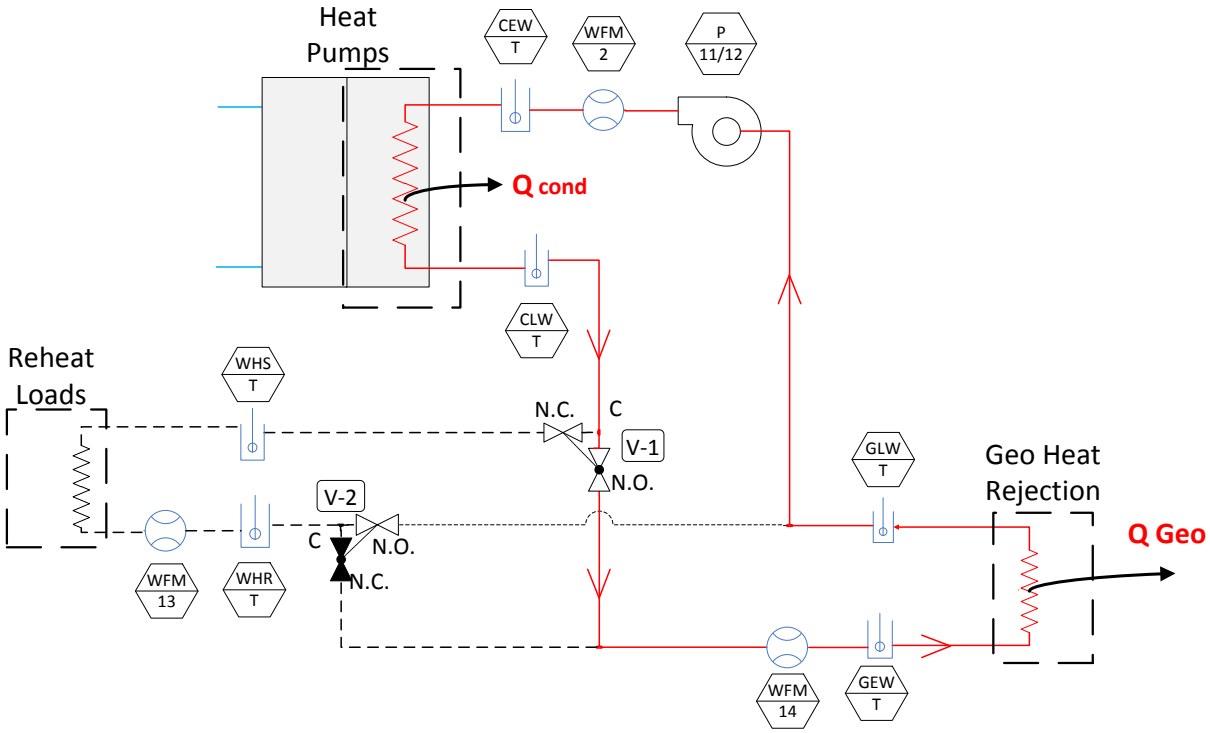

Figure 4-42 - Heat Rejection Energy Balance, Geo-Loop Only

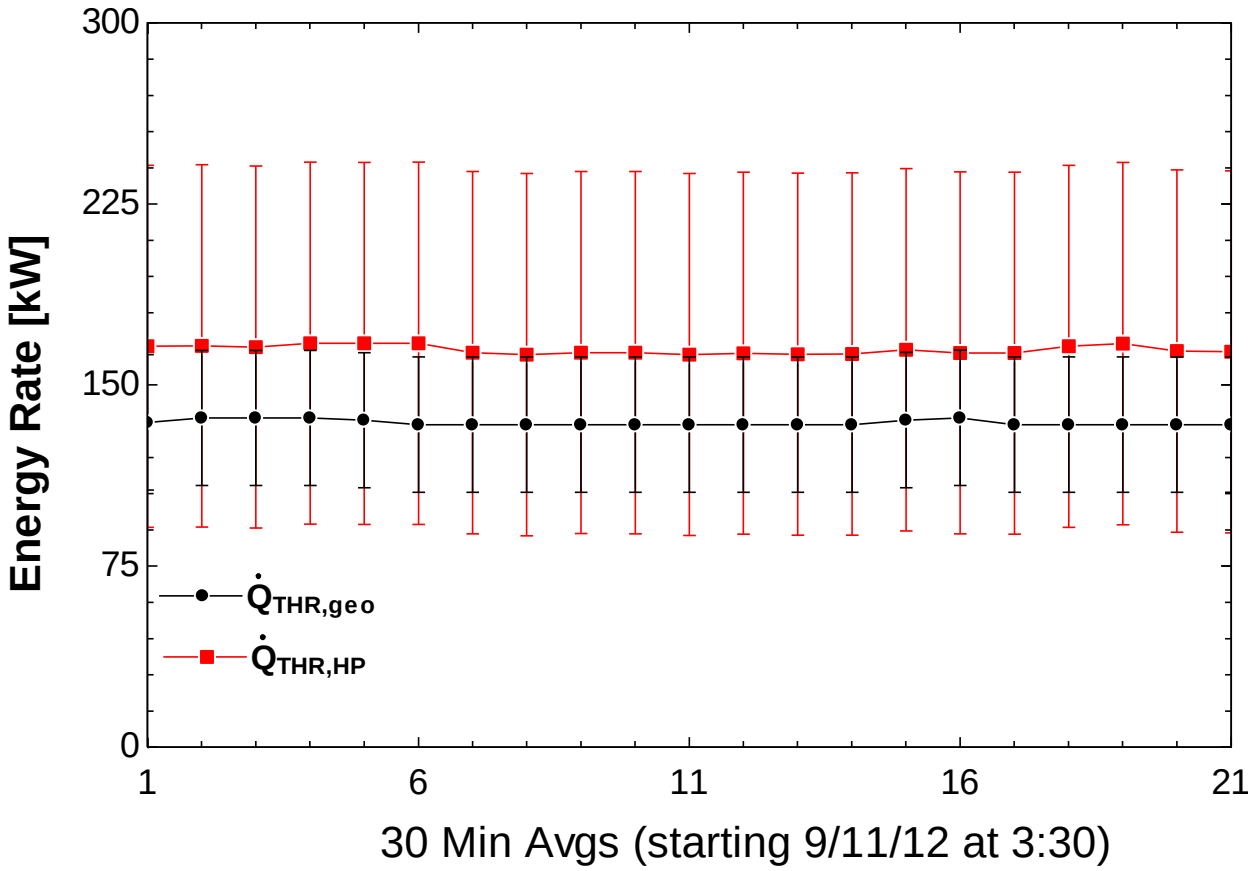

Figure 4-43 - Heat Rejection Energy Balance, Geo-Loop Only

The final heat energy balance verification for the heat rejection loops was tested using the integrated energy measured at the HP condensers, recovered-to-reheat, and geo-field over time periods of one month. The monthly integrated values for the HPs total heat rejected were compared against the sum of the measured integrated energy rejected to the reheat and geo loops. The results showed that the energy balanced within 4% on average and the energy inputs and outputs agreed within measurement uncertainties. The data are shown in Figure 4-44.

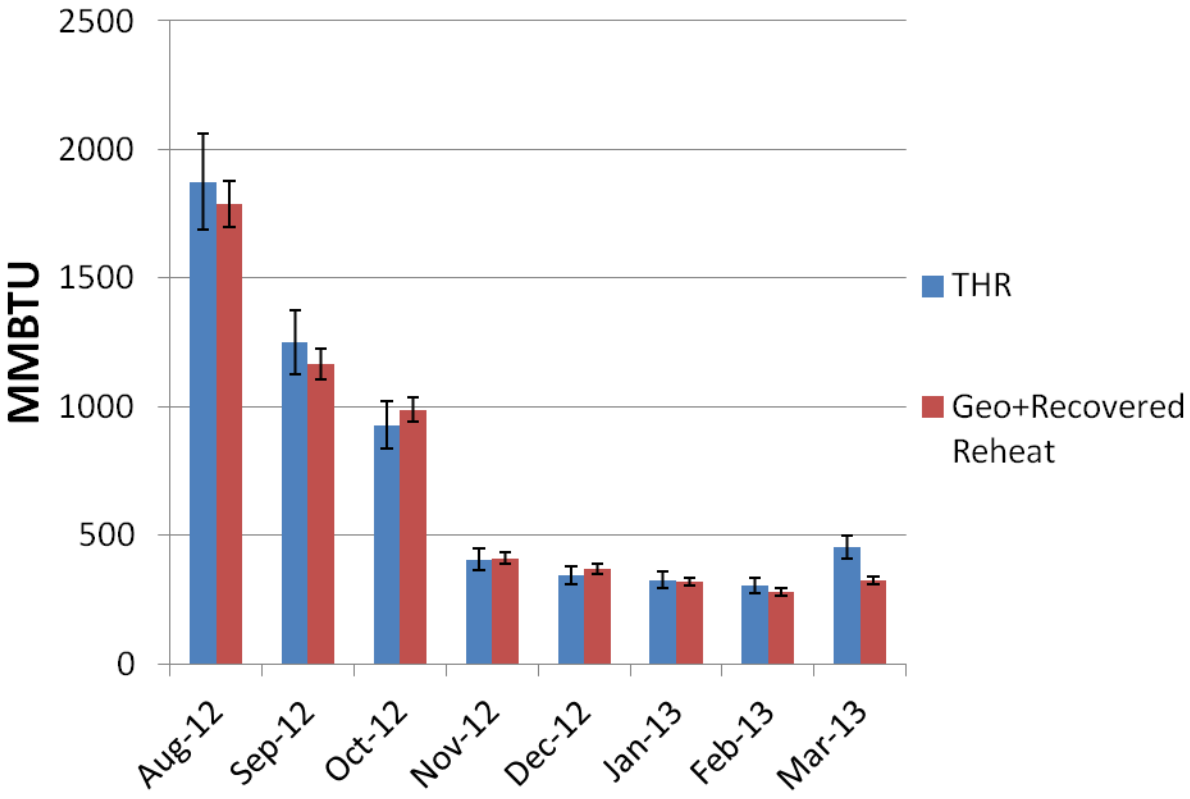

Figure 4-44 - Integrated Heat Rejection Energy Balance

Though it was not a completely independent energy balance comparison, the measurements on the heat pump and campus chilled water supplies could be further verified using downstream temperature sensor BCS-T (see Figure 4-45).

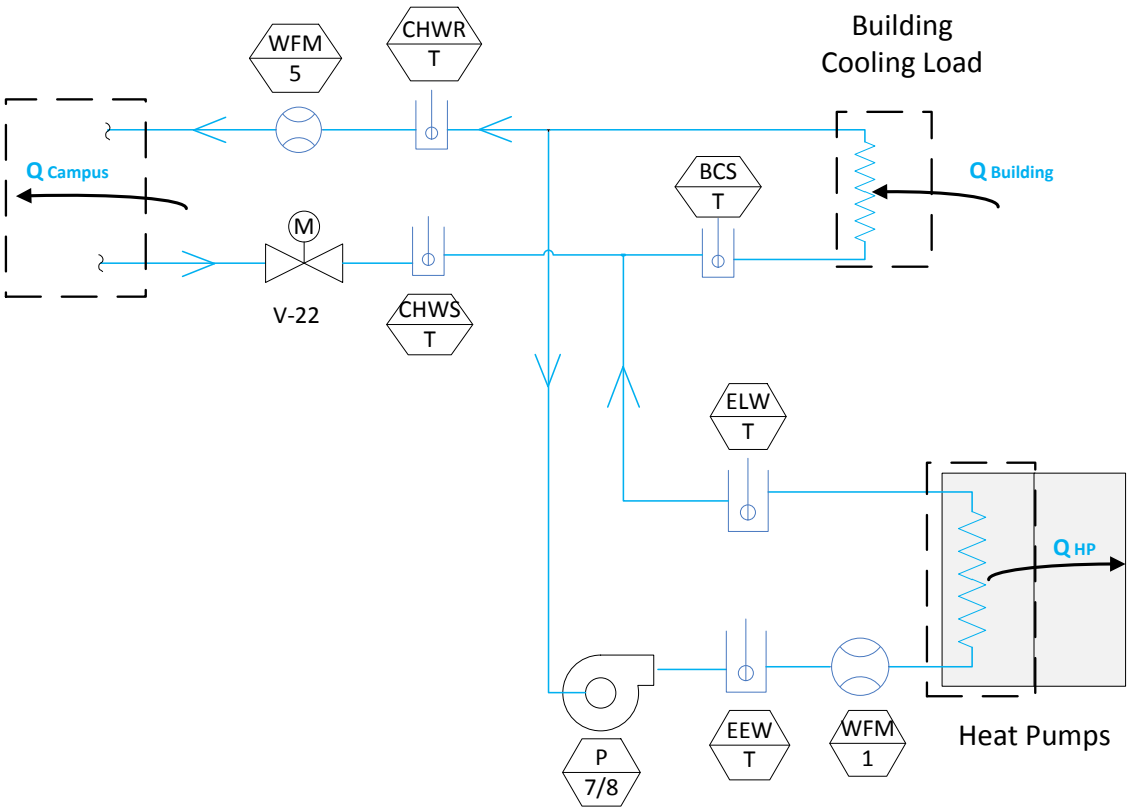

Figure 4-45 – Chilled Water Energy Balance

Measurements of the total supplied chilled water flow rate and the return water temperature from the aggregate building cooling load were not available to make the energy balance completely independent.

The measured cooling rates would balance if conformed to:

$$\dot{Q}_{HP} + \dot{Q}_{campus} = \dot{Q}_{Bldg} \tag{4-11}$$

The measured cooling supplied to the building ($\dot{Q}_{Bldg}$) was calculated using:

$$\dot{Q}_{Bldg} = \left(\dot{V}_{WFM1} + \dot{V}_{WFM5}\right)\rho_{chw}c_{p,chw}(T_{return,avg} - T_{BCS}) \tag{4-12}$$

where $\dot{V}_{WFM1}$ and are the measured evaporator and campus water flow rates in m^3/s,

ρ_{chw} and $c_{p,chw}$ are the density and specific heat of water in SI units at an average conditions,

$T_{return,avg}$ is the average water temperature in K of sensors EEW-T and CHWR-T,

and T_{BCS} is the water temperature measured by sensor BCS-T in K.

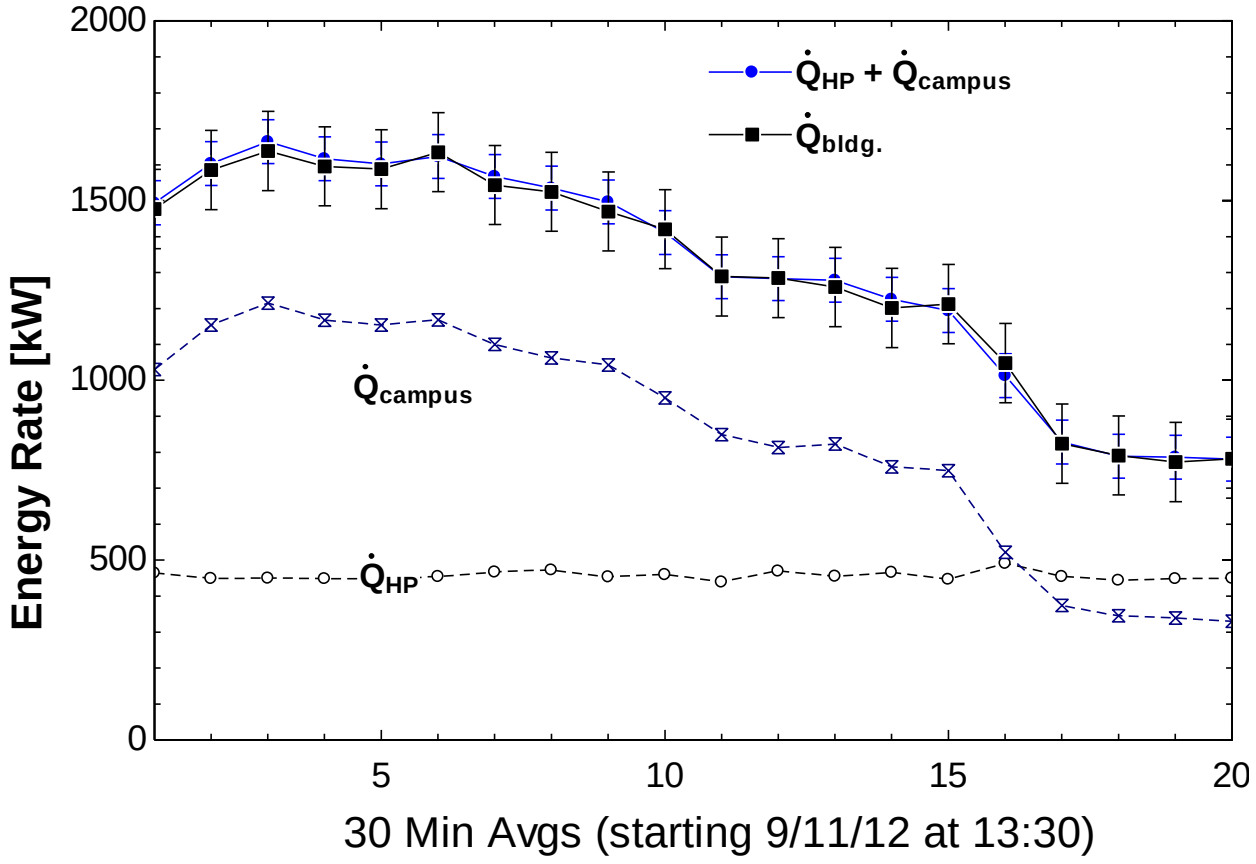

Figure 4-46 - Chilled Water Energy Balance

4.5 Conclusions

The steps used to verify the research sensors produced several sensor measurement corrections. Where necessary, single-point calibrations were defined for the temperature sensors and the calibrated sensor measurements were compared at varying system conditions. Flow meter verifications revealed that all but one flow meter agreed reasonably well with an

ultrasonic flow meter. Due to the close proximity of a pipe elbow and the results of the UFM comparison tests, it was determined appropriate to increase the measurement uncertainty for flow meter WFM-1 from the manufacturer-rated uncertainty of ±2% (of reading) to ±10% (of reading).

The steps to "field-verify" the sensors (i.e. physically removing instrumentation) proved to be a crucial step in the sensor verification process and also the most rewarding. It was found that some temperature sensors were not installed appropriately, including one sensor which read nearly 6°F higher than actual due to deficient installation depth in the thermowell. It was also found that the flow meters monitoring the evaporator and condenser water flow rates were connected to the wrong control data point in the BAS, and subsequently had been calibrated improperly. A significant number of test hours were spent in vain due to the sensor installation issues that were not uncovered until the sensors were field-verified. It is highly recommended for future research to perform sensor field-verifications as a first and fundamental step in the verification process. All sensor calibration and data corrections identified in this Chapter were performed post-data collection, meaning that no changes were made to the controls or data-logging systems.

Chapter 5. Cooling Mode Performance Analysis

5.1 Introduction

Following the installation of additional sensors in July 2012, a performance analysis of the ground-coupled heat pump (GCHP) system in the base operating mode (cooling with heat recovery) was conducted. Chapter 4 presented the means and methods used to verify and validate the instrumentation installed. This chapter outlines the procedures used to compare the field-measured performance of the heat pumps with the manufacturer-expected performance (i.e. rated performance "as-sold"). The measured performance of the WID GCHP system in cooling mode was then compared to other cooling alternatives at the WID. The results of this chapter were used to explore operational strategies for cooling the WID in subsequent chapters. To simplify the reading, the equations used to calculate the quantities presented in this chapter are located in Appendix A and referred to where appropriate. The propagated uncertainties of the measured quantities presented in this chapter are discussed in Appendix A.

5.2 Comparative Analysis of Heat Pump Performance

The in-situ measures of performance for the WID heat pumps during cooling mode operation included cooling capacity and efficiency. The field-measured cooling capacity and efficiency are compared against the manufacturer-predicted capacity and efficiency. Details regarding the equipment specifications of the heat pumps can be found in Appendix B.

5.2.1 Defining Steady Data

In order to establish higher confidence level in the field-measured performance data, steady HP operation is desirable. The criteria for steady state HP operation are based on AHRI Standard 550. (AHRI 2011) For the purposes of the present study, steady state heat pump

operation is a time span of at least forty minutes that satisfied the following criteria: (1) none of the heat pump compressors in the system experienced a change of status (on/off); (2) entering and leaving chilled water and condenser water temperature measurements (four measurements total) do not vary by more than 1°F; and (3) the chilled water flow rate does not vary by more than 1% from the average over the steady state time interval. All measured data were sampled at ten minute intervals, synchronous in time, and recorded on the IBA system.

To verify that heat pump compressors did not cycle on or off during the steady time period, the on/off status Change of Value (COV) for all twelve heat pump compressors were recorded. When an individual compressor within a HP module was energized, the heat pump master computer reported a status change for that compressor, recorded on the IBA as a value of one. Similarly, a value of zero was recorded for each individual compressor when it was cycled off. The compressor status COV points were recorded instantaneously and at disparate times. Therefore, it was necessary to time-synchronize the compressor status data in order to identify steady state periods. Over the month of September, two thousand COV compressor status values were recorded, indicating that the average duration the heat pumps operated steadily was around 20 minutes. An example of the compiled compressor status value tables that were used in identifying steady HP operation is provided in Figure 5-1, where one steady time period is shown at 2:31:09 PM with ten compressors enabled.

Time	M6-2	M6-1	M1-2	M1-1	M3-2	M3-1	m4-1	M4-2	M2-1	M2-2	M5-2	M5-1
9/18/12 2:21:56 PM CDT	Off	Off	On	On	Off	On	Off	Off	On	On	Off	Off
9/18/12 2:23:13 PM CDT	Off	Off	On	On	On	On	Off	Off	On	On	Off	Off
9/18/12 2:24:31 PM CDT	Off	Off	On	On	On	On	On	Off	On	On	Off	Off
9/18/12 2:27:24 PM CDT	Off	Off	On	On	On	On	On	Off	On	On	Off	On
9/18/12 2:28:37 PM CDT	Off	Off	On	On	On	On	On	Off	On	On	On	On
9/18/12 2:31:09 PM CDT	On	Off	On	On	On	On	On	Off	On	On	On	On
9/18/12 3:19:21 PM CDT	On	Off	On	On	On	On	On	Off	On	On	Off	On

Figure 5-1 – Compiled HP compressor status values for all twelve compressors (six HP modules)

Thirteen separate sets of measured HP data from the month of September were identified as meeting the steady state criteria identified above. The measured values for the variables used in the cooling performance validation were averaged over the time period for each steady dataset and those data are provided in Section 0. For each steady state data period, the measured HP cooling capacity was determined and compared with the manufacturer-predicted cooling capacity.

5.2.2 Manufacturer-Predicted and Measured Cooling

Linear regression techniques were used to fit the performance data provided by the HP manufacturer. Additional data were requested from the manufacturer for certain operating conditions that were not published in the manufacturer's catalogs. All heat pump manufacturer performance data used in the present research are attached in Appendix D.

The manufacturer-predicted cooling capacity was determined as a function of the leaving chilled water and entering condenser water temperatures. Sixty-six points of manufacturer performance data were fit with a second-order polynomial with cross terms. All equations for the in-situ heat pump energy performance analysis are found in Appendix D, including: the measured cooling capacity of the heat pumps, the measured uncertainty, the equation

developed from fitting manufacturer-predicted cooling capacity data, the equation for the closeness of fit (R^2) for all equations developed from manufacturer performance data are provided in. Figure 5-2 shows the field-measured HP cooling capacity compared to the manufacturer-predicted cooling capacity for each of the thirteen steady state intervals identified during the month of September 2012.

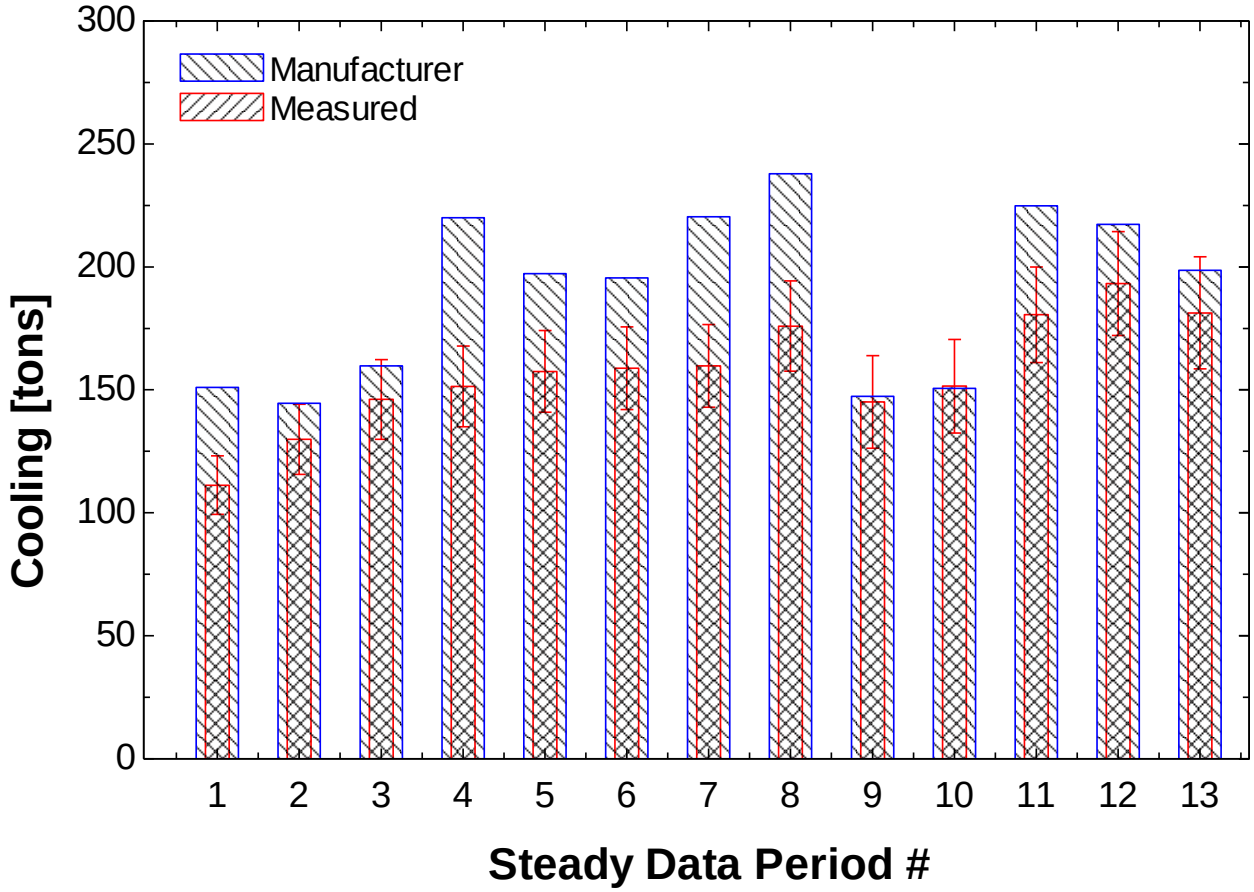

Figure 5-2 – Steady Data periods of measured and manufacturer cooling capacity

The variability in the cooling capacity is attributable to variations in the chilled water leaving temperature and the entering condenser water temperature. With one exception, the field-measured HP cooling capacity was less than the manufacturers-predicted cooling capacity. On average, the measured cooling capacity was 80% of the manufacturer rated performance.

Although the field-measured HP capacity was consistently lower than the manufacturers-rated capacity, six of the thirteen steady data periods did have the measured HP capacity agree with the manufacturer-s rated capacity within the span of measurement uncertainty.

Factors contributing to the difference in measured HP cooling capacity with manufacturer's rated cooling capacity were not immediately evident from the data collected, so additional investigation was required. By comparing the measured averages for each of the steady periods, the measured leaving chilled water temperature being maintained differed significantly from the chilled water set point (44°F). The average chilled water temperatures of each steady time intervals varied from 39°F to 51°F, indicating that the internal controls of the heat pumps may not have been operating as expected. As shown in Figure 5-3, no direct correlation was observed between the measured leaving chilled water temperature and the difference between the measured and manufacturer cooling.

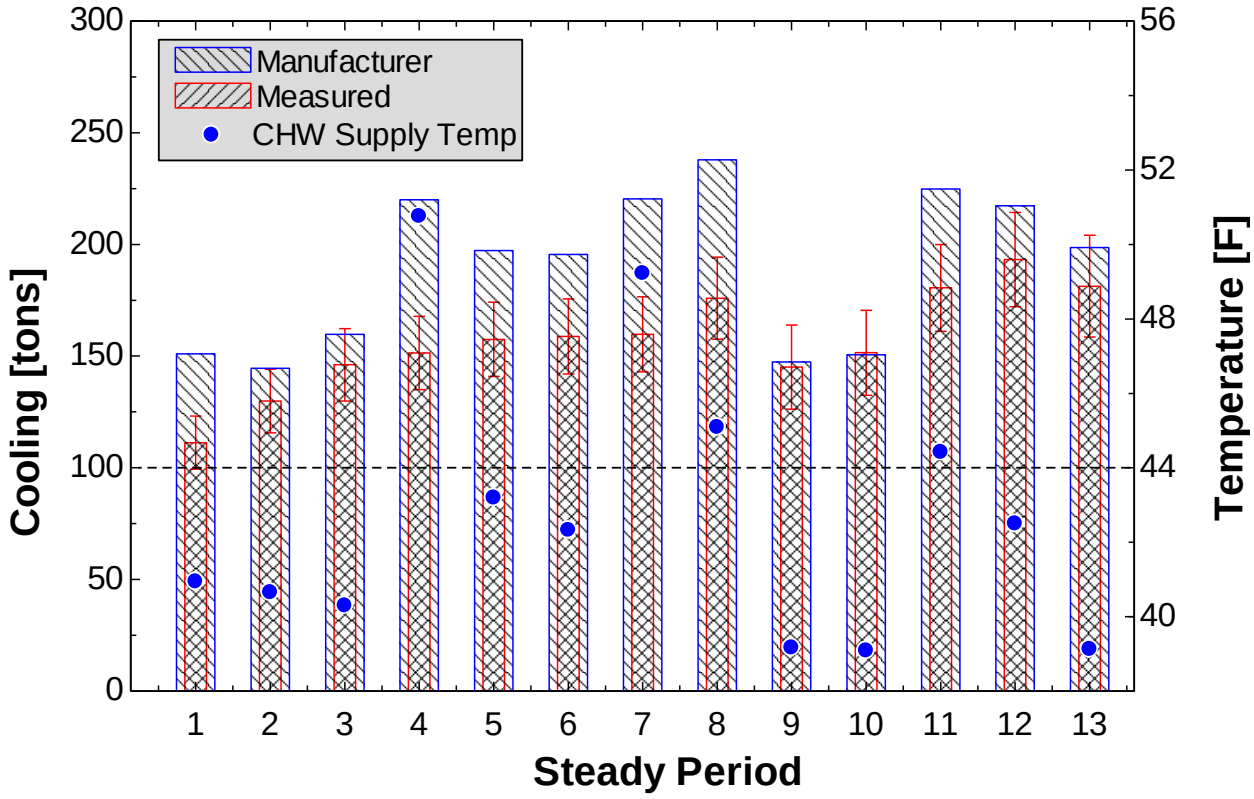

Figure 5-3 – Measured and Manufacturer Cooling, Including measured the chilled water supply temperature

5.2.3 Manufacturer and Measured Efficiency

The HP manufacturer also provides data for the electrical power consumption of the heat pumps at various operating conditions. The measured and manufacturer-predicted electrical consumption rates for the steady data periods were 1% different on average; indicating a strong agreement between the measurements and the manufacturer data. The data are shown in Figure 5-4.

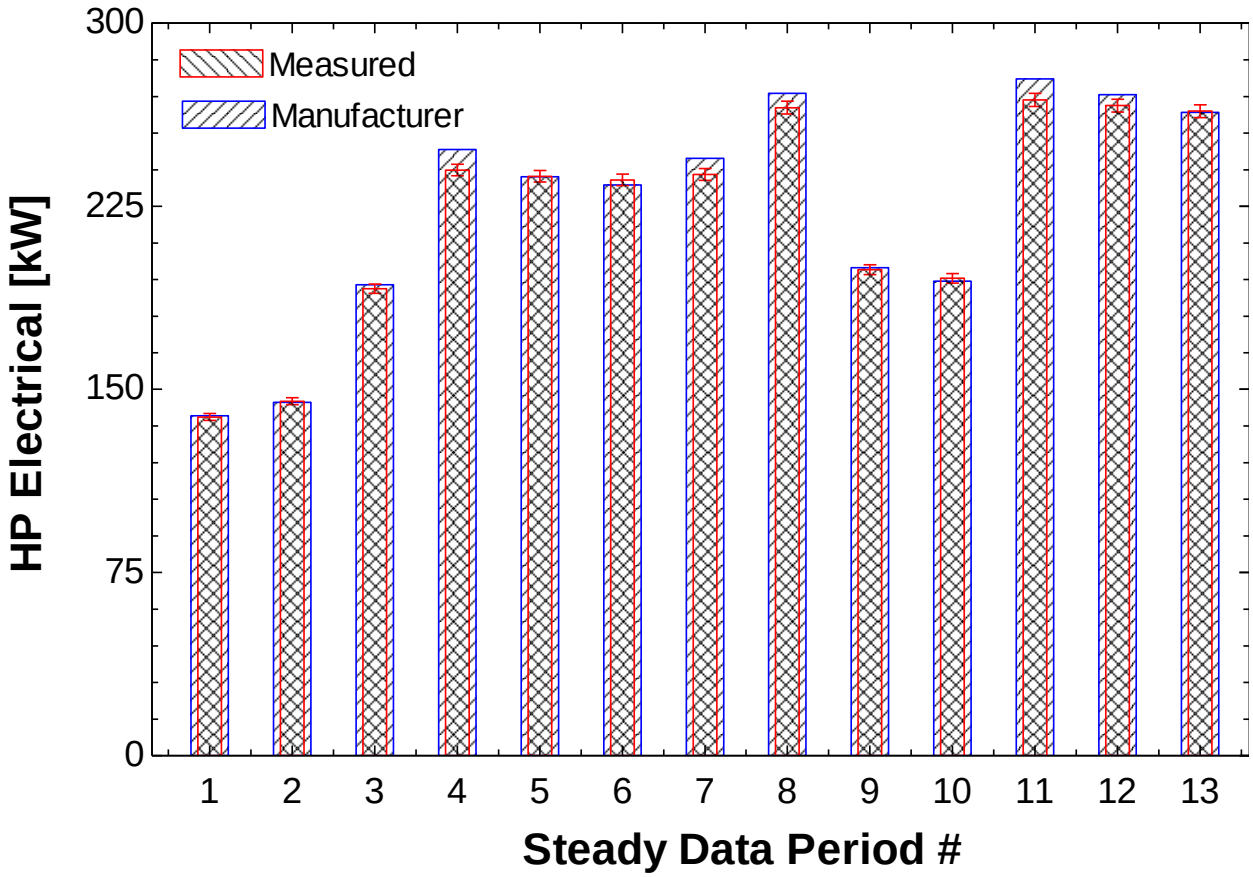

Figure 5-4 – Measured and Manufacturer Electrical Power Consumed by the Heat Pumps

The power and capacity data were combined to determine the HP efficiency. The HP efficiency is expressed as the unitless coefficient of performance, COP, (capacity over input power in consistent units). As expected, the measured heat pump COP for the steady data periods were, on average, 20% lower than the manufacturer-predicted efficiency values. Ten of thirteen measured values had COP values within the manufacturer prediction within the measurement uncertainty. The measured and manufacturer COPs for the steady data periods are provided in Figure 5-5.

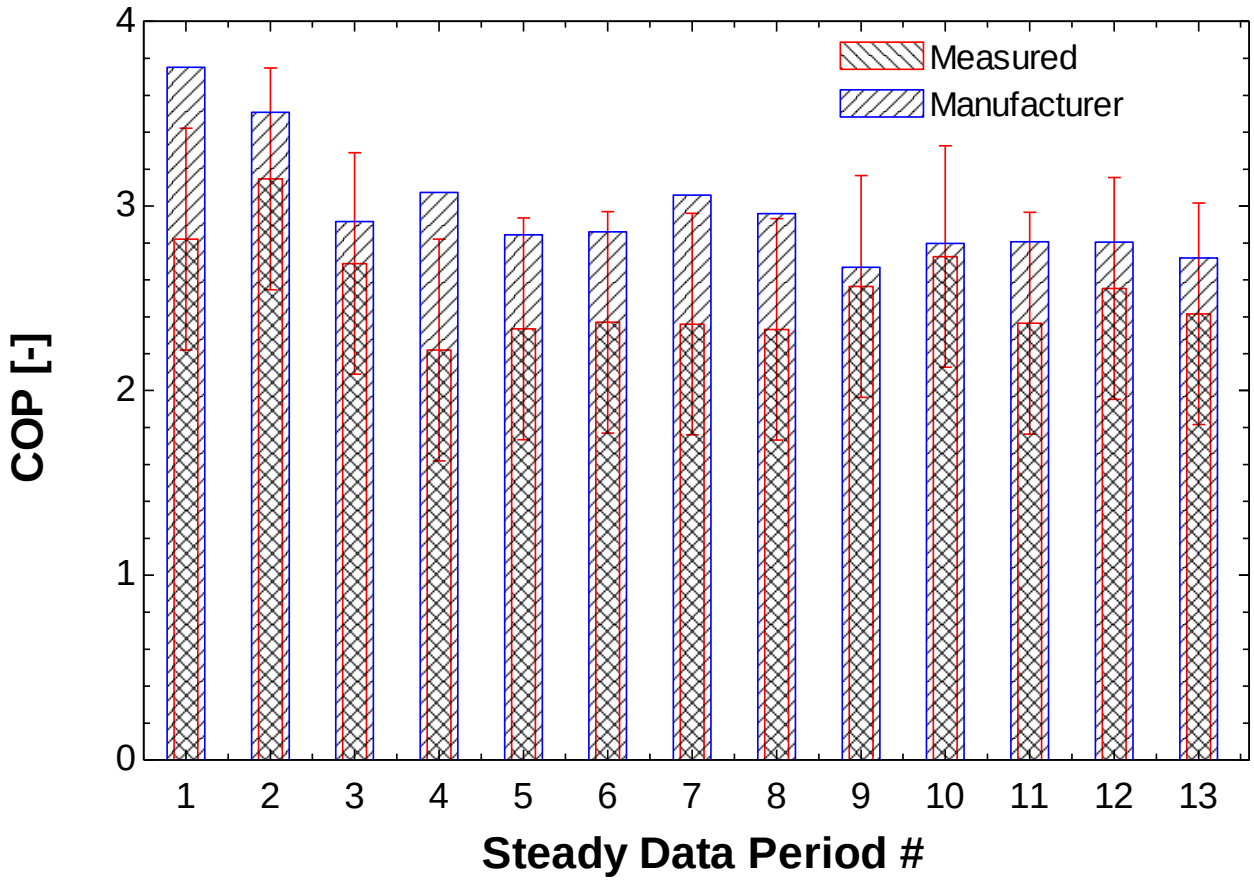

Figure 5-5 - Measured and Manufacturer Efficiency

The comparisons between the measured and manufacturer-predicted heat pump cooling performance indicated the machine operated at roughly 80% of the rated cooling capacity and efficiency, with an appreciable number of steady measurements within the manufacturer rating by the measurement uncertainty. Deviations from the heat pump chilled water set point suggested possible control issues and reasons for the degraded performance during steady and unsteady operation. Measured and manufacturer efficiencies for the steady data periods were observed lower than the efficiency at design conditions and set the expectations for the overall performance of the system. With the performance of the heat pump equipment

assessed, further analysis of the WID's overall cooling performance is discussed in the following sections.

5.3 Measured Performance of the Chilled Water Systems

The WID HP system is not capable of meeting 100% of the building's chilled water requirements. Consequently, a portion of the facility's cooling needs are met by the UW Campus district cooling system. One objective of the present research is to compare the measured efficiency of the GCHP system in cooling mode operation to the efficiency of cooling provided by the campus district cooling system. The proportion of cooling provided by the WID heat pumps and the campus chilled water system were measured independently using the respective supply chilled water temperature, return water temperature, and chilled water volumetric flow rates of each subsystem. All temperature and flow measurements related to the heat pumps were recorded synchronously in ten minute intervals and trended on the IBA.

5.3.1 Measured Peak and Integrated Cooling

As a means of substantiating the behavior of the building cooling load, the design peak cooling rates were compared with the measured peak cooling. The measured cooling capacities of the heat pumps or the campus chilled water supply were calculated using equations provided in Appendix A. The total cooling capacity provided to the building at any instant is the sum of the cooling rate provided by the HPs and campus chilled water. The peak total cooling load measured during the present research was 2334 tons which was very close to the estimated (design) peak cooling load of 2395 tons. The peak cooling capacity observed for the heat pumps was 321 tons which is 20% lower than the design capacity of

385 tons. This reduction in HP capacity is consistent with the measured heat pump performance discussed in section 5.2.2.

The integrated cooling energy consumed by the WID from the HPs and campus chilled water are calculated using the equations provided in Appendix A. The total integrated cooling load of the building is shown in Figure 5-6. The monthly data from second half of 2012 and the beginning half of 2013 were re-ordered from January to December in order to reflect the measured cooling over one calendar year.[41] The average outdoor temperature is included on the right vertical axis to give a sense of the seasonal temperature change. Finally, the integrated cooling provided by the HPs and the campus chilled water system are plotted separately in Figure 5-7 to indicate the proportion of the total cooling provided by each of the chilled water sources.

[41] Data for June 2012 were not available because the required instrumentation was not yet in place. Additionally, heat pump data for May 2013 were not available because the heat pumps were shut down on May 2nd for testing.

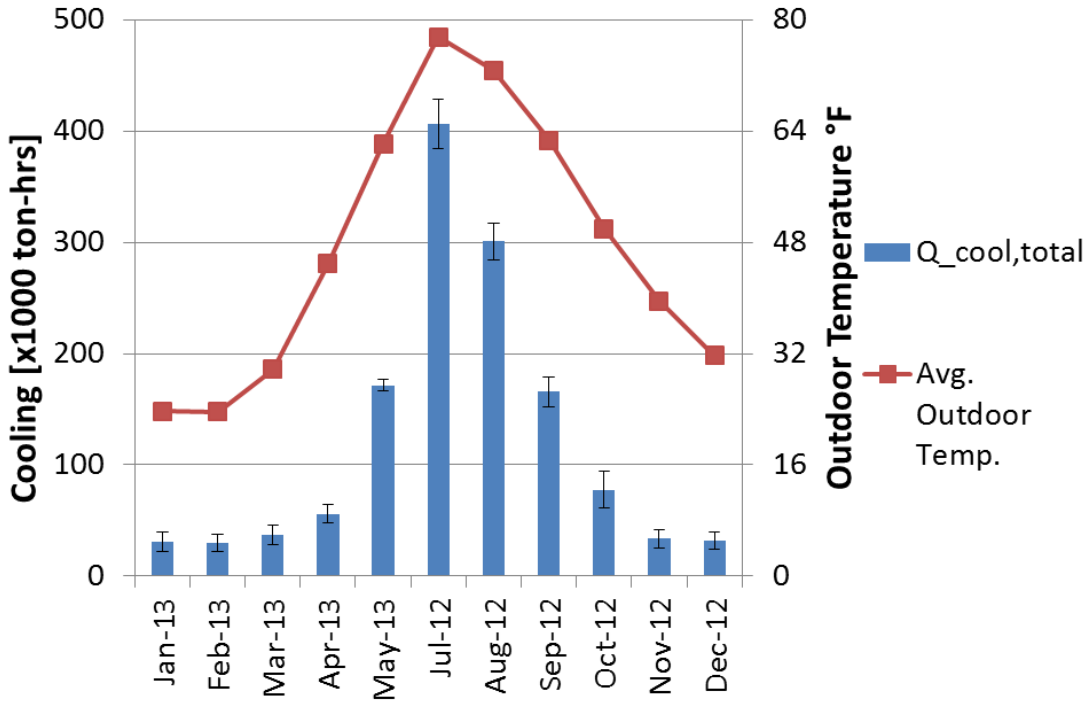

Figure 5-6 – Total Measured Cooling from HPs and Campus over several months

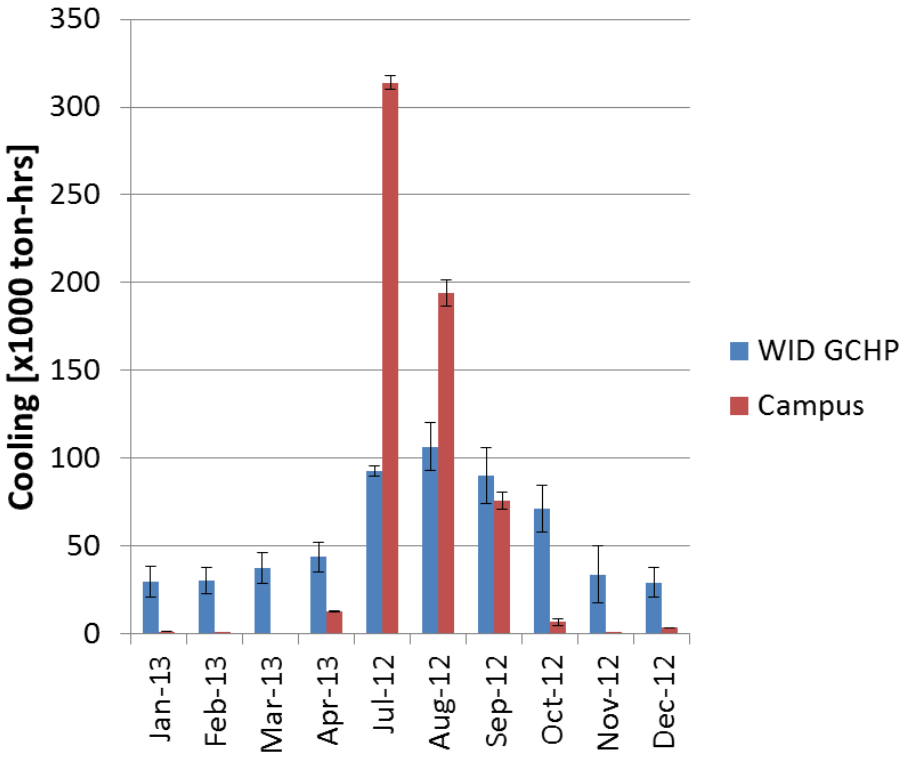

Figure 5-7 - Breakdown of the Total Cooling Provided to the Building

As anticipated, the large integrated building cooling loads during the summer months were are primarily served by the campus district system. Little campus chilled water is used from October to April of the next year, as the WID heat pumps are able to satisfy the building cooling demand. To further analyze the performance of the respective cooling systems, the measured cooling and measured power consumption by the systems were used to calculate the system efficiencies.

5.3.2 Measured GCHP and Campus System Efficiencies

The integrated electrical energy consumed by the system was calculated. The power requirements to operate the WID HP system consisted primarily of the electrical power consumed by the heat pumps themselves (i.e. the heat pump compressors) and the system hydronic pumps. The WID system pumps included: the penthouse reheat pumps P-1 and P-2;

the HP chilled water pumps P-7 and P-8; the HP condenser water pumps P-11 and P-12; and the campus chilled water booster pump P-21. The true power consumed by each hydronic pump was measured independently at ten minute intervals synchronized with the temperature/flow data used to calculate the measured cooling capacity and trended on the IBA. The true electrical power consumed by the heat pumps was measured and trended at ten minute intervals on the IBA, synchronously with the cooling and system pump measurements.

The electrical requirements to operate the system, integrated over each month, are broken down for the heat pumps and system pumps and provided in Figure 5-8. As a secondary means of comparison, the measured energy consumption by the heat pumps and system pumps are compared to the predicted system energy consumption as documented in the energy model created by the WID mechanical design engineers. (Energy Model 2011) On average, the measured heat pump energy consumption was 5% greater than the model predicted heat pump energy and the measured system pump energy consumption was 33% greater on average than the model predicted pump energy. The comparative data are provided in Figure 5-9.

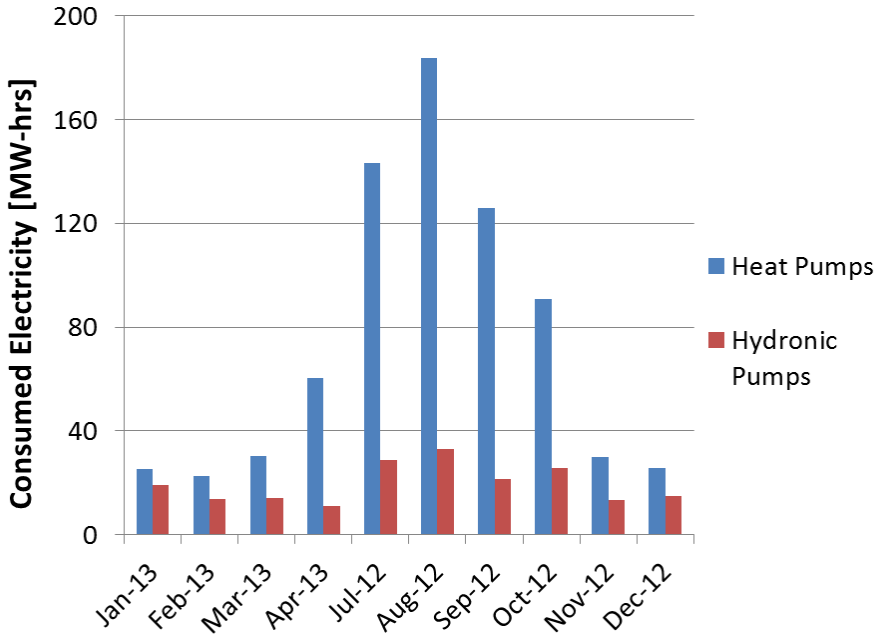

Figure 5-8 - Breakdown of Measured Electrical Consumption of the GCHP System

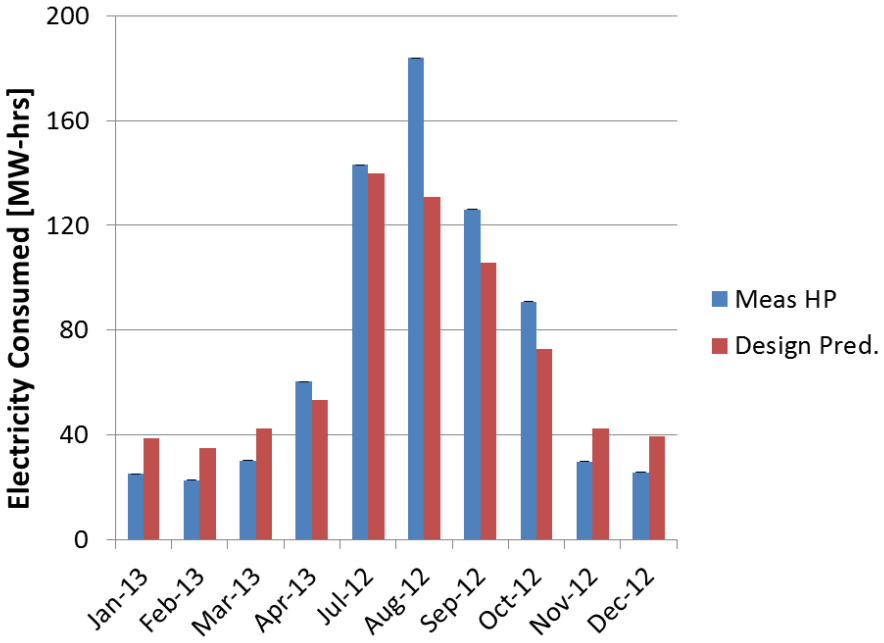

Figure 5-9 - The Integrated Energy Consumed by the Heat Pumps Compared to Predictions in the WID Energy Model

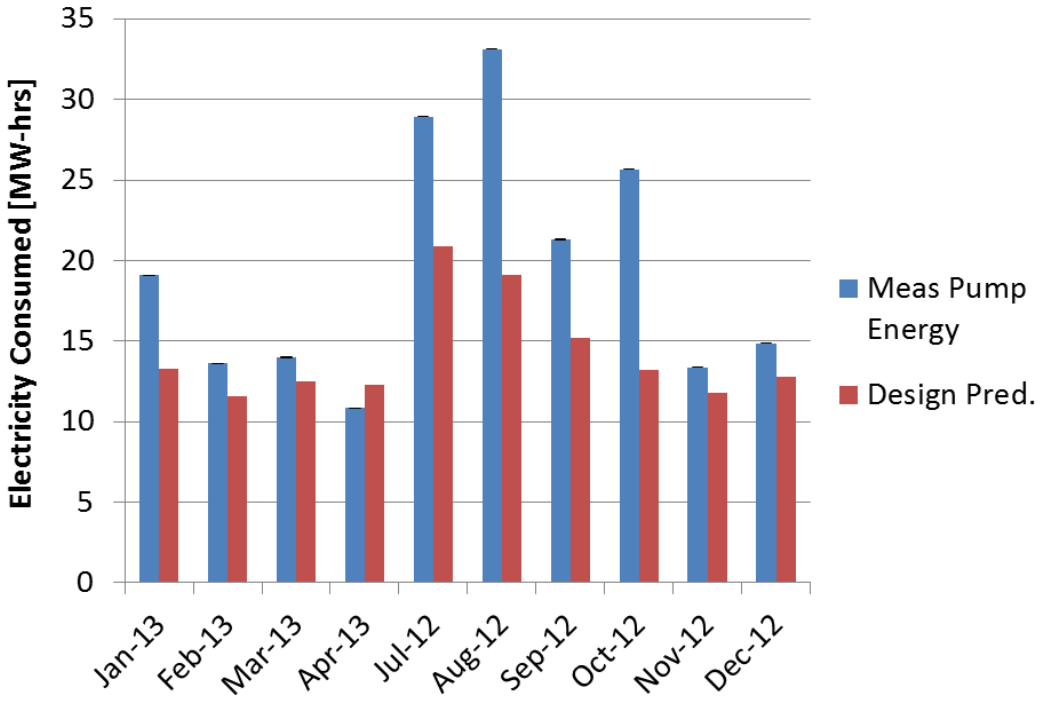

Figure 5-10 - The Energy Consumed by the System Pumps Compared to Predictions in the WID Energy Model

The system efficiency is calculated by averaging the coefficient of performance (COP) using the measured cooling energy provided by the GCHP system and the measured electrical energy input. The measured average COP was integrated over each month using and the uncertainty is calculated using the equation in Appendix A. The results indicated that the GCHP system had performed at an average COP of 2.0 for the months with a larger cooling load and that the heat pumps alone had only performed to their design efficiency during months with little cooling load.[42] The average COP of the WID heat pumps and GCHP

[42] As can be seen in Figure 5-6, relatively small cooling loads were observed from October 2012 through April 2013.

system for each month are provided in Figure 5-11. For additional reference, Figure 5-11 includes the manufacturer-rated efficiency of the WID heat pumps at their design conditions.[43] The monthly efficiencies of the GCHP system are directly compared to the measured efficiencies of the campus chilled water system, shown later in Figure 5-12.

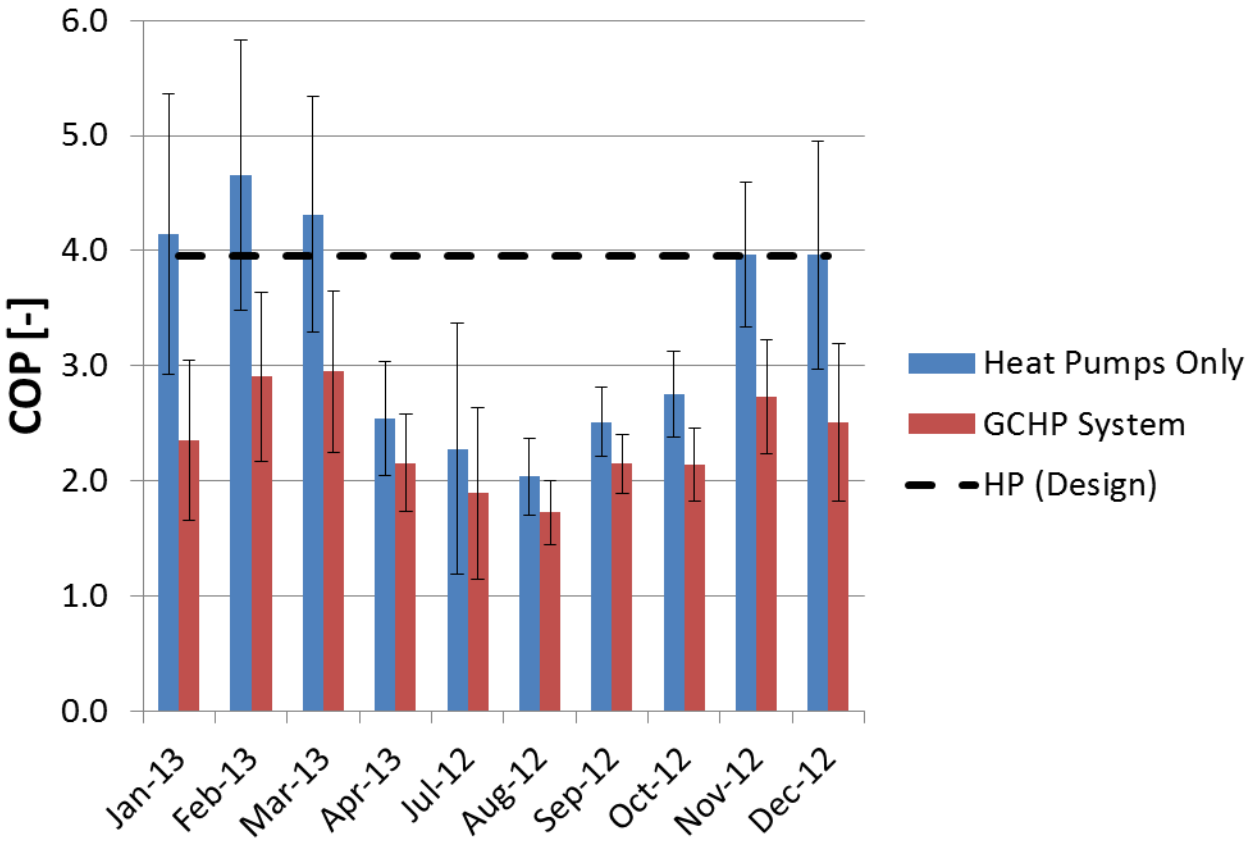

Figure 5-11 - HP and GCHP System Monthly Efficiencies

[43] HP Manufacturer design COP was reported as 3.96 in the WID heat pump equipment submittal document. (HP Submittal 2010)

5.3.3 Campus Chilled Water System and Comparative Efficiencies

The West Campus "Cogeneration" Facility (WCCF) was chosen as the basis for comparison with the WID GCHP system. An overview of the WCCF is provided in Appendix B. Hourly data from July to October of 2012 were provided by FP&M for the measured chilled water capacity (tons) and system electrical consumption (kW) of the chilled water system located in the WCCF. [44] The system electrical consumption included the electricity costs of the chillers as well as the water distribution pumps. The uncertainties of the WCCF data were not provided, but estimated at 10%. The campus cooling and electrical data were integrated over the available months and the average COP was determined. The WCCF and the GCHP system efficiencies for the late summer to early fall months are shown in Figure 5-12. It was observed that the WCCF chilled water system was more efficient than the WID GCHP system by 50% on average.

[44] Regular preventive maintenance windows were reserved for the WCCF chilled water equipment during the winter months. The minimal cooling demand on campus during the winter months was met with chillers at the Walnut Street plant.

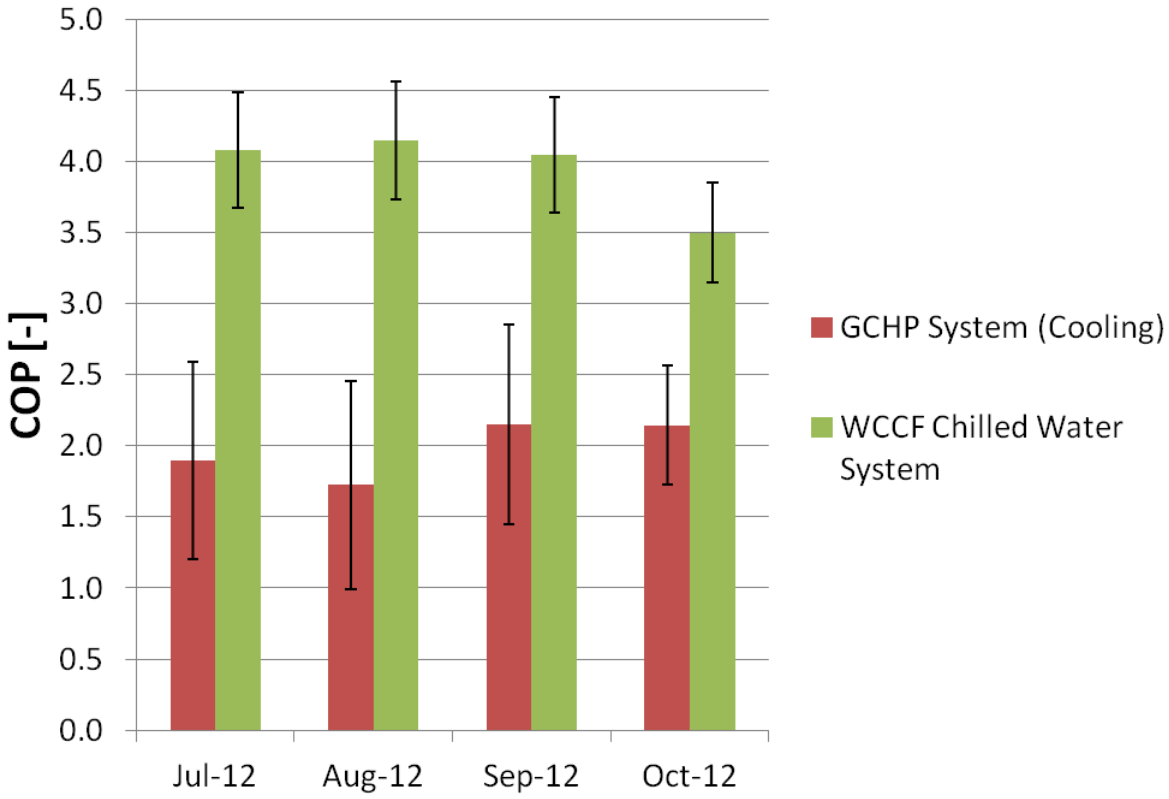

Figure 5-12 – Measured efficiencies for WCCF and WID chilled water systems

Data for the WCCF chilled water system were not available in Spring 2013 because the chillers were not put into operation until near the end of the present research. To estimate the comparative performance over a year, the measured monthly WID GCHP efficiencies were compared with the measured WCCF efficiencies of the previous year where necessary, shown in Figure 5-13.

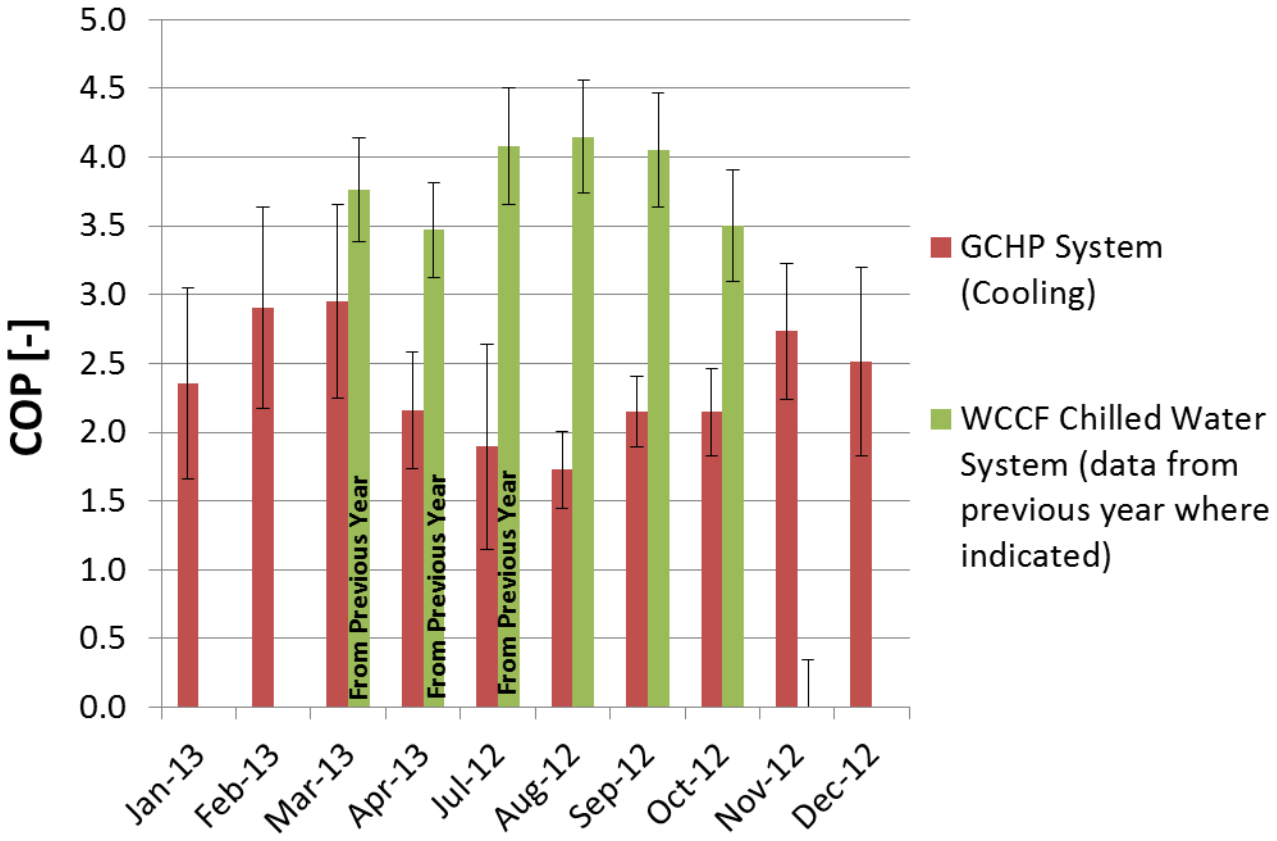

Figure 5-13 - Comparison of WID GCHP and WCCF Efficiencies Over Year

The WCCF chilled water system performance data used in the present research comprised 6000 rows of hourly data and was too large to reproduce in this document. The data are summarized in Table 5-1. The measured cooling capacity and electrical power input of the WCCF system were integrated and summed over each month. It was observed that the WCCF chillers operated on average at 48% of their total nominal cooling capacity from March to November and that the WCCF chilled water system had operated 100% of that time. Therefore, it was concluded that the GCHP and WCCF comparisons were fair because the WCCF had operated at an appreciable capacity and amount of time. In other words, it

would be unfair to compare the WCCF to the WID system had the WCCF operated very little or at relatively low loads. The capacity and time of operation data are included in Table 5-1.

Month	Total Integrated Cooling [10^6 ton-hrs/month]	Total Integrated Electrical [GW-hrs/ month]	System Monthly Avg. COP [-]	System Avg. Capacity [tons]	Monthly avg. Capacity (% of nominal)	System Operational
Jan-12	-	-	-	-	-	No
Feb-12	-	-	-	-	-	No
Mar-12	3.53	3.30	3.76	4,745	24%	Yes
Apr-12	2.78	2.82	3.47	3,866	19%	Yes
May-12	6.55	5.45	4.23	8,804	44%	Yes
Jun-12	9.57	8.12	4.15	13,291	66%	Yes
Jul-12	12.45	10.74	4.08	16,739	84%	Yes
Aug-12	9.73	8.25	4.15	13,077	65%	Yes
Sep-12	6.13	5.32	4.05	8,512	43%	Yes
Oct-12	5.76	5.79	3.50	7,738	39%	Yes
Nov-12	-	-	-	-	-	No
Dec-12	-	-	-	-	-	No

Table 5-1 – Summarized FPM data for WCCF chilled water system

The measured data showed that the WID GCHP had performed less efficiently than the WCCF chilled water system during those periods where the WCCF system was available. The results suggest that, in order for the WID to achieve the energy reduction goals stated in the Basis of Design, it would have been more appropriate to cool the building with campus chilled water during the cooling season, rather than operating the GCHP system. Further investigations were necessary to determine whether the WID GCHP system had been operated as efficiently as possible or if the system could be optimized to operate more efficiently in the future.

5.4 GCHP Underperformance: High Condensing Temperatures and Heat Recovery

As discussed in Section 5.3, the measured efficiency of the GCHP system was low compared to design and the campus chilled water system. It was of further interest to determine the reasons for the system underperformance. The WID GCHP was designed as a heat recovery chiller system. Therefore, the heat recovered by the system was investigated in the following sections to better understand its influence on the overall HP operating performance.

From the measured data, it was observed that the temperatures returning from the geo-field/recovered-reheat to the heat pump condensers were much higher than design conditions, indicating as high as 110°F for a monthly average. The monthly average COP and the monthly average water temperature entering the HP condensers are provided in Figure 5-14, plotted on the left and right axes, respectively. The design entering condenser water temperature is included on the right axis of the figure. For additional reference, average entering condenser water temperatures for the month of August, the time frame with the highest heat pump load and highest condensing temperatures, are provided in Figure 5-15.

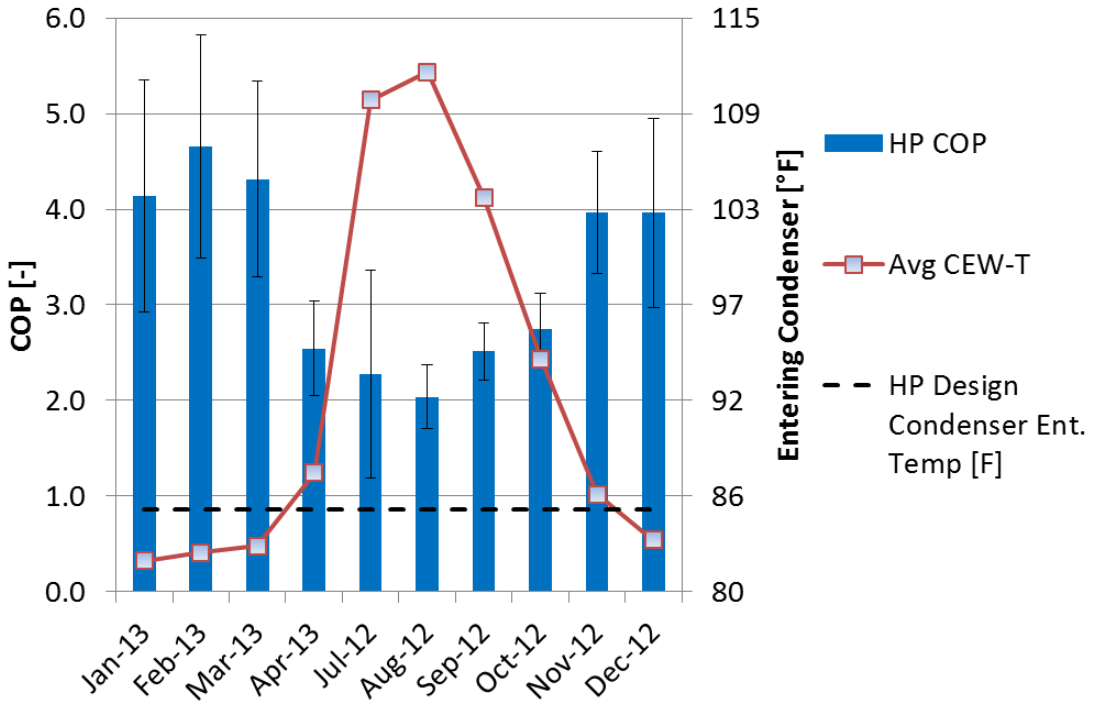

Figure 5-14 - Monthly HP Efficiency and the Average Entering Condenser Water Temperature

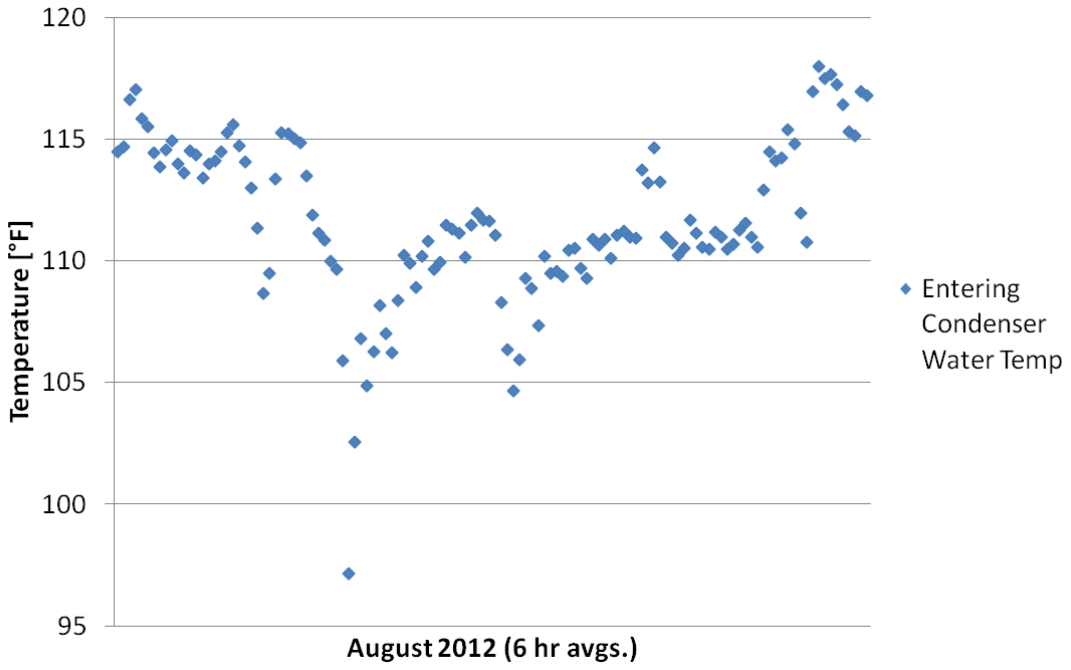

Figure 5-15 - Entering Condenser Water Temperatures for the month of August

The WID hydronic system was designed to allow heat rejected from the HP condensers to be diverted (i.e. "recovered") to the building reheat loop in order to displace the use of campus utility steam for HVAC reheat and to decrease the heat rejection duties of the ground heat exchanger.[45] [46] The measured heat recovered by the system for use in building reheat can be used to determine whether the maximum amount of heat recovery had been achieved and what affects the heat recovery design had on the condenser entering temperature and the efficiency of the heat pumps. The WID air-handling was exhaust driven to meet ventilation requirements, rather than being driven by space conditioning. The reheat coils, located in air terminals throughout the building, were sized to make up for much of the space conditioning requirements and to supply 60% of the WID space heating load.[47]

The building reheat loop also supplied in-floor radiative heaters located in the ground floor of the building. According to equipment submittal drawings, the floor area (i.e. slab area) served by the in-floor heaters was approximately 5000 ft^2. (In-Floor Submittal 2008) The estimated heating capacity of the in-floor system was reported as 45 $Btu/hr/ft^2$, giving a total heating capacity of 225 MBtu/hr. (First Floor Mechanicals 2008)

[45] Steam reheating or recovered-condenser reheating had to be isolated in order to avoid using steam to heat the HP condenser loop and the geo-exchange loop.

[46] It should be noted here that it was possible to satisfy the WID reheat demands with low pressure steam from the campus utility, which was a utility resource that was in abundance on UW campus. The UW utility operators often struggled with finding means of rejecting the low pressure steam heat load. Therefore, it may not have been of significant value to design a mechanical system for a building like the WID to displace the use of low pressure steam from a systems perspective.

[47] BOD page 8-25

According to the Basis of Design, the peak reheat and in-floor heating load was estimated to be twice the peak HP heat rejection at design conditions.[48] By design, the system recovered condenser heat when the HPs produced water at temperatures above a specified setpoint.[49] According to the contractor's schedules, roughly one third of the building's 456 reheat coils were sized for an entering water temperature of 105°F and the remaining two thirds of the reheat terminals were sized for 130°F entering water.[50]

The HP system is capable of providing condenser water at a temperature at or slightly above 105°F; however, the HP system is not able to provide hot water at the higher 130°F temperature. Of course as the condenser leaving water temperature rises, the efficiency of the HP will decrease further so this behavior naturally raises questions about the viability of recovered heat for building reheat.

At design conditions, the manufacturer-predicted total heat rejection (THR) from the HP condensers was 5785.4 MBtu/hr. The measured peak heat recovered from the heat pumps was 2673 MBtu/hr and the total design capacity of the reheat coils plus the in-floor heaters was 3136 MBtu/hr; indicating that the peak measured heat recovered met 85% of the total reheat coil capacity. The design peak heat rejection from the heat pumps, total heating

[48] BOD 8-17

[49] During the research, a lower temperature setpoint of 105°F was suggested because the original setpoint of 130°F was excessive and limiting the system from recovering heat.

[50] The air terminals dedicated to offices and labs in the basement were sized for 105°F entering water temperatures. The rest of the building terminals were sized for 130°F entering water temperatures air terminals.

capacity of the WID reheat coils, and the peak measured heat recovered from the heat pumps is shown in Figure 5-16.

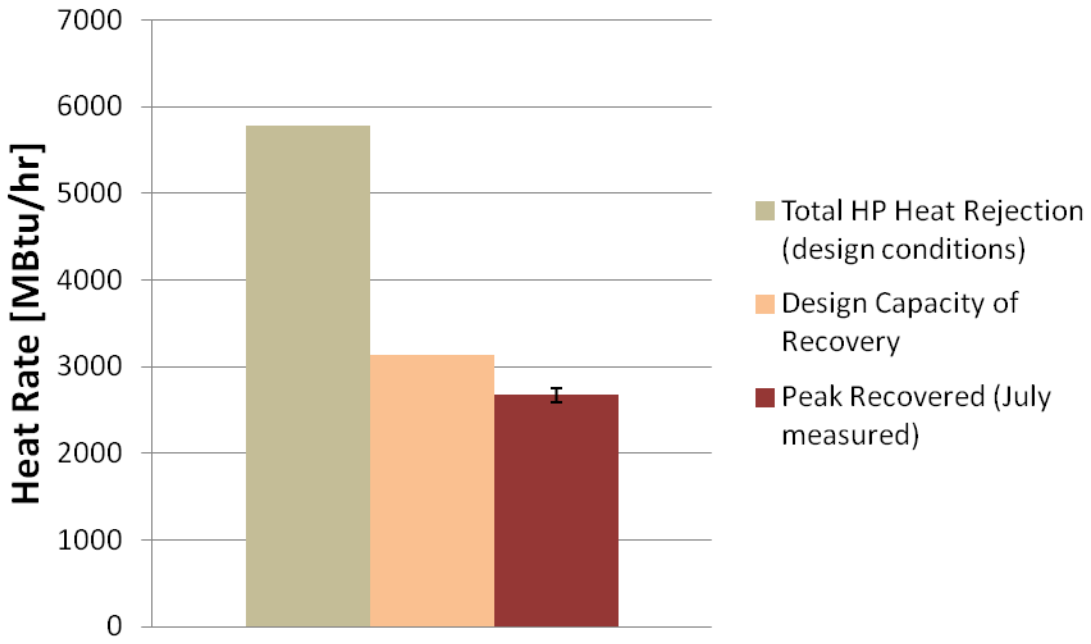

Figure 5-16 - Design and Measured Reheat Recovery, and the Design HP Total Heat Rejection

Only the months from May to October saw heat pump condenser leaving temperatures high enough for the system to recover a noteworthy amount of heat to the reheat loop. During those months, the measured recovered heat was consistently between 400 to 600 MMBtu per month. Referring to Figure 5-13, it was observed that the system COPs were no better during the months where reheat was recovered to the reheat loop. In other words, the time periods where reheat was recovered from the HPs did not provide significant heat rejection necessary to lower the water temperature returning to the HP condensers. The measured heat rejected from the HPs, the heat recovered to reheat, and along with the comparative heat rejected to the geo-field are shown in Figure 5-17.

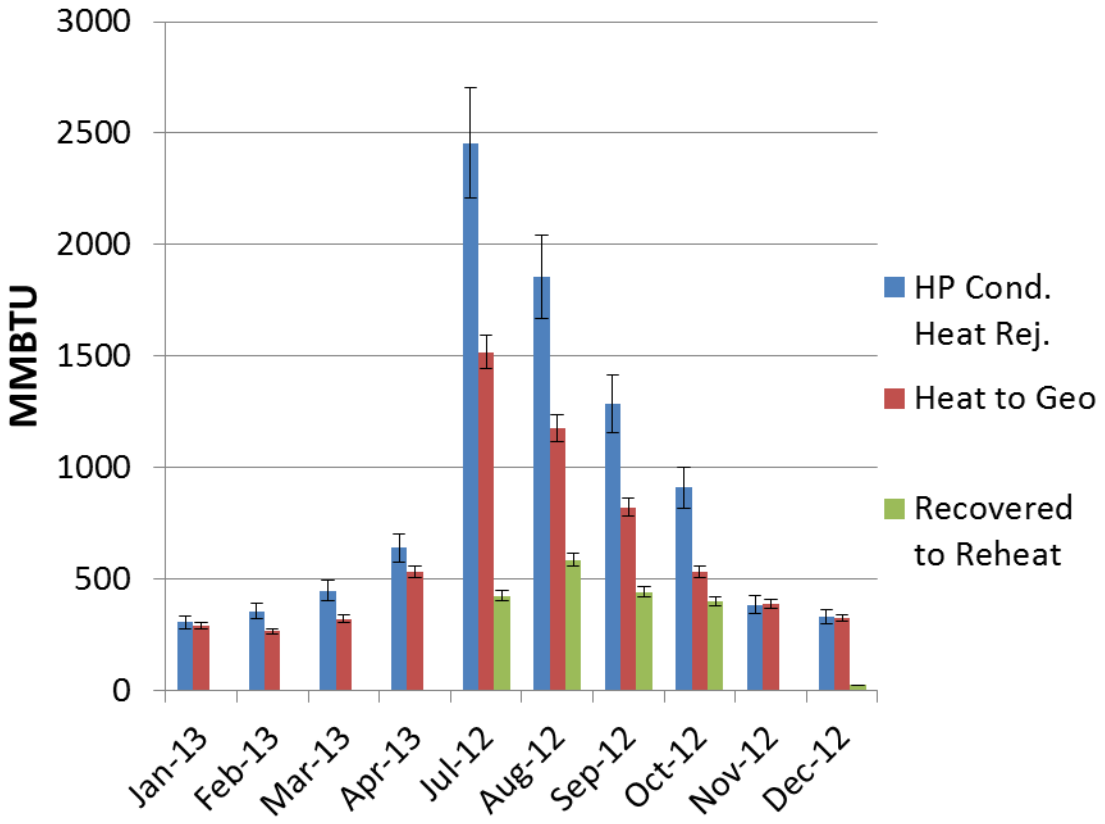

Figure 5-17 - Measured Heat Rejected from HP, to the Geo-field, and Reheat Loops

5.5 Conclusion

The WID heat pumps performed at 80% of the manufacturer-rated cooling capacity during operating periods where quasi-steady conditions were maintained. The measured data showed that the efficiency of the WID GCHP was, on average, 50% less efficient than the campus chilled water system and that the WID system entering condenser water temperatures were much higher than design. The heat recovery functionality of the system had operated as expected, and the measured heat recovered adequately compared to the peak capacity of the reheat coils. The WID GCHP system showed evidence for the risk of designing a heat recovery machine (i.e. high condensing temperatures are desirable and useful) with

inadequate heat rejection capabilities: the resulting high entering condenser temperatures hurt the efficiency of the machine.

Leaking valves in the WID GCHP constrained the system to operate only in cooling mode for the duration of the present research. Therefore, the performance of the system in heating was not possible. Discussed in the following chapter, a numerical model was created to investigate the sizing and heat rejection capabilities of the ground heat exchanger compared to the measured.

Chapter 6. Ground Heat Exchanger Model

6.1 Introduction

As noted in the previous chapter, the measured performance of the WID GCHP system was observed to be lower than design expectations and the manufacturer-indicated performance. The primary reason for the poor system performance was determined to be high entering condenser water temperatures; a consequence of inadequate condenser heat rejection. The heat recovery portion of the heat pump system appears to be operating close to design expectation, leaving only the ground heat exchanger (GHX) as the probable cause of heat rejection inadequacies.

This chapter reports on the simulation of a geofield model in attempts to better understand the factors that may be contributing to the performance issues of the GHX as-installed. The geofield simulations also allow other operating strategies for the system to be considered with a goal of identifying preferred methods of HP operation given the GHX design, its sizing, and measured performance.

6.2 Overview of TRNSYS and the DST Model

A model of the WID geo-exchange bore field was created using TRNSYS. (Klein 2004) TRNSYS has a modular architecture that allows third-party developers to build component modules that can be implemented into larger simulations. The WID GHX was modeled with component Type 557 “Vertical U-Tube Ground Heat Exchanger”, which is based on the Duct Ground Storage model (DST), created by Hellström et al (1989). The DST is a numerical model that calculates the changing temperature of a given ground volume (referred to as “storage”) due to the thermal interactions with and between multiple geo-exchange bores

embedded therein. (Hellström 1989) Figure 6-1 shows the GHX bores in relation to the ground storage volume.

The model can be generally described as a super-position of three heat transfer solutions: (1) a local solution that uses finite difference techniques to solve for the thermal interaction between the GHX bores and the storage volume in multiple sub-regions, (2) a steady-flux analytical solution that accounts for the distribution of heat between the sub-regions, and (3) a global solution that uses finite differences to solve for large scale ground temperatures in two-dimensional radial and vertical meshes within the storage volume. The inputs to the model are: the geometry of the GHX; thermophysical properties of the heat exchanger materials and circulating fluid; temperature and flow rate of the circulating fluid; and the initial temperature conditions of the ground and its surroundings. The model outputs include the temperature of the circulating fluid leaving the GHX, rate of heat transfer from the GHX to the ground, and the average temperature of the ground.

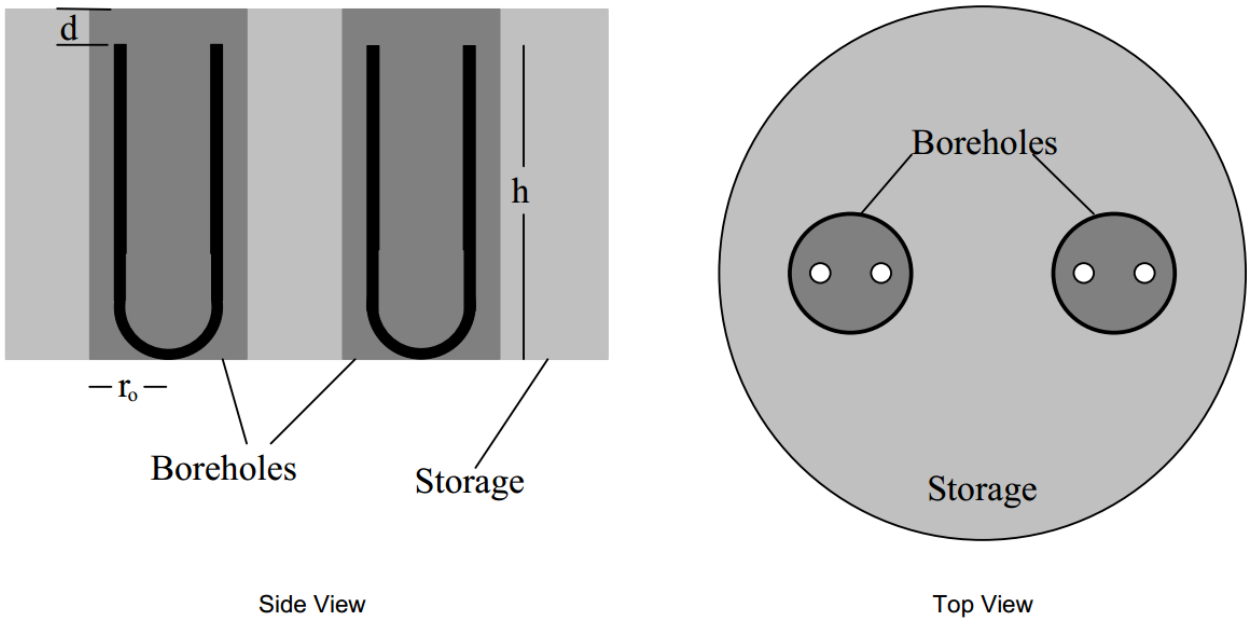

Figure 6-1 - Diagram showing the Ground Storage and the GHX Bores

One major difference between the WID GHX and the DST model is the spatial pattern of the bore field. For symmetry and computational simplicity, the DST assumes that the bores are spaced equidistantly within a cylindrical volume and arranged in a hexagonal pattern. In practice, most vertical GHX systems are laid out in a square or rectangular grid. As discussed, the WID bores were installed along the perimeter of the building. For a given storage volume, the thermal interaction between the bores was assumed to be much greater in the DST model as compared to a perimeter configuration. As discussed in Section 6.4.2, an extended storage volume was determined to approximate greater spacing between the bores and better simulate the interactions between bores in a perimeter configuration.

The DST model has been validated for GHX systems that were not installed in a hexagonal pattern or cylindrical ground volume. Pertzborn validated the model, implemented in

TRNSYS, for two vertical closed-loop GHX systems: (1) a commercial size GHX (360 bores at 400 ft depths, with average spacing of 25 ft) that was laid out in fragmented rectangular grids in a cooling-dominated climate; and (2) another commercial-sized system (39 bores at 280 ft depths, with avg. spacing of 15 ft) that was installed in a long rectangle (~19 x 2) in a heating-dominated climate. (Pertzborn 2011) Shonder validated the model (implemented in TRNSYS) for a vertical closed-loop GHX for a residential, two bore GHX. (Shonder 1999)

Other assumptions made to adapt the DST model that may create differences between the simulation and the actual WID GHX were as follows. The model does not account for the thermal interaction between the WID building and the GHX ground volume. The ground volume was considered to be composed of homogenous isotropic material. Therefore, the model does not account for variable ground material in different regions of the bore field, nor does it account for the possibility of flowing ground water within the field.

6.3 A Single-bore Model

Prior to the construction of the WID, a contractor that specialized in thermal response tests (TRT) was commissioned to determine the thermal conductivity of the site to aide in the modeling/sizing of the GHX. In order to perform the test, one geo-exchange u-tube and bore configuration was installed as similar to the expected geo-exchange bores of the actual system. The test consisted of imposing a constant heat input (via electrical heating) to water loop that is circulated through the u-tube while the inlet and outlet water temperatures were recorded. The data from the TRT test were used to compare with a simple, single-bore DST modeled in TRNSYS.

Where possible, parameter values used in the single-bore model were based on information derived from the TRT report or WID design/construction documentation. In other words, parameters in the model were not manipulated in order to force the model results to match the measured TRT data. The parameters used in the single-bore model are provided in Table 6-1. The definitions of each parameter can be found in the TRNSYS user manual. (Klein 2004) More detailed discussions of the major parameters can be found in the sections that follow. Model inputs include: entering water temperature and water flow rate (recorded at five minute intervals and provided as raw data files from the TRT contractor). The 48 hours of five minute TRT data used in the calibration model are provided in Appendix E.

The DST model requires a specified storage volume that contains the GHX bores. TRNSYS provides the equation necessary to determine the cylindrical storage volume that would be required to contain equally spaced bores at a specified bore spacing, using:

$$V_S = \pi\, N_b D (0.525\, S_b)^2 \tag{6-1}$$

where N_b is the number of bores,

D is the bore depth,

and S_b is the distance between the bores.

As the name suggests, there was only one vertical bore for the single-bore model. Therefore, no spacing between bores and Eq. (6-1) would equal zero. However, it was assumed that an appropriate storage volume would consider the actual spacing between the bore arrangements at WID. A value of 14,234 m^3 was calculated for V_S assuming that S_b was equal to 6.096 m (20 ft).

#	Parameter	Value	Units	Source
1	Storage volume	14234	m^3	Recommended by TRNSYS
2	Borehole depth	121.9	m	TRT Documentation
4	Number of boreholes	1	-	TRT Documentation
5	Borehole radius	0.083312	m	TRT Documentation
9	Thermal conductivity of storage	14.52	kJ/hr-m-K	TRT Documentation
10	Storage heat capacity	2660	kJ/m^3-K	TRT Documentation
12	Outer radius of u-tube pipe	0.02108	m	TRT Documentation
13	Inner radius of u-tube pipe	0.01725	m	WID Geo Submittal
14	Center-to-center half distance	0.02654	m	WID Geo Submittal
15	Fill thermal conductivity	6.231	kJ/hr-m-K	TRT Documentation
16	Pipe thermal conductivity	1.402	kJ/hr-m-K	TRT Documentation
19	Reference borehole flow rate	1817	kg/hr	TRT Documentation
20	Reference temperature	11	C	Estimated
21	Pipe to pipe heat transfer	-1	-	Assumed
22	Fluid specific heat	4.183	kJ/kg-K	Calculated
23	Fluid density	997	kg/m^3	Calculated
29	Maximum storage temperature	54.4	C	TRT Documentation
30	Initial surface temp	11.7	C	TRT Documentation
40	Thermal Conductivity of layer	14.52	kJ/hr-m-K	TRT Documentation
41	Heat capacity of layer	2660	kJ/m^3-K	TRT Documentation
42	Thickness of layer	121.9	m	TRT Documentation

Table 6-1 – Parameters for the Single-Bore (TRT) model

* Parameter values not shown indicate the default value was used. The full list of parameters used in the single-bore model are provided in Appendix E.

As shown in Figure 6-2, the leaving water temperature of the single-bore model agreed well with the measured leaving water temperature, indicating a mean average error of ±0.38°F.[51] The only source of appreciable difference between modeled and measured temperature values occurs in the first two hours, during which time the measured test flow rate and heat input were comparatively low. It can be seen that the model quickly converges with the

[51] The equation for mean average error between the model and the measured data can be found in Appendix E.

measured data once the heat input begins (indicated by the measured outlet temperature quickly rising).

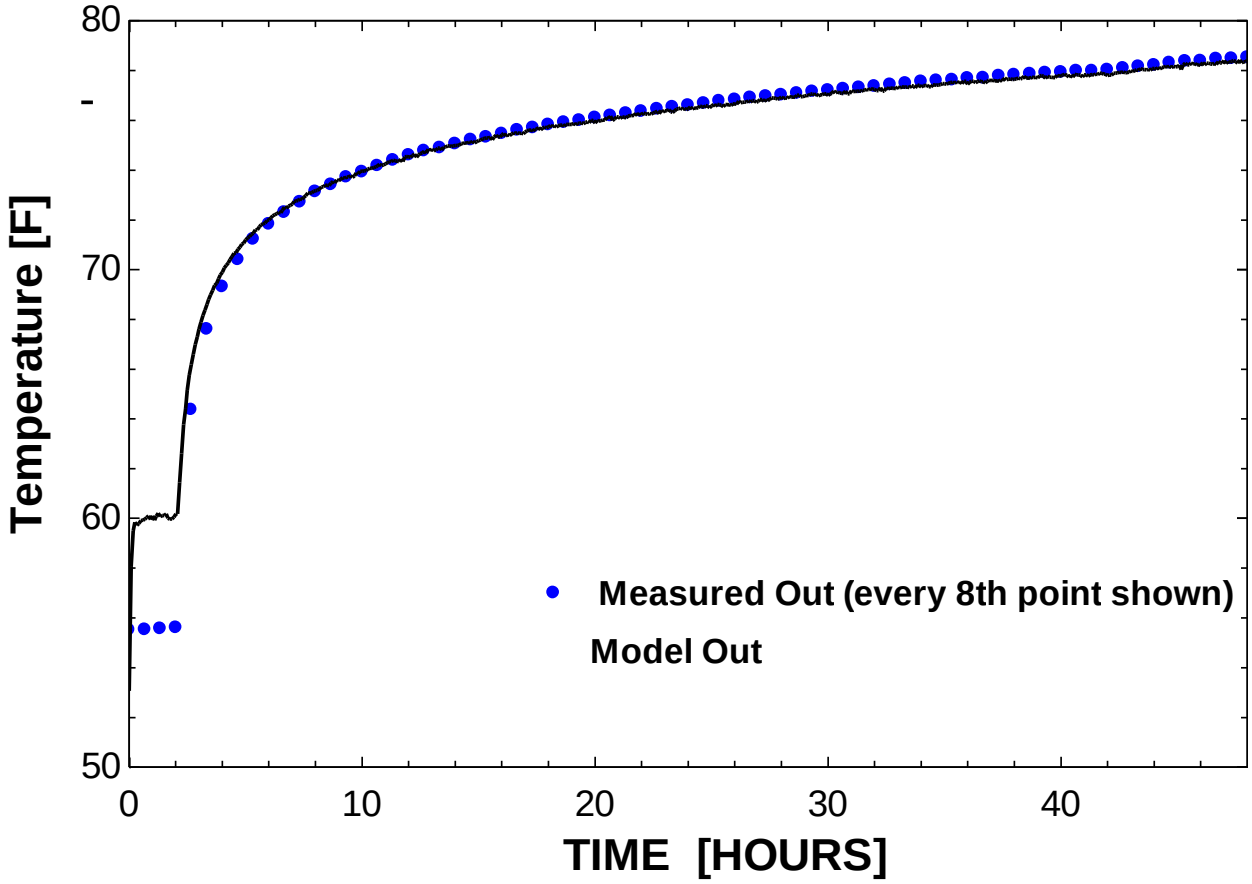

Figure 6-2 – Single-Bore model response compared to measured data

The single-bore model provided a simplified scenario to test the documented GHX parameter values, the units required by the TRNSYS simulation, and to generally organize the modeling methods used in the present research. Parameter sensitivity analyses were conducted, but are more appropriately explained for the full-field model in the following section.

6.4 Full-Field Model

A model was created for the actual WID GHX and storage. As described for the single-bore model, the parameter values used in the full-field model are based on construction and design

documentation where possible. However, it was anticipated that more variability between the GHX bores "as-designed" and "as-built" were likely to be found in the full-field model as opposed to the single-bore (discussed in the previous section). The seventy-seven bores in the full GHX allowed more opportunity for differences in the installation of the bores or changes to the bore hole geometry post-installation (e.g. bore-hole collapse, grout sinkage, etc). Furthermore, the properties of the storage used in the model were based on the results of the TRT conducted at one location in the bore field. Therefore, the full-field model assumes that the properties of the storage are uniform throughout the field.

There are four major differences between the single-bore and the full-field models: (1) the number of bores, (2) the vertical depth of the bores, (3) the storage geometry (e.g. the spatial pattern of the bores, their thermal interaction, and the volume of storage surrounding the bores), and (4) the temperature of the ground at the beginning of the simulation. The number of bores and bore depth of the WID GHX were reported in construction documentation at seventy-seven and three hundred feet, respectively. The full-field model also accounted for the depth of the WID GHX header piping, and updated values for reference borehole flow rate and reference fluid temperature based on the GHX operating conditions. The methods to determine the storage volume and initial conditions of the full-field model are discussed in the following sections. Table 6-2 provides the parameters used in the full-field model that were different than those used in the single-bore model. A full list of the full-field model parameters is provided in Appendix E.

#	Parameter	Value	Units	Source
1	Storage volume	1654000	m^3	See Section 6.4.1
2	Borehole depth	91.4	m	Construction As-Builts
3	Header depth	2.134	m	Construction As-Builts
4	Number of boreholes	77	-	Construction As-Builts
19	Reference borehole flow rate	1764	kg/hr	Calculated
20	Reference temperature	38	C	Estimated
30	Initial surface temperature of storage volume	15.6	C	See Section 6.4.2
42	Thickness of layer	91.4	m	Construction As-Builts

Table 6-2 – Full-field model parameters that differed from single-bore model

6.4.1 Storage Volume Parameter

As discussed, the DST assumes that all bores are spaced uniformly in a hexagonal pattern within a cylindrical storage volume. However, the actual WID GHX bores were arranged in a linear fashion that predominately coincided with the perimeter of the building (Figure 6-3). Figure 6-4 and Figure 6-5 show the difference in the model responses with the storage volume calculated using the default TRNSYS Eq. (6-1) and a larger "extended" storage volume.[52] With all other parameters and input data the same, the smaller storage volume model results in an average storage temperature 17°F higher than that of the model with the larger storage volume after a simulation time of 6000 hours. The daily average leaving water temperature is included in Figure 6-4 for reference. In Figure 6-5, the model with the smaller storage volume shows about half of the total heat transfer capability compared to the larger

[52] The methods used to calculate the extended storage volume are presented following the discussion of the results.

volume model after the simulation has run for about 2000 hours; the measured GHX heat transfer rate is included for reference.

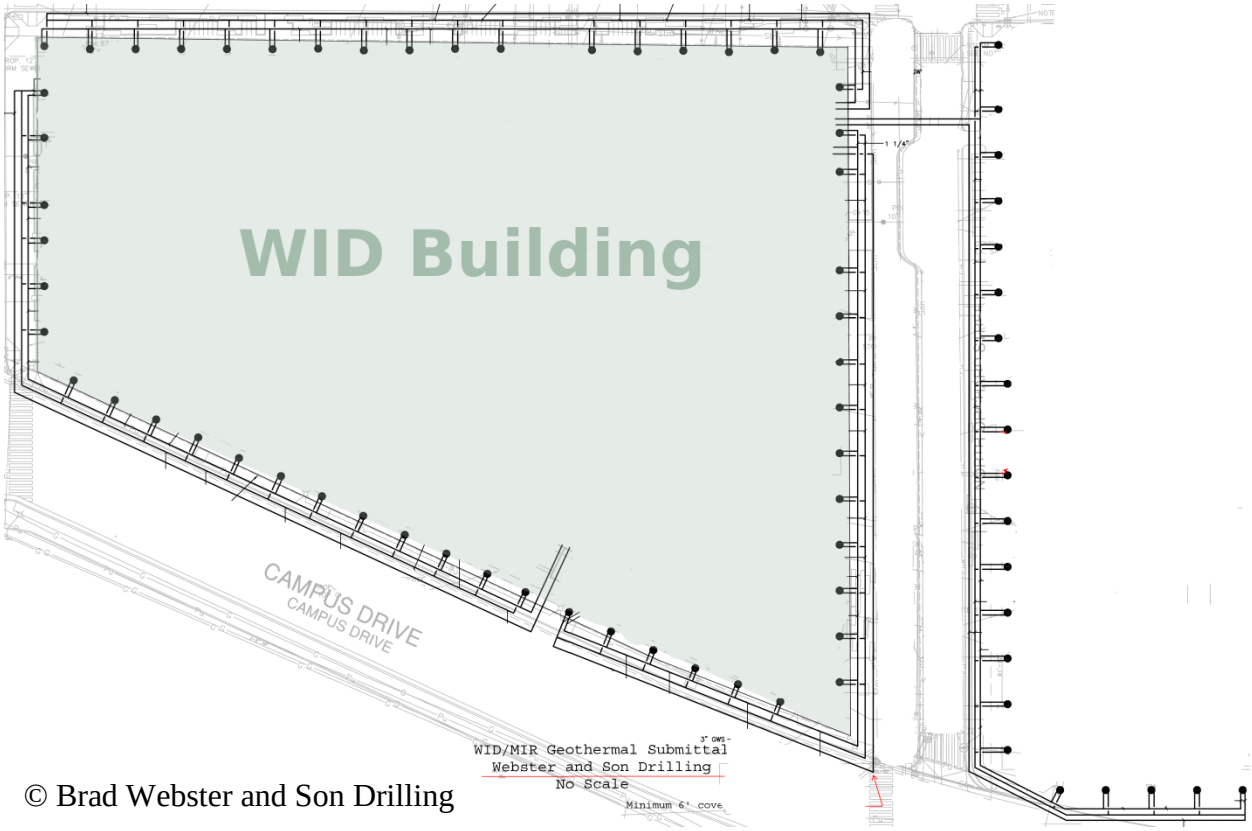

Figure 6-3 - Design schematic of WID perimeter and bore field layout (from top, not to scale)

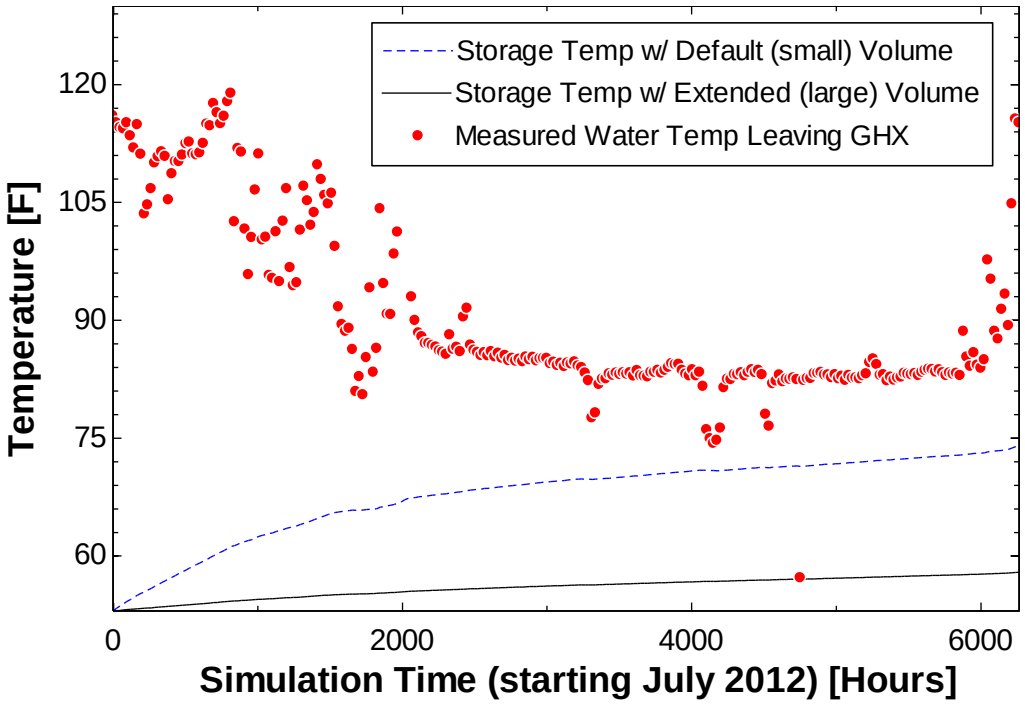

Figure 6-4 – Comparison of average storage temperature response between small and larger storage volumes

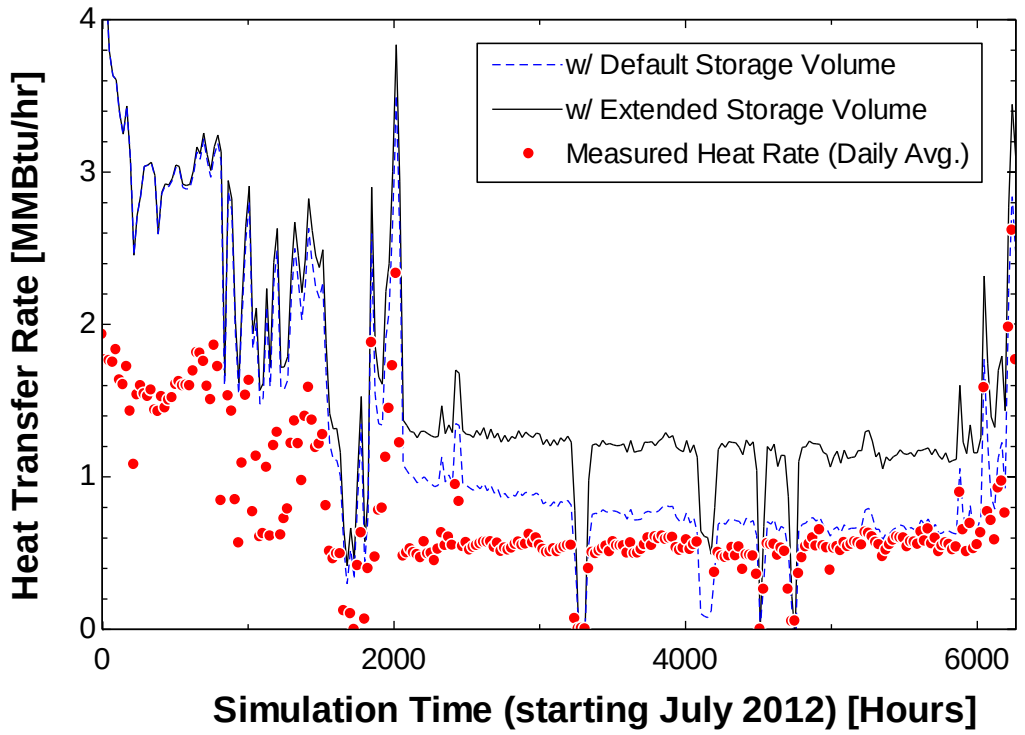

Figure 6-5 - Comparison of modeled heat transfer rate between small and large storage volume models

The results of the above comparisons were intuitive, as the larger storage volume would be expected to show a lesser increase in average temperature due its larger thermal capacity. Additionally, the larger storage volume allows the bores to have greater spacing and without the bores thermally interacting as was observed for the smaller volume model after 2000 simulation hours. At first glance, Figure 6-4 and Figure 6-5 may seem to show that the small volume model is the more accurate of the two models, as the modeled storage temperature and heat transfer rates toward the end of the simulation are much closer to the measured leaving water temperature and measured heat transfer rates, respectively. However, the trend in the heat transfer rates of the large volume model more reasonably reflected the measured heat rejection rates. The larger storage volume was then considered more representative of the WID GHX, and was used for the remainder of the present research. The larger heat transfer rate of the model GHX (large volume) to the actual (measured) GHX in terms of heat transfer ability (shown in Figure 6-5) were investigated and are discussed in Section 6.5.

It was determined that a larger storage volume compared to that given by the cylindrical volume of Eq. (6-1) was needed to better approximate the thermal interaction between the WID GHX bores. The "extended" storage volume was determined by extending the floor area of the storage volume by a distance outside of the actual WID floor area. The floor area that contained the WID bore field was approximately 105,000 ft^2 (9,755 m^2). The thermal wave penetration concept, as described by Nellis, was used to determine the additional area needed to extend the model's storage area. (Nellis 2009) It was assumed that a row of bores could be approximated as a plane wall conducting heat outwardly in one-dimension (Figure

6-6). After one year of steady heat rejection, the radial thermal wave penetration distance (δt) was estimated to be 45 ft, using:

$$\delta t = 2\sqrt{\alpha t} \tag{6-2}$$

where α is the thermal diffusivity of the storage as determined by the TRT (1.41 ft^2/day), and t is 365 days (one year).

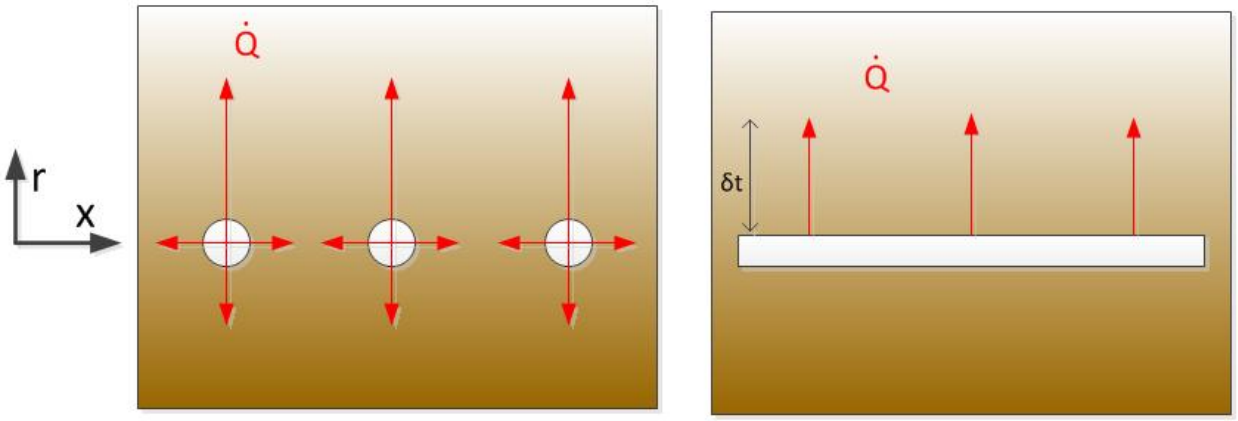

Figure 6-6 –To calculate the thermal wave penetration distance, the bores (left) were approximated as a plane wall (View from above)

The result given by Eq. (6-2) was used to extend the model storage area from the actual WID perimeter in all directions, for a final storage area of 194,670 ft^2. The extended area is shown Figure 6-7 and compared with the actual WID perimeter and the default DST storage area calculated with Eq. (6-1). The extended area was multiplied by the bore depth (300 ft) to calculate the model storage volume as 5.84e7 ft^3 (1,654,000 m^3). Sections of the DST hexagonally-configured bore field and the relative bore spacing for the different storage areas are shown in Figure 6-8.

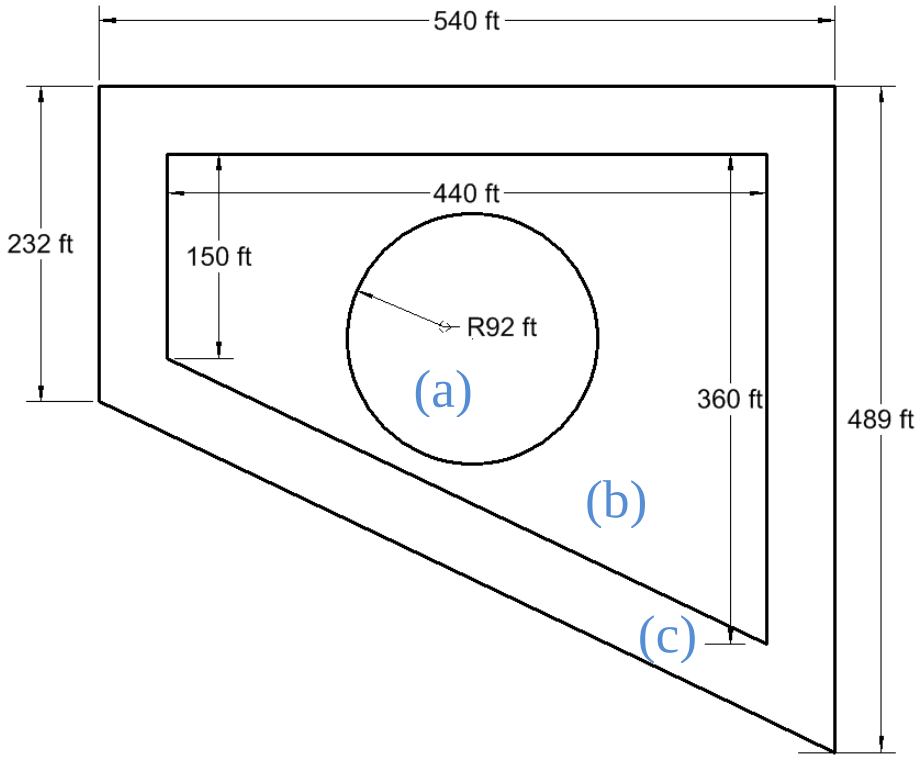

Figure 6-7 – Various floor areas enclosing the WID bore-field: (a) Using Eq. (6-1); (b) actual area surrounding bore-field; and (c) extended area.

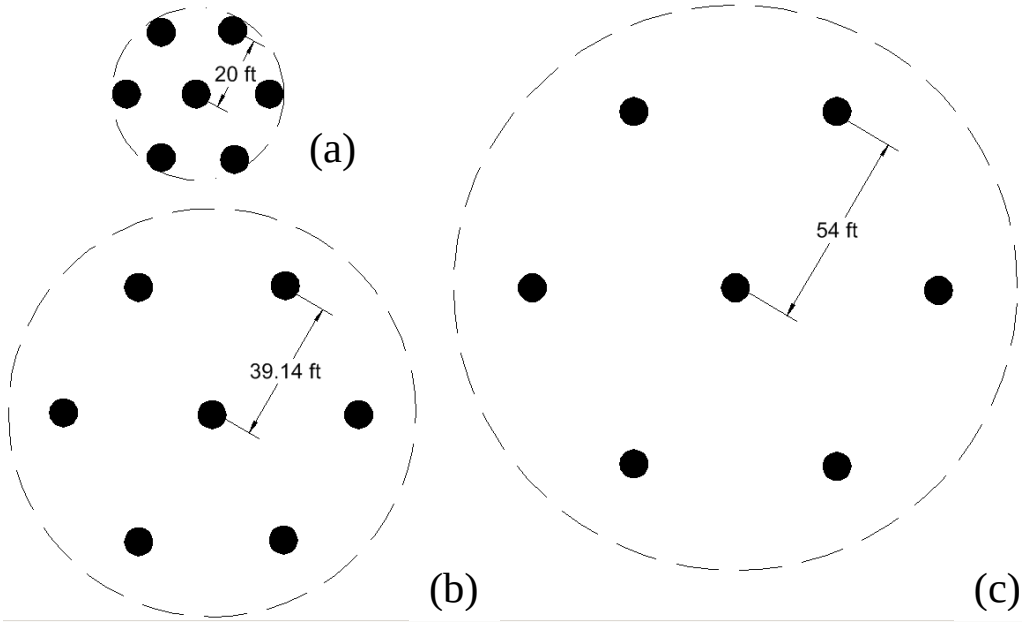

Figure 6-8 – Top view of the DST storage area with spacing from: (a) Default TRNSYS Eq. (6-1) , (b) WID floor area, (c) Extended WID floor area. Bores (solid circles) are exaggerated in size and only 7 bores are shown for display purposes.

Comparisons between small and large storage volume models showed the need for a large volume model to more appropriately reflect the long-term thermal behavior of the WID GHX. Because of the difference in configuration between the DST and the actual WID bore field, an approximate storage volume was determined using known geometries of the WID and concepts in thermal diffusivity. As observed at the beginning of this section, the storage volume showed a close relationship to the average storage temperature response. The initial temperature of the storage volume is discussed in the following section.

6.4.2 Initial Storage Temperature

The temperature condition of the storage volume was not known (i.e. measured) and yet was an important parameter in the model. At the time data collection began for the present research, the WID GCHP system had been operating in cooling mode (i.e. heat rejection to the geo-field) for approximately one year. Over the first year of operation, it was assumed that the average storage temperature had elevated to a temperature between the average water temperatures leaving the GHX and the undisturbed ground temperature as measured by the TRT (53°F).

It was assumed that the temperature conditions produced by the heat pumps during operation in the previous year (2011-2012) were similar, on average, to those measured during the present research (2012-2013). The temperature condition of the ground storage volume after one year of operation (i.e. the beginning of data collection) was determined, simply, by observing the modeled average storage volume temperature change during one simulation year with an initial condition equal to the undisturbed soil temperature (53°F). As shown in Figure 6-9, the model shows that the average ground storage temperature rose by 7°F in the

first year of operation to 60°F. Therefore, the initial storage temperature parameter for the remainder of the modeling work was set to 60°F.

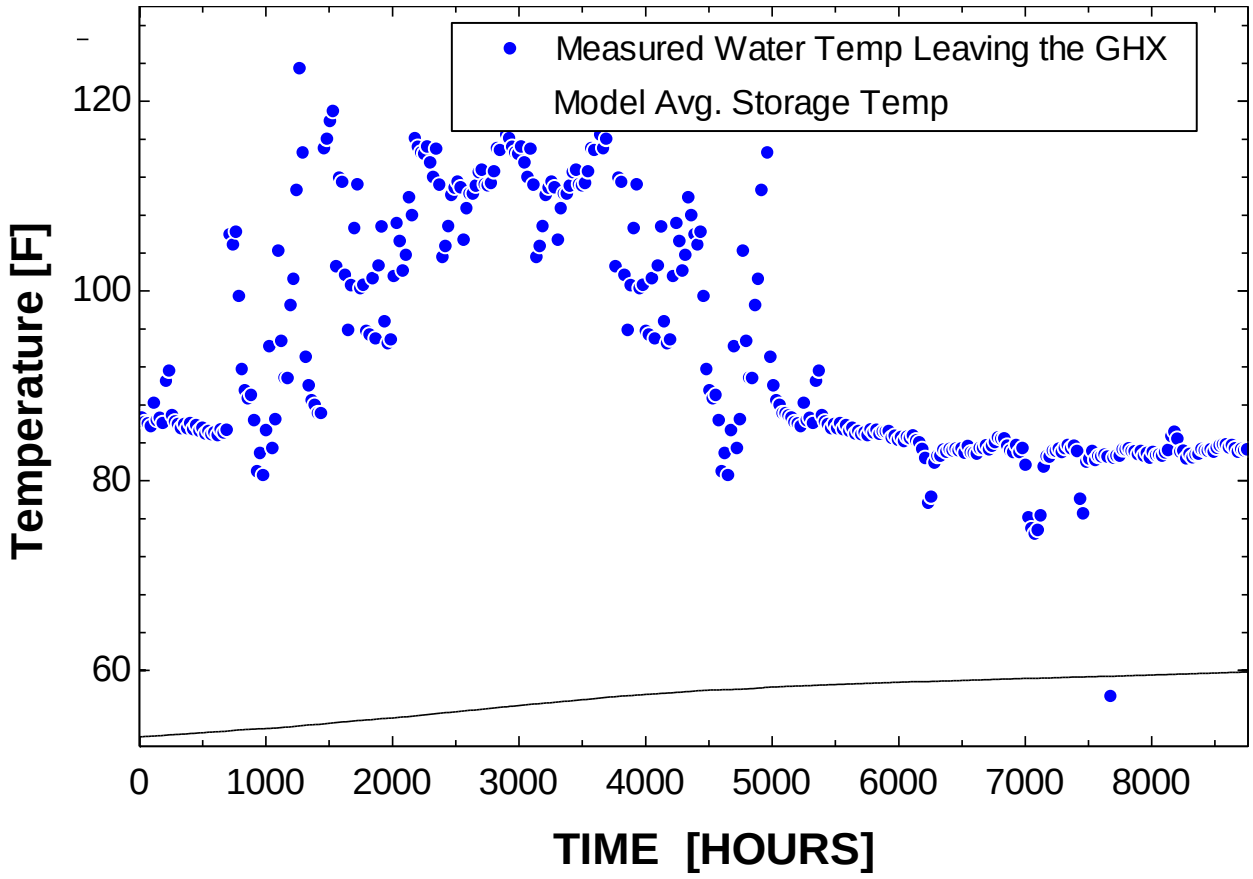

Figure 6-9 – The average storage temperature during one year simulation. The final temperature was used as the initial condition for the model.

6.5 Model Compared to Measured, and Parametric Studies

With the appropriate parameters determined for the full-field model, the measured data for the GHX were compared to the model to investigate possible causes for the deficiencies of the GHX performance as-measured (i.e. high water temperatures returning to the heat pump condensers). Considerations for differences between the GHX as-designed and as-installed were explored, along with known issues regarding possible fouling of the GHX. Hourly average condenser water flow rate and entering geo-field water temperature measurements

from August 2012 to April 2013 were used as inputs to the GHX model. Of the 6288 hours of data available, 480 hours were removed from the comparison because the system was under scheduled maintenance or not operating during those times. The resulting leaving water temperature from the model was compared with the measured leaving geofield water temperature.

It was observed that the GHX model consistently rejected heat from the condenser water at a greater rate than the actual (measured) GHX. Shown in Figure 6-10, daily averages of the model water temperature drop across the GHX was 3.7°F greater for the model.

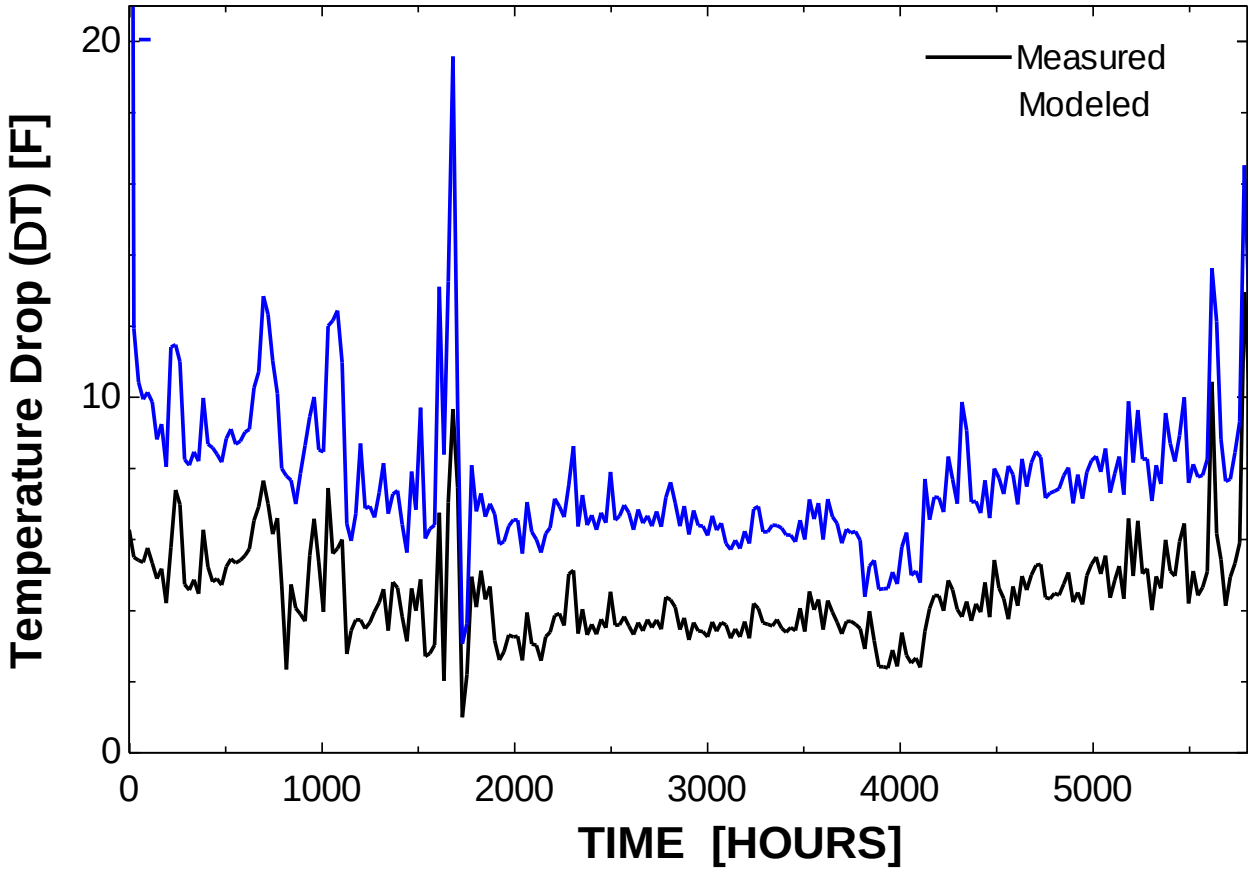

Figure 6-10 – Daily averages of measured and modeled water temperature drop across the GHX

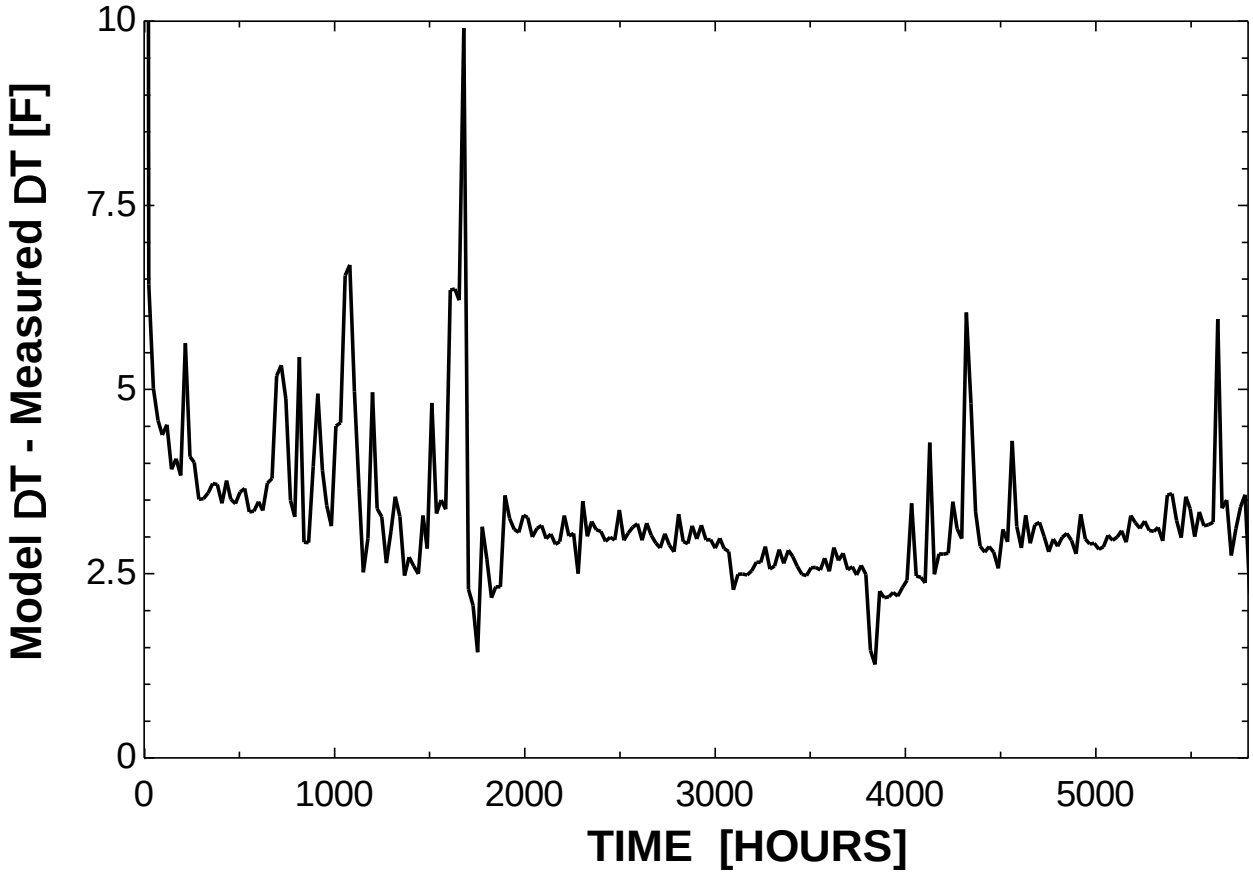

Figure 6-11 – GHX temperature drop difference (daily averages), modeled ΔT minus measured ΔT.

Discussed in the following section, parametric studies were used to explore the changes needed to the model parameters such that the predicted performance better matches the measured data. The parametric investigations were also used to explore anticipated issues with the actual GHX (e.g. fouling) by creating artificial resistances to simulate the lower heat transfer rates of the GHX as measured compared to the model. Only those parameters determined as sensitive (i.e. a parameter change by factor less than 10 was needed to calibrate the model response to the measured) are discussed.

6.5.1 Ground (Storage) Thermal Conductivity

As noted previously, the parameter values for thermal properties of the storage volume were measured by the TRT prior to the installation of the WID GHX. The test was performed in a single test bore at one location in close proximity to the present WID field. It may possible that the storage thermal properties were not uniform through the rest of the field. To address this possibility, the values of the storage thermal conductivity and heat capacity were varied in order to "force" the model to match the measured data. The mean difference error (provided in Appendix E) was minimized in order to characterize the match.

The heat capacity of the storage volume was observed as a relatively insensitive parameter in the model, requiring a value over ten times smaller than the reported value. On the other hand, the thermal conductivity of the storage volume was determined as the most sensitive parameter in the model, because the value needed for the model to match the measured was 5 kJ/hr-m-K (1.4 W/m-K); a factor of three smaller than the reported value. Figure 6-12 shows the agreement between the model and measured data with the decreased storage thermal conductivity value applied. Pertzborn et al showed that, for a site with significant ground water flow, a storage thermal conductivity value needed for the model to match the measured data was a factor of 2 smaller than the original value. (Pertzborn 2011) The smaller-than-reported thermal conductivity value suggested by the model for the WID ground storage volume appeared reasonable, though it may not be the sole reason for the GHX lower performance.

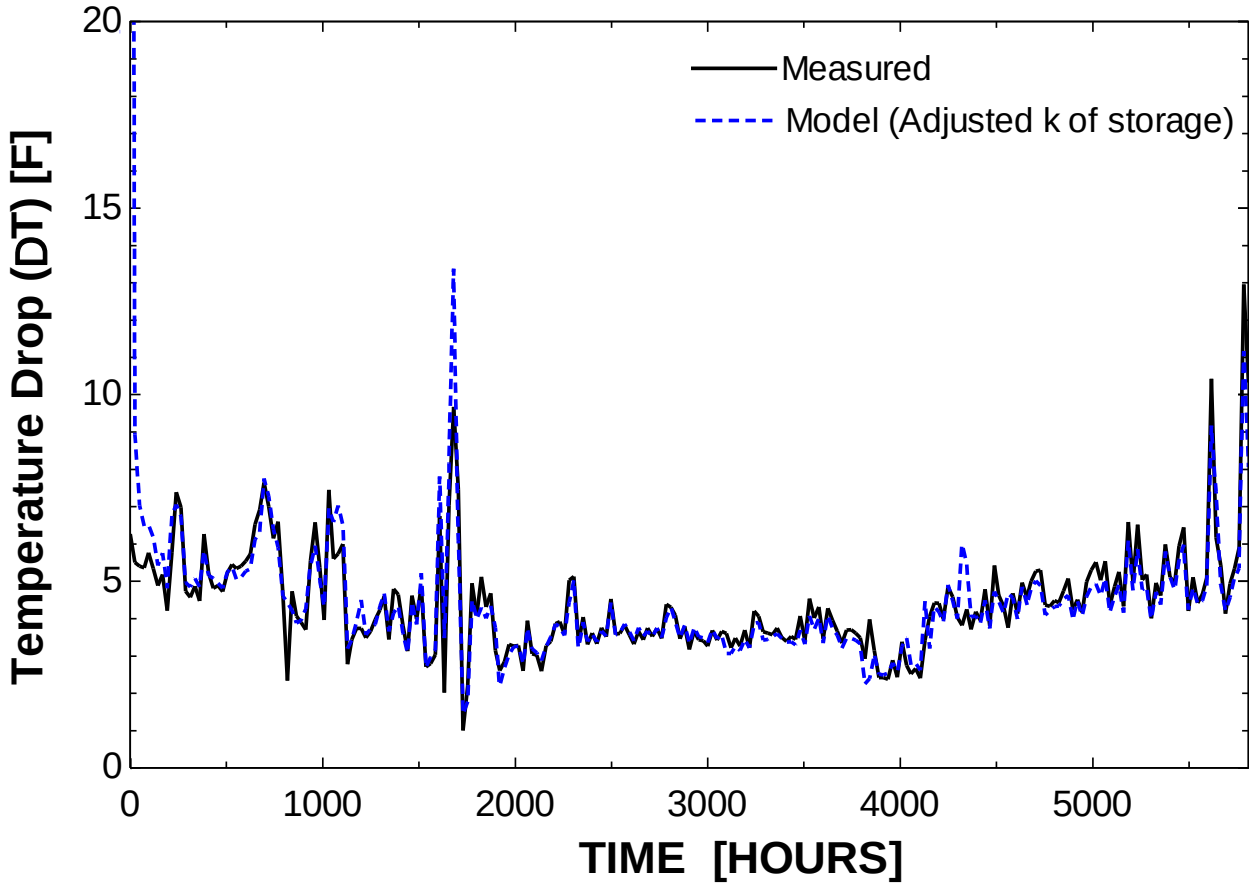

Figure 6-12 - Measured and modeled temp drop with decreased storage thermal conductivity

6.5.2 Fouling in the GHX

The WID hydronic water system is unique on the campus of UW-Madison in that it is the only system that, under normal operation, changes between chilled water and hot water circulation within a given segment of system piping and is directly connected to the campus chilled water supply. Reviewing the system drawings shows that the chilled water within piping nearest the heat pumps would be mixed in with the reheat loop during the switchover from cooling to heating mode, and vice versa. Furthermore, the leaks that were detected in the system valving would increase the likelihood that campus water was entering the condenser/geo water loop.

It is known that that the campus chilled water loop contains iron bacteria, originating from the days when campus utility water was taken directly from Lake Mendota. The intentional and unintentional connectivity between the campus chilled water loop and the WID condenser/geo water loop is believed to have provided an environment for the accelerated propagation of iron bacteria. Many of the pipe segments in the WID chilled water and reheat/in-floor radiative heater loops were believed to be areas of stagnation, adding increased probability for bacteria propagation.

Excessive contamination and plugging of AHU cooling coils was discovered by WID facility technicians and the contamination was typical to that of iron bacteria. Especially due to the high amount of contamination found, it was conceivable that the product of bacteria growth was causing fouling in the GHX. The low temperature drops measured across the GHX were also symptomatic of fouling. In the midst of the present research, additional water filter and chemical treatment stations were added to the WID hydronic loops by the facility technicians. Figure 6-13 shows the contamination “sludge” that was filtered out of the condenser/geo-field water loop.

Figure 6-13 - "Sludge", believed to be from iron-oxide bacteria in the WID hydronic loops, left behind on hand from touching a water filter

To simulate water-side fouling in the GHX model, a resistance to heat conduction was added to the GHX by decreasing the u-tube thermal conductivity (k_u). To make the model match the measured data, k_u needed to be decreased to 0.17 kJ/hr-m-K (0.05 W/m-K); a factor of eight lower than the u-tube manufacturer's reported conductivity value. To determine if the additional u-tube resistance (simulated fouling) was reasonable, the equivalent fouling factor, determined from the additional u-tube resistance, was back-calculated and compared to accepted values of fouling factors.

The conduction resistance for the u-tube was calculated as 0.0004487 [K/W] using:

$$R_u = \frac{\ln\left(\frac{r_{out}}{r_{in}}\right)}{2\pi L k_{u,m}} \tag{6-3}$$

where r_{out} and r_{in} are the outer and inner radii of the u-tube (0.02108 and 0.01725 m, respectively),

L is the total length of the u-tube (183 meters),

$k_{u,m}$ is the u-tube manufacturer's thermal conductivity value (1.402 kJ/hr-m-K).

Using Eq. (6-4), the effective resistance (R_{eff}) was calculated as 0.003695 [K/W], using k_u. Because R_f and the resistance of the u-tube (R_u) were additive (in series), R''_f was calculated by subtracting R_u from the effective resistance:

$$R_f = R_{eff} - R_u \tag{6-4}$$

The fouling factor (R''_f) is defined by:

$$R''_f = \frac{R_f}{A_s} \tag{6-5}$$

where R_f is the resistance to conduction due to fouling and A_s is the surface area of the fouled heat exchanger (u-tube, 19.82 m^2). The calculated R''_f was equal to 64.35 m^2K/kW.

Fouling factors for river water and organic solvents in shell and tube heat exchangers (most similar factor available to the u-tube arrangement and working fluid in the GHX) were published by the Tube Exchanger Manufacturers Association as ranging from 0.35 to 0.53 m^2K/kW. (TEMA 1999) The calculated fouling factor for the WID GHX was 140 times larger than the standard fouling factor value. It is important to note that the TEMA fouling factor value was created for the use of oversizing heat exchangers to meet minimum performance over reasonable intervals between shutdowns and cleanings. In other words, the TEMA value does not consider the time effect of contamination buildup (i.e. greater

resistances for increasing fouling thicknesses). Furthermore, the TEMA value only considers the affects of fouling as a conductive resistance and does not consider the reduction in heat transfer due to changes in the convective heat transfer coefficient (i.e. increased roughness and decreased tube diameter). Fouling in the GHX due to iron bacteria contamination was considered a possible cause for reduced heat transfer capability, but was not found to be the sole reason.

6.5.3 Air Gap or Air Entrainment

Alternative causes of poor GHX heat rejection were explored by simulating added resistance in the GHX grout fill. In the installed GHX system, the effective thermal resistance between the u-tube and ground may vary for the installed bores based on the installation procedure. For example, it may be the case that air became entrained in the grout during the GHX installation, causing an increase in the conductive resistance. Furthermore, expansion and contraction of the u-tubes from thermal and system operating conditions could de-couple the u-tube from the grout in some areas of the GHX.

The TRNSYS GHX model has the ability to account for a gap between the u-tube and grout. This feature of the model assumes that the gap is uniform for all u-tube/grout interfaces with a constant thermal conductivity of the material occupying the gap. A gap of air with a thermal conductivity of 0.08825 kJ/hr-m-K (0.025 W/mK, ideal gas at 53°F and atmospheric pressure) was used to force the model to match the measured data. The gap thickness required to “force” the model to match the measured data was 0.004 m, which translates to 3% of the total grout volume. The determined air gap thickness represents a lower bound for what an actual air gap may have been. A uniform air gap, as in the model, would create a

much larger thermal resistance compared to situations where only portions of the u-tube/grout interface were separated.

Due to the proximity of the WID to the Madison lakes, it was considered possible that gaps between the u-tube piping and the bore grout may become filled in with ground water. Modeling a water filled gap, with a conductivity of 2.054 kJ/hr-m-K (0.57 W/mK, at 53°F and atm. pressure), the gap thickness needed for the model to match was 1 m; a large and unlikely thickness for possible gaps in the actual system considering the bore diameters are only 6 inches. In other words, this gap does not make any sense.

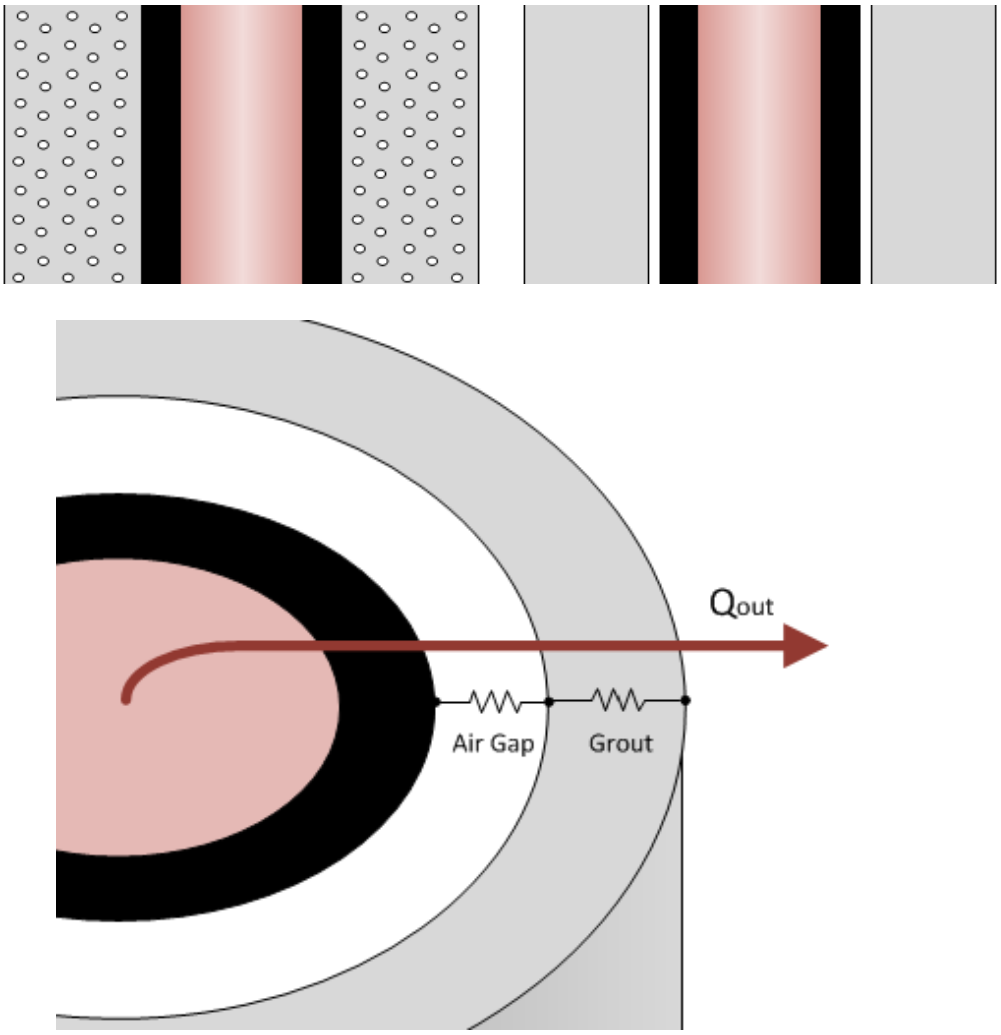

Figure 6-14 - Diagram showing air bubble entrainment and an air gap between the U-tube piping and grout (Top), and the cylindrical resistances in series (bottom).

In summary, parametric investigations were conducted to determine the necessary values that made the model match the measured GHX data. No single parameter was identified as the primary source of difference between the model response and the measured data. The parameters that forced the model to match the measured data, and identified as the most sensitive, were: (1) the storage thermal conductivity, (2) the u-tube resistance (simulating GHX fouling), and (3) an air gap added between the u-tube and grout. It was considered

possible that the actual WID GHX had possessed a combination of the parameter calibrations explored in this section. Discussed in the following section, further simulations were conducted to study the performance of the heat pumps connected to the GHX. Two GHX models were considered: one which is using the model parameters given by construction documentation ("as-designed"); and another which made use of parameters that reflected the measured GHX performance ("as-measured").

6.6 Challenging the GHX – Maximum Estimated Heat Rejection and Cooling Capacity

It was of interest to determine whether the GHX would allow all of the heat pumps to operate, and for what period of time. A simple model of the HPs was implemented in TRNSYS and connected to the full-field GHX to simulate the behavior of the system. The TRNSYS GHX model was used to predict the maximum heat rejection capability of the field and the allowable cooling capacity that would be expected for the WID ground-coupled heat pumps over a typical cooling season of 4 months. The behavior of the system for the full-field GHX modeled "as-designed" (i.e. using the parameters listed in Table) and the GHX model "as-measured" (i.e. the parameter-adjusted GHX model that more closely matches the measured GHX data) were used to determine the HP performance capabilities with regard to cooling capacity, COP, and the expected time the HPs would be allowed to operate before the field became too hot.[53]

[53] To model the "as-measured" GHX model, the storage thermal conductivity was decreased by a factor of three as discussed in Section 6.5. However, any of the parameter tweaks could have been used to simulate the as-measured GHX.

Figure 6-15 provides a summary of the HP and GHX model built in TRNSYS. In the model, the HPs were assumed to operate constantly at a specified capacity fraction (i.e. the number of HP modules operating divided by the total number of modules) and with the design chilled water supply and return temperatures, 45°F and 57.2°F, respectively. HP manufacturer performance data curve fits for the cooling capacity and COP were determined as a function of condenser entering water temperature and used to model the change in the HP operating conditions. The reason for the use of manufacturer HP data (as opposed to actual measured HP performance data as discussed in Chapter 5) was to investigate the design of the GCHP system. The required condenser water mass flow rate and leaving condenser water temperatures were calculated for the heat pumps and used as inputs to the GHX model. The reheat recovery capability of the WID GCHP system was incorporated in the model by assuming the reheat load was equal to 15% of the HP cooling capacity, which was based on the lowest measured monthly percentage of integrated recovered reheat out of the integrated HP cooling (July 2012). Reheat was only recovered from the condenser loop if the condenser leaving water temperature was above 110°F, the setpoint temperature that was used for recovery during the research. The water mass flow redirected to reheat was assumed half of the total condenser water mass flow, based on typical flow rate values observed in the system. The water returning from the reheat loop was mixed in with the condenser water and the drop in temperature due to reheat recovery was calculated before the inlet to the GHX. The leaving geo-field water temperature from the GHX model was returned as an input to the model of the HPs and the process starts over again. The equations used to model the HPs are provided in Appendix E.

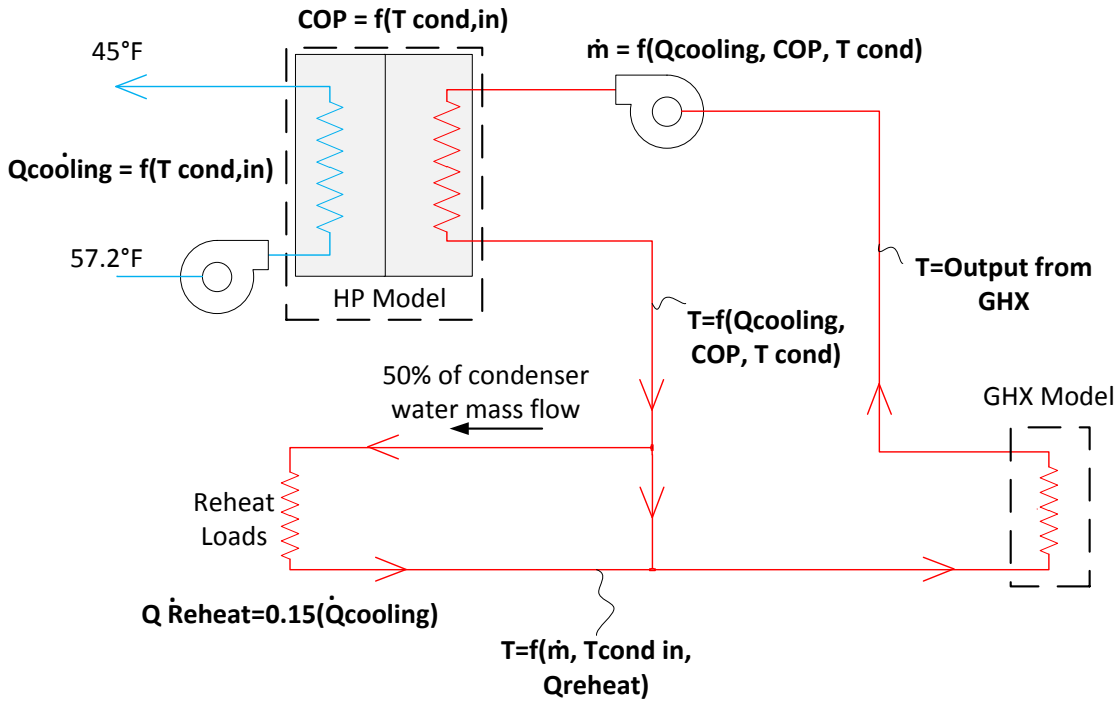

Figure 6-15 - Schematic of couple HP and GHX models in TRNSYS

A limit to the condenser water temperature was built into the model to simulate the heat pumps being unable to operate due to high condensing temperatures. An upper limit for the leaving condenser water temperature was assumed to be 143°F, based on the saturation temperature (153°F) of the HP working fluid (R410a) which corresponds to the refrigerant high pressure cutout setpoint (650 psi) for the HPs with an approach of 10°F between the condenser water inlet and refrigerant compressor inlet. Noting the 20°F drop across the condensers in the model, the max allowed entering condenser water would be 123°F.[54] A T-s diagram showing the saturation temperature of R410a is provided in Figure 6-16.

[54] Manufacturer performance data were not available for entering condenser water temperatures above 115°F. The data curve fits used to model the HPs were extrapolated for the higher condenser temperatures.

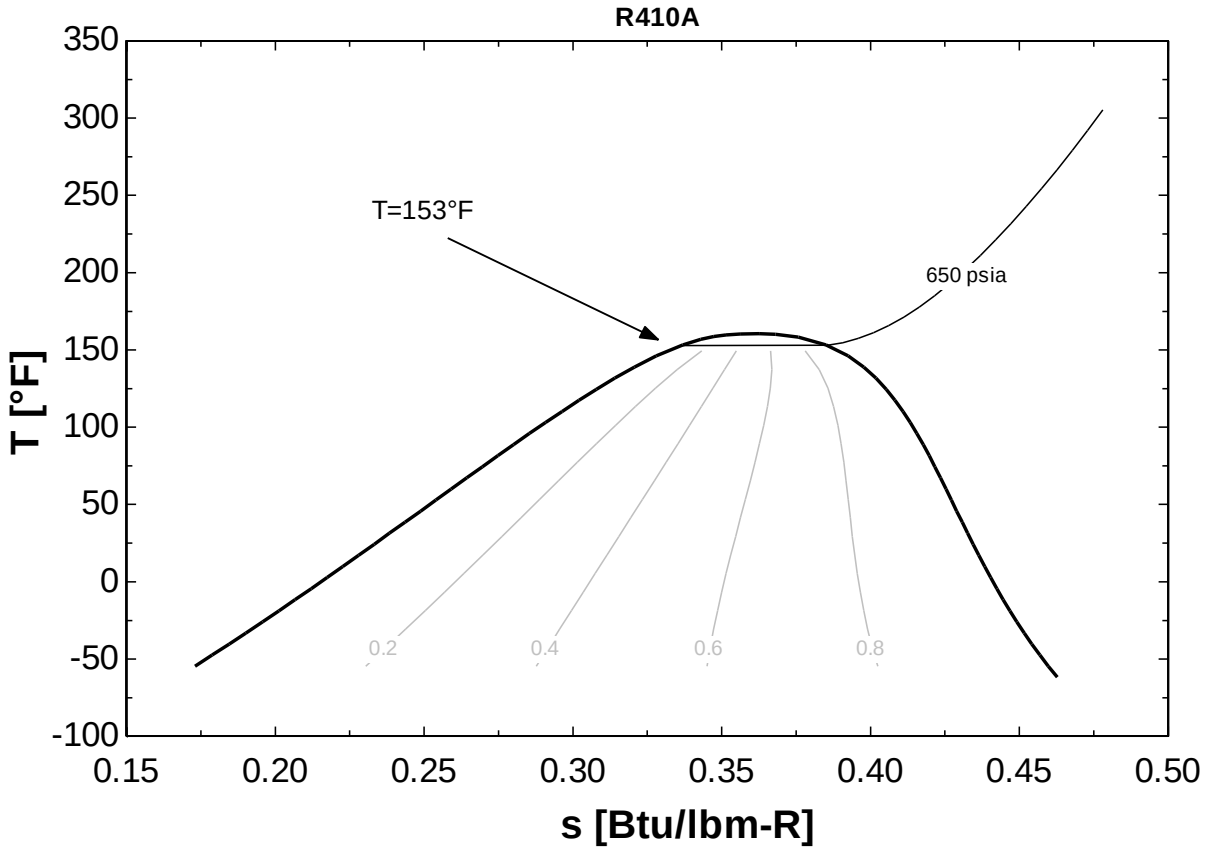

Figure 6-16 – T-s diagram with the saturation temperature for R-410a at the HP cutout pressure (650 psi)

The cutout time (i.e. the time taken for the water temperature returning to the HP condensers to rise to the maximum allowed temperature) was determined for the heat pumps running constantly at various load conditions. Figure 6-17 and Figure 6-18 show the cutout times for various HP capacities with the as-measured and as-designed GHX models, respectively. Using the "as-measured" GHX model, the cutout time for half of the heat pumps running constantly was observed to be 370 hours (15 days). In other words, the model suggests that even with heat recovery, the cutout condenser temperature condition would be reached with the actual WID GHX after running half of the available heat pumps for a period of 15 days.

The as-measured GHX is able to accommodate 40% of the available HPs operating steadily for about 100 days. Using the as-designed GHX model (i.e. the GHX using parameters given by design and manufacturer information), the cutout temperature is reached after all heat pumps operate steadily for only 75 hours. The as-designed GHX, with the assumed reheat heat recovery, is able to accommodate 75% of the heat pumps for four months.

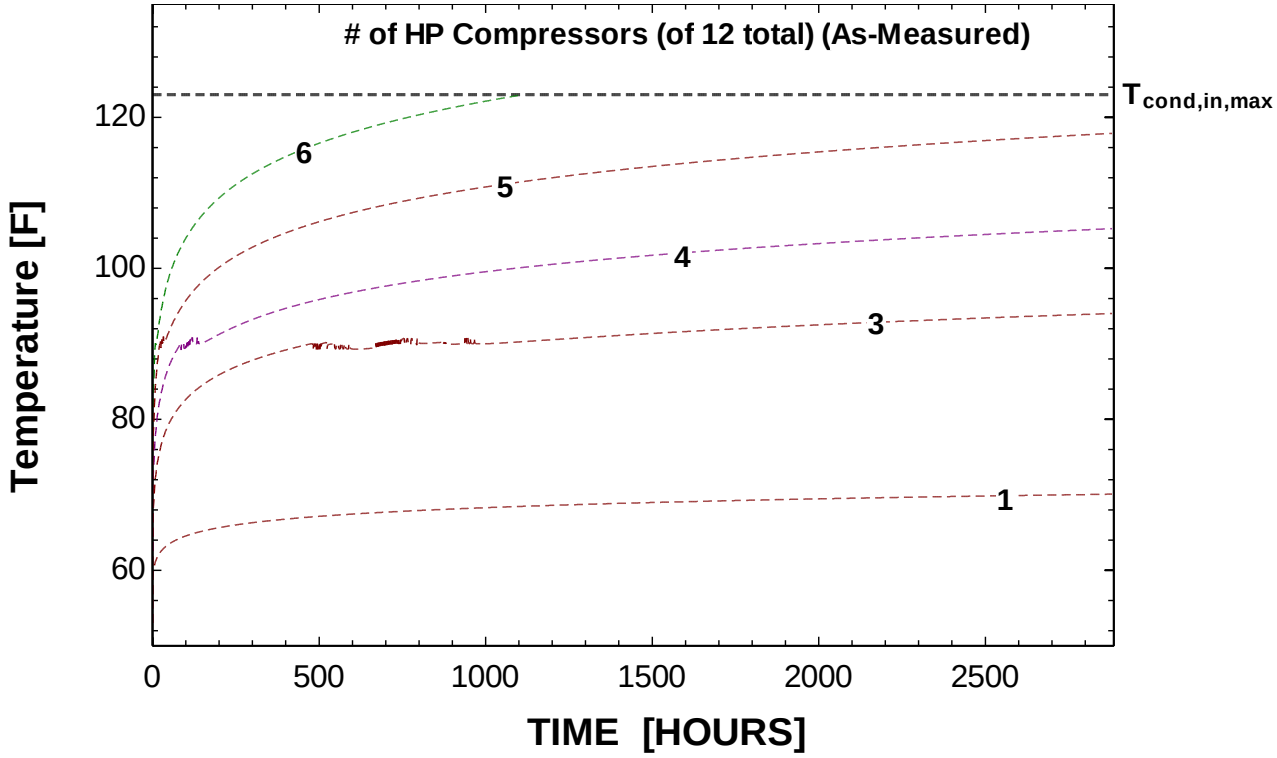

Figure 6-17 – HP cutout times at various capacities with the <u>as-measured</u> GHX model

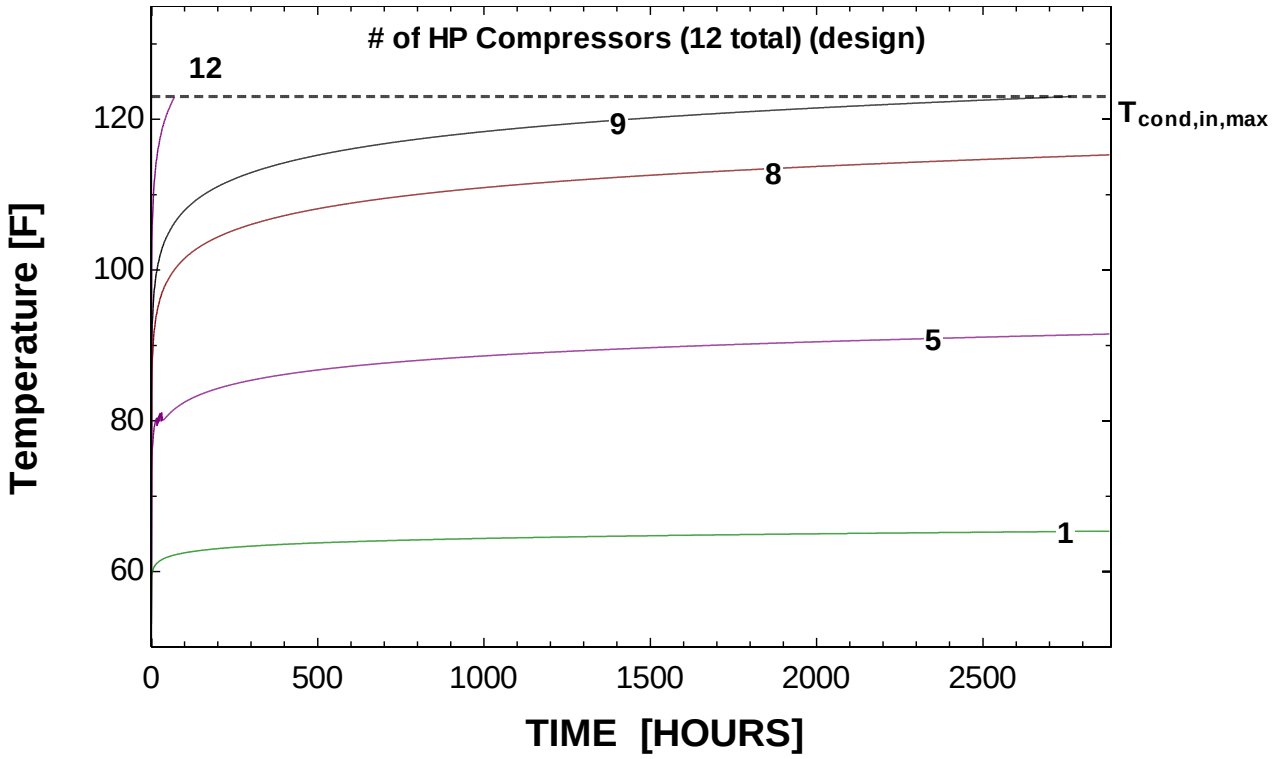

Figure 6-18 - HP cutout times at various capacities with the <u>as-designed</u> GHX model

The model suggests that, even with the GHX as-designed, all of the heat pumps would not be able to operate for more than a few days before reaching the maximum water condenser temperatures. The COPs and cooling capacities associated with various numbers of HPs operating steadily are provided in Figure 6-19 and Figure 6-20.

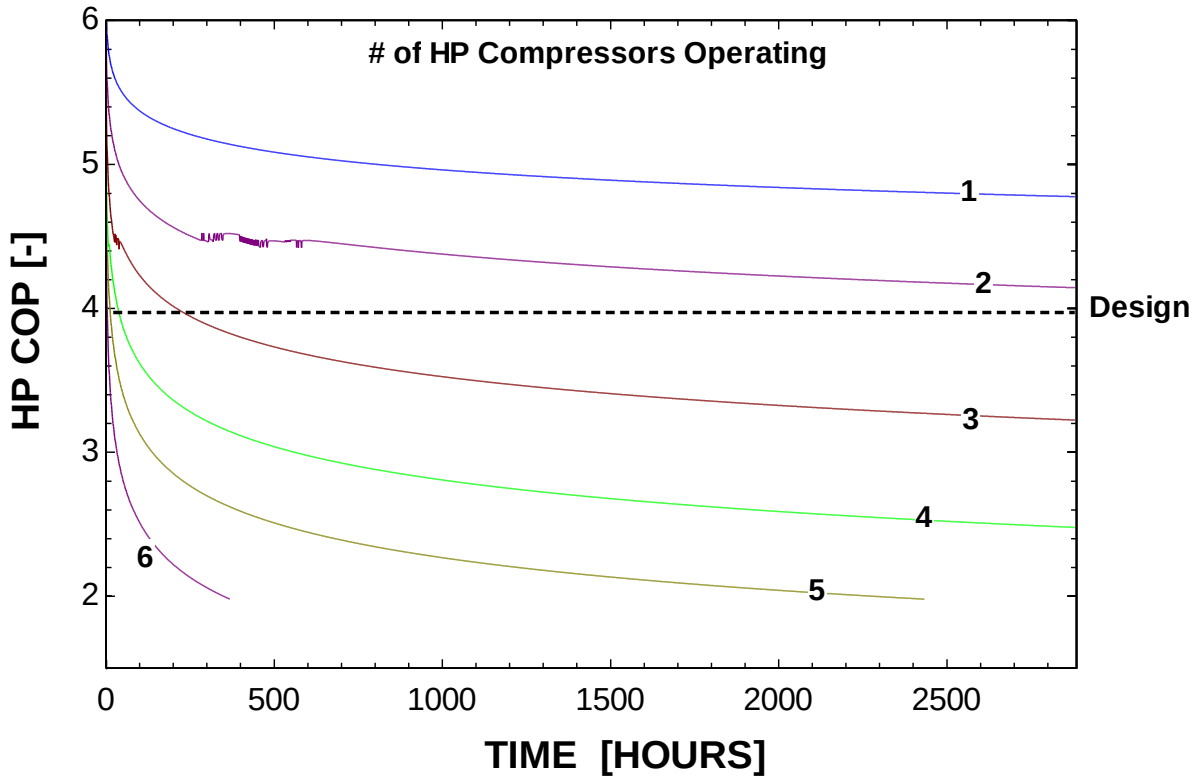

Figure 6-19 - HP COPs at various capacities and time of steady operation with <u>as-measured</u> GHX

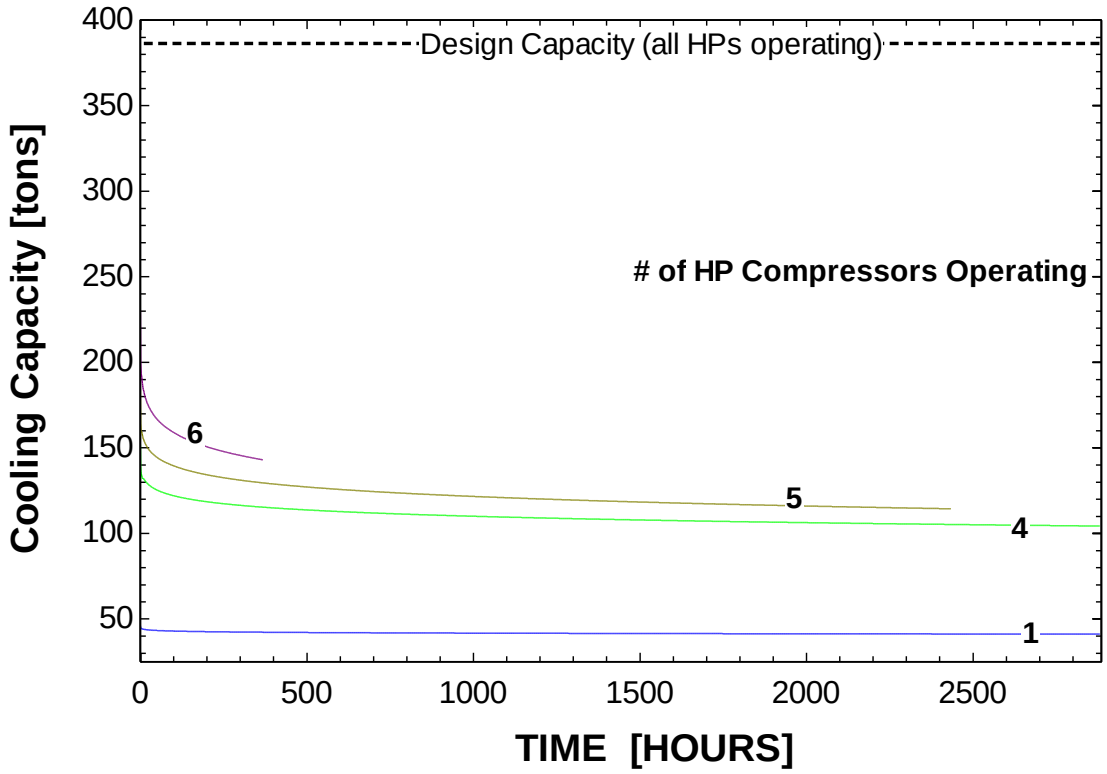

Figure 6-20 - Design HP cooling capacities at various operating capacities with the <u>as-measured</u> GHX

The models indicate that neither the as-measured or as-designed GHX would allow the operation of all twelve of the heat pumps for longer than a few days. Based on the documented properties of the storage, GHX materials, and bore layout it was investigated how many additional GHX bores, within the same volume ground, would be required to allow the cooling mode operation of all of the heat pumps. In Figure 6-21 and Figure 6-22, the entering condenser water temperatures and the HP COPs with all available heat pumps operating are shown for varying numbers of bores in the as-designed GHX model. As shown, between 100 and 150 GHX bores were needed to operate the HPs consistently for more than 2000 hours before reaching cutout temperatures. However, to operate all HPs simultaneously at the design HP COP, between 200 and 250 bores would be needed; approx. 3 times the number of bores installed at the WID.

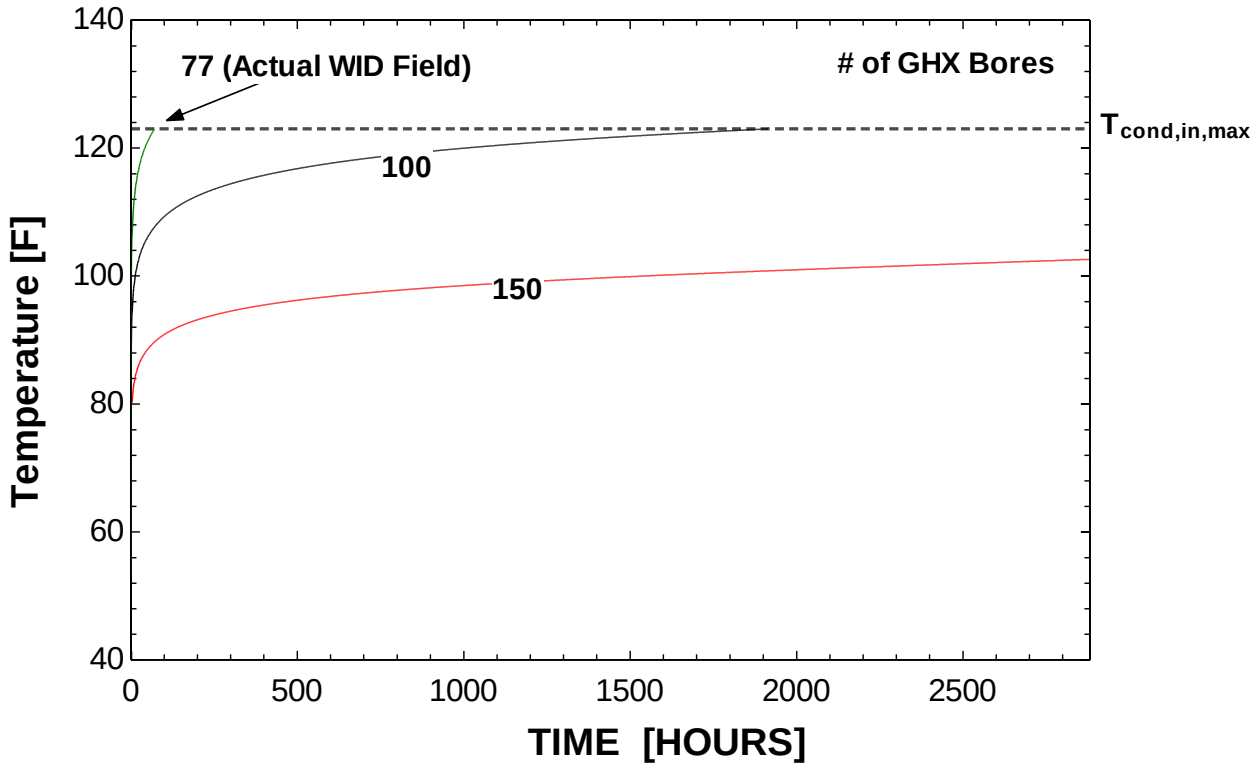

Figure 6-21 – Entering HP condenser water temps with all HPs operating and various numbers of bores (at GHX design parameters)

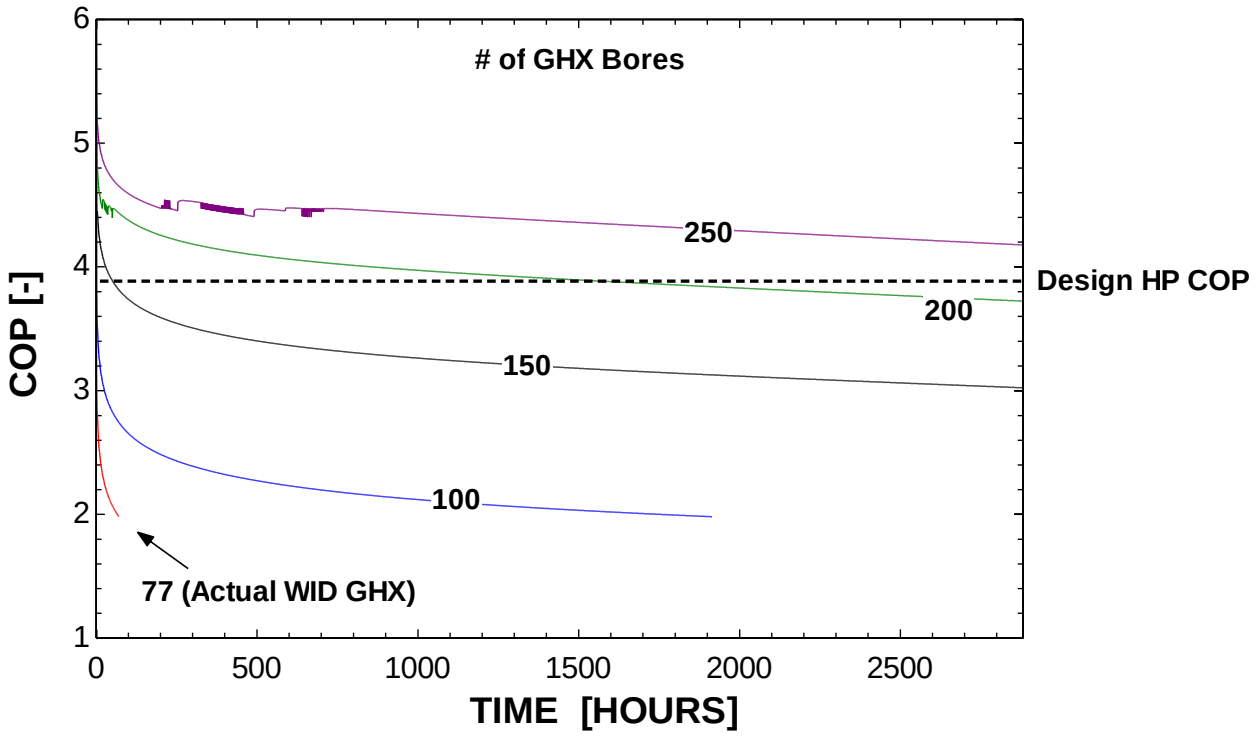

Figure 6-22 - HP COPs with all HPs operating and various numbers of boreholes (at GHX as-designed parameters)

It is important to remind the reader that the heat pump conditions produced in the models discussed in this section are based on the HP manufacturer performance data. In Chapter 5 the measured cooling capacity and COP of the heat pumps were shown to be, on average, 80% of the manufacturer data during steady operation. A more realistic (i.e. as-measured) model of the heat pumps would result in greater condenser temperatures (lower COPs resulting in higher heat rejection requirements) and therefore shorter cutout times, lower COPs, and lower cooling capacities than those shown in this chapter.

6.7 Conclusion

The WID GHX and ground-coupled heat pump system were modeled using TRNSYS to investigate possible causes for the heat rejection inadequacies observed in the system and to

explore potential flaws in the design of the system. Because the WID bores were configured in a perimeter pattern, it was determined necessary to increase the storage volume of the model to simulate greater spacing between the bores. The modeled GHX showed to have greater heat rejection capabilities than the actual GHX by approx. a factor of 2. From the model, possible origins (or combinations thereof) for the poor performance of the GHX were determined to be: (1) the ground thermal conductivity showed to be 3 times less than the reported value; (2) fouling (fouling factor) due to iron-oxide bacteria was 60 times greater than typical fouling factor values; and (3) air gaps between the u-tube and grout were found to be 3% the total volume of the grout.

The model of the GHX as-designed was coupled to a simple heat pump model in order to determine the maximum cooling capacity and efficiency of the heat pumps at various cooling loads. It was observed from the model that the GHX, as-measured, was only capable of rejecting heat to allow 40% of the available heat pumps to run constantly through the cooling season. In order to run the heat pumps at or above their design efficiency, only 20% of the heat pumps could be operated. More interestingly, the GHX, as-designed, could not accommodate the required heat rejection needed to operate 100% of the heat pumps for more than 15 days. The model suggested that 100 to 150 bores were needed to run 100% of the HPs constantly through a typical cooling season, and 200 to 250 bores to run 100% of the HPs at their design efficiencies.

Because of the inherent differences between the model and the actual WID GHX, namely the configuration and spacing of the bores, the model results were considered only estimates and

not conclusive. Tests that allowed the heat pumps to run constantly at set operating capacities would provide valuable measured data with which to validate the models.

Chapter 7. Summary of Results and Conclusion

7.1 Summary of Results

An energy performance analysis was conducted for the ground-coupled heat pump system (GCHP) located at the Wisconsin Institutes for Discovery – a high-performance, LEED Gold certified laboratory facility. Initial explorations of the system revealed two issues that had long term impacts to the research: (1) high-cycling of the heat pumps, (2) and leaks in the valving that were installed to allow the system to operate in either heating or cooling mode. Technical staff from the construction contractor and the heat pump manufacturer reduced the cycling time from three minutes on average to 20 minutes on average. To stop the leaks, the valving was permanently sealed, limiting the system to operate only in cooling mode.

7.1.1 Instrumentation Errors

During the research, instrumentation errors were found and corrected (Chapter 4). The flow meters monitoring the condenser and evaporator water flow rates (installed prior to this research) were improperly labeled and interchanged. The evaporator water flow meter had been installed close to an upstream pipe elbow, resulting in a greater measurement error (±10%, from comparative measurements). The condenser water flow meter had been calibrated for a larger pipe size than the actual condenser water pipe. Re-calibration of the flow meter was performed with the assistance of FP&M.

Due to an excessively long installation mounting, the probe of the sensor monitoring the entering evaporator water had not been fully inserted into the thermowell, causing the temperature reading to be at least 6°F higher than actual. Comparative temperature

measurements indicated offset corrections were needed for several sensors ranging from 0.1 to 3.6°F. Electrical wiring issues caused the sensors connected to BTU meter to be out of operation extended time periods during the research. Four temperature or flow sensors were installed in locations that could not be physically accessed for field-verification.

7.1.2 Heat Pump Performance

The measured in-situ performance of the heat pumps was observed at 80% of the manufacturer-predicted performance (cooling capacity and COP), on average (Chapter 5). Six out of thirteen data periods during quasi-steady operating conditions indicated the measured cooling capacity was within measurement uncertainty of the manufacturer-predicted capacity. The supply chilled water temperature varied as much as 7°F from the setpoint supply temperature for several of the steady measurement intervals, indicating possible issues with the internal controls of the heat pumps. The measured COP of the heat pumps was consistently below manufacturer-predicted COP. However, the measured COP for all compared data intervals were within measurement uncertainty of manufacturer-predicted COP, indicating that the heat pumps operated as expected.

7.1.3 System Performance

For the months that the HPs provided over 40,000 ton-hours of cooling (July to October 2012, and April 2013), the measured monthly average COP of the heat pumps was observed to be from 2 to 2.75, which was 66% of the design efficiency, on average (Chapter 5). The in-situ COP of the GCHP system in cooling mode was compared with the measured COP of the campus chilled water utility. The campus chilled water system was twice as efficient

when compared to the WID GCHP for the months that the campus chillers were operational (May to October). The single largest factor to explain the comparatively low operating efficiency of the GCHP system is that the entering condenser water temperatures were running significantly higher than anticipated in the design. With the functionality of the reheat recovery appearing to perform near design expectations and the measured peak reheat recovery rates matching closely to the expected reheat capacity, the high condenser water temperatures were attributed to the heat rejection capabilities of the ground heat exchanger.

7.1.4 GHX and Heat Pump Model

A model of the ground heat exchanger (GHX) was created in TRNSYS that aided a parametric study to determine possible causes for what was observed to be poor heat rejection capabilities of the GHX as compared to its design (Chapter 6). The study indicated that the GHX design was most sensitive to three parameters, which, when varied, allowed the GHX-modeled leaving water temperature to closely match the measured leaving water temperature: (1) the average thermal conductivity of the ground, (2) the thermal resistance between the grout fill and the u-tube piping (or fouling within the u-tube), and (3) the thermal conductivity of the grout fill. The three identified parameters were compared with reasonable approximations or standard values and it became apparent that none of the identified parameters were likely to be the sole cause of the poor GHX performance. However, it was probable that all three of the parameters contributed.

A model of the GCHP system "as-measured" showed that the design efficiency (COP = 4) could only be attained with one or two HP compressors operating (of twelve total). Three or

more operating heat pumps generate water temperatures returning from the GHX that are too high for the heat pumps to operate at their design efficiency. With the system modeled "as-designed", all twelve of the HPs operating constantly caused the condenser water temperature to reach the maximum allowed temperature (high pressure cutout conditions) after about three days. Therefore, it was not clear how the GHX was sized to accommodate the installed heat pumps.

7.1.5 Recommendations

One recommendation that should be considered to increase the cooling capacity and overall operating efficiency of the WID's primary system would be to disable the ground-coupled heat pump system and utilize campus utilities to satisfy the WID cooling and reheat loads. If the decision is made to retain and continue operating the heat pump system, other means of heat rejection should be sought. For example, heat might be rejected to a separate condenser water system utilizing a cooling tower sited on the roof or other accessible and safe area near the WID. The following sections explore areas of the system design that appeared to cause the main issues with the system's energy performance.

7.2 Concluding Remarks on the System Design

7.2.1 Failure of Valves Due to System Complexity

Butterfly valves V-3 through V-10 were installed in the WID GCHP system for the purpose of allowing the system to operate in either heating or cooling mode. Facility technicians discovered that some or all of the valves were the source of leaking between the condenser and chilled water loops. The added complexity in piping and valving to allow the system to

operate in heating, cooling, or cooling with heat recovery modes increased the possibility for implementation, installation, or equipment flaws. Further research is needed to determine the cause of the valve failures. More dependable valves, or double valves, may be considered for future hydronic heat pump systems that are more complex than conventional systems.

7.2.2 Free Campus Low Pressure Steam

The campus utility steam supply piping within WID was such that the reheat requirements were met by low pressure steam if available, and high pressure steam if not. The overabundance of the free campus low pressure steam made the heat recovery and heating mode capabilities of the WID GCHP system considerably lower in value. The surplus of low pressure steam is a consequence of campus utility power plant operations (e.g. a by-product of power production from natural gas-fired turbines). Further investigation is needed to determine if there are regular/predictable time periods that the campus utility does not have an abundance of low pressure steam. Additionally, further research should determine the energy, efficiency, carbon costs due to WID consumption of campus utility high pressure steam. The analysis would further compare the source energy costs between the campus high pressure steam production and the WID GCHP system operating in heating mode.

7.2.3 Heat Recovery Can Encourage High Condenser Water Temperatures

The heat recovery design of the system has the potential to negatively impact the operating efficiencies of the heat pumps. Heat recovery requires minimum water temperatures to operate, nominally 90°F to 110°F, but depends largely on the sizing of the reheat coils. Further, the heat pumps' efficiency is inversely proportional to the entering condenser water

temperature; the lower the entering temperature the higher the heat pump efficiency (in cooling mode). Therefore, the heat recovery or heat rejection capabilities of the system are important to ensure the condenser water temperature drop between the design reheat supply and entering condenser water temperature is possible. Otherwise, the high condenser water temperatures that are desirable for heat recovery are only possible by sacrificing the efficiency of the heat pumps.

7.2.4 High Reheat Water Supply Temperatures

According to the construction schedule documents, 70% of the WID reheat terminals were designed for entering water temperatures of 130°F. When building reheat is met by campus utility steam, the setpoint temperature for the reheat water is 130°F. In heating mode, the heat pumps were able to provide a maximum (design) temperature of 130°F. However, with all twelve of the heat pumps operating in cooling mode, the heat pumps were only able to produce leaving condenser water temperatures as high as 105°F at design entering condenser water temperature and condenser water flow rate. Therefore, it was not clear how reheat recovery was intended to work with such low (105°F maximum) temperature water compared to the design temperature of the reheat terminals, without sacrificing the efficiency of the heat pumps.

7.2.5 Risk of Steam Heated Condenser Water from Automatic Mode Switch-Over

As discussed, the GCHP system was able to recover condenser leaving water or use campus steam in the building reheat loop. Because the system could automatically switch between

either mode, it was possible that, at switch-over from steam-heated to heat recovery mode, the steam temperature reheat loop water (130°F) would necessarily be directed to the geo-field and then to HP condensers, causing undesirable heat addition to the geo-field and condenser loop. The behavior just described was observed at least once, during which the water temperatures entering the heat pump condensers immediately following switch-over to heat recovery mode were high enough that several of the heat pumps quickly shut down due to high pressure refrigerant cutout (consequence of high temperature entering condenser water).

Fundamentally, the risk stems from the difference between the steam-heated reheat supply setpoint temperature (130°F) and the heat recovery supply setpoint temperature (105°F). The problem would not exist if the two setpoint temperatures were the same. The system controls should also implement logic that increases the time between steam shut-off and heat recovery initiation based on the temperature in the reheat loop. In other words, the steam-heated water in the reheat loop should be allowed to circulate with no further steam heat input until the temperature reaches the heat recovery temperature, before switching to heat recovery mode.

7.2.6 LEED Design and Energy Model

According to the Basis of Design, the GCHP system was installed at the WID to reduce energy consumption and carbon emissions. However, it is difficult to quantify the extent that the WID primary system's design may have been influenced by the requirements of the LEED certification or by the "green" publicity potential of a ground-coupled heat pump system with heat recovery. The WID design engineers created a building energy model in

eQuest, and from reviewing the details of the model it may be possible to determine the following: (1) how the model results (specifically the modeled GCHP system) contributed to the achieved LEED rating; (2) whether the modeled energy saving measures were realistic and what assumptions were employed (e.g. reasonable heat pump COPs); (3) whether the model and early design process considered the efficiencies of the existing campus utilities; (4) what energy saving methods or assumptions were employed in the model that changed in the actual building construction and, knowing the changes, would a more conventional design had saved more energy; and (6) what negative and positive outcomes could be projected using a more conservative/conventional system in the energy model, knowing the implementation challenges that have been realized at the WID.

7.3 Further Actions and Future Research

Several changes to the WID GCHP system were anticipated to occur at the conclusion of the present research. Based on the preliminary recommendations of this research, the WID Green Team and facility technical staff initiated a temporary (one month) shutdown of the WID heat pump system on May 2nd, 2013. The purpose of shutting down the system for a longer period of time was to evaluate the "recovery" of the ground loop. Specifically, this action sought to systematically measure the decrease in return water temperature from the GHX when heat was not being rejected. Depending on the findings from this test, the development of a longer-term plan should be established.

The detected leak between the chilled water and condenser/reheat loops was on the agenda for the WID and campus facility staff to address following the present research. Additionally, there were tentative plans to install a heat exchanger between the campus and heat pump

chilled water loops in order to isolate the high system water pressure and possible iron bacteria believed to be in the campus chilled water system. Finally, the WID, UW Facilities, and the UW Direct Digital Controls group were in on-going discussions regarding an extensive review of the controls and control setpoints within the WID systems. An additional commissioning process was also being considered. Following, or in conjunction with, the above anticipated system changes, future research may consist of the ideas explored in the following sections.

Operating Some of the Heat Pumps in Heating and the Others in Cooling

During the present research, it was not possible to operate some of the heat pumps in cooling mode while simultaneously operating the others in heating mode. Being able to do so would allow for a more balanced system and help avoid the heat rejection constraints observed in the geo-field. For example, a fraction of the twelve heat pumps may be run in heating mode to provide building reheat. The evaporators of the heating heat pumps would be connected hydronically to the condensers of the other six heat pumps, which would be running in cooling mode to provide some portion of the building cooling load. In other words, the heating HPs would absorb heat from the condenser fluid of the cooling HPs. Supplemental heat rejection/absorption would be performed using the GHX. It is possible that a system operating in this manner could realize higher system efficiencies than in the current configuration of the WID GCHP system and reduce the heat rejection/absorption duty of the GHX. However, additional piping and equipment would be needed and a significantly more complex controls scheme. The heat pump electricity costs and the availability of free campus low pressure steam should first be considered.

Locate Additional Heat Rejection/Recovery Opportunities

Additional heat rejection or heat recovery opportunities using the heat pump condenser water would allow more of the heat pumps to operate at higher efficiencies. Connecting the GCHP condenser water to other WID heating systems or portions thereof, such as the WID perimeter heating loop or domestic hot water loop, may allow additional heat rejection. A system that provides ice melting capabilities within the building sidewalks may be one method that would allow for additional heat rejection. The relatively low temperature of the heat pump condenser leaving water, the overabundance of campus utility low pressure steam, and the investment cost of the GHX vs. the heat pumps would make finding additional heat rejection capabilities unlikely to add substantial value. In addition to the cost of additional piping/equipment, the increased complexity of the system should be carefully considered.

Other Campus Chilled Water Systems

To compare the COP of the WID GCHP system to the campus utility, measured data for the chilled water system operations at the West Campus facility were used (Chapter 5). The West Campus facility was chosen for comparison because it had the largest chilled water capacity of the three chilled water utility plants at the time of the present research and possessed the greatest future (planned) capacity. However, because chilled water is generated at multiple facilities on campus, a complete study would consider the performance of all available chilled water systems. Specifically, the schedule of operation, availability and amount of chilled water, dependability, long-term operation plans, and confidence in the measured data should all be considered for the chilled water system performance of each utility.

Data Sensor Fault Detection

Continuous energy monitoring practically necessitates sensor fault detection. Calculations such as the building's monthly carbon footprint (which is publicly displayed in the ground floor of the building) would be impacted by the loss of measurement, rendering the published carbon footprint value inaccurate. Due to the relatively frequent instrumentation faults that were observed during the present research, such as the BTU meter sensors losing power due to electrical issues, it is recommended to establish an automated or routine instrumentation fault detection process. The Intelligent Building Architecture system (IBA) possesses the capability to automate energy monitoring fault detection and alerting.

For example, if a zero reading is recorded for a sensor for a significant period of time, an alarm should be generated that notifies an administrator of the issue. A second level of fault detection would compare that sensor's reading to other measurements in the system to provide basic logic (e.g. the condenser hydronic pumps have been disabled, so there should be no water flow through the condenser – do not generate alarm). A third level of fault detection would compare sensor readings at various times and system conditions in order to detect sensor changes or faults (e.g. when valve V-1 and V-2 are open 100%, temperature sensors CLW-T and WHS-T should reasonably agree within ±0.5°F).

Verification and Calibration for Future Instrumentation

Because several instrumentation errors were found during instrumentation verification, it is recommended that sensor verification and calibration be performed for any instrumentation installed for the purpose of energy monitoring. The verification process would, at a

minimum, require that critical sensor / data point connections are validated (i.e. physically removing the sensor to observe the reading change on the data system). Secondly, measurement comparisons should be made for all sensors where possible. Examples for data comparisons can be found in Chapter 4 of this document. Where sensor comparisons cannot be made, additional instrumentation may be required (e.g. ultrasonic flow meter, surface mounted temperature sensor, or glass thermometer).

Methods to Avoid and Detect Grout Fill Air Entrainment

Air entrained in the grout fill was shown to greatly impact the heat transfer ability of the ground heat exchanger (model). Further research is needed to investigate the likelihood of air entrainment in the grout slurry during the mixing and fill of the borehole. If it becomes possible to access one or more of the WID GHX bores, one or more samples of the grout may be extracted and subjected to a thermal conductivity test. Preferably, the sample(s) would be a radial cross section of the bore from the u-tube to the ground. The results of the test should be compared to the grout manufacturer's reported thermal conductivity. Furthermore, because the grout slurry is mixed on-site during the GHX installation, a review of the mixing procedure for the WID GHX grout may reveal possible causes of grout entrainment and, subsequently, methods to avoid such.

Methods to Detect and Avoid Bore Gap or Bore Collapse

As with the possibility of grout fill air entrainment discussed above, the GHX model showed that the GHX heat rejection capability is sensitive to a gap between the outer u-tube walls and the grout fill. A gap could form from cycles of thermal expansion and contraction of the

u-tubes during operation, or from neglecting to apply an appropriate system pressure inside the u-tubes while the u-tube is being installed. If access to the WID GHX becomes possible, one or more samples of the bore may be extracted to investigate the existence of, or possibility of, a gap between the u-tube and grout. The adhesion strength of the grout to the u-tube outer wall should be considered. Further, a review of the WID GHX u-tube installation procedure may reveal possible causes of bore gap.

U-tube Shank Spacing and Thermal Short Circuit

No information was reported regarding the installation methods used to ensure adequate u-tube shank spacing (i.e. the distance between the upward and downward flowing legs of each u-tube pipe) for the WID GHX. Adequate shank spacing is desirable to promote heat conduction outward from the bore and to discourage heat transfer to the adjacent u-tube leg (i.e. thermal short circuit). The GHX model was created assuming shank spacing based on the reported curvature of the u-tube bend. Though it was not observed to be the most sensitive parameter, the GHX model confirmed that smaller u-tube shank spacing would promote greater thermal short circuiting, and therefore poorer heat rejection capability of the GHX. Further investigations of the installation procedures of the WID GHX may reveal installation improvements for future ground heat exchangers. One possible example might be the need for thermally resistive shank spacers that guarantee spacing between the u-tube legs.

Investigating GHX Fouling

Based on observed contamination in the hydronic loops and the poor heat transfer capability of the GHX, it was hypothesized that contaminate fouling had collected on the walls of the GHX u-tubes. If possible, gaining access to one or more of the GHX u-tubes would allow it to be inspected for fouling or contaminant buildup. The investigation would be best if coordinated with future sidewalk removal or replacement. The inspection may consist of a visual inspection (e.g. an imaging "scope") or a sample removal by scraping the inside of the u-tube.

GHX Fouling Observation U-tube

Future GHX installations and GHX research, particularly those connected to systems that likely produce heat exchanger fouling, should consider the design and implementation of a special "observation" u-tube that would be installed in a similar manner to the actual GHX u-tubes. The observation u-tube would not be installed into the ground; rather it would be left in an accessible location such as a mechanical equipment room. Because the u-tube is connected to the same hydronic system, studies could be conducted using the observation u-tube with almost no impact to the actual GHX system. For example, sections could be cut from the u-tube and studied at regular intervals to investigate fouling or even complete blockage due to fouling. The impact of the fouling to the thermal resistance or water flow could be studied using the observation u-tube. It may also be possible to construct a transparent observation u-tube (with similar material properties of the actual u-tube) in order to aid the fouling investigations.

Works Cited

AHRI. *Standard 330: Standard for Ground-Source Closed-Loop Heat Pumps.* Arlington: Air-conditioning, Heating, and Refrigeration Institute, 1998.

AHRI. *Standard 550/590: Performance Rating of Water-Chilled and Heat Pump Water-Heating Packages Using the Vapor Compression Cycle.* Arlington, VA: Air-Condition, Heating, and Refrigeration Institute, 2011.

Architects. *Interim report on advancement of sustainability inititiatives.* Madison: WID Internal Document, 2008.

ASHRAE. *Fundamentals Handbook - HVAC.* Atlanta: American Society of Heating, Refrigeration, and Air-Conditioning Engineers, Inc., 2011.

ASHRAE. *Measurement, Testing, Adjusting, and Balancing of Building HVAC Systems.* Atlanta: ASHRAE, 2008.

Austin, G., K. Delorey, D. Wilson, J. Madden, P. Stupp. *A New Direction, The Wisconsin Institutes for Discovery: Integrated Project Delivery.* www.discovery.wisc.edu, 2011.

Austin, W.A. III, C. Yavuzturk, and J.D. Spitler. "Development of an in-situ system for measuring ground thermal properties." *ASHRAE Transactions*, 2000: 365-379.

Azar, E., C. Menassa. "Agent-Based Modeling of Occupants and Their Impact on Energy Use in Commercial Buildings." *Journal of Computing in Civil Engineering, Vol. 26 Issue 4* (Journal of Computing in Civil Engineering), 2012: 506-518.

BOD. "WID Basis of Design." *WID Internal Document.* 2011.

Building Database. *Department of Energy.* 2013. https://buildingdata.energy.gov/ (accessed June 4, 2013).

Burr, A.C. *Studies suggest more gains for green building in 2009.* Washington D.C.: CoStar Group, 2008.

Clarke, B.G. "Model Specification to Determine Thermal Conductivity of Soils." *Proceedings of the Institution of Civil Engineers*, 2008: 161-168.

Controls. "As-Commissioned Control Drawings." *WID Internal Document.* WID Controls and Commissioning Engineers, 2012.

Correspondence. "Author e-mail correspondance with the WID Cx team." December 15th, 2011.

Dermisi, S.V. "Effect of LEED ratings and levels on office property assessed and market values." *Journal of Sustainable Real Estate, Vol. 1* (Journal of Sustainabile Real Estate), 2009: 23-47.

DOE. *ANSI/ASHRAE/IES Standard 90.1-2010 Final Determination Quantitative Analysis.* Alexandria, VA: Pacific Northwest National Laboratory, 2011.

EIA. *Annual Energy Outlook.* Washington D.C.: United States Energ Information Agency, 2013.

EISA. "Energy Independence and Security Act." *Public Law 110-140.* Washington D.C., December 19, 2007.

Energy Center of Wisconsin. *Hybrid Ground-Source Heat Pump Installations: Experiences, Improvements and Tools.* Madison: Energy Center of Wisconsin, 2011.

Energy Model. "eQuest Energy Model Results." WID Internal Document, 2011.

Energy Star. 2013. www.energystar.gov/istar/pmpam/ (accessed June 4, 2013).

Eskilson, P. *Thermal analysis of heat extraction boreholes.* University of Lund, Sweden, 1987.

First Floor Mechanicals. *WID Internal Document: Mechanical Elements in the First Floor Pour.* WID General Construction Contractor, 2008.

FP&M. *Facility Information: Campus Map.* 2007. http://www.fpm.wisc.edu/smomap/building.aspx?building=0205&wing= (accessed June 5, 2013).

FP&M. *Utilities Master Plan Report Vol. 1.* Madison: Facilities, Planning, and Management: University of Wisconsin, 2005.

Hellström, Göran. *Duct Ground Heat Storage Model: Manual for Computer Code.* Lund, Sweden: Department of Mathematical Physics, University of Lund, 1989.

HP Submittal. *WID Heat Pump Manufacturer Equipment Submittal.* Madison: WID Internal Document, 2010.

IEC. *IEC 60751: Industrial Platinum Resistance Thermometers and Platinum Temperature Sensors.* Geneva: IEC, 2008.

In-Floor Submittal. "WID Internal Document: Radiant Floor System Re-Submittal." 2008.

Ingersoll, L.R. *Heat conduction with engineering and geological application, 2nd Edition.* New York: McGraw-Hill, 1954.

IPCC. *Climate Change Synthesis Report.* Geneva, Switzerland: Inergovernmental Panel on Climate Change, 2007.

Kavanaugh, S.P., Rafferty, K. *Ground-source heat pumps - Design of geothermal systems for commercial and institutional buildings.* Atlanta: ASHRAE, 1997.

Kelly, Janet. "Discovery building marks first anniversary with Gold LEED." *discovery.wisc.edu.* November 30, 2011. http://discovery.wisc.edu/story.cmsx?sid=20084 (accessed June 3, 2013).

Klein, S.A., W.A. Beckman, J.W. Mitchell, J.A. Duffie, J.W. Thronton, and J.C. Mitchell. *TRNSYS, A Transient System Simulation Program, User's Manual, Version 16.* Madison, WI: Solar Energy Laboratory, University of Wisconsin-Madison, 2004.

Mangasarian, S., Carol Menassa. *Energy consumption evaluation of United States Navy LEED certified buildings for fiscal year 2009.* UW-Madison Civil and Environmental Engineering, 2010.

Matthew, P., Sartor, D., Van Greet O, Reilly S. "Rating energy efficiency and sustainability in laboratories: results and lessons from the Labs21 program." *Proceedings of the ACEEE 2003 Summer Study on Energy Efficiency in Buildings, vol. 4.* 2003. 321-329.

MGE. *West Campus Cogeneration Facility, Meeting Multiple Energy Needs Through the Efficiency of Cogeneration.* Madison: Madison Gas and Electric Company, 2011.

Mogensen, P. "Fluid to duct wall heat transfer in duct system heat storages." *Proceedings of the Internation Conference on Subsurface Heat Storage in Theory and Practice.* Stockholm, 1983. 652-657.

Nellis, G. F., S.A. Klein. *Heat Transfer.* New York: Cambridge, 2009.

NREL. *Evaluation of ANSI/ASHRAE/USGBC/IES Standard 189.1-2009.* Golden, CO: National Renewable Energy Laboratory, 2010.

Pertzborn, A., Scott Hackel, Greg Nellis, and Sanford Klein. "Experimental Validation of a Ground Heat Exchanger Model in a Hybrid Ground Source Heat Pump." *HVAC&R Research 17(6),* 2011: 1101-1114.

Rafferty, K. "A capital cost comparison of commercial grond-source heat pump systems." *Geo-Heat Center Quarterly Bulletin Vol. 16, No. 2,* February 1995.

Rafferty, Kavanaugh and. "Ground-Source Heat Pumps - Design of Geothermal Systems for Commercial and Institutional Buildings." In *ASHRAE,* by ASHRAE. 1997.

Shonder, J.A., V. Baxter, J. Thornton, P. Hughes. "A new comparison of vertical ground heat exchanger design methods for residential applications." *ASHRAE Transactions 105(2),* 1999: 1179-88.

Spitler, J., J. Cullin, M. Bernier, M. Kummert, P. Cui, X. Liu, E. Lee, and D. Fisher. "Preliminary intermodel comparison of ground heat exchanger simulation models." *Proceedings of the 11th International Conference on Thermal Energy Storage.* Stockholm, Sweden, 2009.

Taylor, B.N., and Kuyatt, C.E. *Guidelines for Evaluating and Expressing the Uncertainty of NIST Measurement Results.* Washington D.C.: National Institute of Standards and Technology, 1994.

Taylor, N., C. Menassa. "An Experimental Approach to Optimizing Natural Ventilation in Public Spaces of Complex Buildings." *Construction Research Congress*, 2012: 1651-1661.

TEMA. *Standard of the Tubular Exchanger Manufacturer Association, 8th Ed.* New York: Tubular Exchanger Manufacturer Association, 1999.

TESS. *Type 557: Vertical Ground Heat Exchanger Manual.* As part of TRNSYS User's Manual (2004), 2004.

USA Today. "USA Today." *Green schools: Long on promise, short on delivery.* December 11th, 2012. http://www.usatoday.com/story/news/nation/2012/12/10/green-schools-construction-leed/1753823/ (accessed June 5th, 2013).

UW News. *University of Wisconsin-Madison News.* February 2nd, 2009. http://www.news.wisc.edu/16189 (accessed June 5th, 2013).

WI Statute 196, section 374. *Regulation of Public Utilities.* Madison: State of Wisconsin, 2013.

Witte, Henk J.L. "In Situ Measurement of Ground Thermal Conductivity: A Dutch Perspective." *ASHRAE Transactions, Vol 108, Part 1*, 2002: 262-272.

Woo, S., and O'Neal, D.L. "The Effect of Elbows on the Accuracy of Liquid Flow Measurement with an Insertion Flow Meter." *ASHRAE Transactions*, 2006: 195-201.

Appendix A. Key Equations and Measurement Uncertainties

Key Equations

To consolidate information and remove redundancy in the present report, the key equations (i.e. the equations most crucial to the research and used repetitively) are located in the following sections. Additionally, the equations used to propagate the measurement uncertainties of key variables have also been consolidated herein. The equations are referred to where appropriate within the text.

Measured Cooling Capacity and Integrated Cooling

The general equation for measured cooling capacity in English units is:

$$\dot{Q}_{cooling} = \dot{V}\rho_{chw}c_{p_{chw}}\left(T_{return} - T_{supply}\right) 0.005 \left[\frac{tons}{\frac{Btu}{min}}\right] \quad \textbf{(A-1)}$$

where $\dot{V}$ is the evaporator water volume flow rate in GPM,

ρ_{chw} is water density in lb/gallon,

$c_{p_{chw}}$ is water specific heat in Btu/lb-°F,

and T_{return}, T_{supply} are the water temperatures in °F returning to and supplied from the source of cooling, respectively.

The water density and specific heat values were assumed to be constants at typical chilled water conditions found in the WID chilled water systems. Thermophysical property data in EES were used to determine the density and specific heat of water at an average chilled water

temperature of 50°F and pressure of 50 psi, resulting in values for density and specific heat of 1 [Btu/lb-°F] and 8.344 [lb/gallon], respectively.

For convenience, the constants found in Eq. (A-1) were combined, resulting in a simplified equation for measured cooling capacity:

$$\boxed{\dot{Q}_{cooling} = \dot{V}\left(T_{return} - T_{supply}\right) 0.0417 \left[\frac{tons\ min}{gallon\ °F}\right]} \quad \textbf{(A-2)}$$

At any instant, the total rate of cooling (in tons) provided to the building was calculated using:

$$\dot{Q}_{cool,total} = \dot{Q}_{HP} + \dot{Q}_{campus} \quad \textbf{(A-3)}$$

where $\dot{Q}_{HP}$ is the measured cooling rate provided by the heat pumps in tons,
and $\dot{Q}_{campus}$ is the measured cooling rate provided by the campus chilled water supply in tons.

The measured cooling rates were integrated over the measurement time intervals to find the cooling energy that was provided by the heat pumps and/or the campus chilled water loop. The integrated cooling over each measured interval $(Q_{cool,i})$ in units of kton-hrs was calculated with:

$$Q_{cool,i} = \dot{Q}_{cool,i} \frac{1\ [\text{kton}]}{1000\ [\text{tons}]} \Delta t \frac{1[hr]}{60[min]} \quad \textbf{(A-4)}$$

where $\dot{Q}_{cool,i}$ is the measured cooling rate in tons,
and Δt is the ten minute time interval between the measurements.

The total monthly cooling consumed by WID from either the heat pumps or the campus chilled water supply was calculated by summing the integrated cooling for all intervals during the month:

$$Q_{cool} = \sum Q_{cool,i} \quad \textbf{(A-5)}$$

Measured Heat Rejection Rate and Integrated Heat Rejection

Measured heat rejection rate was calculated similar to the measured cooling found in Eq. (A-1), but utilized more appropriate water property values at condenser water conditions. The water density and specific heat were determined in EES at an average condenser temperature of 100°F and pressure of 50 psi, resulting in density and specific heat values of 8.288 [lb/gallon] and 0.998 [Btu/lb-°F], respectively. Combining the constants and the necessary unit conversion factor, the equation used to calculate the condenser total heat rejection $(\dot{Q}_{THR})$ in MBtu/hr was:

$$\boxed{\dot{Q}_{THR} = \dot{V}\left(T_{leaving} - T_{entering}\right) 0.497 \left[\frac{MBH\ min}{gallon\ °F}\right]} \quad \textbf{(A-6)}$$

where $\dot{V}$ is the water flow rate in GPM,

and $T_{leaving}, T_{entering}$ are the temperatures in °F of the water leaving and entering the source of heat rejection, respectively.

Electrical Power Consumption

The total rate of electrical consumption by the WID GCHP system pumps $(\dot{W}_{pumps})$ at any instant was calculated using:

$$\dot{W}_{pumps} = \dot{W}_{P1} + \dot{W}_{P2} + \dot{W}_{P7} + \dot{W}_{P8} + \dot{W}_{P11} + \dot{W}_{P12} + \dot{W}_{P21} \quad \textbf{(A-7)}$$

where each term is the electrical consumption rate in kW of the indicated pump.

The total electrical consumption rate of the GCHP system at any instant was calculated with:

$$\dot{W}_{system} = \dot{W}_{pumps} + \dot{W}_{HP} \quad \textbf{(A-8)}$$

where $\dot{W}_{pumps}$ is the electrical power consumed by the system pumps in kW,

and $\dot{W}_{HP}$ is the the electrical power consumed by the heat pumps in kW.

The measured electrical energy in MW-hrs was calculated at each time interval using:

$$W_{system,i} = \dot{W}_{system,i} \frac{1\ [\text{MW}]}{1000\ [\text{kW}]} \Delta t \frac{1[hr]}{60[min]} \quad \textbf{(A-9)}$$

where $\dot{W}_{system,i}$ is the measured cooling rate at a specified interval in tons and Δt is the ten minute time interval between the measurements.

The total electrical energy consumed by either the heat pumps, the system pumps, or the the total GCHP system was calculated by summing the integrated electrical energy at each interval for all intervals during the month:

$$W_{elec} = \sum W_{elec,i} \tag{A-10}$$

Measured COP

The efficiency of a chilled water system at any instant was defined as the dimensionless coefficient of performance (COP) and was calculated using:

$$COP = \frac{\dot{Q}_{cool}}{\dot{W}_{elec}} \frac{3.517[kW]}{[ton]} \tag{A-11}$$

where $\dot{Q}_{cool}$ is the cooling capacity of the system in tons and $\dot{W}_{elec}$ is the rate of electricity in kW consumed by the system.

The average efficiency of a system (COP_{avg}) in dimensionless units was calculated, using:

$$COP_{avg} = \frac{Q_{cool}}{W_{elec}} \frac{3.517[MW\ hrs]}{[kton\ hrs]} \tag{A-12}$$

where Q_{cool} is the total cooling in kton-hrs and W_{elec} is the total electrical energy in MW-hrs consumed by the system.

Heat Pump Manufacturer Performance Correlations

The equations for the manufacturer-predicted heat pump performance were developed using second-order polynomial fit with cross terms of the heat pump manufacturer performance data. The manufacturer-predicted cooling capacity ($\dot{Q}_{mfctr}$) in tons was calculated using:

$$\dot{Q}_{mfctr} = N_{modules}\, AF\, [17.929 + 1.676\, ELW + 7.328(10^{-4})ELW^2 + 2.895(10^{-2})CEW - 1.261(10^{-3})CEW^2 - 5.105(10^{-3})\, ELW\, CEW] \quad \textbf{(A-13)}$$

where $N_{modules}$ is the number of operating HP modules (i.e. # of active compressors divided by two),

AF is an adjustment factor provided by the manufacturer,

ELW is the bulk temperature in °F of the water leaving the evaporators,

and CEW is bulk temperature in °F of the water entering the condensers.

All HP manufacturer data assumed that a 10°F water temperature difference existed across the evaporators and condensers. The manufacturer provided data to correct the predicted cooling based on the measured evaporator temperature drop. The adjustment data is provided in Appendix D. The corresponding adjustment factor (AF), found in Eq.(), was calculated using:

$$AF = 0.933 + (0.00667)\Delta T_{evap} \quad \textbf{(A-14)}$$

The manufacturer-predicted electrical power consumption in units of kW was calculated using:

$$\dot{W}_{mfctr} = N_{modules}[39.618 - 0.1626\, ELW + 4.626(10^{-3})ELW^2 - 0.271\, CEW + 5.123(10^{-3})CEW^2 - 1.43(10^{-3})ELW\, CEW] \quad \textbf{(A-15)}$$

where $N_{modules}$ is the number of operating HP modules (i.e. # of active compressors divided by two),

ELW is the bulk temperature in °F of the water leaving the evaporators,

and CEW is bulk temperature in °F of the water entering the condensers.

Measurement Uncertainties

Temperature Sensors

In general, the measurement uncertainties of the temperature sensors used in the present research were defined using the combination of the sensor manufacturer nominal uncertainty and the "Change of Value" (COV) parameter configured in the BAS. The uncertainty of the BTU meter computing was listed by the manufacturer at 0.005%, and was considered negligible.

Sensor Name	Type	Listed Uncertainty (± °F)	COV (± °F)	Total Uncertainty (± °F)
ELW-T	Standard	0.35	0.2	0.55
EEW-T	Standard	0.35	0.3	0.65
CLW-T	Standard	0.35	0.2	0.55
CEW-T	Standard	0.35	0.3	0.65
GEW-T	Standard	0.35	0.2	0.55
GLW-T	Standard	0.35	0.2	0.55

Table A-1– Temperature Sensor Measurement Uncertainties

The BTU meter had sensors calibrated for the temperature difference (ΔT). The BTU meter manufacturer listed the accuracy of ΔT at ±0.15°F, and the accuracy in the BTU meter computing (i.e. the output signal to the BAS) at ±0.005%. The uncertainty of the BTU meter computing was listed by the manufacturer at 0.005%, and was considered negligible.

Water Flow Meter Uncertainties

Sensor Name	Type	Listed Uncertainty (% Rdg)	Final Uncertainty (% Rdg)
WFM-1	Turbine	2	10
WFM-2	Turbine	2	2
WFM-5	Turbine	2	2
WFM-13	E.M.	1	1

Table A-2 – Water Flow Meter Measurement Uncertainties

True Electrical Power Uncertainties

All electrical power measurements in the present research were true power measurements using a multi-circuit electrical monitor. The relative measurement uncertainties were based on the manufacturer listed uncertainty of ±1% of the reading.

Propagated Uncertainties

General Equations

Due to the large number of data rows and the necessity to organize and compile the measured data, many calculations for the present research were computed in MatLAB. Necessarily, the propagated uncertainties were also programmed in MatLAB using the method described in NIST Technical Note 1297. (B. a. Taylor 1994) EES utilized the same method of uncertainty propagation and was available for use to validate the MatLAB results. The general equation used to propagate the measurement uncertainties of the sensors in the present research was:

$$U_Y = \pm \sqrt{\sum_i \left(\frac{\partial Y}{\partial X_i}\right)^2 {U_{X_i}}^2} \quad \textbf{(A-16)}$$

where U_Y is the absolute uncertainty of the calculated value of interest Y,

X is a variable used to calculate the value of interest Y,

and U_X is the absolute uncertainty of the variable X.

Due to the large number of rows for most data sets found in the present research, the propagated uncertainties for integrated total quantities, such as the integrated monthly cooling, were calculated differently than the method described above. The propagated uncertainties for all integrated totals were calculated by summing the uncertainties of the integrated values at each interval, using:

$$U_{integrated,total} = \pm \sum_{i} U_{integrated,i} \quad \textbf{(A-17)}$$

where $U_{integrated,i}$ is the uncertainty of the integrated value at each interval,

and i represents the number of integrated values or the number of intervals to be summed.

Cooling

The propagated uncertainty of the temperature difference across the heat pump evaporators was a constant value and calculated using:

$$U_{\Delta T_{evap}} = \pm\sqrt{(U_{EEW})^2 + (U_{ELW})^2} \quad \textbf{(A-18)}$$

where U_{EEW} is the measurement uncertainty of sensor EEW-T and U_{ELW} is the uncertainty of sensor ELW-T.

The equation used to calculate the propagated uncertainty in tons was:

$$U_{\dot{Q}_{cool}} = \pm\sqrt{(0.0.417)^2\ (V_{WFM1})^2\ \left({\Delta T_{evap}}^2 (Ur_{WFM1})^2 + {U_{\Delta \mathrm{T}_{evap}}}^2\right)} \quad \textbf{(A-19)}$$

where V_{WFM1} is the measured evaporator water volumetric flow rate in GPM,

ΔT_{evap} is the measured temperature drop across the evaporators in °F,

Ur_{WFM1} is the relative uncertainty of flow meter WFM-1,

and $U_{\Delta \mathrm{T}_{evap}}$ is the uncertainty of the evaporator water temperature drop.

Electrical Power

The uncertainty of the electrical power consumed by the heat pumps was calculated using:

$$U_{W_{pumps}} = \pm\sqrt{(Ur_{elec})^2\ \left[\sum_i \left(\dot{W}_i\right)^2\right]} \quad \textbf{(A-20)}$$

where Ur_{elec} is a constant equal to 0.01 (i.e. the relative uncertainty of the electrical power measurements) and $\dot{W}_i$ represents the measured electrical power consumed by pumps P-1, P-2, P-7, P-8, P-11, P-12, and P-21.

COP

The uncertainty of the instantaneous COP of the heat pumps was calculated using:

$$U_{COP} = \pm\sqrt{\frac{(3.517)^2\left(\dot{Q}_{cooling}\right)^2\left(U_{\dot{W}_{HP}}\right)^2 + (U_{\dot{Q}_{cooling}})^2(\dot{W}_{HP})^2}{\left(\dot{W}_{HP}\right)^4}} \quad \textbf{(A-21)}$$

where $\dot{Q}_{cooling}$ is the measured cooling capacity in tons,

$\dot{W}_{HP}$ is the measured electrical power consumed in kW,

$U_{\dot{W}_{HP}}$ is the absolute uncertainty of the heat pump electrical power consumption,

and $U_{\dot{Q}_{cooling}}$ is the absolute uncertainty of the measured cooling capacity. The constant deals with the unit conversion required to make the COP dimensionless.

The average COP was calculated using the same as Eq.(A-21) with the rate values replaced with integrated values (e.g. the cooling capacity would be replaced with the integrated cooling, etc.).

Appendix B. System Overviews

Heat Pumps

The heat pumps consist of six independent heat pump circuits or “modules”. Each module contains two Copeland scroll-type compressors nominally rated at 30 tons cooling/heating capacity each, making the total unit capacity nominally rated at 420 tons. The unit is capable of meeting load demands in increments of 8.33%. The module flow circuits are connected in parallel by common headers for both the evaporator water and condenser water. Solenoid valves on the modulate flow to the heat pump heat evaporators to control the chilled water supply temperature. An additional set of valves modulate the flow to the HP condensers to control the condensing temperature (and subsequently the condensing refrigerant pressure). The HP units do not have supplementary heating or cooling components such as electrical resistance heating. Refer to

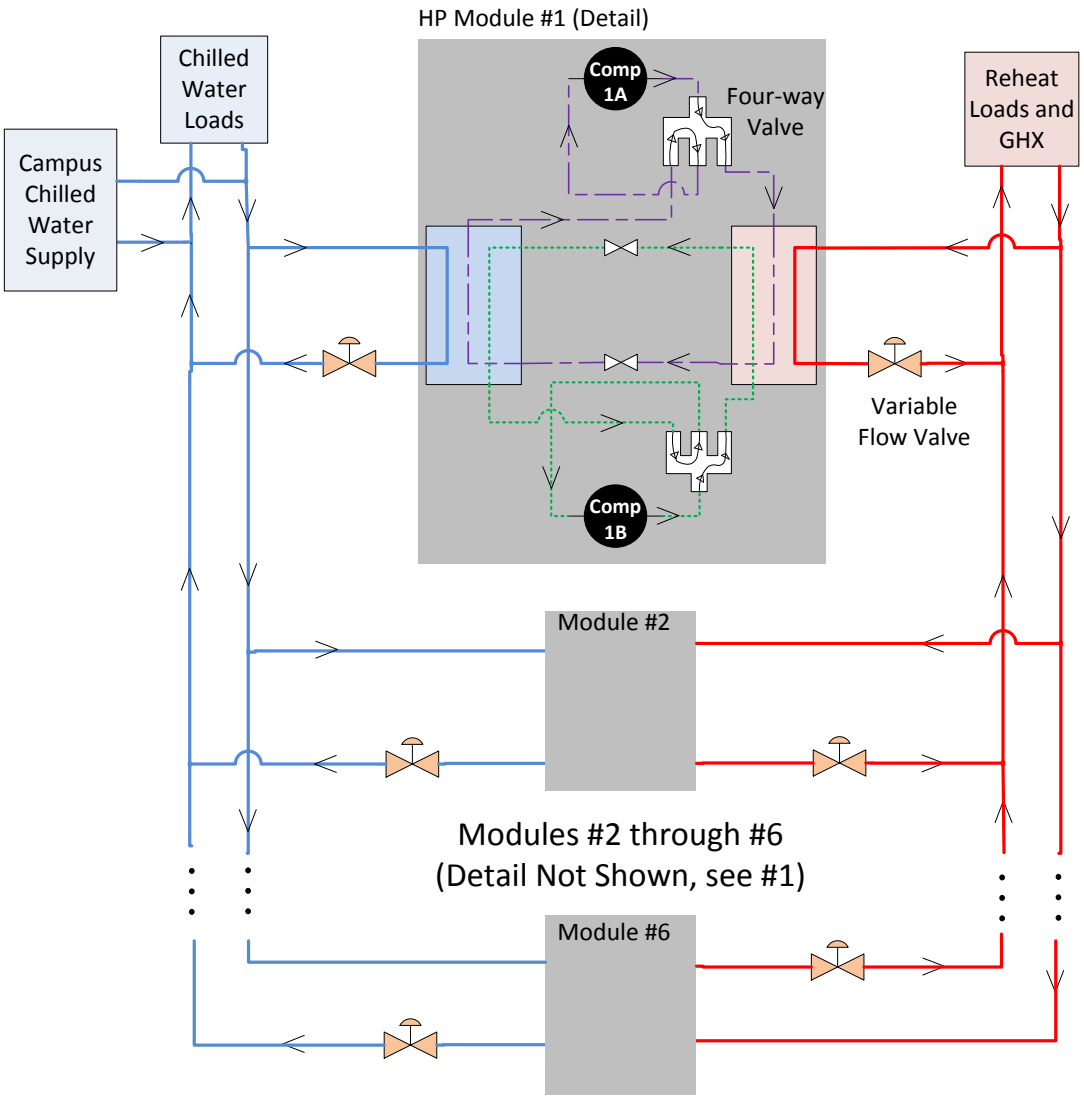

Figure B-1 – Internal flow schematic of the connected heat pump modules, including refrigerant circuits

Heat Recovery

Under certain operating conditions, the ground-coupled heat pump system is capable of supplying hot water to meet building reheat requirements (i.e. similar to what is commonly referred to as heat recovery chillers). A reheat load in the building is created because the discharge air temperature following the dehumidification process within the air-handling units is lower than zone setpoint temperature. The reheat load consists of heating

requirements by the variable air volume (VAV) units that serve the WID air-conditioning zones. Though not readily apparent, the term “reheat load” in this research will also include the heating demand by the radiant flooring system on the ground floor. This system is independent of the VAV reheat system, but is lumped into the term “reheat load” for convenience.

When the HP system is not configured to recover condenser hot water for reheat, the demand is met by steam from the campus district system. The steam is fed to the reheat load by equipment located in the WID penthouse floor including: modulating control valves (“CVxx”), two steam-to-hot water converters (labeled CV-1 and CV-2) and two pumps (labeled P-1 and P-2). This equipment will be referred to as the “steam reheat system” and is shown in Figure 1.

A schematic of the WID penthouse piping layout for the campus utility steam supply can be found in Figure B-2.

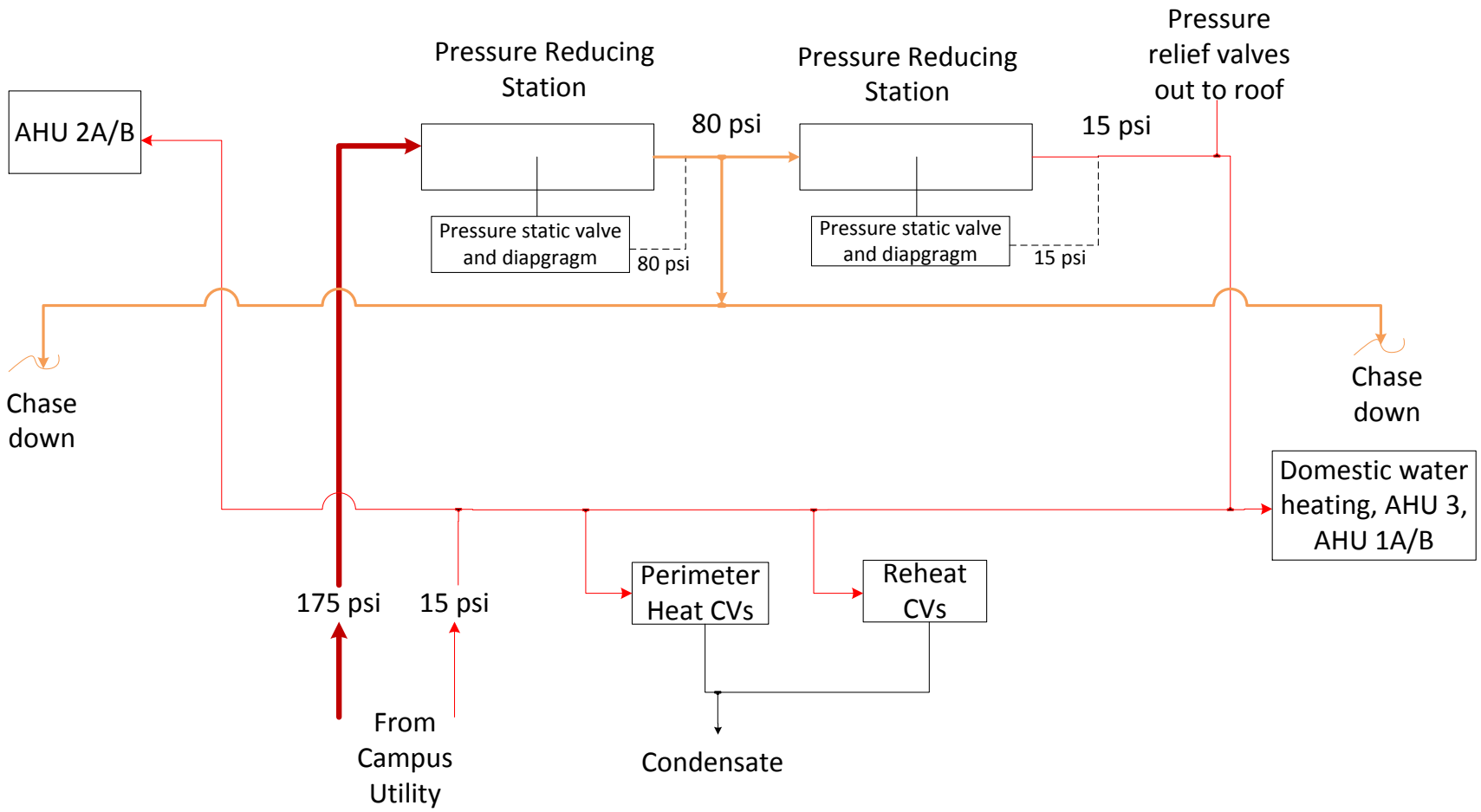

Figure B-2 – Penthouse piping layout for the high pressure and low pressure campus utility steam supply

The steam reheat system denotes equipment that is separate from the equipment that allows reheat heat recovery from the GCHP system, but the two systems are connected to the reheat loads by common piping.

Ground Heat Exchanger

In addition to the cooling and reheat loads, the HPs are connected to a ground heat exchanger (GHX). The field consists of seventy-five boreholes, each with a three hundred foot depth. The bores are located around the perimeter of the building and an additional ground borehole segment is located opposite of Orchard Street. The geoexchange system consists of four sections or "loops" that circulate the HP system hydronic fluid to promote heat transfer. The HP-geoexchange system can be configured to reject or absorb heat from the geoexchange reservoir. The Wisconsin Department of Natural Resources (DNR) classifies any dug bore as a well and prohibits the installation directly underneath a built structure.[55] The WID GHX field was installed in a perimeter pattern lining the outside of the building and one side of the adjacent property.

Auxiliary Equipment

The HP system utilizes seven hydronic pumps each equipped with variable frequency drives (VFD). One pump (labeled P-21) operates to boost the water supply pressure from the campus chilled water loop when required. Two pumps, sized to provide 50% of the design

[55] The WI DNR specifically upholds requirements on the treatment of abandoned wells, with regards to the ability to access the well and well equipment (e.g. u-tubes). Refer to the WI DNR Administrative Code 811.13.

flow rate and operating in a lead-lag sequence, are located on both the evaporator and condenser sides of the HP unit (P-7/P-8 and P-11/P-12 respectively). The HP system includes various valves including isolation valves, bypass valves, and pneumatic modulating valves. The valves are configured to allow and control multiple "Modes of Operation" to be discussed in the following section. Finally, an Orival water filtration system has been installed in-line of the campus chilled water supply to be used when campus chilled water is required.

Proposed "Modes of Operation"

As with all heat pump/chillers, the HP unit has the capability to operate in either heating or cooling modes. Additionally, the by-product of either mode can be "recovered" for use in a secondary application. The HP system has been designed to harness these capabilities and to make proper use of seasonal-dependent conditions in what have been called "Modes of Operation".

Modes of Operation	*Description*
Mode 1 – Cooling Mode with recovered reheat	HP unit evaporator produces chilled water for building cooling load. Hot water from unit condenser is recovered for use in building reheat system while additional heat is rejected to the geo field.
Mode 1a – Cooling Mode with heat rejection to geoexchange.	HP unit evaporator produces chilled water for building cooling load while condenser waste heat is rejected to the geo field.
Mode 2 – Heating Mode with heat absorption from geoexchange.	HP unit evaporator produces hot water for building reheat. Cold condenser water is circulated through the geo field to absorb heat from the Earth.
Mode 2a – Heating Mode with recovered chilled water	HP unit evaporator produces hot water for building reheat. Cold condenser water is recovered for building cooling load with additional heat rejection to geo field.
Mode 3 – Geoexchange Test Mode	HP unit evaporator and condenser are disabled. Water is circulated through geo field to measure field temperatures

Table B-1– HP System Modes of Operation

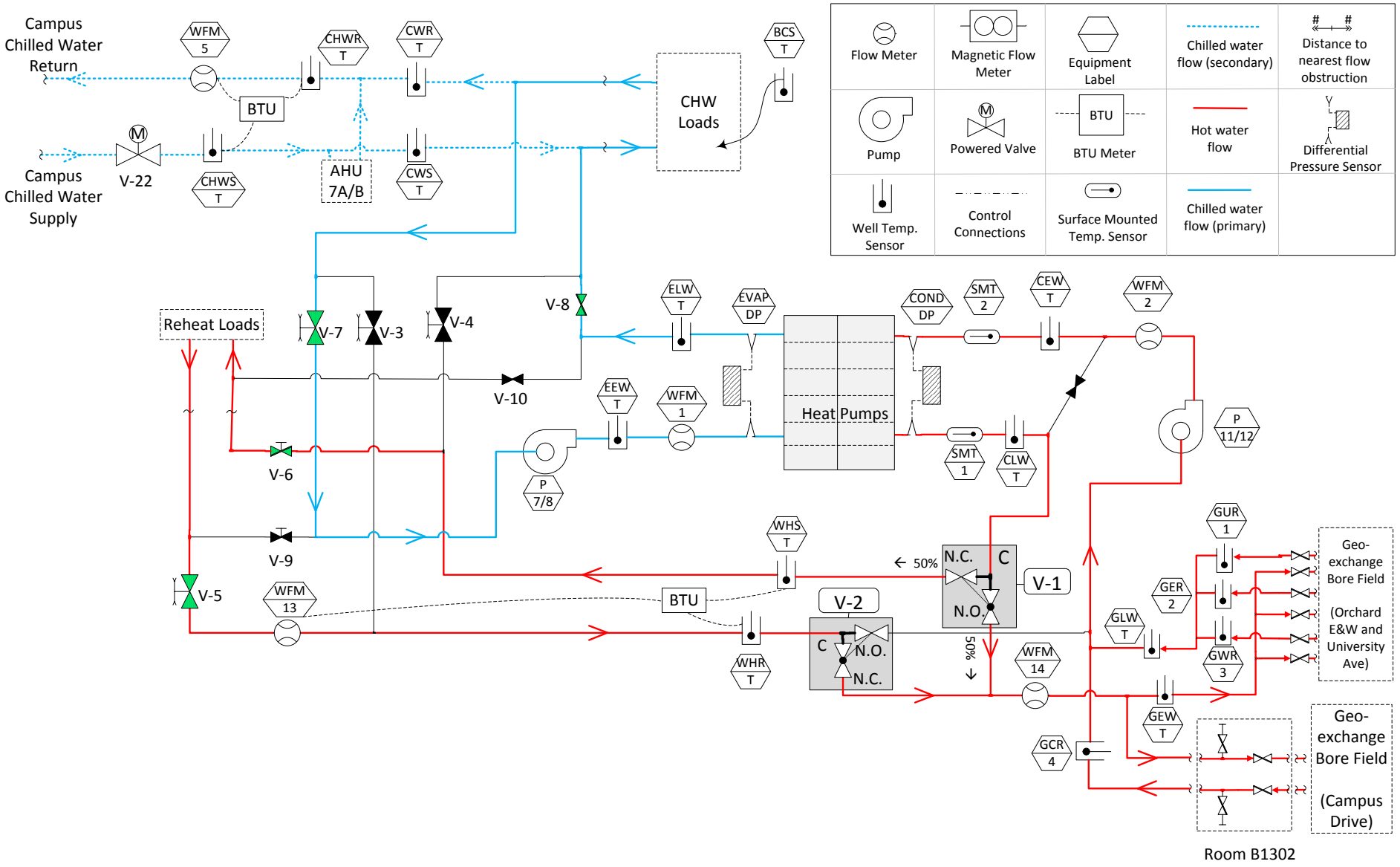

Figure B-3 - GCHP system as operating in cooling mode

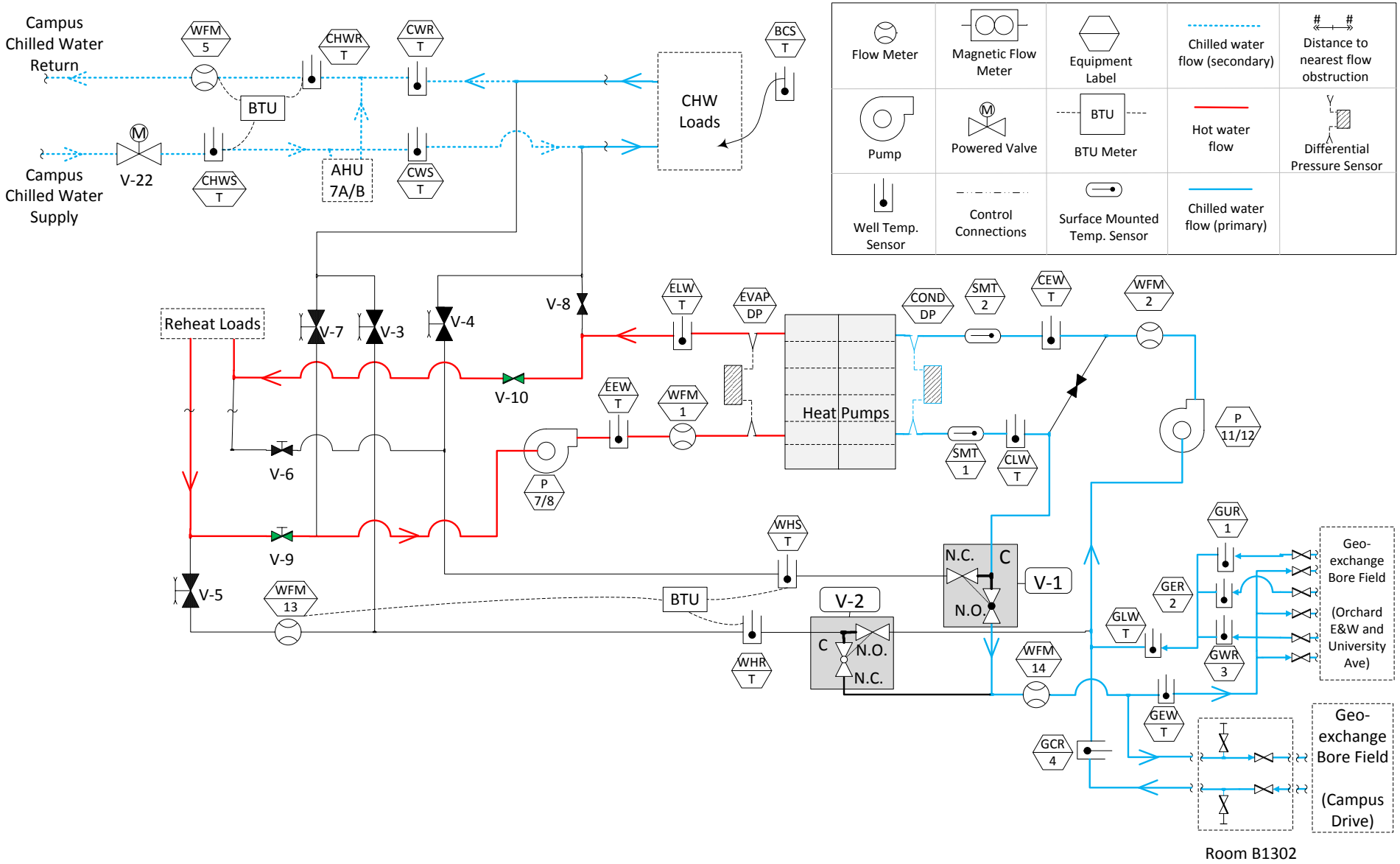

Figure B-4 - GCHP system as operating in heating mode

Overview Campus Utility Chilled Water and Steam: West Campus Cogeneration Facility

Campus utility chilled water was generated at three heating/cooling facilities: Charter Street, Walnut Street, and the West Campus "Cogeneration" Facility (WCCF).[56] A map showing the relative locations of campus utility facilities and the WID is provided in Figure B-5.

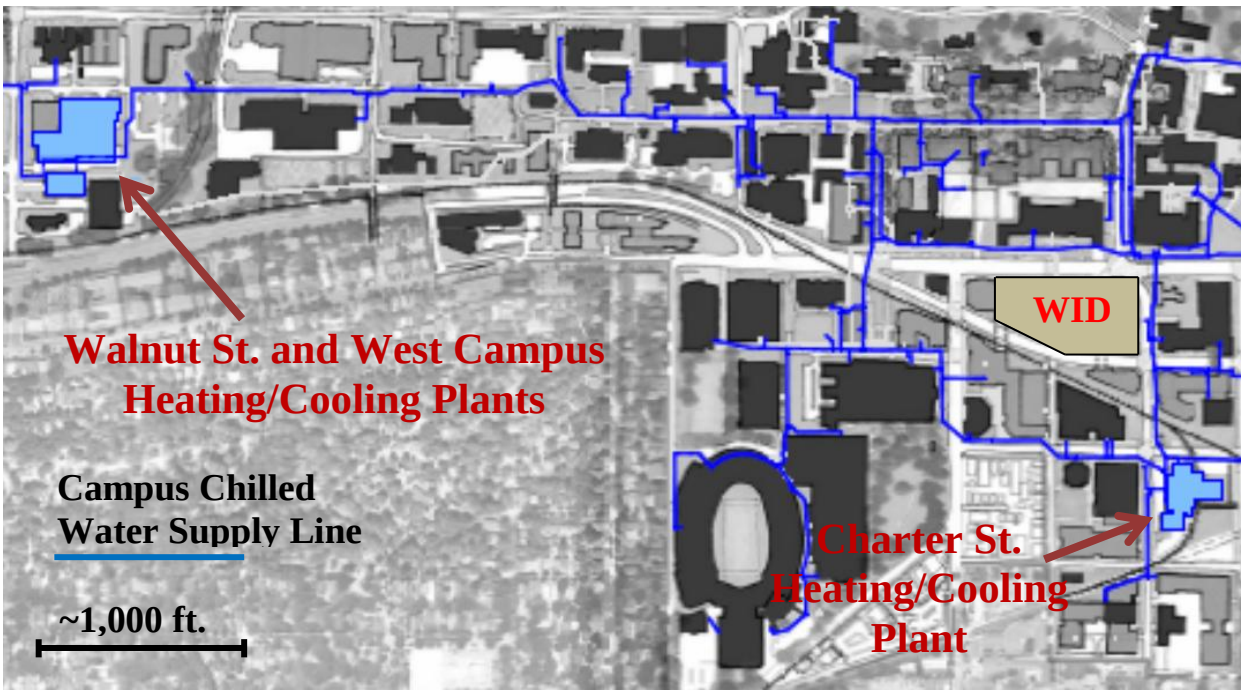

Figure B-5- Campus Map (section) Indicating Locations of the WID, Campus Chilled Water Generation and Supply Piping. From (FP&M 2005), with labeling added

All chilled water supplied to campus shares a common distribution piping. Therefore, it was not possible to determine where the chilled water used by the WID had originated. At the

[56] The university is a provider of campus utilities and a utility customer. The UW-Madison purchases electricity and natural gas from the local power utility (MGE) and municipal water from the city. Three utilities are provided by UW via district utility systems in underground "steam tunnels": steam for facility heating purposes; chilled water for facility cooling; and compressed air for building control pneumatics and sanitation pumping.

time of the present research, the Charter Street facility was inactive due to major equipment conversions from coal-fired to natural gas-based power. Of the campus heating/cooling facilities, the WCCF was the most recently built (beginning operation in 2005) and the only plant with documented plans to increase the chilled water generation capacity. (FP&M 2005) Furthermore, performance data for the chilled water system at WCCF was available from the UW Facilities, Planning, and Management department (FP&M). For these reasons the WCCF was chosen as a test case for comparing WID GCHP efficiency to campus chilled water efficiency. A schematic of the major equipment within the WCCF is provided in Figure B-3.

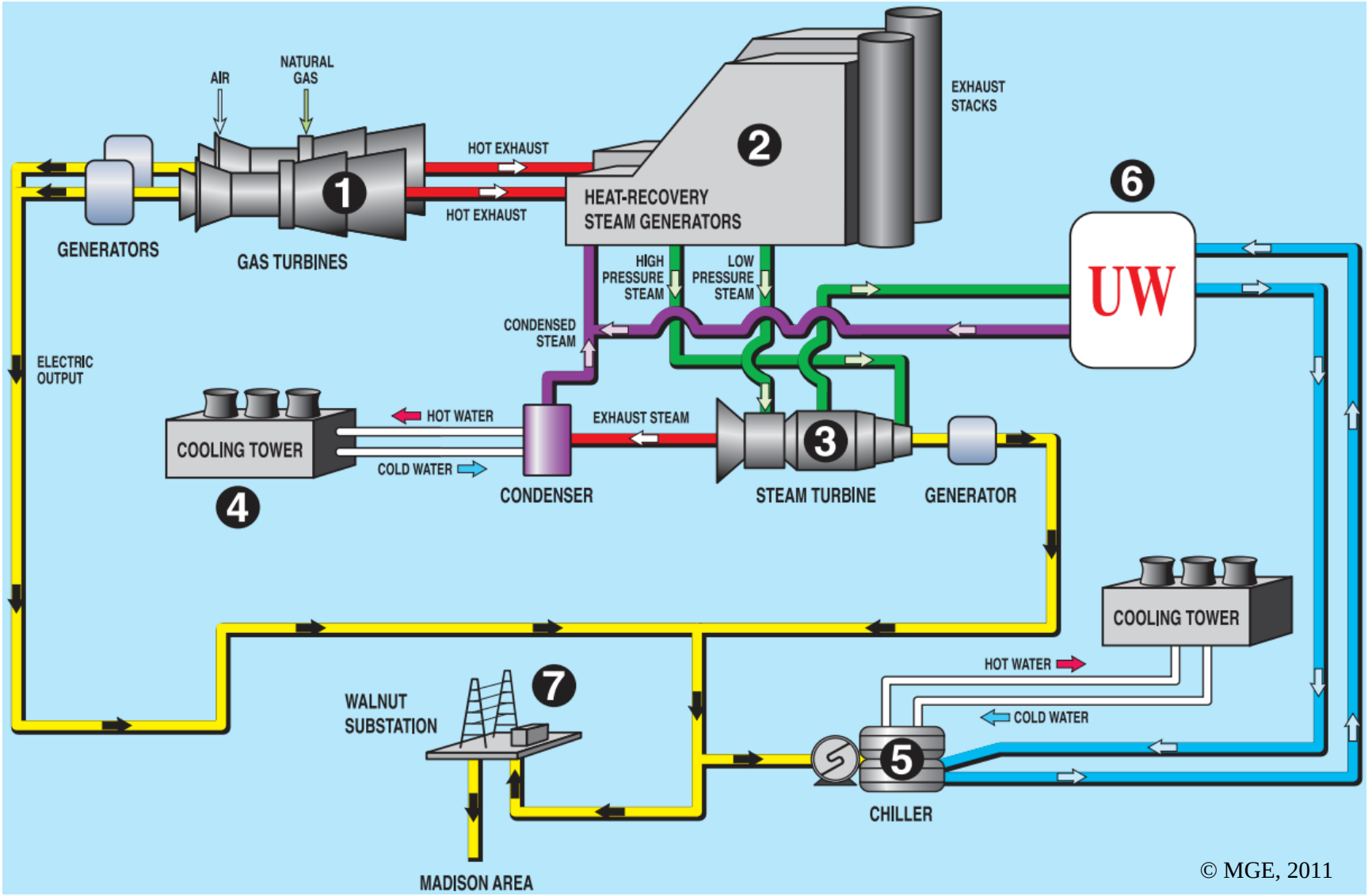

Figure B-6 – System schematic of the West Campus Cogeneration Plant

The UW-Madison owned the WCCF within an agreement with Madison Gas and Electric (MGE). The WCCF property and building were co-owned by UW and MGE; the equipment was owned by UW, and the facility was operated and maintained by MGE.[57] The WCCF generated electricity from natural gas-fired combustion turbines at a maximum capacity of 150 megawatts supplied to the Madison electrical grid. (MGE 2011) The electricity generated in the plant was also supplied to four 5,000 ton chillers within the WCCF. The facility's chilled water capacity was 20,000 tons total, but was designed for the capability to be expanded to 50,000 tons of capacity in the future. (FP&M 2005) A photograph of campus chiller equipment can be found in Figure .

[57] Section 5, pg. 5-27 of (FP&M 2005)

Figure B-7 - Campus Chiller (5000 ton, nominal)

Appendix C. Data Used for Sensor Comparisons

Below are graphical representations of the data used to compare and calibrate temperature sensors as discussed in Section 4.2.2. The temperature sensor of interest (raw and calibrated) is plotted along with the reference temperature sensor(s) with which it was compared.

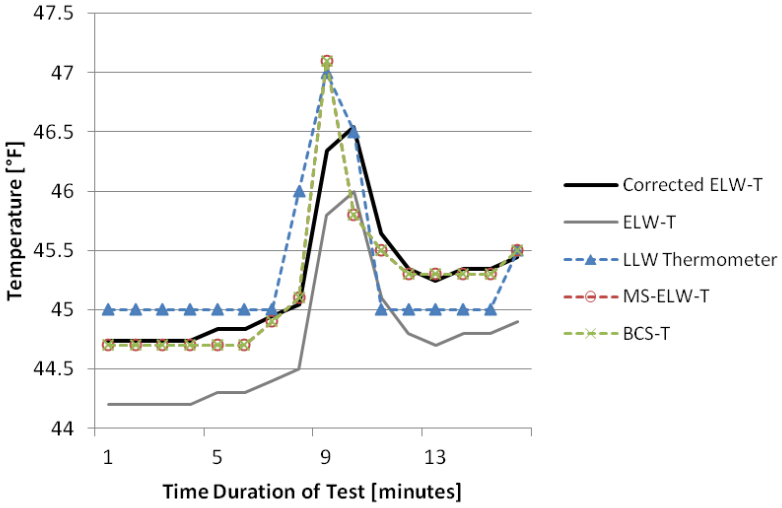

Figure C-1 – ELW-T

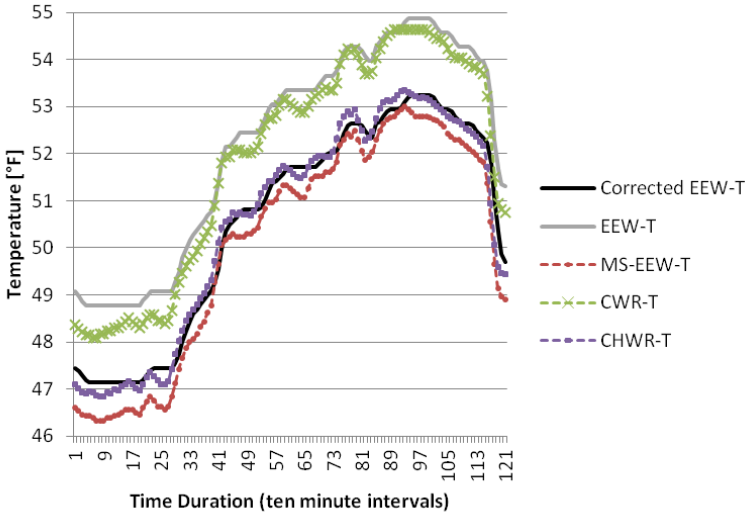

Figure C-2 – EEW-T

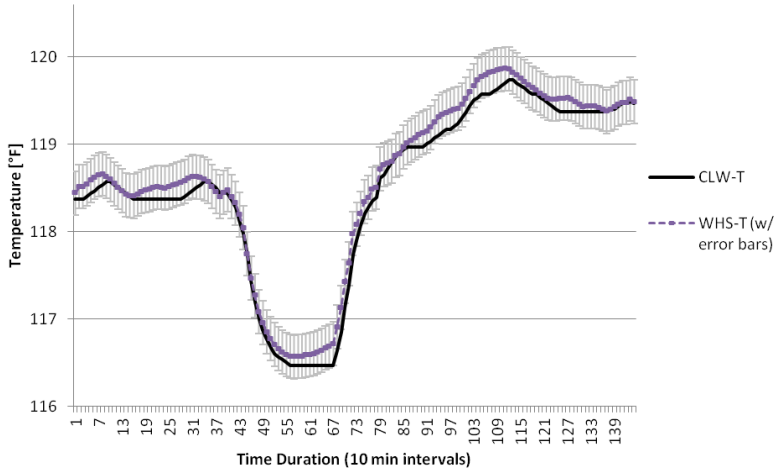

Figure C-3 – Raw CLW-T data compared to reference sensor WHS-T.

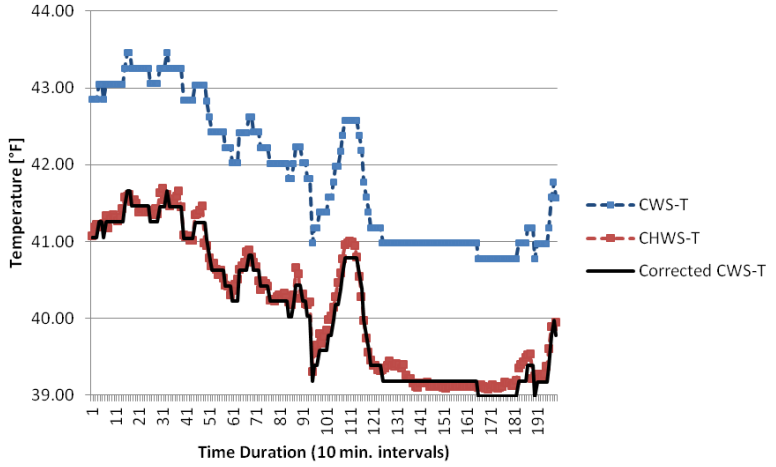

Figure C-4 – CWS-T

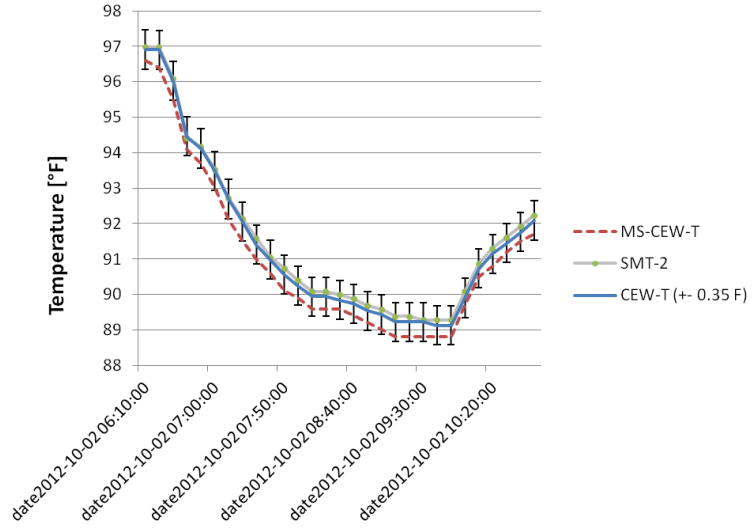

Figure C-5 - CEW-T

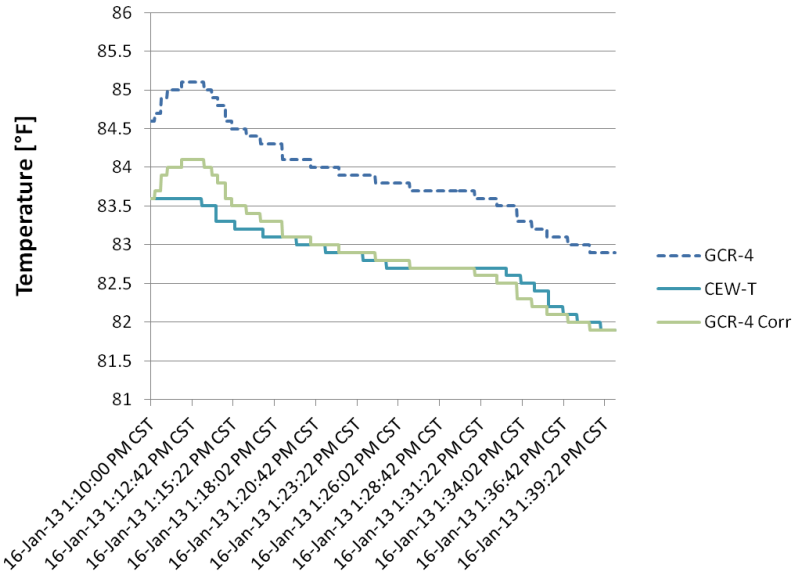

Figure C-6 - GCR-R

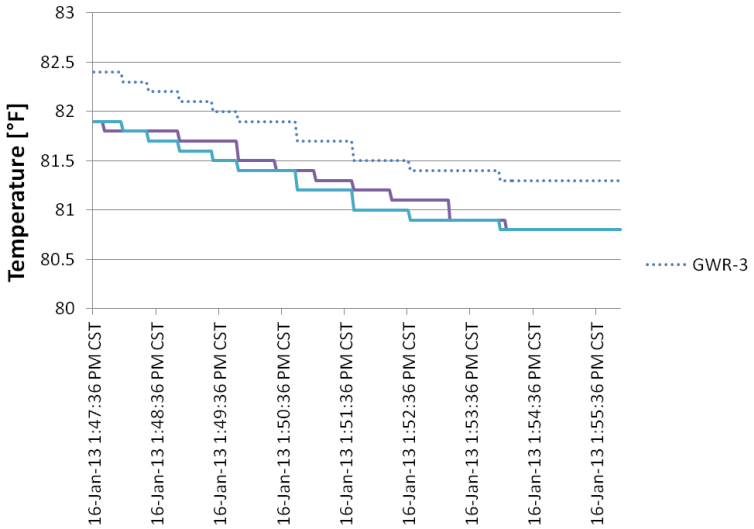

Figure C-7 - GWR-3

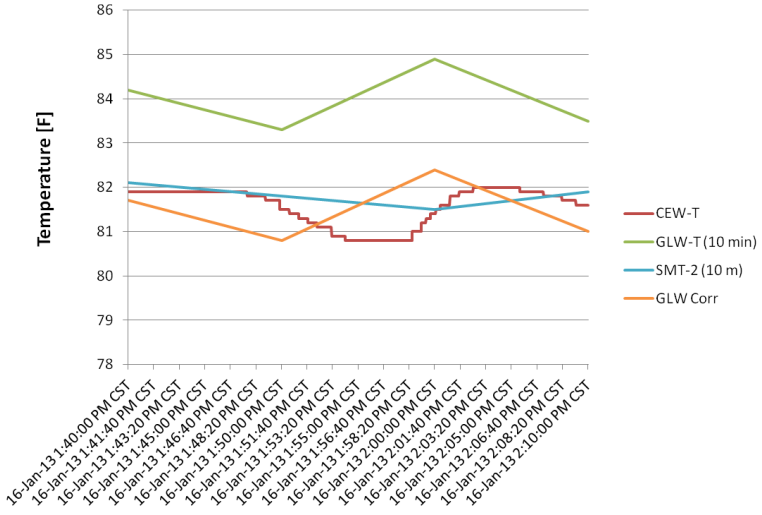

Figure C-8 - GLW-T

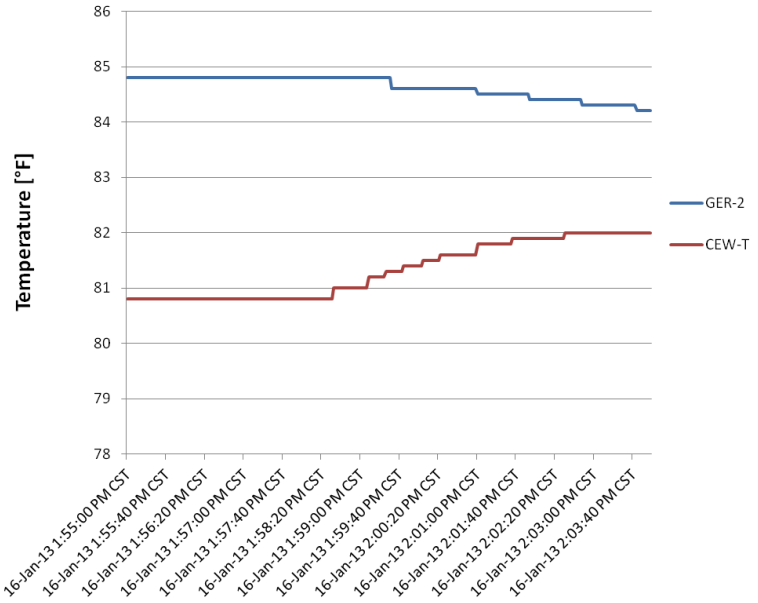

Figure C-9 - GER-2

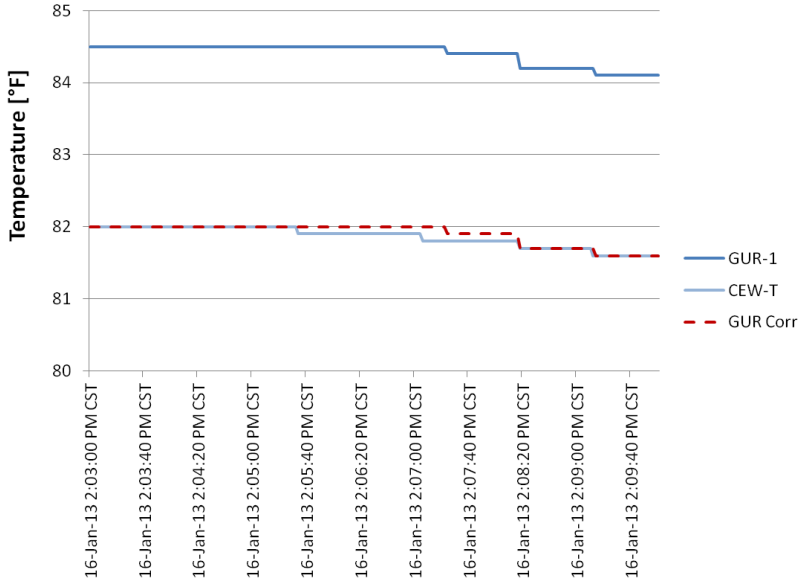

Figure C-10- GUR-1

Closeness of Fit Calculation Procedure

The closeness of fit (R^2) discussed in Section 4.2.2 was calculated using the following:

$$R^2 = \left(1 - \frac{SS_{error}}{SS_{total}}\right) 100[\%]$$

SS_{error} is the sum of squares of the difference between the sensor of interest and the reference calculated by:

$$SS_{error} = \sum_i \left(T_{ref,i} - T_{x,i}\right)^2$$

where $T_{ref,i}$ is the temperature measured by the reference sensor,

and $T_{x,i}$ is the temperature measured by the sensor of interest (i.e. the sensor to be calibrated). The term SS_{total} is the sum of squares of the difference between the reference sensor and the average of the reference sensor measurements, calculated by:

$$SS_{total} = \sum_i \left(T_{ref,i} - \bar{T}_{ref}\right)^2$$

where $\bar{T}_{ref}$ is the average of the reference temperature measurements.

Energy Balance Data

x	W_dot_HP_1	W_dot_HP_2	WFM1	WFM2	ELW	EEW	CEW	CLW
	[kW]	[kW]	[GPM]	[GPM]	[K]	[K]	[K]	[K]
1	161	64.35	287.9	590.2	278.4	286.1	315.2	319.9
2	202.5	33.01	261.1	567.1	278.9	287.1	316.6	321.3
3	202.6	33.02	261.5	571.9	278.9	287.1	316.6	321.3
4	202.6	33.02	260.8	565.5	278.8	287	316.7	321.3
5	203.2	33.13	261.9	566	278.8	286.9	316.7	321.5
6	192.7	44.13	280.4	563.1	279.2	286.9	316.7	321.5
7	171.2	66.23	326.4	578.1	279.7	286.5	316.7	321.6
8	171.1	66.13	333.7	587	279.6	286.3	316.8	321.5
9	170.6	65.9	328.4	595.7	279.4	285.9	316.9	321.5
10	171.2	91.92	348.7	592.6	279.4	285.6	316.8	321.3
11	170.9	95.27	366.2	605.6	279.9	285.6	316.7	321
12	170.5	92.65	353.4	603.6	279.2	285.5	316.6	321.2
13	170.8	86.41	367	593.8	279.4	285.3	316.6	321
14	170	75.93	351.2	597.7	278.8	285.1	316.6	321.3
15	170.7	96.78	368.1	617.5	279.1	284.8	316.6	321.1
16	171.2	76.04	396.5	586.2	278.3	284.2	316.5	321.2
17	170.4	65.12	410.7	569.7	277.8	283	316.6	321.3
18	170.7	65.2	415.1	563.3	277.8	282.8	316.6	321.3
19	171.1	65.35	413.3	569.6	277.7	282.8	316.6	321.3
20	171.3	65.45	406.3	567.7	277.8	283.1	316.8	321.4

Table C-1 – Data used to calculate Energy Balances in Section 4.4.2 - 30 Min Avgs (starting 9/11/12 at 13:30)

x	CEW	CLW	EEW	ELW	WFM2	WFM1	W_dot_HP_1	W_dot_HP_2
	[K]	[K]	[K]	[K]	[GPM]	[GPM]	[kW]	[kW]
1	300.8	303.7	281	278.2	221.1	201	0	50.39
2	300.8	303.7	281.1	278.3	221.4	202.9	0	50.4
3	300.8	303.7	281.1	278.2	220.7	201.8	0	50.34
4	300.8	303.7	281.1	278.3	222.8	203	0	50.41
5	300.8	303.7	281.1	278.3	222.7	202.3	0	50.41
6	300.8	303.7	281	278.1	222.7	202.2	0	50.31
7	300.8	303.6	280.9	278	221.9	201.4	0	50.3
8	300.8	303.6	280.9	278	220.8	201	0	50.25
9	300.8	303.6	280.9	278.1	221.9	203.2	0	50.32
10	300.8	303.7	281	278.2	220.4	202.3	0	50.37
11	300.8	303.7	281.1	278.2	219.4	201.4	0	50.41
12	300.8	303.7	281	278.2	220.2	201.7	0	50.4
13	300.8	303.6	280.9	278	221.1	201.2	0	50.3
14	300.8	303.6	280.8	278	221.2	202.5	0	50.32
15	300.8	303.6	280.9	278	223.6	200.3	0	50.26
16	300.8	303.6	280.9	278	221.8	201.2	0	50.26
17	300.8	303.6	280.8	277.9	221.7	200.7	0	50.18
18	300.8	303.6	280.8	278	222.6	201.8	0	50.24
19	300.8	303.6	280.8	278	222.6	200.8	0	50.21
20	300.8	303.6	280.7	277.8	221.4	200.7	0	50.18
21	300.8	303.6	280.6	277.8	222.4	201.3	0	50.18
22	314.8	318.5	280.5	277.4	695	784.2	162.6	61.6
23	314.9	318.8	280.5	277.5	686.8	755.4	163.7	61.9
24	315.1	319	280.3	277.5	685.7	764.2	164.1	62
25	315.3	319.1	280.3	277.4	680.7	776.3	164.5	62.1
26	315.3	319.2	280.3	277.4	680.6	792.4	165.2	62.4

Table C-2 – Data Used in Low Cooling Load HP Energy Balance

x	CEW	CLW	WFM2	GEW	GLW	WHR	WHS	V1	V2	WFM13	WFM14
	[K]	[K]	[GPM]	[K]	[K]	[K]	[K]	[%]	[%]	[GPM]	[GPM]
1	315.2	319.9	590.2	319	314.9	317.1	319.6	100	100	305.6	603.3
2	316.6	321.3	567.1	320.2	316.8	318.7	321.5	100	100	278	589.7
3	316.6	321.3	571.9	320.3	316.9	318.8	321.5	100	100	278.4	584.1
4	316.7	321.3	565.5	320.2	316.9	318.9	321.5	100	100	278.4	586.1
5	316.7	321.5	566	320.2	316.9	318.7	321.6	100	100	277.2	588.1
6	316.7	321.5	563.1	320.3	316.9	318.7	321.6	100	100	272.4	578.7
7	316.7	321.6	578.1	320.2	316.9	318.7	321.6	100	100	283.6	594.2
8	316.8	321.5	587	320.2	317	318.8	321.6	100	100	294.8	604.1
9	316.9	321.5	595.7	320	317	318.4	321.5	100	100	306.4	619.6
10	316.8	321.3	592.6	319.9	316.9	318.3	321.3	100	100	302	611.9
11	316.7	321	605.6	319.5	316.8	318	321.1	100	100	318	625.9
12	316.6	321.2	603.6	319.7	316.7	318.2	321.1	100	100	318	630.3
13	316.6	321	593.8	319.6	316.7	318.2	321.1	100	100	306.4	613.1
14	316.6	321.3	597.7	319.7	316.8	318.1	321.3	100	100	311.2	616.1
15	316.6	321.1	617.5	319.5	316.8	318	321	100	100	320	628.7
16	316.5	321.2	586.2	319.9	316.8	318.2	321.3	100	100	288	600.6
17	316.6	321.3	569.7	319.8	316.7	318.3	321.2	100	100	276	591.6
18	316.6	321.3	563.3	320	316.8	318.5	321.3	100	100	270.8	587
19	316.6	321.3	569.6	320.1	316.8	318.6	321.4	100	100	273.6	593.4
20	316.8	321.4	567.7	320.1	316.9	318.8	321.5	100	100	272.8	580.9

Table C-3 - Data Used for Energy Balances with Geo and RH in Series

x	CEW	CLW	WFM13	WFM14	WFM2	WHR	WHS	GEW	V1	V2	GLW
	[K]	[K]	[GPM]	[GPM]	[GPM]	[K]	[K]	[K]	[%]	[%]	[K]
1	314.6	317.8	274.4	310.2	571.4	315.2	317.7	317.8	100	0	313.8
2	314.2	317.3	286.8	316.7	582.6	314.8	317.3	317.4	100	0	313.3
3	313.9	316.9	299.6	313.8	594.9	314.4	316.9	316.9	100	0	313
4	313.6	316.6	299.6	322.8	589.7	314.1	316.6	316.6	100	0	312.7
5	313.2	316.3	294	332.1	591.1	313.7	316.3	316.4	100	0	312.5
6	313.1	316.2	305.6	330.4	602	313.6	316.1	316.2	100	0	312.3
7	312.8	315.8	364.8	301.6	664.1	313.3	315.8	315.8	100	0	312.2
8	312.7	315.3	406.8	292.2	705.2	312.8	315.3	315.3	100	0	311.8
9	312.2	314.7	427.6	286.8	719.8	312.1	314.7	314.7	100	0	311.5
10	311.8	314.4	424.4	276.6	709.1	311.9	314.4	314.5	100	0	311.2
11	311.7	314.5	406.8	302.9	700.1	312.2	314.6	314.6	100	0	311
12	311.9	314.8	390.8	297.5	685.6	312.6	314.9	314.9	100	0	311
13	312.2	315	386.4	305.8	686.3	312.8	315.1	315	100	0	311
14	312.2	315.1	361.2	309.5	663.9	313	315.3	315.2	100	0	311.2
15	312.5	315.8	353.6	317.7	661.1	313.6	316	315.9	100	0	311.3
16	313.2	316.8	356.8	316.6	663.7	314.6	316.9	316.8	100	0	311.6
17	313.7	317.4	358	322.2	663.6	315.2	317.5	317.5	100	0	312.1
18	314.1	317.7	352.4	315.1	658	315.6	317.8	317.8	100	0	312.4
19	314.6	318.9	334.8	324.4	645.7	316.4	319	318.9	100	0	312.7
20	314.7	319	322.8	317.3	629.4	316.8	319.2	318.6	100	0	313.9

Table C-4 – Data used in Heat Rejection Energy Balances, Geo and RH in parallel

x	CEW	CLW	GEW	GLW	V1	V2	WFM13	WFM14	WHR	WHS	WFM1
	[K]	[K]	[K]	[K]	[%]	[%]	[GPM]	[GPM]	[K]	[K]	[GPM]
1	300.8	303.7	303.7	301	0	0	0	191	304.8	298.3	221.1
2	300.8	303.7	303.7	301	0	0	0	191	304.7	298.3	221.4
3	300.8	303.7	303.7	301	0	0	0	191	304.7	298.3	220.7
4	300.8	303.7	303.7	301	0	0	0	191	304.7	298.3	222.8
5	300.8	303.7	303.7	301	0	0	0	191	304.7	298.3	222.7
6	300.8	303.7	303.6	301	0	0	0	191	304.7	298.3	222.7
7	300.8	303.6	303.6	301	0	0	0	191	304.7	298.3	221.9
8	300.8	303.6	303.6	301	0	0	0	191	304.7	298.3	220.8
9	300.8	303.6	303.6	301	0	0	0	191	304.7	298.3	221.9
10	300.8	303.7	303.6	301	0	0	0	191	304.7	298.3	220.4
11	300.8	303.7	303.6	301	0	0	0	191	304.7	298.3	219.4
12	300.8	303.7	303.6	301	0	0	0	191	304.7	298.3	220.2
13	300.8	303.6	303.6	301	0	0	0	191	304.7	298.3	221.1
14	300.8	303.6	303.6	301	0	0	0	191	304.7	298.3	221.2
15	300.8	303.6	303.6	300.9	0	0	0	191	304.7	298.3	223.6
16	300.8	303.6	303.6	300.9	0	0	0	191	304.7	298.3	221.8
17	300.8	303.6	303.6	300.9	0	0	0	191	304.7	298.3	221.7
18	300.8	303.6	303.6	300.9	0	0	0	191	304.7	298.3	222.6
19	300.8	303.6	303.6	300.9	0	0	0	191	304.7	298.2	222.6
20	300.8	303.6	303.6	300.9	0	0	0	191	304.6	298.2	221.4
21	300.8	303.6	303.6	300.9	0	0	0	191	304.7	298.2	222.4

Table C-5 - Data Used in Heat Rejection Energy Balance, Geo-Loop Only

x	BCS	CHWR	CHWS	EEW	ELW	WFM1	WFM5
	[K]	[K]	[K]	[K]	[K]	[GPM]	[GPM]
1	278.1	286.2	277.9	286.1	278.4	287.9	468.9
2	278.3	287.1	277.9	287.1	278.9	261.1	475.1
3	278.2	287.1	277.7	287.1	278.9	261.5	491.5
4	278.1	287	277.6	287	278.8	260.8	470.9
5	278.1	287.1	277.8	286.9	278.8	261.9	470.9
6	278.2	286.9	277.8	286.9	279.2	280.4	487.4
7	278.6	286.5	277.7	286.5	279.7	326.4	473
8	278.5	286.2	277.6	286.3	279.6	333.7	468.9
9	278.3	285.9	277.6	285.9	279.4	328.4	473
10	278.2	285.5	277.4	285.6	279.4	348.7	444.2
11	278.5	285.7	277.6	285.6	279.9	366.2	399
12	278.3	285.4	277.6	285.5	279.2	353.4	392.8
13	278.4	285.3	277.6	285.3	279.4	367	401
14	278.3	285	277.5	285.1	278.8	351.2	382.5
15	278.1	284.8	277.5	284.8	279.1	368.1	386.6
16	277.8	283.9	277.5	284.2	278.3	396.5	306.4
17	277.7	282.9	277.4	283	277.8	410.7	257.1
18	277.6	282.8	277.4	282.8	277.8	415.1	240.6
19	277.7	282.9	277.4	282.8	277.7	413.3	236.5
20	277.7	283.1	277.6	283.1	277.8	406.3	228.3

Table C-6 - Date Used for Chilled Water Supply Energy Balance

Pump Curves for Flow Rate Verification

An industry standard method for verifying flow meter readings typically comes from measuring the differential pressure across the hydronic pumps then using the manufacturer pump curves to find the expected pump flow rate (ASHRAE 2008). The WIDMIR "As-Released" mechanical design documents note the specifications for chilled water pumps P-7/P-8 and condenser pumps P-11/P-12 necessary for locating the appropriate manufacturer performance curves. For the range of flow rates observed from the chilled water hydronic pumps (0 to 500 GPM for the heat pump chilled water and 0 to 700 GPM for condenser water) the pump curves indicate relatively constant differential pressures and therefore were not useful for flow verification.

It was not possible to conduct ex-situ tests, whereby the hydronic pumps would be put "in hand" and the pump speed increased until lower differential pressures occur with which to read the expected flow rate from the pump curve. As a reference, flow rates as high as 900 GPM would be necessary to read from the flow curve a differential pressure that is 10 psi different than the constant differential pressure seen at the typical flow range. In other words, the pumps would need to be forced to generate a flow rate almost three times the design flow rate in order to use the manufacturer pump curves. Because the pumping potential in the chilled water loop is dependent on the load behavior, it is not possible and/or not practical to artificially force the pumps to operate in this manner. Increasing the pump drives to their maximum (100%) would not necessarily increase the flow rate to the pump's flow capacity (1200 GPM), as the flow is dependent on pressure drop through the loop (cooling load).

Chilled Water Pumps (P-7 and P-8)

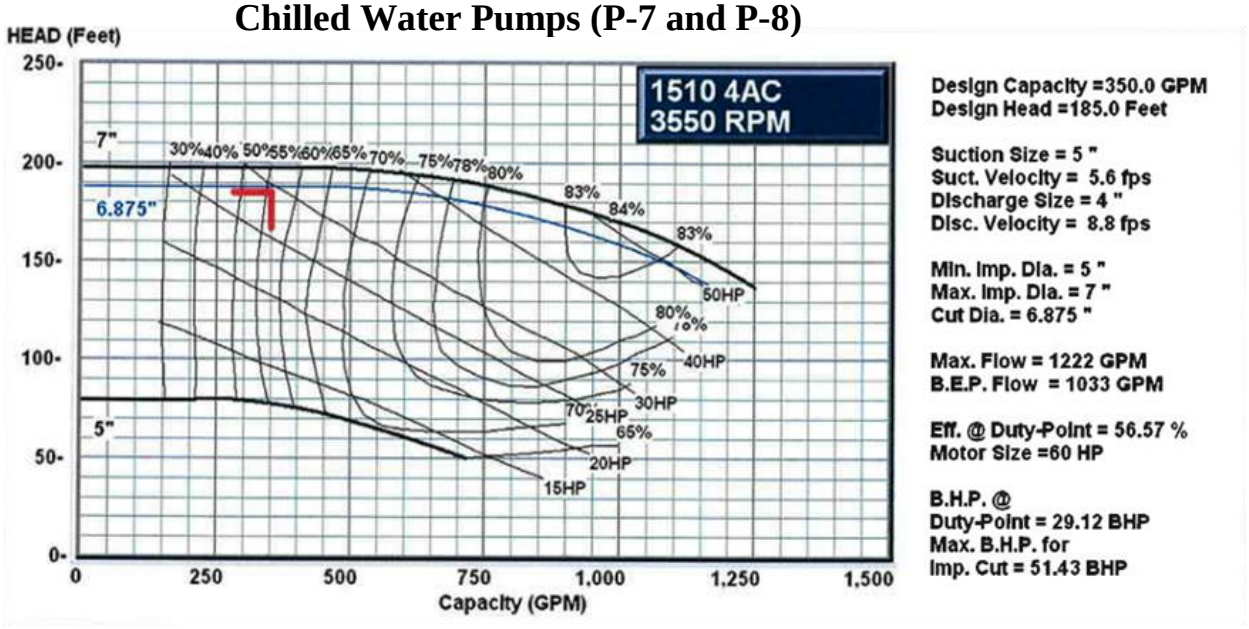

Condenser Pumps (P-11 and P-12)

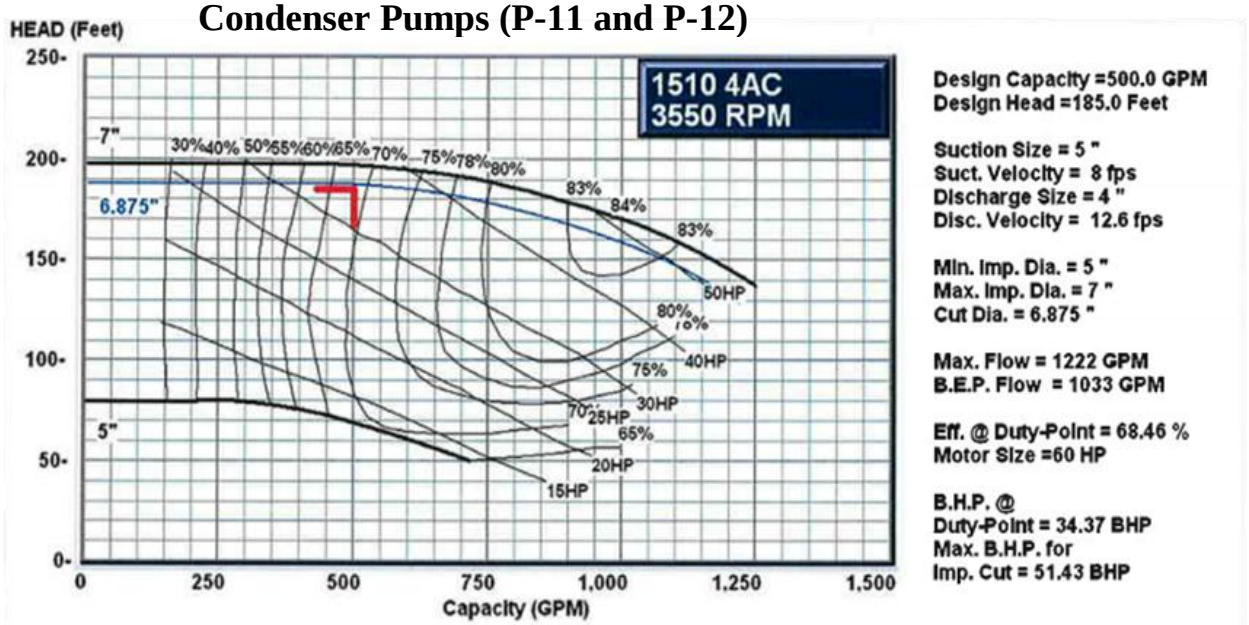

Figure C-11 - Manufacturer pump performance curves for the chilled water hydronic pumps.

Appendix D. Data for In-situ Heat Pump Performance Analysis

This section contains the tabulated performance data provided by the heat pump manufacturer.

Leaving Chilled Water (°F)	Entering Condenser Water (°F)	Cooling (tons)	Power (kW)	kW/ton	EER (BTU/W-hr)
40	75	65.8	44.9	0.682	17.6
42	75	68.4	45.1	0.659	18.2
44	75	71.0	45.4	0.639	18.8
45	75	72.4	45.6	0.630	19.1
46	75	73.8	45.7	0.619	19.4
48	75	76.6	46.0	0.601	20.0
50	75	79.5	46.4	0.584	20.6
40	80	64.1	47.1	0.735	16.3
42	80	66.6	47.3	0.710	16.9
44	80	69.2	47.6	0.688	17.5
45	80	70.6	47.7	0.676	17.7
46	80	71.9	47.9	0.666	18.0
48	80	74.6	48.1	0.645	18.6
50	80	77.4	48.5	0.627	19.2
40	85	62.4	49.5	0.793	15.1
42	85	64.8	49.7	0.767	15.7
44	85	67.4	49.9	0.740	16.2
45	85	68.7	50.1	0.729	16.5
46	85	70.0	50.2	0.717	16.7
48	85	72.6	50.5	0.696	17.3
50	85	75.4	50.7	0.672	17.8
40	90	60.6	52.1	0.860	14.0
42	90	63.0	52.3	0.830	14.5
44	90	65.5	52.5	0.802	15.0
45	90	66.7	52.6	0.789	15.2
46	90	68.0	52.7	0.775	15.5
48	90	70.6	53.0	0.751	16.0
50	90	73.2	53.3	0.728	16.5
40	95	58.8	54.8	0.932	12.9
42	95	61.1	55.0	0.900	13.3
44	95	63.5	55.3	0.871	13.8
45	95	64.7	55.4	0.856	14.0
46	95	66.0	55.5	0.841	14.3
48	95	68.5	55.7	0.813	14.7
50	95	71.1	56.0	0.788	15.2

Table D-1 - Heat Pump Manufacturer Product Catalog, Version: F148PC0911, 70 Ton Package

Leaving Source Water (°F)	Entering Source Water (°F)	Leaving Chilled Water (°F)	Cooling (tons)	EER (BTU/W-hr)	THR (MBTU/hr)	Load Flow (GPM)	Source Flow (GPM)
110	100	42	58.4	11.7	905	140	180.9
110	100	44	60.7	12.1	933.7	145.7	186.6
110	100	46	63.1	12.6	963.2	151.4	192.5
110	100	48	65.6	13	993.5	157.3	198.6
110	100	50	68.1	13.5	1024.5	163.4	204.8
115	105	42	56.3	10.7	891.4	135.1	178.2
115	105	44	58.6	11.1	919.3	140.5	183.8
115	105	46	60.9	11.5	947.9	146.1	189.5
115	105	48	63.3	11.9	977.2	151.8	195.3
115	105	50	65.8	12.3	1007.3	157.7	201.3
120	110	42	54.2	9.7	877.9	129.9	175.5
120	110	44	56.4	10.1	904.9	135.2	180.9
120	110	46	58.6	10.5	932.6	140.6	186.4
120	110	48	60.9	10.9	961.1	146.2	192.1
120	110	50	63.3	11.2	990.2	151.8	197.9
130	120	50	58.2	9.3	955.9	139.6	191.1
125	115	50	60.8	10.2	973.1	145.8	194.5
130	120	48	56	8.9	928.7	134.3	185.6
125	115	48	58.5	9.9	944.9	140.3	188.9
130	120	46	53.9	8.6	902.1	129.1	180.3
125	115	46	56.3	9.5	917.4	135	183.4
130	120	44	51.7	8.3	876.1	124.1	175.1
125	115	44	54.1	9.2	890.5	129.7	178
130	120	42	49.7	8	850.8	119.1	170.1
125	115	42	52	8.8	864.3	124.6	172.8

Table D-2 - Additional Heat Pump Manufacturer Data, Provided Upon Request by Author

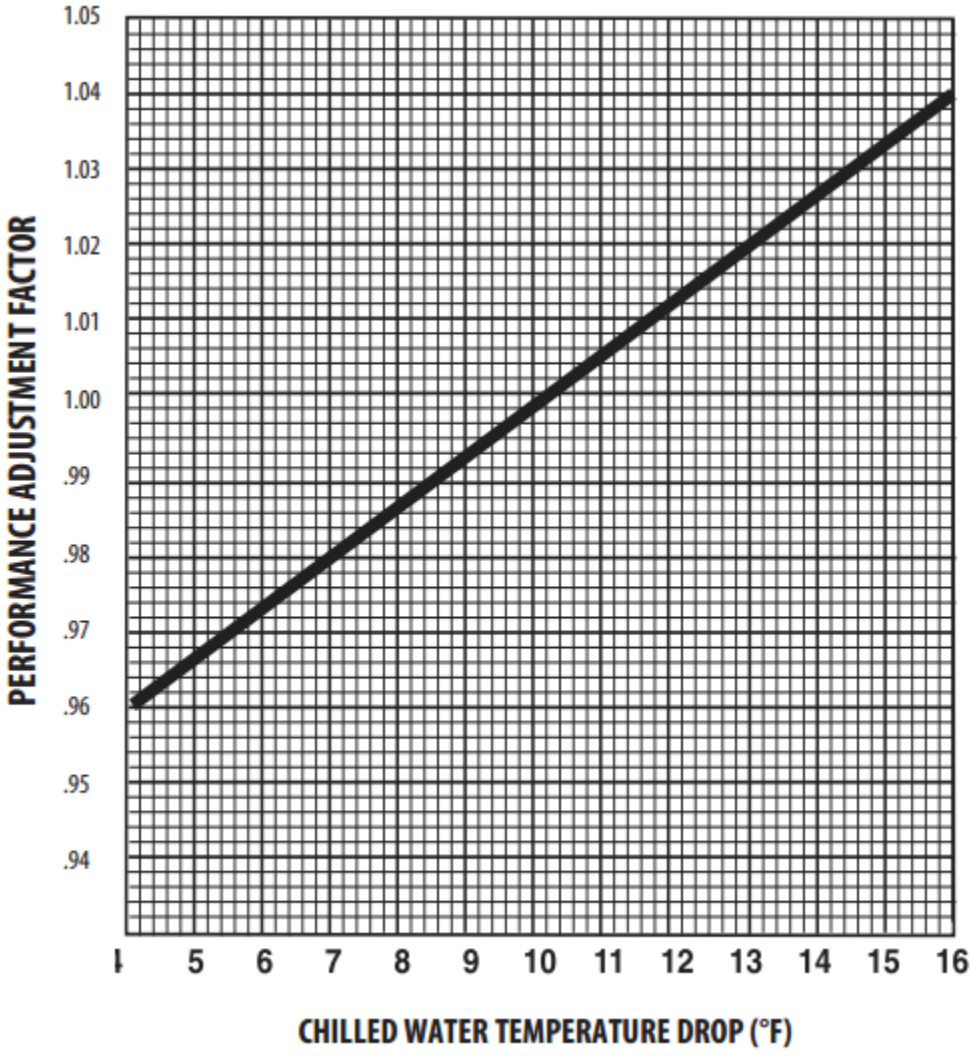

Figure D-1 - HP Manufacturer Adjustment Factor based on Evaporator Temperature Drop

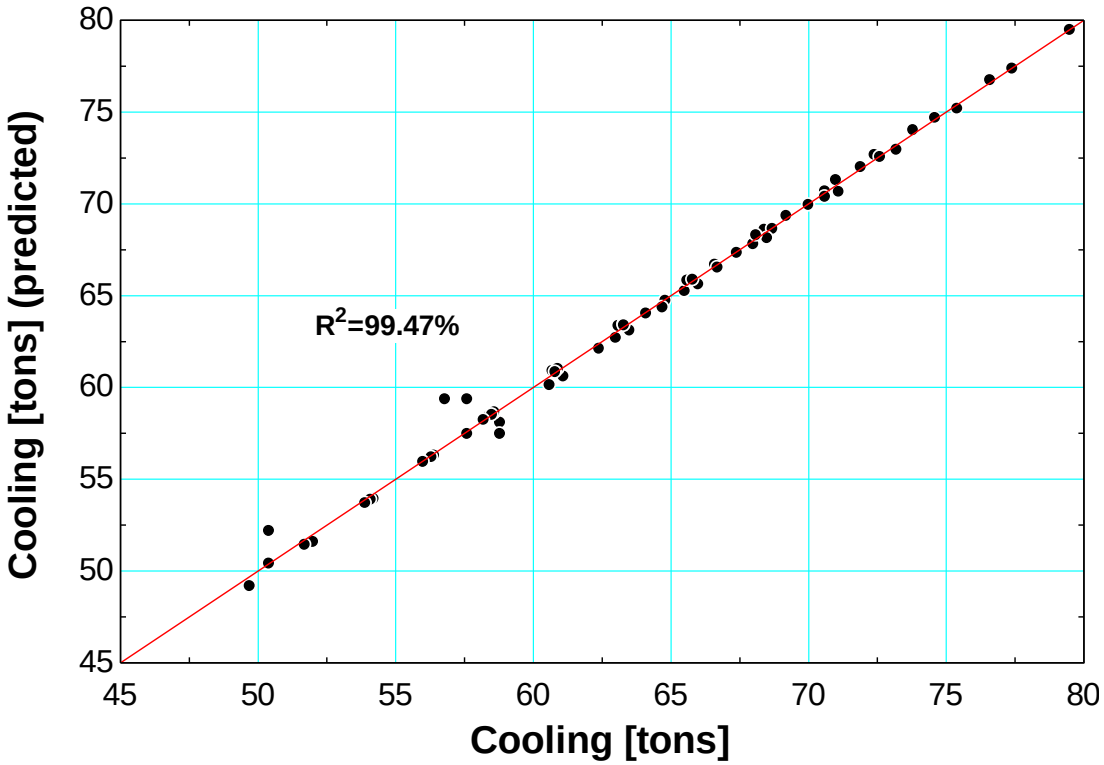

Figure D-2 – Figure showing goodness of fit for Heat Pump Manufacturer Cooling Capacity Data

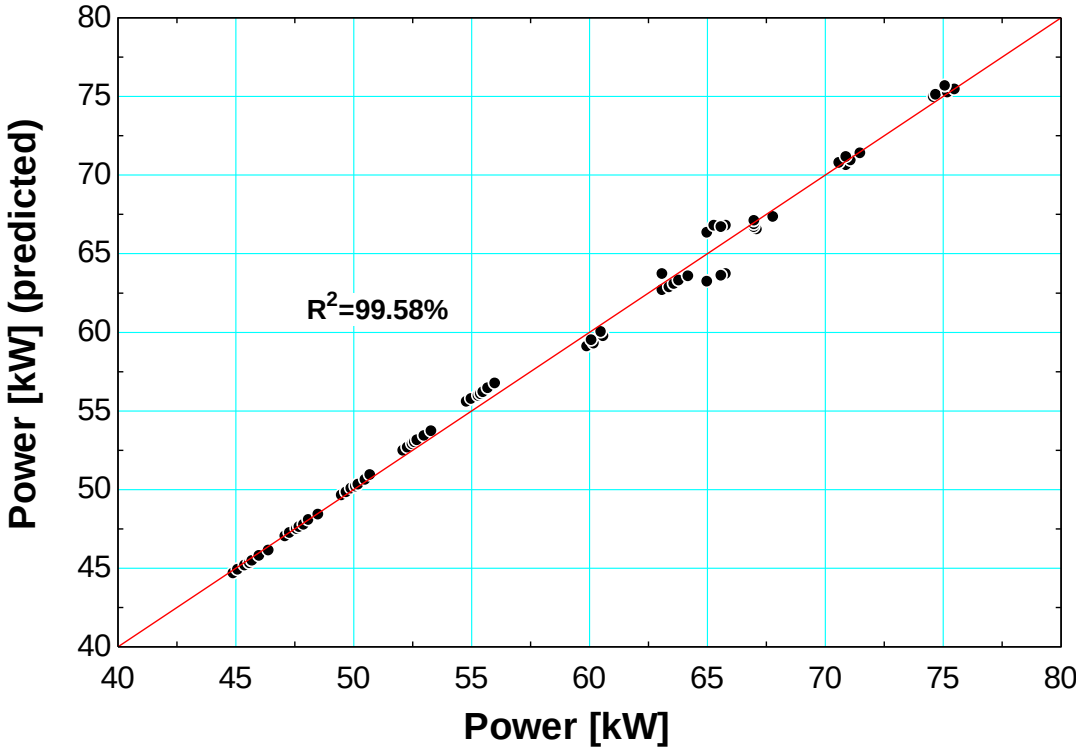

Figure D-3 – Figure displaying goodness of fit of Heat Pump Manufacturer electrical power consumption data

Measured (Steady) Data used to Compared HP Performance to Manufacturer

Steady Data Segment	Timestamp	Active Module and Compressor (a/b)	# of Comps.	# of HXs	ELW [F]	EEW [F]	CEW [F]	CLW [F]	WFM1 [GPM]	W_dot_HP [kW]
1	2012-09-20 09:00:00	2, 4 ,3a	5	3	40.95	53.86	95.1	100.7	206.3	138.7
2	2012-09-15 15:50:00	1, 5, 6b	5	3	40.66	51.6	98.39	104.1	284.2	145.1
3	2012-09-14 16:10:00	1, 5, 6	6	3	40.31	50.52	107.3	114	342.6	191.2
4	2012-09-30 16:20:00	1, 2, 3a, 4b, 5a	7	5	50.76	62.6	114.3	118.9	306.7	239.8
5	2012-09-12 14:30:00	1, 5, 6, 4b	7	4	43.20	57.76	111.4	119.9	259.3	237.3
6	2012-09-11 15:30:00	1, 2, 3a, 6	7	4	42.33	56.92	110.3	118.7	260.9	235.7
7	2012-09-28 17:00:00	1, 2, 6, 3a	7	4	49.23	64.55	113.3	119.4	250.2	238
8	2012-09-28 14:50:00	1, 2, 3, 6	8	4	45.10	61.71	111.3	118.1	254	265.4
9	2012-09-13 02:10:00	1, 6, 4b, 5a	6	4	39.18	45.15	110.3	117.1	581	199.1
10	2012-09-11 01:30:02	3, 4, 5a, 6a	6	4	39.10	45.56	108	115.3	560.6	195.5
11	2012-09-28 22:30:00	1, 2, 3a, 4b, 6	8	5	44.43	56.95	113.2	118.5	345.7	268.5
12	2012-09-26 20:40:01	1, 3, 5, 6	8	4	42.51	53.7	111.4	118.5	413.7	266.2
13	2012-09-17 15:40:00	1, 2, 3, 4a, 6b	8	5	39.14	45.63	109.4	118	667.9	263.9

Table D-3 - Averaged Measurements for Steady Time Periods for Validating HP Performance

Appendix E. Additional Information for TRNSYS GHX Models

Absolute Mean Difference

The absolute mean difference (MD) was used to determine the error of the model:

$$MD = \frac{\sum_i |Model_i - Measured_i|}{i} \quad \textbf{(E-1)}$$

where Model and Measured are the respective leaving water temperatures in °F,

and i is the number of time steps in the simulation.

DST Model Parameters and Input Data

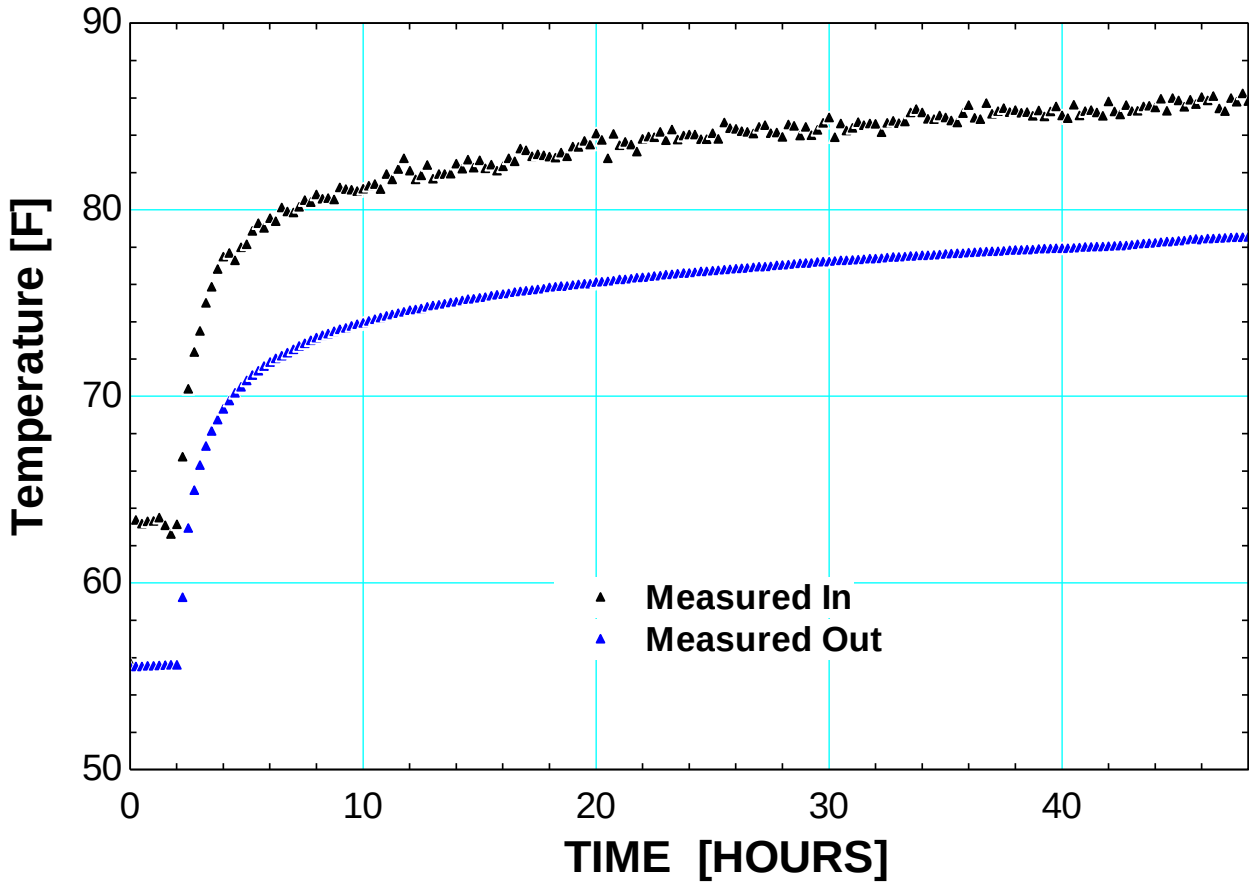

Figure E-1 - TRT data provided by the contractor for Single-bore model

#	Parameter	Value	Units
1	Storage volume	14234	m^3
2	Borehole depth	121.9	m
3	Header depth	0	m
4	Number of boreholes	1	-
5	Borehole radius	0.083312	m
6	No. of boreholes in series	1	-
7	Number of radial regions	1	-
8	Number of vertical regions	10	-
9	Storage thermal conductivity	14.52	kJ/hr.m.K
10	Storage heat capacity	2660	kJ/m^3/K
11	Negative of u-tubes/bore	-1	-
12	Outer radius of u-tube pipe	0.02108	m
13	Inner radius of u-tube pipe	0.01725	m
14	Center-to-center half distance	0.02654	m
15	Fill thermal conductivity	6.231	kJ/hr.m.K
16	Pipe thermal conductivity	1.401895	kJ/hr.m.K
17	Gap thermal conductivity	5.04	kJ/hr.m.K
18	Gap thickness	0	m
19	Reference borehole flow rate	1817	kg/hr
20	Reference temperature	11	C
21	Pipe to pipe heat transfer	-1	-
22	Fluid specific heat	4.183	kJ/kg.K
23	Fluid density	997	kg/m^3
24	Insulation indicator	0	-
25	Insulation height fraction	0.5	-
26	Insulation thickness	0.0254	m
27	Insulation thermal conductivity	1	kJ/hr.m.K
28	Number of simulation years	1	-
29	Maximum storage temperature	54.4	C
30	Initial surface temperature of storage volume	15.6	C
31	Initial thermal gradient of storage volume	0	any
32	Number of preheating years	0	-
33	Maximum preheat temperature	30	C
34	Minimum preheat temperature	10	C
35	Preheat phase delay	90	day
36	Average air temperature - preheat years	20	C
37	Amplitude of air temperature - preheat years	15	deltaC
38	Air temperature phase delay - preheat years	240	day
39	Number of ground layers	1	-
40	Thermal conductivity of layer	14.52	kJ/hr.m.K
41	Heat capacity of layer	2660	kJ/m^3/K
42	Thickness of layer	121.9	m

Table E-1 - Parameters for Single-bore DST model

#	Parameter	Value	Unit
1	Storage volume	1654000	m^3
2	Borehole depth	91.4	m
3	Header depth	2.134	m
4	Number of boreholes	77	-
5	Borehole radius	0.083312	m
6	No. of boreholes in series	1	-
7	Number of radial regions	1	-
8	Number of vertical regions	10	-
9	Storage thermal conductivity	14.52	kJ/hr-m-K
10	Storage heat capacity	2660	kJ/m^3/K
11	Negative of u-tubes/bore	-1	-
12	Outer radius of u-tube pipe	0.02108	m
13	Inner radius of u-tube pipe	0.017247	m
14	Center-to-center half distance	0.026543	m
15	Fill thermal conductivity	6.231	kJ/hr-m-K
16	Pipe thermal conductivity	1.402	kJ/hr-m-K
17	Gap thermal conductivity	5.04	kJ/hr-m-K
18	Gap thickness	0	m
19	Reference borehole flow rate	1700	kg/hr
20	Reference temperature	38	C
21	Pipe to pipe heat transfer	-1	-
22	Fluid specific heat	4.183	kJ/kg.K
23	Fluid density	997	kg/m^3
24	Insulation indicator	0	-
25	Insulation height fraction	0.5	-
26	Insulation thickness	0.0254	m
27	Insulation thermal conductivity	1	kJ/hr-m-K
28	Number of simulation years	1	-
29	Maximum storage temperature	54.4	C
30	Initial surface temperature of storage volume	15.6	C
31	Initial thermal gradient of storage volume	0	any
32	Number of preheating years	0	-
33	Maximum preheat temperature	30	C
34	Minimum preheat temperature	10	C
35	Preheat phase delay	90	day
36	Average air temperature - preheat years	20	C
37	Amplitude of air temperature - preheat years	15	deltaC
38	Air temperature phase delay - preheat years	240	day
39	Number of ground layers	1	-
40	Thermal conductivity of layer	14.52	kJ/hr-m-K
41	Heat capacity of layer	2660	kJ/m^3/K
42	Thickness of layer	91.4	m

Table E-2 – Parameters for the Full-Field DST model

Challenging the GHX Model, Heat Pump Model Equations

Inputs and Constants

Capacity_frac "Allows simulation of the HPs running at varying capacities of their total capacity (i.e. the number of HP modules in operation)."

Correction "Adjusts manufacturer HP performance data closer to actual (measured) HP performance"

T_max_allowed_F = 123 "The condenser entering water temperature in °F that will shut off the HPs"

cp = 4.183 "specific heat of water in kJ/kg-K"

T_cond_in_F "water temp entering condensers (i.e. water temp leaving the GHX, continuously output from the DST model)"

Equations

Cool_max_tons = LT(T_cond_in_F,T_max_allowed_F)*(548.539-1.2956*T_cond_in_F-0.0068226*T_cond_in_F**2)*Capacity_frac*Corection "HP manufacturer performance data

curve fit for cooling capacity as function of entering condenser water temp (assumes chilled water supply temperature is 44°F. If water temp

entering condensers is greater than allowed temperature, cooling goes to zero (i.e. HPs shut off due to high refrigerant pressure)"

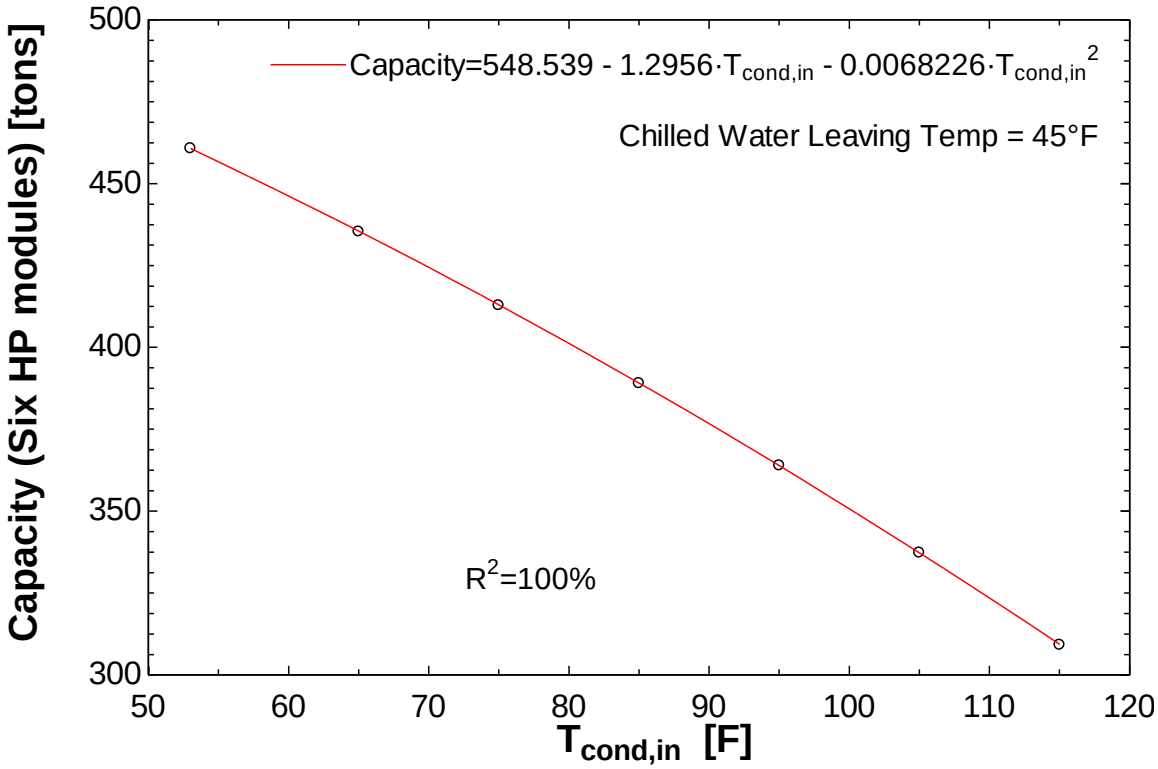

COP = (12.0876-0.119419*T_cond_in_F+0.000302791*T_cond_in_F**2)*Correction

"HP manufacturer performance data curve fit for COP as a function of entering condenser water temp (assumed chilled water supply temperature at 45°F. "

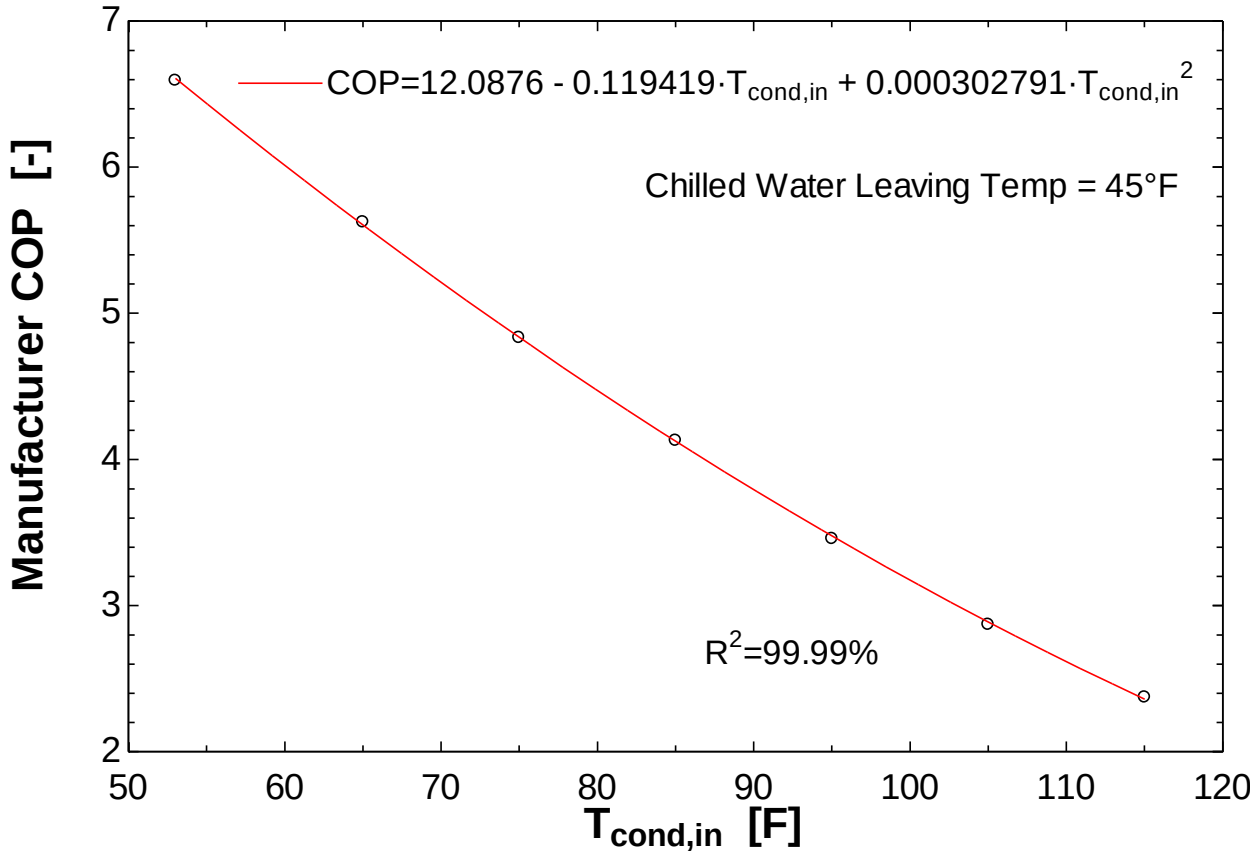

T_cond_out_F = T_cond_in_F+20 "20°F water temperature rise across the condensers"

Power_HP_tons = Cool_max_tons/COP "electrical power in tons required by HPs"

THR_tons = Cool_max_tons+Power_HP_tons "total heat rejection in tons"

DELTAK = (T_cond_out_F+459.67)/1.8-(T_cond_in_F+459.67)/1.8 "temperature rise across condensers converted from °F to K"

$$m\_dot\_kghr = \frac{THR\_tons\ 12660.6672}{(cp{*}DELTAK)}$$ "required condenser water mass flow rate in kg/hr (input to DST). Constant converts tons to kJ/hr"

T_cond_out_K = (T_cond_out_F+459.67)/1.8 "convert condenser out water temperature to K"

$$T_{reh,out,K} = T_{cond,out,K} - GT\left(T_{cond,outF}, 110\right)\left(0.15 Cool_{max,tons}\right)\frac{12660.6672}{\left(cp\ \dot{m}_{kghr}\right)}\ 2$$

"calculates the water temp returning from reheat. The HP cooling is converted to kJ/hr. Assumes water mass flow in reheat is equal to one half of mass flow through GHX. The Greater Than (GT) flag only allows reheat water temp to be calculated (i.e. reheat to be recovered) if leaving condenser water temperature is above 110°F setpoint, otherwise reheat leaving temperature is equal to the condenser leaving temperature."

T_reh_out_F = 1.8*T_reh_out_K-459.67 "return from recovered reheat water temp in °F"

T_geo_in_K = (T_cond_out_K+T_reh_out_K)/2 "Water temperature entering the GHX in K"

T_geo_in_F = 1.8*T_geo_in_K-459.67 "water temp entering the GHX converted to °F (for plotting)"

T_geo_in_C = T_geo_in_K-273.15 “water temp entering the GHX converted to °C (input to DST)”